Synthesis of new Covalent Triazine Frameworks for Carbon Dioxide Photoreduction

Marcelo Alves Favaro

N°d'ordre NNT : 2020LYSE1077

THESE de DOCTORAT DE L'UNIVERSITE DE LYON
opérée au sein de
l'Université Claude Bernard Lyon 1

Ecole Doctorale N° ED206

Spécialité de doctorat: **Chimie**
Discipline: **Chimie Industrielle Durable**

Soutenue publiquement le 27/04/2020, par:
Marcelo Alves Fávaro

Synthèse de nouveaux "Covalent Triazine Frameworks" pour la photoréduction du dioxyde de carbone

---

Devant le jury composé de :

Prof. Albonetti, Stefania	Examinatrice	Università di Bologna
Prof. Andrioletti, Bruno	Président du jury	Université Claude Bernard Lyon 1
Dr. Canivet, Jérôme	Directeur de thèse	CNRS - Lyon
Dr. Carenco, Sophie	Rapporteure	CNRS - Paris
Prof. Claver, Carmen	Examinatrice	Universitat Rovira i Virgili
Prof. De Vos, Dirk	Rapporteur	Université de Louvain
Prof. Liauw, Marcelo	Examinateur	RWTH-Aachen University
Prof. Palkovits, Regina	Directrice de thèse	RWTH-Aachen University

Fakultät für Mathematik, Informatik und Naturwissenschaften | RWTH AACHEN UNIVERSITY

Synthesis of new Covalent Triazine Frameworks for Carbon Dioxide Photoreduction

Von der Fakultät für Mathematik, Informatik und Naturwissenschaften
der RWTH Aachen University

zur Erlangung des akademischen Grades eines
Doktors der Naturwissenschaften genehmigte Dissertation
vorgelegt von

„Alves Fávaro, Marcelo, M.Sc.“
aus
„Orlândia, Brasil“

Berichter*:* Prof. Dr. Regina Palkovits
Dr. Jérôme Canivet

Tag der mündlichen Prüfung: 27-04-2020

The present doctoral thesis was mainly carried out at the Institut für Technische und Makromolekulare Chemie (ITMC) of RWTH Aachen University between November 2016 and November 2019 under the supervision of Prof. Dr. Regina Palkovits. Part of the thesis was carried out at the IRCELYON (CNRS, Universite Claude Bernard Lyon 1) between February 2018 and November 2018 under the supervision of Dr. Jérôme Canivet and Prof. Dr. Alessandra Quadrelli.

Acknowledgments

Undertaking this PhD has been a truly life-changing experience for me and it would not have been possible to do without the support and guidance that I received from many people.

First, I would like to express my deepest gratitude to my supervisors: Regina Palkovits (ITMC, RWTH-Aachen), Jérôme Canivet (IRCELYON) and Alessandra Quadrelli (CPE-Lyon). I'm grateful for all their support, encouragement, exceptional knowledge, trust and guidance during this research project and thesis writing.

Further, I would like to thank the jury members for accepting to review and give their contributions to this work.

A special thanks to Florian Wisser, for all the support, advice, discussions and for helping me to develop new skills and knowledge.

In addition, it was incredible to be part of the SINCHEM program. I want to thank the Erasmus program for funding, Prof. Stefania Albonetti for the coordination and Stefanie Mersmann for helping with the bureaucratic issues. I am extremely honored to be part of the SINCHEM program. Thanks to the other PhD students, Akash, Ravi, Daniel, Ulisse, Valeriia, Sonia, Tran, Aisha, Payal, Kristine, Iqra, Shiming, Danilo, Pooja, Matilde, Tapish, Phouc, Chalechew, Paola, Ana Patricia, Samantha, Ferenc, Medet and Hua for making this journey unforgettable.

I am also very grateful to my colleagues from Palkovits group, including all scientific and administrative members of ITMC. Thanks to my colleagues: Jens, Christian "Puffo", Daniel, Liao Longfei, Ylenia, Keanu, Ximeng, Andree, Feng Zeng, Tobias, Guido, Carsten, and in especial, my friends Chalechew and Xinde Wang (Jacob).

From Lyon, I also would like to acknowledge the scientific members and administrative staff from IRCELYON, in particular, my colleagues: Yorck, Rémy, Yoann, Baptiste, Mehdi, Emmanuel, Cécile, Yann, Katia, Ranin, Alejandra, Ana Rita, Alisa, Partha, Ashta and David from the ING group.

I acknowledge my former professor, Regina Frem, whose passion and affection drove me through this incredible pathway.

I am grateful to my friends Marco and Daniele, for the support and encouragement, since they were the first to know about my aspiration to study overseas. For the support of Vinicius, Juliana, Gleidina, Michael, Felipe and Cinthia, the friends Lyon gave to me.

I also would like to thanks my beloved family, my parents, Mário and Lucinara that always encouraged me to pursue my dreams, even though very far from them. Thanks to my brothers and sisters, Gabriel, Lucas, Ângelo, Eugênio, Carolina, Maria and João Paulo, and my sisters-in-law Aline and Susana, for always seeing the best on me and for making me give my best every day.

I want to thank my grandparents, Mário Eugênio, José Nilton (in Memoriam) and Alda, whose ancestrality has influenced me until now. For always being proud to have a scientist's grandson.

Finally, I thank Rebeca, my beloved partner, for all the love and support. For making me believe that we are capable of great deeds, for always seeing me as an incredible human being. For never letting me give up, for the deepest conversations, for sharing our existence in this extraordinary journey. To you, all my love, passion and admiration.

Abstract

Using sunlight as a renewable source of energy to promote carbon dioxide (CO_2) conversion is an interesting approach to address sustainable chemicals and fuels production as well as mitigation of climate change. However, in most photocatalytic systems, the utilization of a homogeneous photosensitizer represents a key limitation for a long-term reactions due to its low stability. Therefore, novel, more efficient and stable photocatalyst materials and photocatalytic processes are required.

Here, the strategy of structuration at the molecular-level of CTF photocatalysts is presented, seeking to enhance their long-term stability. The integration of photo-active centers into a molecularly defined support improve their photocatalytic stability. Moreover, the incorporation of chelating moieties, such as bipyridine, offers a unique possibility for heterogenization of organometallic complex, profiting at the same time from enhanced selectivity and activity from the molecular catalyst and easy handling and separation from its heterogeneous nature. Macroligands, a solid acting like the ligand in the corresponding molecular complex, is a pivotal strategy to bridge the gap between homogeneous and heterogeneous catalysis.

In this thesis, the synthesis of simple CTFs through condensation was done in order to optimize the parameters and highlight the main advantages and drawbacks of this method. Additionally, the approach was extended to the synthesis of functionalized materials, based on bipyridine ligands. Using the strategy of modular design, the content of a ligand within the framework was precisely controlled for the first time. Additionally, by judiciously chosen the proper tailored precursor and its content, it is possible to carefully control properties like light absorption and porosity, pushing the boundaries of molecular control on the synthesis of CTFs.

In this regard, CTFs based on bipyridine were precisely designed in order to contain both, a photoactive moiety and a chelating site for the heterogenization of molecular catalysts within the structure. In our all-in-one concept, a (Cp*)-Rhodium complex was heterogenized within CTFs macroligands containing different amounts of bipyridine. Those materials catalyze the carbon dioxide photoreduction to formate, driven by visible light at TOFs around 4 h^{-1}.

Zusammenfassung

Die Nutzung des Sonnenlichts als erneuerbare Energiequelle zur Förderung der Umwandlung von Kohlendioxid (CO_2) ist ein interessanter Ansatz zur Bekämpfung der nachhaltigen Produktion von Chemikalien und Kraftstoffen sowie zur Eindämmung des Klimawandels. In den meisten photokatalytischen Systemen stellt die Verwendung eines homogenen Photosensibilisators aufgrund seiner geringen Stabilität jedoch eine wesentliche Einschränkung für Langzeitreaktionen dar. Daher sind neuartige, effizientere und stabilere Photokatalysatormaterialien und photokatalytische Verfahren erforderlich.

In dieser Arbeit wird eine Strategie zur Strukturierung von CTF-Photokatalysatoren auf molekularer Ebene präsentiert, um deren Langzeitstabilität zu verbessern. Die Integration photoaktiver Zentren in einen molekular definierten Träger verbessert deren photokatalytische Stabilität. Darüber hinaus bietet der Einbau von Chelatzentren wie Bipyridin eine einzigartige Möglichkeit zur Heterogenisierung des metallorganischen Komplexes, wobei gleichzeitig von einer erhöhten Selektivität und Aktivität des molekularen Katalysators sowie einer einfachen Handhabung und Trennung von seiner heterogenen Natur profitiert wird. Makroliganden, ein Feststoff, der wie der Ligand im entsprechenden Molekülkomplex wirkt, sind eine Schlüsselstrategie, um die Lücke zwischen homogener und heterogener Katalyse zu schließen.

In dieser Arbeit wird die Synthese einfacher CTFs durch Kondensation untersucht, die Parameter optimiert und die Vor- und Nachteile dieser Methode hervorgehoben. Zusätzlich wurde der Ansatz auf die Synthese funktionalisierter Materialien auf Basis von Bipyridinliganden erweitert. Mit der Strategie eines modularen Aufbaus konnte erstmals der Gehalt eines Liganden innerhalb des Netzwerks präzise gesteuert werden. Darüber hinaus ist es durch sorgfältige Auswahl des richtigen maßgeschneiderten Precursors möglich, Eigenschaften wie Lichtabsorption und Porosität sorgfältig zu kontrollieren und die Grenzen der molekularen Kontrolle bei der Synthese von CTFs zu verschieben.

Es wurden CTFs auf der Basis von Bipyridin entworfen, um sowohl eine photoaktive Einheit als auch eine Chelatierungsstelle für die Heterogenisierung molekularer Katalysatoren innerhalb der Struktur zu enthalten. In unserem All-in-One-Konzept wurden (Cp*) - Rhodium-Komplexe in CTFs-Makroliganden heterogenisiert, die unterschiedliche Mengen an Bipyridin enthielten. Diese Materialien katalysieren die Kohlendioxid-Photoreduktion, angetrieben durch sichtbares Licht mit TOFs von bis zu 4 h^{-1}.

Résumé

L'utilisation de la lumière solaire comme source d'énergie renouvelable pour promouvoir la conversion du dioxyde de carbone (CO_2) est une approche intéressante pour aborder la production durable de produits chimiques et de combustibles ainsi que pour lutter contre le dérèglement climatique. Cependant, dans la plupart des systèmes photocatalytiques, l'utilisation d'un photosensibilisateur homogène représente une limitation clé pour les réactions à long terme en raison de sa faible stabilité. Par conséquent, de nouveaux matériaux photocatalyseurs et processus photocatalytiques plus efficaces et stables sont nécessaires.

Ici, la stratégie de structuration au niveau moléculaire des photocatalyseurs CTF est présentée, cherchant à améliorer leur stabilité à long terme. L'intégration de centres photoactifs dans un support moléculaire défini améliore leur stabilité photocatalytique. De plus, l'incorporation de fractions chélatantes, telles que la bipyridine, offre une possibilité unique d'hétérogénéisation de complexes organométalliques, bénéficiant à la fois d'une sélectivité et d'une activité améliorées comparées au catalyseur moléculaire analogue et d'une manipulation et d'une séparation facile grâce à sa nature hétérogène. L'utlisation de macroligand, solides agissant comme le ligand dans le complexe moléculaire correspondant, est une stratégie attrayante pour combler l'écart entre la catalyse homogène et hétérogène.

Dans cette thèse, la synthèse de CTF simple par condensation a été réalisée afin d'optimiser les paramètres et de mettre en évidence les principaux avantages et inconvénients de cette méthode. De plus, l'approche a été étendue à la synthèse de matériaux fonctionnalisés, basés sur des ligands bipyridiniques. En utilisant la stratégie de conception modulaire, le contenu d'un ligand dans le matériaux a été précisément contrôlé pour la première fois. De plus, en choisissant judicieusement le précurseur adapté et son contenu, il est possible de contrôler soigneusement les propriétés comme l'absorption de la lumière et la porosité, repoussant les limites du contrôle moléculaire sur la synthèse des CTF.

À cet égard, les CTF basés sur la bipyridine ont été précisément conçus afin de contenir à la fois un fragment photoactif et un site de chélation pour l'hétérogénéisation des catalyseurs moléculaires au sein de la structure. Dans notre concept tout-en-un, un complexe rhodium a été hétérogénéisé au sein de macroligands CTF contenant différentes quantités de bipyridine. Ces matériaux catalysent la photoréduction du dioxyde de carbone en formiate activée par la lumière visible avec des activité de l'ordre de 4 h^{-1}.

Summary

Chapter 1 - Introduction:

In the actual scenario, most of the energy produced in the world still relies on fossil resources. To produce energy, power plants burn carbon-based fuels to generate steam, which drives large turbines to produce electricity. However, the combustion of fossil fuels generates carbon dioxide (CO_2) as a by-product.

As a greenhouse gas, CO_2 absorbs the heat emitted from our planet's surface, keeping it warm. However, the increase in the concentration of atmospheric greenhouse gases since the 19th century consequently rose overall Earth's temperature, resulting in climate change. With the rising temperatures, many critical environmental issues can be observed, extreme weather events, ocean acidification, rising in the sea level, global warming and shifting in wildlife populations and their habitats are some of them.

Therefore, decreasing the emissions and setting priorities and strategies to convert atmospheric CO_2 are urgent demands to mitigate climate collapse. Although carbon capture and storage technologies offer a solution, these processes have some limitations for large scale applications. Another solution would be to capture and further convert the CO_2 in useful fuels and chemical compounds, closing the carbon cycle and mitigating the climate emergency. In this regard, CO_2 can be converted by three processes: thermal hydrogenation, electrochemical reduction, and photochemical reduction. Nevertheless, using light as a sole source of energy to drive CO_2 reduction reaction is a sustainable way to address the problem.

However, CO_2 conversion is a challenge. Because together with the intrinsic properties of gases, like low density and readily creation of mixtures, making storage and transportation difficult, the catalytic system has to overcome enormous energy barriers to promote CO_2 reduction. In this context, porous organic polymers are attracting considerable attention as catalysts for CO_2 reduction. This class of materials became popular mainly due to its structural properties like porous nature, with enhanced specific surface area, which consequently boosts the accessibility of reactants and products during catalysis. Additionally, the easy tuning of their structural features compared to the classic inorganic porous materials like zeolites, allow the design and synthesis of polymers containing different functions that are essential to lower the energy barrier in CO_2 conversion.

Many classes of porous organic polymers have been tested as a catalyst in the energy field, including CO_2 photoreduction. Among them, Covalent Triazine Frameworks (CTFs) have shown remarkable activity in the production of clean energy. These frameworks, containing triazine moieties, were discovered by Arne Thomas et al. and became famous, especially in photocatalysis, after the seminal work of Antonietti et al. in which he employed a graphitic carbon nitride, comprising of s-triazine and heptazine units, as a single catalyst to drive both half-reactions on water splitting. From 2008 on, CTFs have been applied in many fields. Besides clean hydrogen production through water splitting and CO_2 conversion, these triazine-based materials have been employed as gas adsorbent and separation media, support for metal nanoparticles and molecular metalorganic complexes, cathode, and anode in electrochemical processes and energy storage systems, water purification and others.

CTFs can be synthesized in many ways. Each method leads to materials with different features. The most common is the ionothermal approach, in which nitriles are mixed with zinc chloride and charged in an ampule that is sealed and heated up to form a very porous black powder. In another approach, nitriles are trimerized by trifluoromethanesulphonic acid to produce photoactive CTFs. This method is called super acid due to the utilization of triflic acid for trimerization. Other methods are available but are not frequently reported in the literature.

Nevertheless, all these approaches have drawbacks. In the first case, the ionothermal conditions are so harsh that they produce partially carbonized materials, and for this reason, unsuitable for photo and optical applications. For the acid approach, the main drawback is the building block limitation, since this method does not work for pyridine-based monomers.

More recently, CTFs have been synthesized by condensing amidine chloride with an aldehyde. Such approach leads to the production of photoactive materials containing partial layered structure. Moreover, modular design can be used to develop materials in a precise and molecularly controlled fashion. However, up to now, only non-functionalized building blocks have been employed in the synthesis of CTF through condensation.

In this project, the aim is to push the boundaries of the CTFs synthesis, studying the novel condensation approach systematically, in order to address their main limitations and advantages. For this purpose, the project started with the synthesis of simple CTFs

already reported in the literature, based on the condensation of terephthalamidine chloride and terephthaldehyde. Further, the same approach was employed in the synthesis of functionalized CTFs.

Taking advantage of the fact that the newly established condensation protocol leads to the production of photoactive materials, the synthesis of functionalized CTFs based on bipyridine ligands was described. Such CTF was employed as macroligand to support the molecular rhodium Cp* complex, know to drive selectively the CO_2 reduction to formate under visible light irradiation. For the first time, the synthesis of complex CTFs prepared by condensation is reported.

Chapter 2 - Challenges:

The challenges in the synthesis of CTFs by condensation start with the synthesis of precursors, poorly reported in the literature. Additionally, the design and synthesis of a stable and active photocatalyst are also addressed in the challenges. Since the characterization of porous polymers is an ongoing challenge, the main issues regarding the elucidation of the catalyst's structure are discussed in this chapter.

First, the synthesis of CTFs begins with the preparation of precursors, aldehydes and amidine chlorides. The aldehyde can be synthesized through a vast number of different reactions. To quote some of them: oxidation of alcohols, Swern oxidation, Sommelet reaction, Kornblum oxidation and others. The pathway chosen will mainly depend on the structure of the building block needed. On the other hand, the synthesis of amidine chlorides presents a real challenge. Between other reactions like Pinner reaction and Garigipati's reaction, the addition of Lithium bis(trimethylsilyl)amide (LiHMDS) to nitrile precursor represents a straightforward way for the synthesis of these monomers. In the beginning, phenyl-based monomers were synthesized and purified. Later, the same protocols of synthesis and purification employed to produce the phenyl-based precursors were used to produce functionalized building units.

Moreover, regarding the challenges in designing a photocatalyst, the materials described in this thesis followed the same strategy employed by Wisser et al. The "all-in-one" strategy is an exciting way to address the lack of stability of photocatalysts for long-term CO_2 reduction. Since one fundamental limitation in photocatalytic CO_2 reduction

reaction is the utilization of a homogeneous organic photosensitizer, which degrades over time and consequently slows down or completely stops the reaction within a few hours, the strategy described by Wisser and co-workers, is the incorporation of a photosensitizing unit within the framework's backbone. In our case, the design of a photocatalyst was done by using triazine as a heterogeneous photosensitizing unit together with bipyridine monomers as a chelating unit. With the bipyridine, it is possible to support homogeneous molecular catalysts like rhodium Cp* for selective conversion of carbon dioxide into formate under visible light irradiation. Therefore, the fully heterogeneous system was designed based on the "all-in-one" strategy previously presented, in order to address and overcome the main challenges for long-term photocatalytic CO_2 reduction.

It is known that the characterization of amorphous porous polymers is an ongoing challenge. Due to the lack of long-term order, it is often challenging to get insights into the structural properties of these materials. To better understand the structure and features of these CTFs synthesized through condensation, the results were combined. In this way, better insight and explanation of the phenomena that govern these new CTFs can be adequately explained, establishing a structure-activity relationship for further optimization of their structures.

Chapter 3 - Synthesis and characterization of precursors

As stated before, the synthesis of amidine chlorides presents the real challenge in the synthesis of CTFs by condensation. These monomers were synthesized through the addition of Lithium bis(trimethylsilyl)amide to the nitrile precursor in THF under an inert atmosphere. The complete experimental procedure was published elsewhere. Even though the synthesis of amidine chlorides proceeds smoothly to the final products, when the reaction is quenched with hydrochloric acid in ethanol, other by-products are generated together with the amidine chloride. From these by-products, lithium chloride and ammonium chloride have been reported previously. In the case of ammonium chloride, this persistent contamination can be noticed in the liquid ^{1}H-NMR as a prominent triplet that appears in the region of 7.28 ppm. Since the traditional purification methods like flash column chromatography and recrystallization had failed to yield a pure amidine chloride, the crude product had to be purified by exchanging the counter-ion of

amidine chloride. Inspired by the work of Morshedi and co-workers, the amidine's counter-ion was exchanged from chloride to tetraphenylborate. This option relies on the entirely different properties the counter-ion gives to the compound.

In contrast to the amidine chloride, amidine tetraphenylborate is not soluble in water. In this way, it is possible to wash out the by-products salts formed during the synthesis of the monomer. Since the organic counter-ion could present significant steric effects during the synthesis of a CTF polymer, the amidine's counter-ion was once again exchanged to a halide, this time to bromide. All these monomers were employed on the synthesis of CTFs.

By employing the same experimental procedure, the bipyridine-based building block was synthesized. The choice for bipyridine units relies on the chelating property of this building block. For our targeted application, the heterogenization of a molecular catalyst would profit from an enhanced selectivity and activity, characteristic for homogeneous photocatalysts. On the other hand, the fully heterogeneous system would profit from recyclability and easy separation, bridging both worlds homogeneous and heterogeneous in one single material.

Considering that the synthesis of bipyridine-based amidine starts with the nitrile, and that typically the synthesis of nitrile compounds is done by cyanation of halide precursors, the pathway to synthesize 2,2'-bipyridine-5,5'-dicarbonitrile was developed in order to use less toxic compounds than cyanides. The starting material was the commercially available 5,5'-dimethyl-2,2'-bipyridine, which was oxidized in water by $KMnO_4$ to obtain the dicarboxylic acid. Further, the carboxylic acid was esterified in ethanol/sulfuric acid mixture. The resulting ester reacted with ammonia in a saturated solution of ethanol/ethylene glycol to selectively produce 2,2'-bipyridine-5,5'-dicarboxamide in high yields. In the last step, the carboxamide was dehydrated to nitrile using phosphorus oxychloride under the ultrasonic bath. Although this pathway has many steps and the overall yield is slightly lower (70% compared to 90% from cyanation reactions), at the end only with simple recrystallization in acetonitrile, we were able to recover the pure nitrile. In contrast, for cyanation, extensive purification steps have to be carried out.

Together with bipyridine-based amidines, biphenyl-based precursors were also employed in the synthesis of CTFs. These ligands were chosen as a non-functionalized

counter-part of bipyridine-based monomers. Thereby, when both bipyridine and biphenyl-based precursors are employed in the synthesis of CTFs, the aim is to achieve materials containing symmetric pore structure. Moreover, by taking advantage of the modular approach, only possible when CTFs are synthesized by condensation, the synthesis of CTFs containing different amounts of bipyridine ligands was carried out. So for the first time, the precise molecular control over the content of a ligand within the CTF material was accomplished pushing, therefore, the boundaries of CTF synthesis into a more precise and molecularly controlled manner.

Chapter 4 - Synthesis through condensation

In order to better understand the newly established condensation approach for the synthesis of CTFs, this project first addressed the synthesis of simpler materials based on the reaction between terephthalamidine chloride and terephthalaldehyde. The materials were synthesized systematically to better understand the limitations and advantages of this method.

Owing to the partial layered structure due to the arrangements of bidimensional sheets, the position at which stacking happens in these CTFs is crucial to the material and can give different features. When the AB stacking position is predominant, the material is denser due to the perfect arrangements of layers, in which the triazine center of the first layer is precisely in the vacancy for the next one. This well-packed material presented a very low surface area of 2-10 m^2/g due to pore blocking. On the other hand, the AA stacking position is exceptionally beneficial. In this last case, the layers are aligned in a way that the triazine ring is at the same position in all layers, creating a channel of aligned vacancies and consequently boosting their specific surface area up to 500 m^2/g. The materials were also analyzed by powder XRD, confirming the different stacking positions.

Together with N_2 physisorption and XRD, the characterization of these materials was done by FT-IR, solid-state NMR, XPS, and UV-Vis. From FT-IR spectroscopy, the main stretching vibrations from the triazine was confirmed at 1515 and 1356 cm^{-1}. These stretches can be assigned to C=N and –C-N-, respectively. Solid-state NMR also confirmed the triazine ring within the material's framework, and it is in agreement with the materials published in the literature. However, the XPS analysis showed a small

deviation. From the literature, the material holds three types of nitrogen species: pyrrolic, pyridinic, and pyridine oxide, following exactly this order of relevance. In contrast, the materials synthesized in this project have shown a more significant contribution of pyridinic nitrogens over pyrrolic. Such observation can be explained by the prolonged time employed in the synthesis. From solid-state UV-Vis spectroscopy, the bandgap was found to be the same as from the previously reported material.

Since amidine had its counter-ion exchanged as purification strategy, CTFs were synthesized employing amidines with different counter-ions in order to check their influence over the framework's structure. Condensation reactions using terephthalamidine chloride, tetraphenylborate, and bromide were carried out. Notably, the CTF synthesized with terephthalamidine bromide showed the highest specific surface area, reaching up to 505 m^2/g. The materials synthesized with both terephthalamidine chloride and tetraphenylborate showed lower specific surface area, achieving 335 and 157 m^2/g, respectively. Additionally, from solid-state NMR, no significant deviation was found in the structure of these materials.

Furthermore, the synthesis of a CTF by condensing terephthalamidine bromide and terephthalaldehyde using a microwave-assisted reaction was reported for the first time. The choice for microwave reaction relies on a faster synthesis of the material combined with the lower energy input and the easy scaling-up of microwave reaction in detriment of the synthesis under conventional heating. In this context, the reaction resulted in a CTF as porous as the previously reported ones. According to nitrogen physisorption experiments measured at 77K, the specific surface area of sample synthesized under microwave irradiation achieved 560 m^2/g. The main difference from the material synthesized under conventional heating relies on a higher contribution of macropores in the material synthesized under the microwave, even though both contain microporous structure.

To conclude, the polycondensation approach was successfully employed in the synthesis of simple CTFs. The materials were characterized by FT-IR, solid-state NMR, N_2 physisorption, solid-state UV-Vis, XPS, and XRD. According to the results, the stacking position is a critical feature, leading to highly microporous materials in case of AA or to denser and non-porous structures due to pore-blocking when AB is predominant. Moreover, the counter-ion of the amidine precursor can influence the pore structure of these materials. The results showed good agreement with the previously reported studies.

Chapter 5 - Synthesis, characterization and application of bipyridine-based CTFs:

After establishing a protocol for the synthesis and purification of precursors, functionalized amidine chlorides were employed in the synthesis of CTFs. Targeting the photocatalytic conversion of carbon dioxide, the design of a series of bipyridine-based CTFs containing different amounts of ligands was done. The materials were employed as macroligands for heterogenization of molecular rhodium Cp* complex, known to drive the conversion of CO_2 selectively to formate under visible light irradiation.

Since the condensation approach is based on a reaction between two mols of amidine chloride and one mol of aldehyde, the materials were conveniently synthesized containing amounts of 0, 33, 66, and 100% bipyridine ligands. As a non-functionalized CTF, the material corresponding to 0% was synthesized only with biphenyl precursors. The synthesis followed the same protocol established before. The characterization proceeded by using FT-IR, solid-state NMR, solid-state UV-Vis, XPS, XRD, and elemental analysis. Additionally, nitrogen, water vapor and acetonitrile adsorption experiments gave insights over the porous structure of these materials. Although all the materials are amorphous, lacking long-range order, as evidenced by XRD experiments, the sharp and well-defined bands found in FT-IR, suggests at least local organization. From FT-IR experiments, not only the main stretching vibration of the triazine moiety can be seen at 1510 and 1379 cm^{-1}, but also stretching vibration of both ligands bipyridine and biphenyl. The same trend can be observed in solid-state NMR. The resulting spectra of all samples contain the signal from the carbons located in the triazine ring at higher chemical shifts, while the signals from biphenyl and bipyridine change in intensity according to their content within the framework.

Elemental analysis shows increasing nitrogen content in the series, following the increase of bipyridine ligand withing the CTFs. Moreover, according to XPS analysis, only pyridinic and pyridine oxide nitrogen species were found, suggesting the complete polymerization and further oxidation of the 1,3,5-dihydrotriazine units. The increment in the nitrogen content brings some consequences on the adsorption properties of this series. First, from N_2 physisorption experiments, the increase in nitrogen content is followed by a decrease in specific surface area. Specific surface areas of 572, 400, 368, and 235 m^2/g were found for materials containing 0, 33, 66, and 100% bipyridine ligand, respectively. Since the quadrupolar moment of the nitrogen gas result in repulsive interaction with the

nitrogen atoms containing in the surface of these materials, such a decrease in the specific surface area was expected.

Moreover, as a consequence of increasing the nitrogen content within the framework, the wettability of this series, also changes significantly. From acetonitrile and water adsorption experiments, the Henry constant and also the pore filling degree were correlated to the hydrophobic and hydrophilic properties. According to the results, the pure biphenyl-based material is the most hydrophobic from the series, showing the weakest solvent-solid interaction. In contrast, on the other extreme, the pure bipyridine-based material showed the strongest solid-solvent interaction, being the most hydrophilic material. The material containing 33% of bipyridine ligand, showed a linear behavior when the repulsive carbon-solvent interaction equilibrates the formation of hydrogen bonds between nitrogen-solvent. The material is followed by the one containing 66% in bipyridine ligand, which showed a stronger hydrophilic property. In the series, all materials have shown small flexibility, evidenced by the long time needed for equilibrating the pressures during the measurement and also from the disconnected adsorption and desorption branches in N_2, acetonitrile, and water adsorption experiments.

Solid-state UV-Vis experiments studied the optical properties of this series. According to the Tauc plot analysis, all the materials have different bandgaps, evidencing the precise control over optical properties like absorption of light by judiciously choosing the building units that compose the framework. Bandgaps of 2.93, 2.83, 2.75 and 2.53 eV were found for CTFs containing 0, 33, 66 and 100% bipyridine ligand, respectively.

Taking advantage of the fact that the condensation approach leads to photoactive materials, CTF containing 66% of bipyridine was infiltrated with the molecular catalyst rhodium Cp*. The infiltration was confirmed by the presence of signals from the Cp* ring in the solid-state-NMR. The fully heterogeneous photocatalytic system was tested in CO_2 reduction under visible light irradiation and achieved a remarkable TOF of 3.97 h-1. Such activity is among the highest already reported for fully heterogeneous photocatalysts systems.

In conclusion, taking advantage of the modular design for the synthesis of a series of bipyridine-based CTFs allowed the control over the ligand content. This achievement is a step forward to the molecular control and precision in the synthesis of these materials. Furthermore, the characterization analysis evidenced that properties like bandgap, and

consequently, the light absorption can be tuned by judiciously choosing the building blocks that integrate the polymer structure. Additionally to the control in optical properties, physical ones like wettability and hydrophobicity/hydrophilicity can be tuned. The CTF containing 66% of bipyridine ligand was employed as macroligand for the heterogenization of rhodium Cp*. The full heterogeneous system showed remarkable activity in photocatalytic CO_2 reduction under visible light irradiation.

Chapter 6 - Synthesis, characterization and application of porphyrin-based CTF:

Porphyrins are heterocyclic organic compounds composed of four pyrrole subunits interconnected via double bonds. Due to their large conjugated structure, porphyrins are typically colorful compounds strongly absorbing in the visible spectra. Additionally, the macrocycle can be metallated with different metal species to form a single atom organometallic complex.

The incorporation of this specialized macrocycle within the structure of porous organic materials have found application in many fields of research, especially photocatalysis. Since the synthesis of the amidine monomer 5,10,15,20-tetrakis(4'-amidinophenyl)porphyrin had failed, the nitrile precursor, 5,10,15,20-tetrakis(4'-cyanophenyl)porphyrin was employed in the synthesis of CTF through the acid approach. A purple porous polymer based on porphyrin and triazine units was recovered. With a specific surface area of 670 m^2/g, the material was characterized by FT-IR, XRD, N_2 physisorption and XPS.

Even though the significant color change indicated the insertion of rhodium and copper within the porphyrin-based CTF structure, these materials failed to reduce CO_2 under visible light irradiation. Seeking for another application, CTF-PORF was metallated with iron and applied in methane oxidation. Although the material did not show remarkable activity, when compared to the state-of-art, this was the first example of a catalyst 100% selective. Only formate was observed as product, at a rate of 603.2 $\mu mol/g_{cat}/h$.

Chapter 7 – Conclusion and Outlook:

In conclusion, the main advantages and drawbacks of the condensation approach for the synthesis of CTFs were investigated. In this context, the synthesis of precursor and further purification is a critical step in the preparation of porous CTFs. The same protocol was employed in the synthesis of functionalized CTFs for the first time. Using the modular design, a series of bipyridine-based CTFs for the heterogenization of molecular catalysts, targeting photocatalytic carbon dioxide reduction was developed. Remarkably, the content of bipyridine ligand within the CTF backbone was precisely controlled. Such control over the structure consequently allows the control of properties like light absorption, bandgap, and porous structure. The materials exhibited encouraging photocatalytic activity.

As an outlook, since a remarkable step has being given in direction of the molecular control and precision concerning the synthesis of CTFs through condensation, new functionalized starting materials should be tested. Materials designed for the most varied applications can be synthesized. In a near-future perspective, porphyrin-based CTFs will be developed, since materials containing this special macrocycle have shown remarkable activity in reactions in the clean energy production fields.

Résumé Substantielle

Chapitre 1 - Introduction:

Dans le scénario actuel, la majeure partie de l'énergie produite dans le monde dépend encore des ressources fossiles. Pour produire de l'énergie, les centrales électriques brûlent des carburants à base de carbone pour produire de la vapeur qui entraîne de grandes turbines pour produire de l'électricité. Cependant, l'utilisation de combustibles fossiles génèrent du dioxyde de carbone (CO_2) comme sous-produit.

En tant que gaz à effet de serre, le CO_2 absorbe la chaleur émise par la surface de notre planète, la maintenant au chaud. L'augmentation de la concentration des gaz à effet de serre atmosphériques depuis le 19e siècle a par conséquent augmenté la température globale de la Terre, entraînant un changement climatique. Avec l'augmentation des températures, de nombreux problèmes environnementaux critiques peuvent être observés, notamment les événements météorologiques extrêmes, l'acidification des océans, l'élévation du niveau de la meret le déplacement des populations d'animaux sauvages et de leurs habitats.

Par conséquent, la réduction des émissions et l'établissement de stratégies pour convertir le CO_2 atmosphérique sont des demandes urgentes pour ralentir et limiter le changement climatique. Bien que les technologies de capture et de stockage du dioxyde de carbone offrent une solution, ces processus ont certaines limites pour les applications à grande échelle. Une autre solution consisterait à capturer et à convertir le CO_2 en combustibles et en composés chimiques, en fermant le cycle du carbone. À cet égard, le CO_2 peut être converti par trois processus: l'hydrogénation thermique, la réduction électrochimique et la réduction photochimique. Néanmoins, l'utilisation de la lumière comme seule source d'énergie pour stimuler la réaction de réduction du CO_2 est une solution durable pour résoudre ce problème.

Cependant, la conversion du CO_2 reste un défi. En effet, associé aux propriétés intrinsèques des gaz, le système catalytique doit surmonter d'énormes barrières énergétiques pour favoriser la réduction du CO_2. Dans ce contexte, les polymères organiques poreux attirent une attention considérable en tant que catalyseurs de réduction du CO_2. Cette classe de matériaux est devenue populaire principalement en raison de leurs propriétés structurelles comme leur nature poreuse, qui augmente par conséquent

l'accessibilité des réactifs et des produits pendant la catalyse. De plus, l'ajustement de leurs caractéristiques structurelles par rapport aux matériaux poreux inorganiques classiques comme les zéolites, permet la conception et la synthèse de polymères contenant différentes fonctions qui sont essentielles pour abaisser la barrière énergétique dans la conversion du CO_2.

De nombreuses classes de polymères organiques poreux ont été testées comme catalyseur non seulement sur la photoréduction du CO_2 mais aussi dans le domaine de l'énergie. Parmi eux, les Covalent Triazine Frameworks (CTF) ont montré une activité remarquable dans la production d'énergie propre. Ces solides, contenant des fragments triazine, ont été découverts par Arne Thomas *et al.* et sont devenus célèbres, en particulier dans la photocatalyse, après le travail séminal d'Antonietti *et al.* dans lequel il a utilisé un nitrure de carbone graphitique, comprenant des unités triazine et heptazine, comme catalyseur unique pour conduire les deux demi-réactions lors du fractionnement de l'eau. Depuis 2008, les CTF ont été appliqués dans de nombreux domaines. Outre la production d'hydrogène propre grâce au fractionnement de l'eau et à la conversion du CO_2, ces matériaux à base de triazine ont été utilisés comme adsorbants gazeux et pour la séparation de gaz, comme support pour des nanoparticules métalliques et des complexes moléculaires organométalliques, comme cathode et anode dans des processus électrochimiques et des systèmes de stockage d'énergie, ou encoire pour la purification de l'eau entre autres.

Les CTF peuvent être synthétisés de plusieurs façons. Chaque méthode conduit à des matériaux aux caractéristiques différentes. La plus courante est l'approche ionothermique, dans laquelle les nitriles sont mélangés avec du chlorure de zinc et chargés dans une ampoule qui est scellée et chauffée pour former une poudre noire très poreuse. Dans une autre approche, les nitriles sont trimérisés par l'acide trifluorométhane sulfonique pour produire des CTF photoactifs. Cette méthode est appelée super acide en raison de l'utilisation d'acide triflique pour la trimérisation. D'autres méthodes sont disponibles mais ne sont pas fréquemment rapportées dans la littérature.

Néanmoins, toutes ces approches présentent des inconvénients. Dans le premier cas, les conditions ionothermiques sont si dures qu'elles produisent des matériaux partiellement carbonisés et pour cette raison inadaptés aux applications photo et optiques. Pour l'approche acide, le principal inconvénient est la nature limitée des composants accessibles, car cette méthode ne fonctionne pas pour les monomères à base de pyridine.

Plus récemment, les CTF ont été synthétisés en condensant du chlorure d'amidine avec un aldéhyde. Une telle approche conduit à la production de matériaux photoactifs contenant une structure en couches partielles. De plus, la conception modulaire peut être utilisée pour développer des matériaux d'une manière précise et contrôlée moléculairement. Cependant, jusqu'à présent, seuls des blocs de construction non fonctionnalisés ont été utilisés dans la synthèse de CTF par condensation.

Dans ce projet, l'objectif est de repousser les limites de la synthèse des CTF en étudiant systématiquement une nouvelle approche de condensation afin de répondre à leurs principales limites et avantages. Ce projet débute donc par le développement d'une voie de synthèse de CTF simple déjà rapportée dans la littérature et basée sur la condensation de chlorure de téréphtalamidine et de téréphtalaldéhyde. De plus, la même approche a été employée dans la synthèse des CTF fonctionnalisés.

Profitant du fait que le protocole de condensation nouvellement établi conduit à la production de matériaux photoactifs, la synthèse de CTF fonctionnalisés à base de ligands bipyridiniques a été décrite. Un tel CTF a été utilisé comme macroligand pour immobiliser un complexe moléculaire de rhodium Cp* (Cp* = pentamethylcyclopentadiène) capable de catalyser la réduction du CO_2 à formater sous irradiation de lumière visible de manière sélective. Pour la première fois, la synthèse de CTF complexes préparés par condensation est rapportée.

Chapitre 2 - Défis:

Les défis de la synthèse des CTF par condensation commencent par la synthèse des précurseurs, mal rapportés dans la littérature. De plus, la conception et la synthèse d'un photocatalyseur stable et actif sont également abordées. La caractérisation des polymères poreux étant un défi permanent, les principales questions concernant l'élucidation de la structure du catalyseur sont discutées dans ce chapitre.

Tout d'abord, la synthèse des CTF commence par la préparation de précurseurs, d'aldéhydes et de chlorure d'amidines. L'aldéhyde peut être synthétisé par un grand nombre de réactions différentes parmi lesquelles l'oxydation des alcools, l'oxydation de Swern, la réaction de Sommelet etl'oxydation de Kornblum entre autres. La voie choisie dépendra principalement de la structure du bloc de construction nécessaire. En revanche,

la synthèse du chlorure d'amidines est plus complexe. Entre autres réactions comme la réaction de Pinner et la réaction de Garigipati, l'addition de bis(triméthylsilyl)amide de lithium (LiHMDS) au précurseur de nitrile représente une manière simple pour la synthèse de ces monomères. Au début, les monomères à base de phényl ont été synthétisés et purifiés. Plus tard, le même protocole de synthèse et de purification a été utilisé pour produire des unités de construction fonctionnalisées.

De plus, concernant les défis de la conception d'un photocatalyseur, les matériaux décrits dans cette thèse ont suivi la même stratégie employée par Wisser *et al*. La stratégie «tout-en-un» est un moyen idéal de remédier au manque de stabilité des photocatalyseurs pour une réduction à long terme du CO_2. Étant donné qu'une limitation fondamentale de la réaction de réduction photocatalytique du CO_2 est l'utilisation d'un photosensibilisateur organique homogène, qui se dégrade au fil du temps, ralentissant ou arrêtant complètement la réaction en quelques heures, la stratégie décrite par Wisser et ses collègues consiste en l'incorporation d'une unité de photosensibilisation dans le squelette du catalyseur solide. Dans notre cas, la conception d'un photocatalyseur a été réalisée en utilisant la triazine comme unité de photosensibilisation hétérogène avec des monomères bipyridiniques comme unité de chélation du site catalytique. Avec la bipyridine, il est possible de supporter des catalyseurs moléculaires homogènes comme le rhodium Cp* pour la conversion sélective du dioxyde de carbone en formiate sous irradiation à la lumière visible. Par conséquent, le système entièrement hétérogène a été conçu sur la base de la stratégie «tout-en-un» présentée précédemment afin de relever et de surmonter les principaux défis de la réduction photocatalytique à long terme du CO_2.

Il est connu que la caractérisation des polymères poreux amorphes est un défi permanent. En raison du manque d'ordre à long terme, il est souvent difficile d'obtenir des informations fiables sur les propriétés structurelles de ces matériaux. Pour mieux comprendre la structure et les caractéristiques de ces CTF synthétisés par condensation, les résultats de différentes tehcniques analytiques ont été combinés. De cette façon, une meilleure compréhension et explication des phénomènes qui régissent ces nouveaux CTF peuvent être expliquées de manière adéquate, établissant une relation structure-activité pour une optimisation supplémentaire de leurs structures.

Chapitre 3 - Synthèse et caractérisation des précurseurs

Comme indiqué précédemment, la synthèse du chlorure d'amidines présentes le véritable défi dans la synthèse des CTF par condensation. Ces monomères ont été synthétisés par l'addition de bis(triméthylsilyl)amide de lithium au précurseur de nitrile dans du THF sous atmosphère inerte. La procédure expérimentale complète a été publiée par ailleurs. Même si la synthèse des chlorures d'amidine se déroule dans des conditions douces vers les produits finaux, lorsque la réaction est stoppée avec de l'acide chlorhydrique dans l'éthanol, d'autres sous-produits sont générés avec le chlorure d'amidine. De ces sous-produits, du chlorure de lithium et du chlorure d'ammonium ont été signalés précédemment. Dans le cas du chlorure d'ammonium, cette contamination persistante peut être observée dans la RMN ^{1}H liquide sous la forme d'un triplet proéminent qui apparaît dans la région de 7,28 ppm. Étant donné que les méthodes de purification traditionnelles comme la chromatographie sur colonne et la recristallisation n'avaient pas permis d'obtenir un chlorure d'amidine pur, le produit brut devait être purifié en échangeant le contre-ion du chlorure d'amidine. Inspiré par le travail de Morshedi et de ses collègues, le contre-ion de l'amidine a été échangé du chlorure au tétraphénylborate. Cette option repose sur les propriétés entièrement différentes que le contre-ion donne au composé.

Contrairement au chlorure d'amidine, le tétraphénylborate d'amidine n'est pas soluble dans l'eau. De cette manière, il est possible de laver les sous-produits des sels formés lors de la synthèse du monomère. Le contre-ion organique pouvant présenter des effets stériques importants lors de la synthèse d'un polymère CTF, le contre-ion de l'amidine a été à nouveau échangé en halogénure, cette fois en bromure. Tous ces monomères ont été utilisés pour la synthèse de CTF.

En utilisant la même procédure expérimentale, le bloc de construction à base de bipyridine a été synthétisé. Le choix des unités de bipyridine repose sur la propriété chélatante de ce bloc de construction. Pour notre application ciblée, l'hétérogénéisation d'un catalyseur moléculaire permetttrait d'obtenir une sélectivité et une activité accrues, caractéristique des photocatalyseurs homogènes. D'autre part, le système entièrement hétérogène bénéficierait de la recyclabilité et de la séparation aisée, reliant les deux mondes homogènes et hétérogènes en un seul matériau.

Étant donné que la synthèse de l'amidine à base de bipyridine commence avec le nitrile et généralement la synthèse du composé nitrile se fait par cyanation des précurseurs d'halogénures, la voie de synthèse du 2,2'-bipyridine-5,5'-dicarbonitrile a été développée afin d'utiliser des composés moins toxiques que les cyanures. Le matériau de départ était la 5,5'-diméthyl-2,2'-bipyridine disponible dans le commerce, qui a été oxydée dans l'eau par $KMnO_4$ pour obtenir l'acide dicarboxylique. En outre, l'acide carboxylique a été estérifié dans un mélange éthanol / acide sulfurique. L'ester résultant a réagi avec de l'ammoniac dans une solution saturée d'éthanol / éthylène glycol pour produire sélectivement du 2,2'-bipyridine-5,5'-dicarboxamide avec des rendements élevés. Dans la dernière étape, le carboxamide a été déshydraté en nitrile en utilisant de l'oxychlorure de phosphore sous le bain à ultrasons. Bien que cette voie comporte de nombreuses étapes et que le rendement global soit légèrement inférieur (70% contre 90% à partir de réactions de cyanation), au final uniquement avec une simple recristallisation dans l'acétonitrile, nous avons pu récupérer le nitrile pur. En revanche, pour la cyanation, des étapes de purification importantes doivent être effectuées.

Avec des amidines à base de bipyridine, des précurseurs à base de biphényle ont également été utilisés dans la synthèse de CTF. Ces ligands ont été choisis comme contre-partie non fonctionnalisée de monomères à base de bipyridine. Ainsi, les deux précurseurs, à base de bipyridine et à base de biphényle, sont utilisés dans la synthèse de CTF, dans le but d'obtenir des matériaux contenant une structure de pores symétrique. De plus, en tirant parti de l'approche modulaire, uniquement possible lorsque les CTF sont synthétisés par condensation, la synthèse de CTF contenant différentes quantités de ligands bipyridiniques a été réalisée. Ainsi, pour la première fois, le contrôle moléculaire précis du contenu d'un ligand dans un matériau CTF a été accompli, repoussant les limites de la synthèse du CTF d'une manière plus précise et contrôlée moléculairement.

Chapitre 4 - Synthèse par condensation

Afin de mieux comprendre l'approche de condensation nouvellement établie pour la synthèse des CTF, ce projet a d'abord abordé la synthèse de matériaux plus simples basés sur la réaction entre le chlorure de téréphtalamidine et le téréphtalaldéhyde. Les matériaux ont été synthétisés systématiquement pour mieux comprendre les limites et les avantages de cette méthode.

En raison de la structure en couches partielles due aux dispositions des feuillets bidimensionnels, la position à laquelle l'empilement se produit dans ces CTF est cruciale pour le matériau et peut donner différentes caractéristiques. Lorsque la position d'empilement AB est prédominante, le matériau est plus dense en raison de la disposition parfaite des couches, dans laquelle le centre de triazine de la première couche est précisément dans l'espace vide de la suivante. Ce matériau présente donct une très faible surface spécifique de 2 à 10 m^2/g en raison du blocage des pores. D'un autre côté, la position d'empilement AA est exceptionnellement avantageuse. Dans ce dernier cas, les couches sont alignées de manière à ce que le cycle triazine soit à la même position dans toutes les couches, créant un canal de lacunes alignées et augmentant par conséquent leur surface spécifique jusqu'à 500 m^2/g. Les matériaux ont également été analysés par diffraction des rayons X (DRX) sur poudre, confirmant les différentes positions d'empilement.

Avec la physisorption de l'azote et le DRX, la caractérisation de ces matériaux a été effectuée par infrarouge à transformée de fourrier (FT-IR), RMN à l'état solide, spectrométrie photoélectronique X (XPS) et spectrsocopie UV-Vis. De la spectroscopie FT-IR, les principales vibrations d'étirement de la triazine ont été confirmées à 1515 et 1356 cm^{-1}. Ces signaux peuvent être attribués aux liaisons C=N et –C-N-, respectivement. La RMN à l'état solide a également confirmé le cycle triazine dans la structure du matériau et est en accord avec les matériaux publiés dans la littérature. Cependant, l'analyse XPS a montré une petite déviation. D'après la littérature, le matériau contient trois types d'espèces d'azote: pyrrolique, pyridinique et oxyde de pyridine, suivant exactement cet ordre de pertinence. En revanche, les matériaux synthétisés dans ce projet ont montré une contribution plus importante des azotes pyridiniques par rapport aux pyrroliques. Une telle observation peut s'expliquer par le temps prolongé employé dans la synthèse. De la spectroscopie UV-Vis à l'état solide, la bande interdite s'est avérée être la même que celle rapportée précédemment.

Étant donné que l'amidine a eu son contre-ion échangé comme stratégie de purification, les CTF ont été synthétisés en utilisant des amidines avec différents contre-ions afin de vérifier leur influence sur la structure du matériau. Des réactions de condensation utilisant du chlorure de téréphtalamidine, du tétraphénylborate et du bromure ont été réalisées. Notamment, le CTF synthétisé avec du bromure de téréphtalamidine a montré la surface spécifique la plus élevée, atteignant jusqu'à 505

m^2/g. Les matériaux synthétisés à la fois avec du chlorure de téréphtalamidine et du tétraphénylborate ont montré une surface spécifique plus faible, atteignant respectivement 335 et 157 m^2/g. A partir de la RMN à l'état solide, aucune divergence significative n'a pas été trouvée dans la structure de ces matériaux.

De plus, la synthèse d'un CTF par condensation de bromure de téréphtalamidine et de téréphtalaldéhyde en utilisant une réaction assistée par micro-ondes a été rapportée pour la première fois. Un protocole alternatif par micron-onde a permis une synthèse plus rapide du matériau combinée à un apport d'énergie plus faible et une mise à l'échelle facile de la réaction comparé à la synthèse sous chauffage conventionnel. Dans ce contexte, la réaction a abouti à un CTF aussi poreux que ceux rapportés précédemment. Selon des expériences de physisorption d'azote mesurée à 77 K, la surface spécifique de l'échantillon synthétisé sous irradiation micro-ondes a atteint 560 m^2/g. La principale différence avec le matériau synthétisé sous chauffage conventionnel repose sur une contribution plus élevée des macropores dans le matériau synthétisé sous micro-ondes, même si les deux contiennent une structure microporeuse.

Pour conclure, l'approche de polycondensation a été utilisée avec succès dans la synthèse de CTF simples. Les matériaux ont été caractérisés par FT-IR, RMN à l'état solide, physisorption N_2, UV-Vis à l'état solide, XPS et DRX. Selon les résultats, la position d'empilement est une caractéristique critique, conduisant à des matériaux hautement microporeux en cas d'AA ou à des structures plus denses et non poreuses en raison du blocage des pores lorsque AB est prédominant. De plus, le contre-ion du précurseur d'amidine peut influencer la structure des pores de ces matériaux. Les résultats ont montré un bon accord avec les études précédemment rapportées.

Chapitre 5 - Synthèse, caractérisation et application des FFC à base de bipyridine:

Après avoir établi un protocole pour la synthèse et la purification des précurseurs, le chlorure d'amidines fonctionnalisé a été utilisé dans la synthèse des CTF. Ciblant la conversion photocatalytique du dioxyde de carbone, la conception d'une série de CTF à base de bipyridine contenant différentes quantités de ligands a été réalisée. Les matériaux ont été utilisés comme macroligands pour l'hétérogénéisation du complexe moléculaire de rhodium Cp*, connu pour conduire sélectivement la conversion du CO_2 en formiate sous irradiation de lumière visible.

Puisque l'approche de condensation est basée sur une réaction entre deux moles de chlorure d'amidine pour un aldéhyde, les matériaux ont été commodément synthétisés contenant des quantités de 0, 33, 66 et 100% de ligands bipyridiniques. En tant que CTF non fonctionnalisé, le matériau correspondant à 0% a été synthétisé uniquement avec des précurseurs de biphényle. La synthèse a suivi le même protocole établi auparavant. La caractérisation a été réalisée en utilisant les techniques de FT-IR, RMN à l'état solide, UV-Vis à l'état solide, XPS, DRX et l'analyse élémentaire. De plus, des expériences de physisorption d'azote, de vapeur d'eau et d'acétonitrile ont donné un aperçu de la structure poreuse de ces matériaux. Bien que tous les matériaux soient amorphes, manquant d'ordre à longue distance, comme en témoignent les expériences DRX, les bandes nettes et bien définies trouvées dans FT-IR, suggèrent au moins une organisation locale. D'après les expériences FT-IR, non seulement la principale vibration d'étirement de la fraction triazine peut être observée à 1510 et 1379 cm^{-1}, mais également les bandes des deux ligands bipyridine et biphényle. La même tendance peut être observée en RMN à l'état solide. Les spectres résultants de tous les échantillons contiennent le signal du carbone situé dans le cycle triazine à des déplacements chimiques plus élevés, tandis que les signaux du biphényle et de la bipyridine changent d'intensité en fonction de leur contenu dans le cadre.

L'analyse élémentaire montre une augmentation de la teneur en azote dans la série, suite à l'augmentation du ligand bipyridine avec les CTF. De plus, selon l'analyse XPS, seules des espèces d'azote pyridinique et d'oxyde de pyridine ont été trouvées, suggérant la polymérisation complète et l'oxydation supplémentaire des unités 1,3,5-dihydrotriazine. L'augmentation de la teneur en azote entraîne certaines conséquences sur les propriétés d'adsorption de cette série. Tout d'abord, à partir des expériences de physisorption du N_2, l'augmentation de la teneur en azote est suivie d'une diminution de la surface spécifique. Des surfaces spécifiques de 572, 400, 368 et 235 m^2/g ont été trouvées pour des matériaux contenant respectivement 0, 33, 66 et 100% de ligand bipyridine. Étant donné que le moment quadrupolaire de l'azote gazeux entraîne une interaction répulsive avec les atomes d'azote contenus dans la surface de ces matériaux, une telle diminution de la surface spécifique était attendue.

De plus, les conséquences de l'augmentation de la teneur en azote dans le cadre, la mouillabilité de cette série, changent également de manière significative. À partir d'expériences d'adsorption d'acétonitrile et d'eau, la constante de Henry ainsi que le degré

de remplissage des pores ont été corrélés aux propriétés hydrophobes et hydrophiles. Selon les résultats, le matériau à base de biphényle pur est le plus hydrophobe de la série, montrant l'interaction solvant-solide la plus faible. En revanche, à l'autre extrême, le matériau à base de bipyridine pure a montré l'interaction solide-solvant la plus forte, soit le matériau le plus hydrophile.. Dans la série, tous les matériaux ont montré une faible flexibilité, comme en témoigne le longtemps nécessaire pour équilibrer les pressions pendant la mesure et également des branches d'adsorption et de désorption déconnectées dans le N_2, l'acétonitrile et les expériences d'adsorption d'eau.

Des expériences UV-Vis à l'état solide ont étudié les propriétés optiques de cette série. Selon l'analyse du tracé de Tauc, tous les matériaux ont des bandes interdites différentes, ce qui prouve le contrôle précis des propriétés optiques comme l'absorption de la lumière en choisissant judicieusement les unités de construction qui composent le réseau. Des bandes interdites de 2.93, 2.83, 2.75 et 2.53 eV ont été trouvées pour les CTF contenant respectivement 0, 33, 66 et 100% de ligand bipyridine.

Profitant du fait que l'approche de condensation conduit à des matériaux photoactifs, du CTF contenant 66% de bipyridine a été infiltré avec le catalyseur moléculaire rhodium Cp*. L'infiltration a été confirmée par la présence de signaux du cycle Cp* dans la RMN à l'état solide. Le système photocatalytique entièrement hétérogène a été testé en réduction de CO_2 sous irradiation à la lumière visible et a obtenu un TOF remarquable de 3.97 h^{-1}. Une telle activité est parmi les photocatalyseurs les plus élevés déjà enregistrés dans cette réaction pour des systèmes entièrement hétérogènes.

En conclusion, tirer parti de la conception modulaire pour la synthèse d'une série de CTF à base de bipyridine a permis le contrôle de la teneur en ligand. Cette réalisation est un pas en avant vers le contrôle moléculaire et la précision dans la synthèse de ces matériaux. En outre, leur caractérisation précise a mis en évidence que des propriétés telles que la bande interdite et, par conséquent, l'absorption de la lumière peuvent être ajustées en choisissant judicieusement les blocs de construction qui intègrent la structure polymère. En plus du contrôle des propriétés optiques, des propriétés physiques comme la mouillabilité et l'hydrophobie/l'hydrophilie peuvent être ajustées. Le CTF contenant 66% de ligand bipyridine a été utilisé comme macroligand pour l'hétérogénéisation du rhodium Cp*. Le système hétérogène complet a montré une activité remarquable dans la réduction photocatalytique du CO_2 sous irradiation de lumière visible.

Chapitre 6 - Synthèse, caractérisation et application du CTF à base de porphyrine:

Les porphyrines sont des composés organiques hétérocycliques composés de quatre sous-unités pyrroles interconnectées via des doubles liaisons. En raison de sa grande structure conjuguée, les porphyrines sont généralement des composés colorés qui absorbent fortement dans les spectres visibles. De plus, le macrocycle peut être métallé avec différentes espèces métalliques pour former un complexe organométallique.

L'incorporation de ce macrocycle dans la structure des matériaux organiques poreux a trouvé une application dans de nombreux domaines de recherche, notamment la photocatalyse. Comme la synthèse du monomère amidine 5,10,15,20-tétrakis(4'-amidinophenyl)porphyrine avait échoué, le précurseur nitrile, 5,10,15,20-tétrakis(4'-cyanophenyl)porphyrine a été utilisé dans synthèse du CTF par l'approche acide. Un polymère violet poreux à base de porphyrine et de triazine a été récupéré. Possédant une surface spécifique de 670 m^2/g, le matériau a été caractérisé par FT-IR, DRX, physisorption N_2 et XPS.

Même si le changement de couleur significatif indiquait l'insertion de rhodium et de cuivre dans la structure CTF à base de porphyrine (CTF-PORF), ces matériaux n'ont pas réussi à réduire le CO_2 sous irradiation à la lumière visible. Cherchant une autre application, le CTF-PORF a été métallé par descations fer(II) et appliqué en oxydation de méthane. Bien que le matériau n'ait pas montré d'activité remarquable, par rapport à l'état de l'art, il s'agissait du premier exemple de matériau 100% sélectif testé comme catalyseur. Seul du formiate a été produit, à raison de 603.2 µmol/gcat/h.

Chapitre 7 - Conclusion et perspectives:

En conclusion, les principaux avantages et inconvénients de l'approche de condensation pour la synthèse des CTF ont été étudiés. Dans ce contexte, la synthèse du précurseur et une purification supplémentaire sont une étape critique dans la préparation de polymères CTF poreux. Le même protocole a été utilisé pour la première fois dans la synthèse de CTF fonctionnalisés. En utilisant la conception modulaire, une série de CTF à base de bipyridine pour l'hétérogénéisation des catalyseurs moléculaires, ciblant la réduction photocatalytique du dioxyde de carbone a été développée. Remarquablement,

le contenu du ligand bipyridine dans le squelette du CTF a été contrôlé avec précision. Un tel contrôle sur la structure permet par conséquent le contrôle de propriétés telles que l'absorption de la lumière, la bande interdite et la structure poreuse. Les matériaux présentent une activité photocatalytique encourageante.

À titre de perspective, étant donné qu'une étape remarquable a été donnée dans le sens du contrôle moléculaire et de la précision concernant la synthèse des CTF par condensation, de nouveaux matériaux de départ fonctionnalisés devraient être testés. Les matériaux conçus pour les applications les plus variées peuvent être synthétisés. Dans un avenir proche, des CTF à base de porphyrine seront développés, car les matériaux contenant ce type de macrocycle ont montré une activité remarquable dans le domaines de la production d'énergie propre.

Table of Contents

CHAPTER 1

CHAPTER 2

CHAPTER 3

CHAPTER 4

CHAPTER 5

CHAPTER 6

CHAPTER 7

REFERENCES

CHAPTER 1: INTRODUCTION

1. INTRODUCTION

Nowadays, the world is still dependent on fossil resources to produce energy. Moreover, the increase of almost 130% in energy production in the last 41 years shows that energy demand is rising due to the growing population and ascending standards of living [1]. Typically, power plants burn carbon fuels, including natural gas, petroleum and coal to generate steam, which drives large turbines to produce electricity. However, the combustion of fossil fuels generates as a by-product a major greenhouse gas, carbon dioxide (CO_2) [2].

Greenhouse gases, such as CO_2, absorb most of the Earth's emitted longwave infrared radiation. This absorbed energy makes the molecules to vibrate. Successively, the molecules release this energy by emitting longwave radiation, some of which radiates back to Earth's surface, keeping our planet warm. Increasing the concentration of greenhouse gases in the atmosphere will consequently rise the overall Earth's temperature, resulting in climate change. The enormous amount of CO_2 emission since the 19^{th} century has resulted in critical environmental issues, like ocean acidification, extreme weather events, rising in the sea level, global warming and shifting in wildlife populations and their habitats.

In 2018, the concentration of atmospheric carbon dioxide has reached the maximum ever recorded, 407.4 ppm. If little or no action to mitigate the climate change is taken, according to the Intergovernmental Panel on Climate Change (IPCC), CO_2 levels could reach 950 ppm by 2100 [3]. Such an imminent threat to civilization has triggered climate emergency in many countries. Therefore, setting priorities and strategies to decrease the emissions and mitigating atmospheric CO_2 concentration are vital responsibilities and demands urgent attention.

Carbon capture and storage (CCS) technologies are an option. However, drawbacks like high energy consumption, equipment corrosion and high temperatures to regenerate CO_2 absorbents offer practical limitations to address the problem. Another strategy involves the capture and further conversion of CO_2 into valuable chemicals and fuel. CO_2 can be converted using processes like thermal hydrogenation, electrochemical or photochemical reduction. Using CO_2 as a building block can generate products including carbon monoxide (CO), methanol (CH_3OH), formic acid (HCOOH) and methane (CH_4) [4]. In an ideal future, the shift towards a more sustainable society would

include the utilization of CO_2, not only for the production of energy but also for providing vital chemical compounds for industrial processes, serving as the anthropogenic carbon cycle.

Nevertheless, the utilization of carbon dioxide have to overcome a series of practical problems. The first one is handling. Gases have intrinsic properties such as low density, high diffusivity and readily creation of mixtures, which make storage and transportation difficult. Besides the practical problems of producing fuels or chemicals from CO_2, there is also a thermodynamic issue [5]. Due to its inertness, significant energy barriers have to be overcome to activate CO_2 molecules in order to make them reactive.

To address these difficulties of handling and converting gases, it is mandatory, for science and technology, to find a way to manipulate gases under milder conditions. Materials containing nano-confined spaces may be suitable for this purpose. Such materials are called porous. They possess voids through their structure that is often filled with fluids in the liquid phase (e.g. solvents) or gases. Although conventional porous materials like zeolite and activated carbon have been crucial in the past, we need to develop suitable materials with tunable chemical composition and physical environments to overcome the challenges related to converting CO_2.

1.1. POROUS MATERIALS

Porous materials can be found almost everywhere. It can be natural, like wood, rocks, soil, bones, but it can also be artificial or created by human beings, like cement, ceramics, zeolites. Over the years, mankind has been using these materials for the most different applications. Energy management, vibration suppression, heat insulation, sound absorption, and fluid filtration are between the vast possible applications for porous materials [6].

In science, porous materials have attracted interest in many fields. Indeed, the presence of structural voids opens tremendous possibilities. Either by using its specific surface area to interact with atoms or molecules, or using its bulk structure as a porous media.

Porous materials can be classified in many ways. One of them is by their pore size. According to IUPAC, porous materials can be distributed in macro, meso and

microporous [7]. Macroporous when the porous widths more than 50 nm, mesoporous when porous widths between 2 and 50 nm, and microporous when the pore aperture widths less than 2 nm. Eventually, the size, shape and volume of pores, are strictly connected with the ability of the porous material to perform certain functions in the desired application. One example is the filtration or separation of compounds by their size, such application would require a material with a homogeneous distribution of pore sizes and shapes.

Another way of grouping porous materials is by their nature or content. Inorganic porous materials have a wide composition, varying from silicon and aluminum-based materials to metal foams. Perhaps, the most representative material from the inorganic class of porous materials is zeolites [8-9]. Zeolites are three-dimensional microporous aluminosilicates materials that can accommodate a wide variety of cations in their structure. They are composed basically by $(AlO_4)^{5-}$ and $(SiO_4)^{4-}$, in which all silicon and aluminum atoms are coordinated in a tetrahedral geometry within shared oxygen atoms. There are nearly 245 different trypes of zeolite structures nowadays. They can be found in nature, mainly formed by volcanic activity, or synthesized in laboratory. Zeolites have been employed in many different applications. From industrial to domestic uses, zeolites had become vital in many petrochemistry processes, especially regarding cracking, isomerization and synthesis of hydrocarbons.

Hybrid inorganic-organic porous materials are also possible. Composed of organic multi-dentate molecules and metallic clusters organized in a three-dimensional net-like structure, Metal-Organic Frameworks (MOFs) are the best representation of the hybrid porous materials group [10]. Their structure is based on metal-oxygen bonds, and consequently, it has lower stability compared to the inorganic porous materials. Although the recent examples of MOFs reported in the literature present materials with crystalline structure and outstanding properties, things were not like this in the past.

This class of hybrid porous materials started its development in the early ’80s. The first example of net-like materials was developed by Kinoshita *et al*. The framework comprised of copper ions connected by adiponitrile linkers. With a diamond-like structure, these nets were elucidated using the geometry principles of crystal chemistry established by A. F. Wells in 1954. Although the porous structure was also elucidated, it could not be used as a functional purpose since the structure collapsed upon the removal of solvents trapped in its voids. Figure 1 shows the structure of

$[Cu(C_4H_4N_2)_{3/2}(CH_3CN)](PF_6).0{,}5C_3H_6O$ compound developed by Kinoshita in 1959. [11]

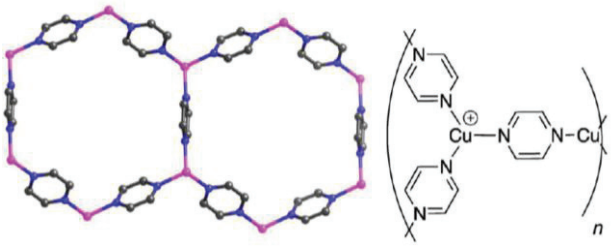

Figure 1 - Structure of the first coordination polymer synthesized by Kinoshita et al. Adapted with permission from: Kinoshita, Y.; Matsubara, I.; Higuchi, T.; Saito, Y. The Crystal Structure of Bis(adiponitrilo)copper(I) Nitrate. *Bull. Chem. Soc. Jpn*., vol. 32, no. 11, pp. 1221-1226, 1959.

In order to achieve more stable materials, Yaghi proposed a solution in 1999: exchanging the adiponitrile ligand by multi-dentate rigid linkers like benzene-based carboxylic acids. Also exchanging the metal ion for a cluster composed by more than one metallic atoms, resulting in a more rigid structure, also preventing the metal center from changing its oxidation state and consequently its geometry. This way, Yaghi and co-workers managed to remove all the solvent out of the porous material, surprisingly achieving for the first time, a material with superficial area of 2000 m^2/g in a highly crystalline framework named MOF-5 [12]. Figure 2 depicts the structure of MOF-5, comprising of Zn_4O clusters connected by 1,4-benzodicarboxylate molecules. The yellow sphere highlights the pore in the structure.

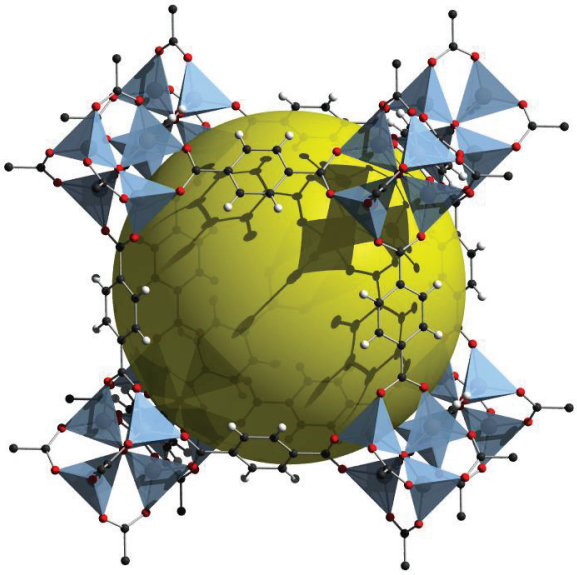

Figure 2 - Structure of MOF-5. Adapted with permission from: Rosi, N. L.; Eckert, J.; Eddaoudi, M.; Vodak, D. T.; Kim, J.; O'Keeffe, M.; Yaghi, O. M. Hydrogen Storage in Microporous Metal-Organic Frameworks. *Science* 2003, v. 300, issue 5622, pp. 1127-1129.

Currently, the class of metal-organic framework has been extensively studied by the scientific community. New geometries, composition, functionalities, were investigated, resulting in an outstanding number of different materials in the past years. Additionally, other aspects were also improved: design, prediction of functionalities, computational studies and structural control were slowly rationalized, revolutionizing the field of material chemistry.

The last class of porous materials divided by its nature, is composed purely by organic matter. They are called porous organic materials. Most porous organic materials are based on carbon, oxygen, nitrogen and hydrogen, but elements like boron, sulfur, phosphorus and others, can integrate their composition. They can be divided into two main groups: porous organic molecular cages and porous organic polymers.

The first subclass is based on a discrete molecular structure, connected by weak interactions. There are many different types of porous molecules, Porous organic cages (POCs) [13], hydrogen-bonded organic frameworks (HOFs) [14], and supramolecular organic frameworks (SOFs) [15] are some examples. In such structures, porosity can either be intrinsic or extrinsic. Intrinsic is when the molecular connections result in a structure that contains an internal void. On the other hand, extrinsic porosity is related to the voids formed between molecules, due to the inefficient packing. Significant diversity of shapes, geometry and functions can be found in porous organic molecular cages. They can be crystalline or amorphous, in solid or liquid state, soluble or not and represent a recent but significant class of material under development.

The second subclass of porous organic materials is called porous organic networks. In contrast with the porous molecular cages, they are based on a framework extended in three dimensions, having more a polymer character than a discrete structure. These networks are based on covalent bonds and as a consequence, more chemical and thermal stable than the hybrids MOFs.

Porous organic networks can be divided according to their specific structural features. A broad variety of polymerization and cross-linking reactions can be employed to connect the building units into frameworks. Therefore, depending on the polymerization reaction, specific linkages are formed, leading to singular properties. The main classes of porous organic polymers are Polymers of Intrinsic Microporosity (PIMs) [16], Hypercrosslinked Polymers (HCPs) [17], Covalent Organic Frameworks (COFs)

[18], Conjugated Microporous Polymers (CMPs) [19], Porous Aromatic Frameworks (PAFs) [20] and Covalent Triazine Frameworks (CTFs) [21].

Figure 3 shows the classification of porous materials divided by their nature, highlighting the different classes of porous organic polymers.

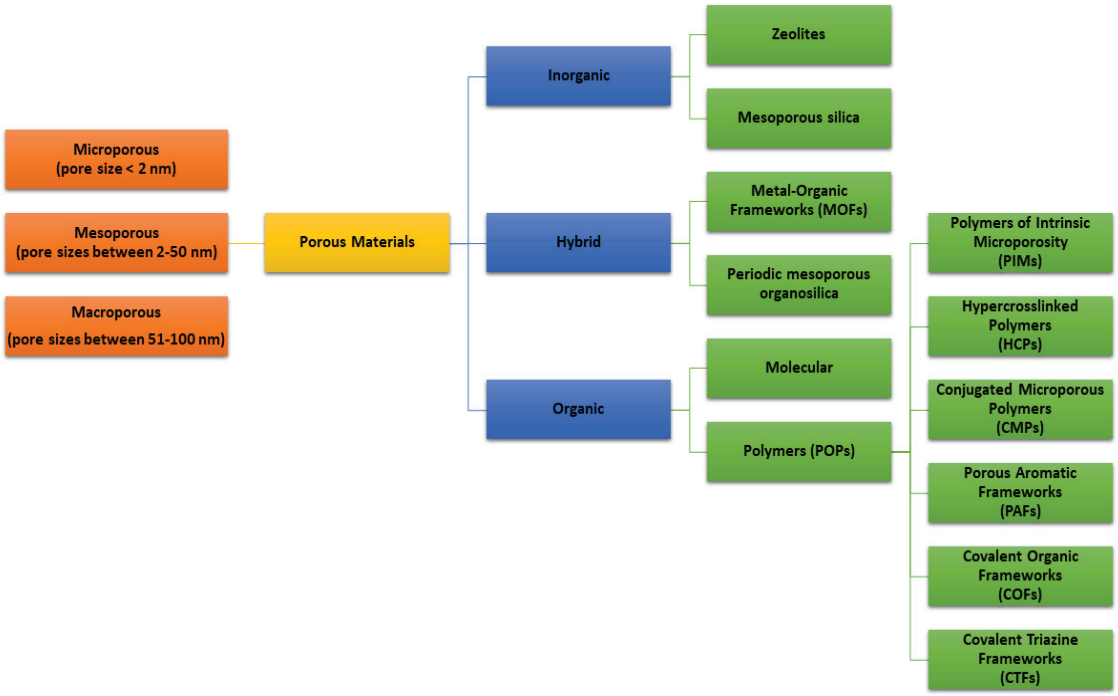

Figure 3 – Classification of porous materials.

Among many possible motives and classes of porous organic materials, this project focus on the development of novel CTFs. These porous organic polymers are interesting mainly due to the triazine properties. Triazine is a nitrogen-containing heterocyclic compound of general formula $H_3C_3N_3$. This compound exists in three different isomeric forms: 1,2,3-triazine; 1,2,4-triazine and 1,3,5-triazine (commonly named s-triazine). Figure 4 illustrates the structure of these three isomeric forms.

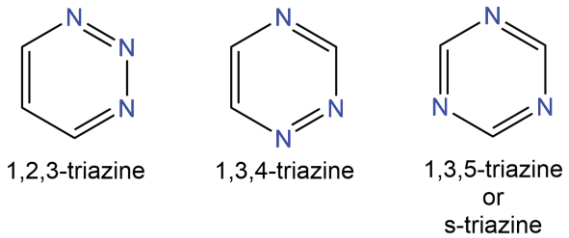

Figure 4 – Structure of triazine isomers.

While discrete triazine-based complexes have found interesting applications in the biological field, their polymeric frameworks have been extensively explored for clean energy production and catalysis.

The interest in triazine-based materials, especially in photocatalysis has dramatically increased after 2008. In this year, Antonietti *et al.* reported the production of hydrogen from water under visible-light irradiation, using the metal-free graphitic carbon nitride (g-C_3N_4) as photocatalyst [22]. The production of hydrogen from water and sunlight is an ideal source of clean energy, it is independent of fossil fuels and has zero-emission of greenhouse gases.

Carbon nitride is based on two different structures, triazine and a tri-s-triazine (heptazine). Both structures coexist and are commonly connected through planar amino groups. The tri-s-triazine unit is thermodynamically more stable than s-triazine, therefore it's difficult to synthesize carbon nitrides based only on s-triazine.

By virtue of its similar structure, the incorporation of triazine units into the backbone of polymeric organophotocatalysts has been considered a strategy to enhance the hydrogen production from water. Moreover, due to the presence of nitrogen atoms with a free electronic pair and the acceptor character of the triazine ring, the heteroatom acts as an active site for interfacial redox reactions and can play a role in many interesting reactions, including water splitting and carbon dioxide reduction. For these reasons, the main target of this project is the investigation and development of novel CTFs designed for photocatalytic carbon dioxide reduction.

From enhancing hydrogen production through water splitting under visible-light irradiation to a better performance in carbon dioxide adsorption and conversion, the heteroatom effect can explain many of the exiting features presented in CTFs. In this way, the next section will describe the structural features of these triazine-based polymers, the different synthetic approaches and later, the design aspects of this class of porous organic polymers.

1.2 COVALENT TRIAZINE FRAMEWORKS

The development of porous organic polymers (POPs) based on triazine units started in 2008 when Arne Thomas *et al.* reported the synthesis of a series of triazine-

based materials and introduced the concept of Covalent Triazine Framework (CTF) [23]. CTFs have notably many exciting features. It is a material based on permanent and strong covalent interactions, leading to high physical and chemical stability. It's high specific surface area and open structure results in good accessibility and dispersion. Additionaly, similar to MOFs and other classes of POPs, CTFs can be designed. The rational design can be achieved by judiciously choosing the right precursors (or building blocks), or by employing a particular synthetic method [24].

Within all these characteristics listed above, CTFs can found applications in many different fields like gas adsorption and separation, electronics, and catalysis. Specifically in heterogeneous catalysis, CTFs have being employed in many key reactions in the energy field [25]. Notably, CTFs can be used in photo, electro and thermo-catalysis. Of course that for each application, the material has to fulfill some requirements. For exemple, CTF has to be photoactive, adsorbing light under visible region (or UV for some applications) to be used as photocatalyst. In the same way, high conductivity is a requirement to employ CTF as electrocatalyst and thermostability for thermocatalysis.

Investigating novel synthetic methods, to enhance control on the molecular architecture is a key step to boost properties for desired applications. In this sense, different synthetic approaches have been used to produce triazine-based materials. The methods will be described in the next pages, followed by some insights on the rational design of CTFs.

1.2.1 SYNTHESIS APPROACH

Over the years, Covalent Triazine Frameworks have evolved from a simple porous polymer to a class of multifunctional reticular materials, experimenting big chemical diversity not only regarding the building blocks but also the synthetic procedure. There are many different ways to synthesize triazine-based porous organic polymers. Therefore, deciding the synthetic approach is definitely a crucial step. The features presented in the final material will depend exclusively on how the building blocks were connected to form an extended three-dimensional solid. In this regard, the synthesis approach plays a role in the features of the final material, and consequently on the addressed application [25]. The next section explains all the procedures employed in the synthesis of CTFs.

1.2.1.1 IONOTHERMAL

The ionothermal method was first reported by Thomas, Antonietti and Kuhn in 2008 [23]. The approach is based on the trimerization of nitriles under molten zinc chloride to give a Covalent Triazine Framework. It is by far the most used method in the synthesis of CTFs. In this approach, nitriles are ground together with $ZnCl_2$ in a specific ratio and charged in a glass ampoule. The ampoule is sealed and heated up in oven over a period of time to result in a monolith which is then ground, washed with dilute HCl to remove the remaining salt, and organic solvents, such as acetone or THF, to remove the unreacted precursors.

The method can be used within a broad variety of different precursors like thiophene, bipyridine and other functionalized building blocks like porphyrin. Usually, when the ionothermal method is employed, the final material presents a very high superficial area, due to the presence of molten $ZnCl_2$, which acts as both catalyst for the trimerization, and porogenic template at the same time. The resulting CTFs can be either crystalline or amorphous. In the first report, Thomas and co-workers stated that especially when the precursor is planar and with the nitrile function in opposite direction, the method results in crystalline materials, however, this is not always true, and other factors might influence the short and long-range organization in these frameworks. One advantage of the ionothermal method is that both compounds used in the synthesis, $ZnCl_2$ and nitriles, are cheap precursors. Furthermore, there are no limitations in terms of geometry, size or nature of the building blocks.

The main drawback when using this approach is the unavoidable carbonization. Due to the harsh conditions of the synthesis, irreversible reaction pathways takes place, including C-H bond cleavage and thermal decomposition of cyano-alkyl groups via C-C coupling of neighboring aromatic nitriles, accompanied by nitrogen loss. As a consequence, the bandgap of a material synthesized by the ionothermal route is too narrow, wherefore they are not suitable for photophysical applications. These CTFs are often used as support of more active species like metal complexes or nanoparticles. Additionally to the carbonization, it is very difficult to completely remove all the $ZnCl_2$ from the final material, becoming a serious contamination problem depending on the application. Figure 5 shows the nitrile trimerization in molten zinc chloride, first forming small oligomers and later the final framework.

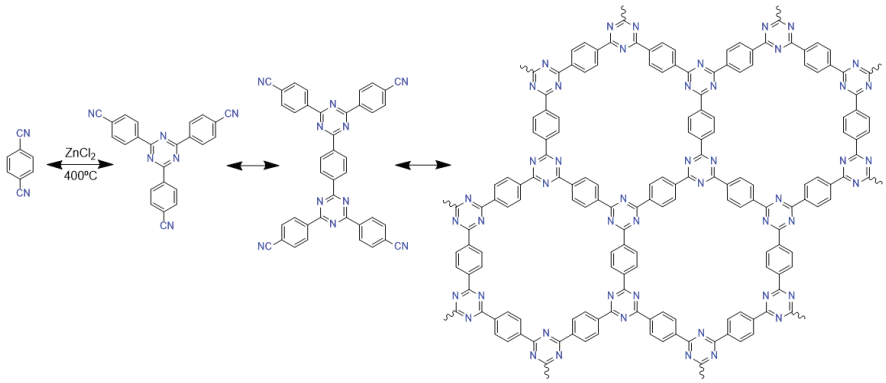

Figure 5 – Synthesis of CTF-1 through nitrile trimerization in molten zinc chloride.

1.2.1.2 ACID

The second most used method is often called "superacid" or "strong acid" approach. The name comes from the utilization of trifluoromethanesulfonic acid as a catalyst for the cyclotrimerization of nitriles, leading to CTF structures. The first report regarding this method was published in 2012 by Cooper *et al* [26]. It consists basically of mixing the precursor (nitrile) and the acid at room temperature. After neutralization of the acid with ammonia solution, the solid is recovered by filtration, ground and washed thoughtfully with water and organic solvents to afford a CTF. Since the synthesis is done at room temperature, there is no problem such as carbonization.

The approach admits some variations. Synthesis under microwave irradiation is one of them. It leads to a lower time consumption for the synthesis and also, in contrast to the materials synthesized at room temperature, to a crystalline CTFs. Another variation is the utilization of solvents like chloroform to solubilize the precursor before trimerization. Additionally, the method can be used to synthesize CTFs in different morphologies, like hollow nanoporous, bi-dimensional sheets and membranes [27].

The advantage of using this procedure lies in the lower number of defects in comparison with the ionothermal method since it avoids high temperatures and the consequent degradation of the framework due to carbonization.

Besides being a straightforward approach, it has some drawbacks. The first one is the difficulty to scale-up, since the trifluoromethanesulfonic acid is powerful and corrosive chemical, it is dangerous to handle in large amounts. The second drawback is the building block limitation. The superacid procedure does not work for building blocks

containing nitrogen heteroatoms in their structure. The reason might be the insolubility after protonation.

1.2.1.3 FRIEDEL-CRAFTS

Triazine-based frameworks can be synthesized by Friedel-Crafts reaction [28]. Figure 6 illustrates the reaction between cyanuric chloride (node) and 1,3,5-triphenylbenzene (linker). The formation of a strong electrophile from the triazine and $AlCl_3$, results in electrophilic aromatic substitution on triphenyl benzene to give the triazine-based polymer. This approach has some advantages like easy handling, mild synthesis conditions, cheaper starting materials and a high yield of the final material. Although all materials synthesized by this route result in amorphous solids due to the irreversibility of bonds formation and fast kinetics of Friedel-Crafts reaction.

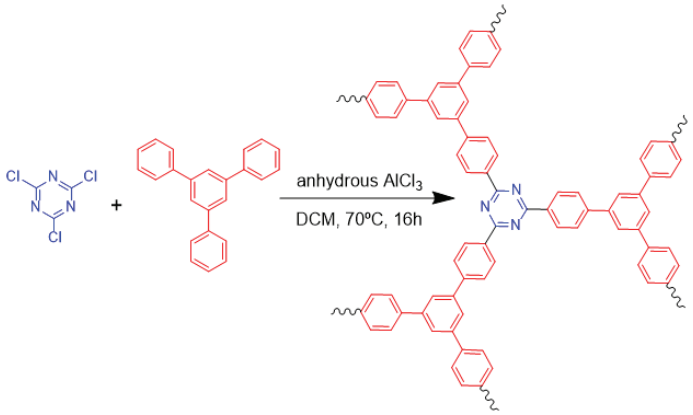

Figure 6 – Resulting structure of Triazine-based polymer MCTP-1 synthesized through Friedel-Crafts reaction.

Materials synthesized by Friedel-Crafts reaction are often described as triazine-based frameworks, not Covalent Triazine Frameworks. Many aspects differ CTFs from the triazine-based polymers. The first is the type of reaction. Friedel-Crafts reaction produces polymers more likely hypercrosslinked polymers. They are synthesized in a fast and completely random process through the formation of C-C bonds. On the other hand, CTFs are most likely bi-dimensional materials, stacked to form a layered structure, only CTFs based on tetrahedral building blocks are three-dimensional. Moreover, in contrast to triazine-based polymers, the in situ triazine formation in CTFs through the trimerization reaction happens over C-N bond formation.

Another aspect regarding the order of these materials, triazine-based polymers will always be amorphous while CTFs, depending on the approach, can be crystalline. The superficial area of some triazine-based polymers surpasses the CTFs with the highest surface area. Additionally, it is possible to observe the consequences of a random synthesis process on the pore size distribution, while triazine-based materials present a broad distribution, CTFs usually have very narrow distributions of pore sizes. In other terms, triazine-based polymers are more likely hypercrosslinked polymers that possess a triazine building unit in its composition, not a covalent triazine framework synthesized by Friedel-Crafts reaction.

1.2.1.4 AROMATIC AMIDES IN P_2O_5

Another method to synthesize CTFs was discovered recently by Jong-Beom Baek *et al* [29]. It consists of using aromatic primary amines as monomer and phosphorus pentoxide as a catalyst for trimerization. It is known that P_2O_5 can dehydrate amines to nitriles and it can also promote the trimerization of nitriles in s-triazine. The material synthesized by this method presents the highest surface area when compared to the preview's methods, in addition to the high crystallinity. Besides these characteristics, there is a lack of information about optical and structural properties for the CTFs synthesized by this approach, for this reason, the application for this material has been focussed only on gas adsorption.

1.2.1.5 CONDENSATION

One of the most recent methods to synthesize CTFs was published in 2018 by Cooper *et al* [30]. As its name says, the polycondensation is based on the condensation between an aldehyde and amidine chlorides. The reaction leads to 1,3,5-dihydrotriazine, which is further oxidized by the solvent (dimethyl sulfoxide) to the triazine center [31]. Figure 7 shows the mechanism in detail.

The materials synthesized by polycondensation possess characteristics that cannot be achieved by a different approach, such as partial layered structure, yellow to orange color, visible light absorption, optical band gap, and so far, no limitation regarding the nature and geometry of the building blocks. Because of the active optical bandgap, the

main application is in photocatalysis. Cooper *et al.* showed the activity for these materials in photocatalytic water splitting, specifically in hydrogen evolution reaction. For a metal-free material, the activity was higher than carbon nitride, the first purely organic material proven to split water under visible light irradiation. Such a remarkable achievement highlights the importance of CTF development for clean energy production.

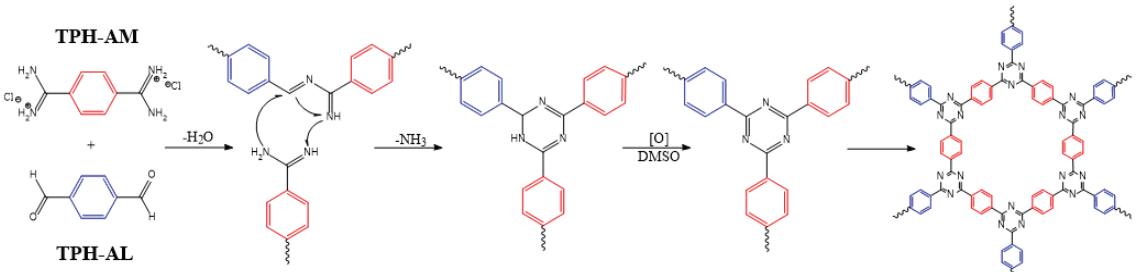

Figure 7 – Condensation mechanism for the synthesis of CTF.

A recent improvement in the condensation approach has been made by Liu *et al* [32]. In order to achieve more crystalline CTFs, the group changed the starting material from aldehyde to alcohol. Since alcohol can be oxidized to aldehyde by DMSO under air, the in-situ oxidation, slows down the nucleation rate, leading to fewer nuclei, and bigger crystallite, therefore improving crystallinity. Figure 8 shows the in-situ oxidation of alcohol to aldehyde for the synthesis of crystalline CTFs.

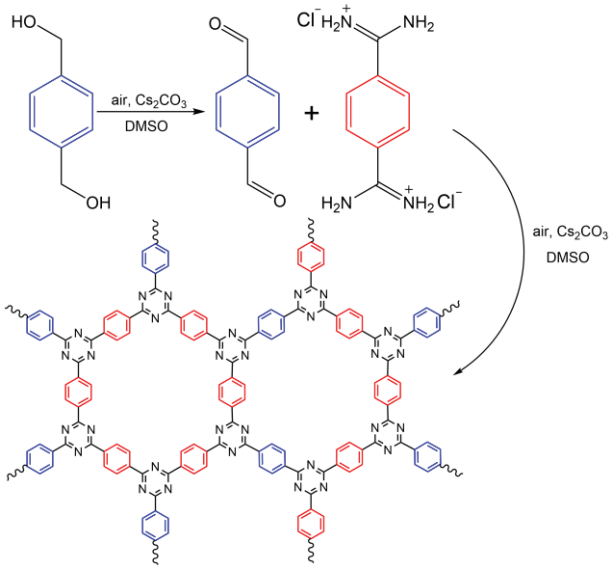

Figure 8 – Synthesis of crystalline CTFs through condensation of alcohols and amidine chloride.

1.2.2 MODULAR DESIGN

The rational design of a polymeric material is a fascinating strategy to control features and functionalities [33]. The bottom-up approach employed in the construction

of porous materials opens an avenue for the discovery and development of many unexplored new materials and devices. Additionally, the precise design can be used for enhancing the activity in a particular application. Although the strategy employed in the design of porous organic polymer might vary from class to class, it can be divided into two main groups: the design of crystalline and amorphous frameworks [21].

Crystalline porous polymers can be designed by using the breakthrough concept of "reticular chemistry" [34-35]. By definition, the word reticular comes from reticulate which means "in the form of a network". Crystalline materials resemble a net or framework in which atoms occupy specific positions in a spatial arrangement. So, reticular synthesis is the assembly of pre-designed rigid building blocks by chemical bonds into an extended three-dimensional network-like structure.

If in a microscopic view, the building blocks that constitute the framework have a specific way to connect, resulting in a specific geometry, on the macroscopic view, these molecules covalently bonded and extended through the three dimensions, gives the topology. The first materials designed and synthesized using the principles of reticular chemistry were MOFs. The inorganic metal clusters and organic linkers were schematically represented by polygons that assembled to form vertices and edges in a three-dimensional structure. Later, the same principles were extended to Covalent Organic Frameworks [36].

In theory, an infinite number of possible nets arrangement could be achieved by the combination of a vast diversity of organic building units. However, Yaghi and O'Keeffe, analyzing the structures achieved from MOF synthesis, stated that commonly, simple highly symmetric topologies are fundamentally essential and favorable in material synthesis. So, all the 300 different COFs already reported, are based on eight regular net-like topologies.

Although the design of 3D and 2D crystalline porous organic materials rely on the analysis of their topology, a distinction has to be made. The topology of 2D materials is strictly related to the arrangements of layers, which are not bonded covalently. Therefore, the stacking position is an essential aspect in the design of 2D materials. Figure 9 illustrates all the five 2D topologies that have been confirmed experimentally [37].

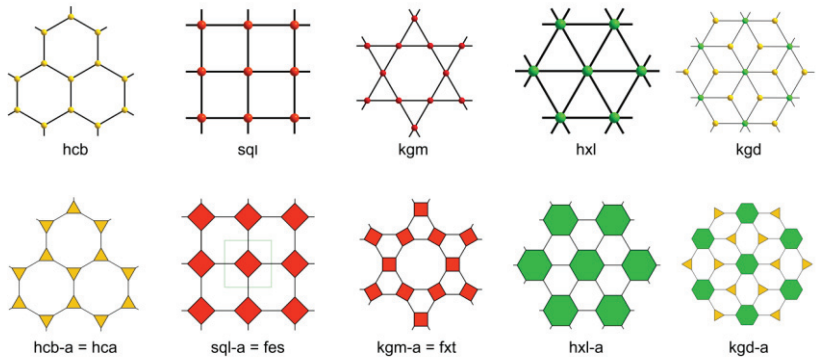

Figure 9 – Bi-dimensional topologies found experimentally in COFs. Adapted with permission from: Diercks, C. S.; Yaghi, O. M. The atom, the molecule, and the covalent organic framework. *Science* 2003, vol. 355, no. 6328.

Crystallinity is not a necessary feature in a porous organic polymer. Literature is full of examples of amorphous POP materials with outstanding properties and interesting potential applications in many different fields [38]. However, the rational design of amorphous porous organic polymers still an ongoing challenge. The main problems are consequences of the lack of long-range organization in these materials. First, the issue to predict and characterize their structures, and secondly, to rationalize their topology. In amorphous porous materials, the topology is often described through models and is mainly used to elucidate their structure not to design a material. Therefore, the designing process of amorphous porous polymers can be faced differently: by focusing on the functionality instead of topology [39].

So, driven by a specific application, a material can be designed to fulfill a series of requirements. The design, in this case, incorporate not only the functional target structure but also the kind of reaction used to link the building units into a framework. Additionally, secondary properties may be taking into account. Features like stability (thermal, mechanical and chemical), porosity (if intrinsic or extrinsic, homogeneous or hierarchical pore size distribution), processability, easy of handling, adsorption and desorption kinetics, thermal transport behavior, among others, should also be considered.

In theory, the enormous diversity of functional building blocks combined with the vast library of reactions used to connect them, make it seems like an easy task. In practice, there are significant challenges in achieving structural control in solid-state polymers and in anticipate functions from the structure.

In the case of CTFs, the rational design depends mainly on the type of synthesis employed. From all different routes for the synthesis of CTFs described in section 1.2.1,

only the condensation method is suitable for modular design. The modular design is a bottom-up strategy characterized by functional partitioning into discrete scalable modules. In essence, it is the construction of a bulk material by connecting different building blocks in a specific fashion. It is different from the reticular chemistry, because this last strategy is based on the analysis of material's topology, and up to now, the class of CTFs have not shown precise topology control.

In all the other methods employed in the synthesis of CTF, controlling the position of modules (building blocks) in a specific manner is not possible. This can be easily noted in the synthesis of materials based on multicomponent. Besides the condensation approach, the synthesis of materials based in two or more building units, using all the routes mentioned above, would lead to materials with a completely random organization.

Up to now, just a few examples of CTFs designed by a modular approach can be found in the literature. Because the triazine ring is always formed from the condensation of two molecules of amidine chloride and one aldehyde, it is possible to predict the positioning of functionalities into the material. Liu *et al* [32] took advantage of the polycondensation method for the synthesis of materials using functionalized aldehydes. Figure 10 depicts the structure of the precursors and their exact position in the CTF. backbone.

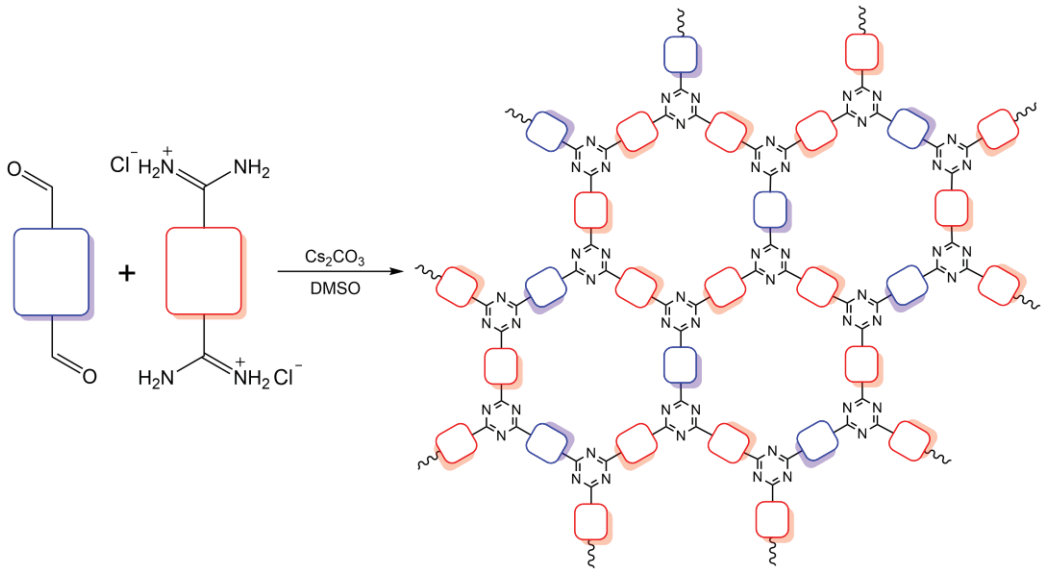

Figure 10 – Structure of precursors and the positioning of building blocks into CTF backbone.

Until the date, CTF synthesis through condensation still limited to the utilization of non-functionalized amidine chlorides. The difficult synthesis and purification of

functionalized amidine chlorides is the main limitation. In order to increase the possibilities and broaden the scope of polycondensation approach utilization, this project aims to use functionalized amidine chlorides in the synthesis of CTFs. Therefore, designing structures combining molecular control and precision over functionalities in CTFs is a key step to achieve high-performing materials in many fields. The next section will describe the main applications of CTFs in different areas.

1.3 APPLICATIONS

The development of novel materials and their application in recent years have shown that porosity plays a role in possible breakthroughs in many fields of research. Due to their intrinsic properties, like large surface area, open channels, the possibility to control the shape and functions of void's environment, combined with a vast diversity of precursors, porous organic polymers have received the status of multifunctional platform materials, going far from limits in established applications, and opening avenues for new fields.

The use of porous organic polymers can be tracked to 1930 when the first commercial application of Polymers of Intrinsic Microporosity (PIM) was conceived as ion-exchange resins [40]. After that, the discovery of new classes of materials, possessing different functionalities and features, boosted the application of porous organic polymers. Currently, the most promising applications of porous organic polymers are: gas adsorption and separation, catalysis, drug delivery, sensors, energy conversion, and others.

Naturally, the application of a certain class of porous organic polymer is strictly linked to their structural features. In the case of CTFs, the main applications are gas adsorption and separation, and heterogeneous catalysis. However, it is possible to find few studies reporting the application of CTFs in energy storage and conversion, and as pollutant removal. The different applications will be divided into subsections to better explain each one.

1.3.1 GAS ADSORPTION AND SEPARATION

Many aspects of modern life are associated with gas utilization. Hydrogen, methane, carbon dioxide, ammonia and others, are examples of gases employed in key process for the maintenance of our society. Moreover, due to their intrinsic properties, there is a need to find proper ways to store, handle and safely transport these gasses. Porous materials offer a unique opportunity due to their relatively high surface area and confined spaces.

Different microporous materials have been used as a sorbent for gases. Zeolites, activated carbons, MOFs and porous polymers are some of them, although the first three, presents significant drawbacks. Zeolite and activated carbon have a low physical interaction within the guest gas molecules, mainly due to the lack of specific functions to enhance the interaction. Metal-Organic Frameworks, on the other hand, can possess a vast library of functionalized pores, but such materials suffer from low stability, especially when adsorbing gases in a humid environment or harsh conditions. Therefore, porous organic polymers represent an emerging class of materials for gas adsorption. Some of the features that makes porous organic polymers good candidates for gas adsorption application are: permanent porosity, numerous structural topologies and functionalities, lightweight skeletons (offering the advantage of a higher adsorption capacity per gram) and last, the covalent bonds that hold the structure makes these materials much more stable than the other classes of porous materials, ensuring stability during the utilization in multiple cycles.

In order to enhance the gas uptake, two strategies can be considered. The first one is increasing the specific surface area. A highly porous material would adsorb gas molecules through their voids due to the strong capillarity force, presenting a high adsorption under low pressure, and therefore boosting gas adsorption through physisorption. The second strategy regards the utilization of functional pores to enhance the interaction between the porous polymer backbone and the guest gas molecules. Such strategy increases the adsorption of gases through chemisorption.

For instance, hydrogen is a promising source of clean and sustainable energy, however, its storage still a critical issue for hydrogen energy utilization. CTFs are particularly good candidates for hydrogen storage due to their high surface area and tailorable pores environment.

Thomas *et al.* primarily reported the synthesis of CTF troughs ionothermal route and also investigated the utilization of biphenyl-based CTFs for hydrogen storage. The material, possessing a high surface area of 2475 m^2/g, achieved a performance of 1.55 wt% in hydrogen storage at 1 bar and 77K. Such accomplishment is comparable with other porous materials reported in the literature [23].

In another study, Han *et al.*, employed tetragonal building blocks and a high ratio of zinc chloride to monomer, for the synthesis of CTFs with hierarchical pore distribution [41]. Due to carbonization, mesopores were formed, even though micropores were still predominant. The material showed a surface area of 1250 m^2/g and an uptake of 2.34 wt% of hydrogen in the same conditions. The high hydrogen uptake is attributed to the presence of both micropores, suitable for hydrogen adsorption, and mesopores, favoring gas diffusion.

In 2017, Coskun *et al.* employed a chemical activation to enhance the textural properties of CTFs [42]. The process consisted of carbonizing the CTF with an equivalent amount of KOH at 500-900°C, during 5h under an inert atmosphere. Such chemical processes resulted in deepening and narrowing the pathways in the interconnected pore structure. After activation, CTF-1 showed remarkable improvement in its superficial area, from 1034 to 2367 m^2/g. Furthermore, the formation of a well interconnected microporous structure can be observed by the increase in micropore volume, from 0.047 to 0.511 cm^3/g. As a result of the chemical activation, the group boosted the hydrogen uptake for CTF-1 from 0.96 wt% to 2.46 wt% at 77K and 1 bar.

Another gas commonly studied in adsorption experiments is carbon dioxide [43]. Due to human activities, the atmospheric concentration of CO_2 had increased rapidly in the last years. Such imbalance has triggered climate emergency. One way of mitigating the global warming is the capture and storage of CO_2. Even though some technologies for CO_2 capture are already available, e.g., amine scrubbing, they have huge drawbacks like very high energy consumption. Therefore, finding a suitable porous material capable of selectively adsorb CO_2 is desired.

CTFs have shown excellent capability in CO_2 adsorption. In the same case as hydrogen, due to the relative small size of CO_2 molecule, the improvement of microporous structure can enhance the carbon dioxide uptake. Moreover, the basic nature

of the nitrogen-containing in the triazine unit, enhances the carbon dioxide uptake, creating active CO_2-philic sites that stabilize the gas molecules.

Janiak *et al.* showed that materials prepared by the ionothermal route have better performance in CO_2 adsorption than CTFs prepared with trifluoromethanesulfonic acid-catalyzed trimerization [44]. The reason, rely on the higher surface area and the bigger micropore volumes. Additionally, the reaction condition can dramatically change the microporous structure, including pore size distribution and superficial area, leading to different potential in carbon dioxide uptake.

In theory, the higher the relative surface area, better the performance on gas uptake. Yang *et al*. synthesized a series of Covalent Triazine Frameworks using precursors with different lengths [45]. Figure 11 shows the structure of the repetition units for PCTFs 1-4 and its resulting specific surface area, calculated using the BET theory. The group was expecting an increase in the relative superficial area when bigger is the length of the branches in the precursor. However, the measurements showed the opposite. CTFs are usually amorphous materials with a stacked 2D layered structure. Therefore, when longer is the precursor, stronger is the π-π interaction between the layers, leading to a denser material with a lower specific surface area.

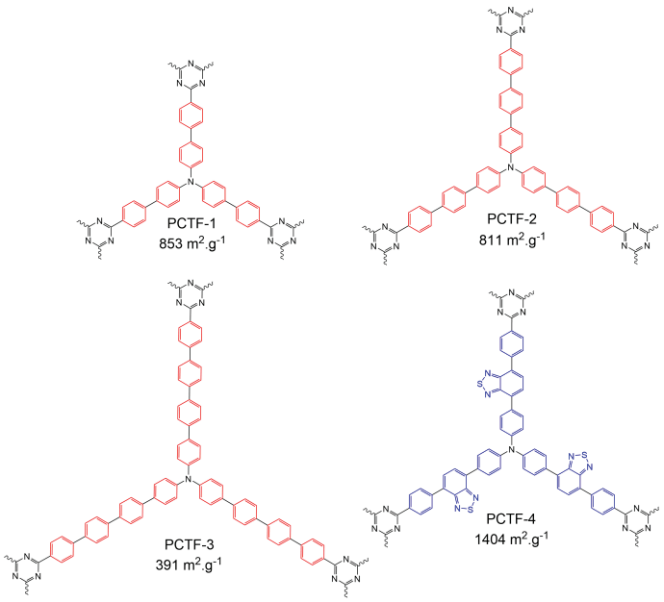

Figure 11 – Structure of repetition unit for PCTF series and their relative specific surface area.

Even though the microporous structure is dominant in all series, the low relative surface area decreases dramatically the gas adsorption performance. The CO_2 uptake were found to be: 13.2, 12.5 and 8.89 wt% for PCTF-1, PCTF-2 and PCTF-3 respectively.

However, much better performance was found for PCTF-4. This last material was synthesized with a precursor containing the same length as PCTF-3, but including thiadiazole groups. As a consequence of inserting such a group can be seen in the specific surface area, 811 m^2/g for PCTF-3 and 1404 m^2/g for PCTF-4. The explanation relies on the layered structure of CTFs. The insertion of thiadiazole groups disturbs the interactions between the layers, thus leading to a non-efficient space packing, resulting in a material with a higher superficial area. Combined with the high specific surface area, PCTF-4 possesses a high total pore volume, comprising in 92% of ultramicropores, making it a very good candidate in gas adsorption. PCTF-4 showed excellent CO_2 uptake of 20.5 wt% at 273K and 1 bar.

Moreover, in the case of carbon dioxide, not only the physical but also the chemical pore environment plays a role in adsorption. Coskun's group employed a charged building block in the synthesis of CTF to increase the CO_2 affinity [46]. The material, synthesized by ionothermal trimerization of cyanophenyl substituted viologen dication, showed a remarkable CO_2 uptake of 26.12 wt%. Furthermore, the incorporation of charged species into the CTF backbone, promoted efficiently the conversion of CO_2 into cyclic carbonates.

More recently, Das *et al*. synthesized a CTF based on the trimerization of triazole-substituted perfluorinated aromatic nitriles for both hydrogen and carbon dioxide storage [47]. Figure 12 depicts the monomer's structure and the adsorption isotherms for hydrogen, carbon dioxide and methane.

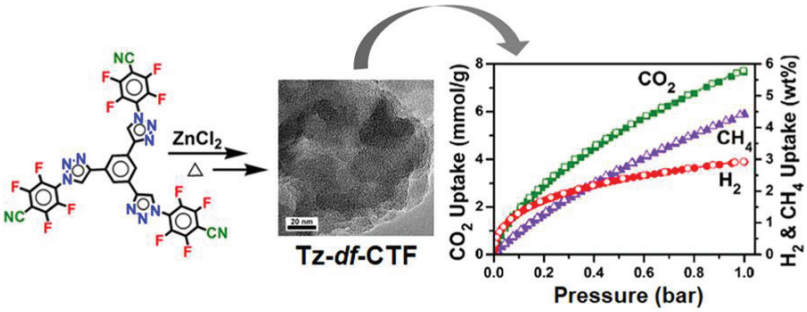

Figure 12 – Structure of Tz-PFCN building block and Tz-*df*-CTF the isotherm adsorption for H_2, CO_2 and CH_4 uptake. Adapted with permission from: Mukherjee, S.; Das, M.; Manna, A.; Krishna, R.; Das, S. Newly designed 1,2,3-triazole functionalized covalent triazine frameworks with exceptionally high uptake capacity for both CO_2 and H_2. *J. Mater. Chem. A*, 2019,v. 7, pp. 1055-1068.

The study is based on a dual strategy. First, integrating a large number of fluorine functionality (C-F), results in a material with high surface area, comprising in a higher degree of ultra-microporosity (pores widths less than 0.7 nm), due to the thermal

decomposition of C-F bonds. Such a strategy certainly improves the uptake of small gas molecules like hydrogen. On the other hand, the utilization of a building block with high nitrogen content, enhance the carbon dioxide uptake, due to the basic nature of the triazole unit, creating active CO_2-philic sites. The group synthesized the same material in three different temperatures, 400, 500 and 600°C. With superficial areas of 1550, 1878 and 2106 m^2/g, respectively. The material synthesized at 600°C showed a hydrogen uptake of 2.91 wt% at 77K and 1 bar, and 7.65 mmol/g for CO_2 at 273K and 1 bar. It has been among the highest hydrogen and carbon dioxide uptakes for porous materials.

Membranes technology provides a very energy-efficient method for gas separation. Some examples of common industrial gas mixtures separated using membrane-based techniques are O_2/N_2 for oxygen-enriched air, H_2/N_2 for hydrogen recovery in the ammonia production process, H_2/CH_4 for hydrocarbon processing and CO_2/CH_4 for natural gas application. Gas separation is usually investigated in terms of two properties: selectivity and permeability. Selectivity is determined by the ratio of permeability coefficients of the more permeable over the less permeable gas in the mixture. Permeability is described as the product of permeance and membrane thickness. Selectivity and permeability have a tradeoff relation. Materials with high permeability are in general, less selective. The relation is described as Robeson's limit in membrane gas separation [48-49].

Membranes with higher selectivity would result in a purer product after separation. Moreover, higher permeability would decrease the quantity of membrane area needed to treat a specific amount of gas, reducing the cost of membrane units. Polymer-based porous membranes highly permeable and selectivity are desirable.

In this context, Zhu and co-workers developed a method to synthesize CTF-based membranes with the acid approach [27]. The precursor is mixed with acid at low temperature, the resulting viscous solution is poured into a flat glass dish and allowed to spread, forming a thin layer. After a temperature treatment of 100 °C for 20 min, the reaction is quenched with the addition of water at room temperature. After being washed with dilute NaOH solution, to neutralize the excess of acid, the membranes were tested for CO_2/N_2 separation. The microporous membrane based on 4,4′-biphenyldicarbonitrile trimerization (TFM-1) showed increased selectivity for the separation of CO_2 over N_2, achieving permselectivity of 29 ± 2, with a CO_2 permeability of 518 ± 25 barrer.

In another study, Ying *et al.* produced a membrane by vacuum filtration of a liquid dispersion of CTF-1 mixed with graphene oxide nanosheets in isopore cellulose acetate support [50]. The resulting ultrathin membranes possess a tunable thickness, depending on the amount of liquid dispersion filtrated. Efficient separation of H_2 from CO_2 was achieved with very high permeance for H_2 ($1.7x10^{-6}$ $mol.m^{-2}.s^{-1}.Pa^{-1}$).

Theoretical studies have shown that CTF membranes are interesting materials for water desalination [51]. Moreover, when investigated in the separation of He and H_2 over Ne, CO_2, Ar, N_2, CO, and CH_4, CTF membranes showed superior performance compared to conventional carbon and silica membranes [52].

1.3.2 HETEROGENEOUS CATALYSIS

Catalysis plays a role in modern society. It is fundamental to the development and transformation of chemical compounds and materials in many different fields, including energy and food production and the pharmaceutical industry. In addition, on a planet with continuous environmental and economic challenges, catalysis is an essential field to address the transition to a more sustainable world.

Because of its intrinsic features like high porosity, tailorable chemical composition and pore structure, covalent triazine frameworks have superior qualities in catalysis: its tailorable structure allows the synthesis of materials with an active precursor or the insertion of functional groups to host the active moiety; its high specific superficial area promote the accessibility and a high dispersion of catalytic sites; the interconnected pore structure results in an efficient mass transportation of reactants through the material; their well-defined structure enables the visualization of the catalytic mechanism, in comparison with similar homogeneous reaction, leading to a better understanding of the interactions between catalytic site and reactants. For all the reasons mentioned above, CTFs have been extensively studied as a catalyst.

As stated before, the type of synthesis will directly affect the final material's features, driving its properties towards a specific application. To simplify, due to carbonization, CTFs synthesized through the ionothermal method possess high thermostability and conductive properties, essential features for thermo and electrocatalytic applications. Moreover, the inertness of materials synthesized by this

route is a requisite for a good support in catalysis [53]. In photocatalysis, the catalyst has to adsorb light in the visible spectra and promote the generation of electron-hole pairs. Only materials with an active bandgap can be used as photocatalyst. Therefore, only CTFs synthesized through the acid and condensation methods are suitable.

This section will be divided according to the type of energy employed in the catalytic reaction. Thermocatalysis, electrocatalysis and photocatalysis use temperature (thermal energy), electrical current and light as driving forces for catalytic transformations. Such separation was done to better cover the aspects of CTFs as catalysts.

1.3.2.1 THERMOCATALYSIS

Covalent Triazine Framework have emerged as a prominent class of porous organic material for high-performance catalysts. Their performance is linked to structural features like high thermal stability, inertness, chemical stability under acid or basic environment, rigid structure, and high nitrogen content, characteristics only found in CTFs. As catalysts, CTFs can be designed in two ways. The first is the incorporation of an organic active unit into the backbone of the material. Such a strategy is often called heterogenization and the resulting CTF an organocatalyst. Alternatively, CTFs can be designed as hosts for more active species like metal nanoparticles or molecular organometallic compounds.

Due to their basic nature and high surface area, CTFs turned out to be suitable for CO_2 conversion into epoxides. In 2012 and 2013, Thomas and co-workers showed the potential of CTF as a metal-free catalyst in cycloaddition of CO_2 to epichlorohydrin. CTFs based on 1,4-dicyanobenzene and 2,6-dicyanopyridine, synthesized through ionothermal route at 600°C, exhibit conversion of 100% within 4 h at 130°C and 6.9 bar of CO_2, achieving selectivity of 95.8 and 94.6% to cyclic carbonate, respectively [54].

In 2017, Coskun's group employed a charged CTF as a metal-free catalyst in cyclic carbonates production through CO_2 addition. The material, based on cationic viologen motifs showed similar conversion and enhanced selectivity of 100% towards the carbonate within 12 h at 90°C and 100 bar of CO_2. The CTF was recycled up to 5 times without apparent loss in activity [46].

As support, CTFs have been applied in many reactions. Palkovits *et al.* showed the benefits of N-heterocyclic moieties in CTFs when stabilizing a nanoparticle [55-56]. CTFs containing Ruthenium nanoparticle was synthesized through the coordination-reduction method. First, the precursor $RuCl_3.xH_2O$ and CTF were refluxed in ethanol. Then the Ru-coordinated species were reduced under hydrogen. Figure 13 shows the coordination and stabilization of Ru NPs on CTFs.

The material showed superior activity in the oxidation of 5-hydroxymethylfurfural when CTF was used as support, in comparison to conventional ruthenium on carbon or alumina (Al_2O_3). Additionally to the stabilization of NP through the triazine moieties, the porous nature of the support assure high dispersion of the active species and at the same time, offers as a steric impediment to the growth of metal clusters, preventing agglomeration and consequently deactivation.

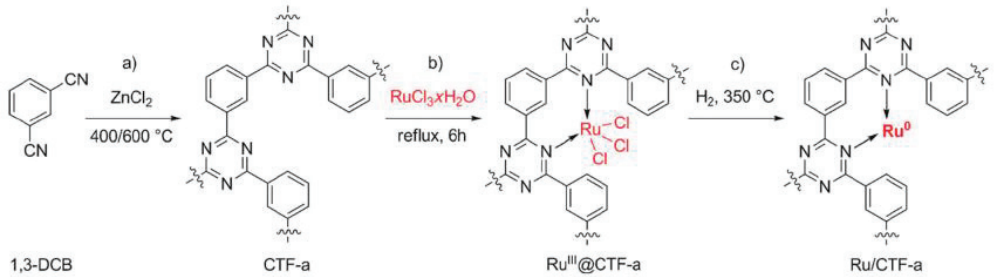

Figure 13 – Synthesis and support of Ru NPs into CTF. Adapted with permission from: Artz,J.; Mallmann, S.; Palkovits, R. Selective Aerobic Oxidation of HMF to 2,5-Diformylfuran on Covalent Triazine Frameworks-Supported Ru Catalysts. *ChemSusChem* 2015, 8, 672-679.

Her group was also the first to report the immobilization of a molecular catalyst within a CTF. The utilization of a CTF based on 2,6-dicyanopyridine, allow the coordination of the precursor $K_2[PtCl_4]$ into the pyridinic moieties. Resembling the molecular Periana catalyst, the group was able to selectively oxidaze methane to methylbisulfate, an intermediate for methanol production. Achieving comparable TON and slightly lower selectivity (75% for $K_2[PtCl_4]$-CTF against 81% for Periana-type catalysts), the Pt-supported CTF surpass the molecular one in recyclability, being easily separated by filtration. The system is stable and kept the same activity for at least five cycles [57]. Even though high costs are expected for the utilization of CTFs in industrial scale, the group showed an interesting strategy in supporting molecular catalysts in N-rich building blocks. Such strategy was further used to design supported molecular catalysts, bridging heterogeneous and homogeneous catalysis.

Using the aforementioned strategy, Yoon *et al.* supported Ruthenium and Iridium complexes into bipyridine-based CTFs [58-59]. The resulting immobilized catalysts were used in the hydrogenation of CO_2 to formate. The binding functionalized building unit was incorporated into the framework backbone to mimic the homogeneous homologous. Both materials convert CO_2 to formate under mild conditions. Furthermore, the CTF-immobilized complex outperformed the state-of-art, a Ru-complex immobilized on the surface of silica particles.

1.3.2.2 ELECTROCATALYSIS

The first study on the application of CTFs as electrocatalysts was reported by Kamiya and co-workers. The material, based on the ionothermal trimerization of 2,6-dicyanopyridine, was synthesized together with conductive carbon nanoparticles (CP), in order to increase its conductivity. Finally, the impregnation with platinum chloride salt, resulted in the active electrocatalyst Pt-CTF/CP for Oxygen Reduction Reaction (ORR). In comparison with other supports, Pt-CTF/CP showed activity close to benchmark electrocatalysts Pt/C, however, a high methanol tolerance in acidic media was observed. Such property enables the utilization of this material in direct methanol fuel cells (DMFCs) [60].

Oxygen reduction reaction (ORR) is an important cathodic reaction in energy conversion systems such as fuel cells and metal-air batteries. Oxygen reduction in aqueous solutions can occur mainly through two different pathways: a four-electron reduction from O_2 to H_2O or a two-electron reduction from O_2 to H_2O_2 [61]. Between many metals evaluated, Platinum still the best catalyst for ORR. However, its price limits the commercialization of fuel cells on a large scale. Therefore, the development of electrocatalysts composed only by abundant elements is a key goal in the energy sector.

Using the same strategy, Kamiya and co-workers, synthesized a copper-based CTF modified with conductive carbon nanoparticles [62]. The Cu-CTF/CP showed improved conductivity and enhanced stability compared to the molecular Cu-based catalysts, due to the conductive carbon nanoparticles and the CTF structure, respectively. The activity was also very high among Cu-based electrocatalysts, achieving the onset potential of 810 mV versus the reversible hydrogen electrode (RHE) at neutral pH.

Although Kamiya and co-workers performed the synthesis of CTFs with conductive carbon nanoparticles as a strategy to enhance their conductivity, the synthesis through ionothermal route, especially at high temperatures, favors the formation of conductive materials, due to carbonization.

Similarly to ORR, hydrogen evolution reaction (HER) is an important cathodic reaction for the development of clean and renewable energy. In electrochemical water splitting, HER is the two-electron transfer half-reaction that produces hydrogen from water ($2\ H^+ + 2\ e^- \rightarrow H_2$) [63]. Pt is also a remarkable catalyst in HER, exhibiting a very low overpotential for this application. Basically, the overpotential (η) is the difference between the thermodynamically determined potential and the potential at which a certain redox reaction really happens. In electrocatalytic reaction, the existence of overpotential means the cell requires more energy than thermodynamically calculated to trigger a redox reaction.

In this context, Yi *et al.,* reported the synthesis of a cobalt single-atom porphyrin-based CTF for both ORR and HER [64]. The material was synthesized in three different temperatures, the most active is the one produced at high temperature (600°C). CoSAs/PTF-600 showed high activity in ORR, exhibiting a positive half-wave potential of 808 mV (vs. RHE) in alkaline solution (0.1M KOH), which is slightly more positive than 20 wt% Pt/C (0.806 mV), a benchmark catalyst in ORR. Moreover, the same material achieved a very low overpotential for hydrogen evolution reaction. Performing the HER with 94 mV of overpotential, an increase in 40 mV when compared to Pt/C (54 mV) at a current density of 10 mA/cm^2.

Electrochemical conversion of carbon dioxide has also emerged as an interesting field of application for CTFs. As stated before, the conversion of CO_2 is a way to mitigate the climate emergency, sustainably producing chemicals and fuel. Therefore, significant efforts have been done to develop suitable catalysts for such application.

Taking advantage that porphyrin-based materials result in very active MN_4 (M=metal) single atoms sites, homogeneously dispersed, Zhuang *el al.* synthesized a Nickel-containing porphyrin-based CTF (NiPor-CTF) for the electrocatalytic conversion of CO_2. Taking advantages of the high surface area, conjugated backbone structure and high content of NiN_4 single atoms sites, NiPor-CTF generated a high current density (52.9 mA/cm^2) at -0.9 V (vs. RHE), when converting CO_2 to CO. The Faradaic Efficiency (FE)

reached the maximum of 97% at -0.9V and only CO and H_2 were detected as products [65].

1.3.2.3 PHOTOCATALYSIS

Using sunlight as a renewable source of energy to promote chemical transformation in key reactions of the energy field is an interesting approach to address sustainable energy production. Therefore, novel, more efficient and stable photocatalyst materials and photocatalytic processes are required.

The interest in the utilization of porous organic polymers in photocatalysis, initiated to overcome the main limitations of inorganic semiconductors. Even though they are very robust catalysts, their poor light absorption in visible spectra, scarcity of precursors and the difficulty to tune their electronic and optical structure, imply some disadvantages on their utilization. On the other hand, the utilization of POPs as photocatalysts offer some advantages like tunable bandgap structure, pore environment and chemical composition, strong visible light absorption and well-defined structure.

The utilization of organic polymers in photocatalysis experienced a widespread interest after the resurgence of graphite carbon nitride (g-C_3N_4) in 2008, when Antonietti, Domen and co-workers showed the heptazine-based polymer could catalyze both half-reactions in water splitting under visible light irradiation [22]. After this, many classes of POPs, including covalent organic frameworks (COFs), conjugated microporous polymers (CMPs) and covalent triazine frameworks (CTFs) were developed as photocatalysts.

Some prerequisites for the utilization of POPs in photocatalysis may limit the application of certain materials. Appropriate band alignment and efficient charge separation and transfer are requirements to promote photoredox reactions. In the case of CTFs, materials synthesized through the ionothermal method are not suitable for photocatalysis. The harsh conditions employed in the synthesis result in carbonized materials, with a black appearance and narrow bandgap (~1eV). However, Lotsch and co-workers reported the synthesis of CTF-like material through an ionothermal approach at low temperature (300°C) that is capable to drive catalytic water splitting under visible light irradiation in the presence of a sacrificial compound. Because the low temperature of synthesis, the solid does not have an extended structure like a CTF, in contrast to the polymer in which the extensive repetition of building blocks results in a large extended interconnected structure, oligomers present just a few numbers of connected repetition

units. The resulting material was named phenyl-triazine oligomers (PTO-300) and showed an efficient hydrogen evolution rate of 1080 $\mu mol.h^{-1}.g^{-1}$ under the irradiation of simulated sunlight [66].

The interest in the application of CTFs in water splitting comes from the properties of incorporated triazine unit in highly conjugated polymeric structures. This nitrogen-rich aromatic ring with an electron-withdrawing character acts as an active site for photoredox reactions. Finding suitable methods for the synthesis of photo-active CTFs led to further developments. In this context, Cooper *et al.* synthesized a series of CTFs by trifluoromethanesulfonic acid trimerization at room temperature [67]. In the series CTF-1 to CTF-4, the number indicates the amount of para-phenylene spacers between the triazine units within the material's structure. With an active bandgap of 2.73 eV and the highest specific surface area calculated by the BET equation (560 $m^2.g^{-1}$), CTF-2 presented the best activity in photocatalytic water splitting from the series, 296 ± 11 $\mu mol.g^{-1}.h^{-1}$. Extending the space between the triazine units by the gradual increase in the number of phenylene moieties, decrease the thermodynamic driving force for water splitting, however at the same time, it broadens the visible-light absorbance. The photocatalytic activity of a CTF system is governed by a synergetic effect between bandgap structure, light absorbance and specific surface area, therefore, it can be regulated by judiciously choosing the building blocks and the reaction to connect them into a framework.

Lately, the synthesis of CTFs through condensation, enabling better control over the molecular structure, enhanced their tunability and made possible the design and synthesis of better photocatalysts. The first study on the synthesis of CTF through amidine and aldehyde condensation, reported by Wang and co-workers, also described the properties of these materials in photocatalytic HER. Combining partial layered structure, broad visible light absorption and suitable bandgap, CTF-HUST-2, based on the condensation of terephthalamidine dihydrochloride and 4,4'-biphenyldicarboxaldehyde, showed the highest activity in HER, reaching an outstanding rate of 2647 $\mu mol.h^{-1}.g^{-1}$ in the presence of a sacrificial compound and visible light irradiation. This value is among the highest reported rates in HER for POPs [30, 32].

Improving the crystallinity of these CTFs synthesized by condensation dramatically enhanced their HER activity. The same team reported the synthesis of a crystalline CTFs by replacing the aldehyde precursor for an alcohol. The slow in situ

oxidation of alcohol to aldehyde, decreased the nucleation rate, improving significantly their crystallinity. In contrast to CTF-HUST-1, synthesized by condensation of aldehyde and amidine hydrochloride, which showed a HER activity of 1460 $\mu mol.h^{-1}.g^{-1}$, CTF-HUST-C1, the crystalline equivalent, achieved a rate on hydrogen evolution of 5100 $\mu mol.h^{-1}.g^{-1}$ in the presence of sacrificial reagent. By electrochemical impedance spectroscopy (EIS) the group stated that the charge transport in crystalline CTF-HUST-C1 is better than in CTF-HUST-1 [32]. Together with a better charge transport ability, the crystalline material has a broader visible light absorption, which is beneficial to enhance their photocatalytic performance.

Taking advantage of the synthesis of covalent triazine frameworks through condensation, Guo *et al.* synthesized three CTFs by condensing terephthalamidine dihydrochloride with 3,6-dicarbaldehyde-N-ethylcarbazole, 2,8-dicarbaldehyde-dibenzothiophe and 2,8-dicarbaldehyde-dibenzofuran [68]. The materials were named CTF-N, CTF-S and CTF-O, respectively, representing the heteroatom that composes the aldehyde building block. Figure 14 illustrates the structure of the precursor as well as the solid-state NMR of the materials.

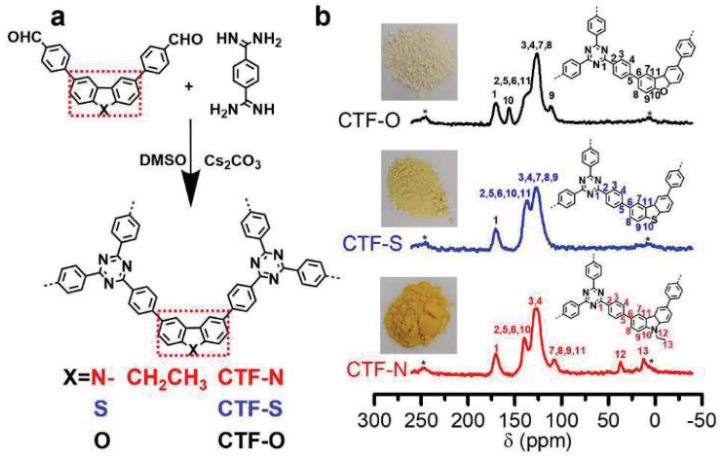

Figure 14 – Structure of precursors and solid state NMR of the resulting materials. Adapted with permission from: Guoa, L.; Niub, Y.; Xua, H.; Lic, Q.; Razzaquea, S.; Huanga, Q.; Jin, S.; Tan, B. Engineering Heteroatom with Atomic Precision in Donor-Acceptor Covalent Triazine Frameworks to Boost Photocatalytic Hydrogen Production. *J. Mater. Chem. A*, 2018,6, 19775-19781.

Using theoretical calculations, the group was able to study the electronic structure of CTFs, confirming their donor-acceptor connection. A progressive increase in the energy of highest occupied molecular orbital (HOMO) levels, was observed following the order N<S<O, suggesting the gradual decrease in electron donor ability. Possessing the narrowest bandgap (2.17 eV) and consequently the broadest visible light absorption,

CTF-N showed the highest activity in HER. The material achieved 538 μmol.h^{-1} using triethanolamine (TEOA) as sacrificial agent and Pt as cocatalyst.

In addition to HER, CTFs were also employed on photocatalytic carbon dioxide conversion. Cao *et al.*, reported the synthesis of CTF through ionothermal trimerization of 2,6-dicyanopyridine and further grafting of rhenium complex ($Re(CO)_5Cl$) into the pyridine units for CO_2-to-CO conversion [69]. Even though the group irradiated the material with a broader light spectrum (200-1100 nm) and not only with the visible region, Re-CTF-py notably showed a CO evolution rate of 353 μmol.h^{-1}.g^{-1} in the solid-gas system after 10 hours of irradiation. A small fraction of CH_4 was also detected among the products, however, CO was the majoritarian product.

In another report, Bi and co-workers described the synthesis of CTF-1 through trimerization in acid at room temperature followed by wet impregnation of cobalt chloride and further activation in an oven at 250°C. The cobalt-modified CTF-1 was employed as photocatalyst in CO_2-to-CO conversion in a mixture of acetonitrile, water and triethanolamine (volume ratio of 1:2:3) in the presence of $[Ru(bpy)_3]Cl_2.6H_2O$ as a photosensitizer. Co/CTF-1 exhibited a CO evolution rate of 50 μmol.h^{-1}.g^{-1} after 4h irradiation under visible light [70].

Further examples of heterogeneous photocatalysts include the utilization of triazine-based materials for NADH regeneration in artificial photosynthesis [71], CO_2 reduction [72] and water splitting. However, since these materials are classified as covalent organic frameworks (COFs), hypercrosslinked polymers (HCPs) and other classes of POPs, they will not be in focus. Other applications of CTFs are described in the next section.

1.3.3 OTHER APPLICATIONS

Further applications include the utilization of CTFs as absorbents for pollutants removal, supercapacitors, and cathode for Li-ion batteries. In all cases, their features are the main driving force for such applications.

In the first case, the high specific superficial area and the interconnected porous system provide great applicability in absorption. Moreover, the extended π-conjugated system, improve the interaction of CTFs with aromatic compounds through π-π

interactions. Furthermore, the basic nitrogen atoms from the triazine center benefit the metal uptake. According to Janiak and co-workers, CTF-1, synthesized through ionothermal route at 600°C have 20 times more gravimetric uptake of surfactants from water than carbon black [73]. From the two surfactants tested, sodium dodecylsulfate and alkyl polyglycolether, CTF-1 have shown much better absorption properties. The reason relies on the higher specific surface area, 1390 m^2/g for CTF-1, compared to 150 m^2/g for carbon black.

Lin *et al.* synthesized a magnetic CTF composite for adsorption of perfluorinated compounds in environmental water samples. The material was synthesized by the ionothermal route, with addition to Fe_2O_3 [74]. After optimizing the desorption step, the group developed a reproducible method for the detection of perfluorinated compounds with a very low limit of detection (0.62 - 1.39 $ng.L^{-1}$) in a wide linear range (5–4000 $ng.L^{-1}$). The material did not show any change even after 50 cycles.

In another study, Zhong *et al.* employed the acid approach for the synthesis of a CTF with mixed ligands (1,4-dicyanobenzene and 4,4′-biphenyldicarbonitrile) in a molar ratio of 1:1 [75]. The group performed adsorption of benzene, naphthalene, and phenol, simulating typical volatile aromatic contaminants from industrial waste. After adsorption, the group regenerated the CTF under simulated sunlight. The defective CTF showed great capability in absorbing and self-regenerate under light irradiation. Even after four cycles, the percentage of material regenerated was still 90%, much higher than the CTFs synthesized with a unique monomer. This work emphasizes the potential of CTFs as solar-driven self-cleaning adsorbents for the removal of aromatic pollutants from water.

Supercapacitors are electrochemical energy storage devices that store and release energy by reversible adsorption and desorption of ions at the interfaces between electrode and electrolytes. In supercapacitors, the heteroatom effect plays a role in increasing the capacitance, while a high specific surface area with a hierarchical porous structure accelerates electrolyte ions transfer. Therefore, due to its features, CTFs offer great potential for high performance in energy storage. Zhu *el al.* developed a composite based on graphene and CTF-1 [76]. After pyrolysis, the porous carbon nanosheets exhibited 2D morphology, high nitrogen content and specific superficial area. Such material presented remarkable energy storage performance, achieving 340 $F.g^{-1}$ at 0.1 $A.g^{-1}$ and 10000 stable charge-discharge cycles at 5 $A.g^{-1}$.

Deng and co-workers reported the synthesis of a CTF series based on 7,7,8,8-Tetracyanoquinodimethane [77]. The materials were synthesized through ionothermal method using different temperatures. Due to very high specific surface area (up to 3663 m^2/g), nitrogen content of 8.13% and conductive properties, the materials showed outstanding performance in supercapacitors. Achieving a capacitance of 383 $F.g^{-1}$ in alkaline conditions and no apparent degradation after 10000 cycles.

Covalent Triazine Frameworks have also been explored in ion batteries. Their porous nature and high nitrogen content make CTFs a promising material for ion-based batteries. Rechargeable lithium-sulfur (Li-S) batteries have received considerable attention in the past years due to their very high energy density. However, they have a low cycle lifetime. Such a problem arises mainly due to the dissolution of intermediate lithium polysulfide into the organic electrolytes during the charge/discharge cycle. To overcome this problem, the encapsulation of elemental sulfur (cathode) with a conductive material is one strategy. Coskun and co-workers developed a CTF containing very homogeneously dispersed sulfur for this application [78]. The group synthesized the material through an ionothermal route by mixing 1,4-dicyanobenzene and elemental sulfur. The mixture was heated, first at 160°C, to dissolve and promote the ring-opening of elemental sulfur, and then at 400°C for simultaneous trimerization of nitriles and insertion of sulfur into the CTF backbone. When tested as a cathode, the battery exhibits a profile consistent with previously works reported in the literature. The discharge curve shows two plateaus, corresponding to two-step reduction, including the formation of Lithium-polysulfide (Li_2S_n) at 2.35 V and Lithium sulfide (Li_2S) at 2.1V. Furthermore, during charging, Li_2S is oxidized to Li_2S_n at 2.3V and further to sulfur at 2.4V. The battery achieved a remarkable initial coulombic efficiency (ICE) of 94.4%, much higher than most of organic-based matrix/sulfur materials tested in the literature.

Further improvement was made by employing tetrafluoroterephthalonitrile and elemental sulfur for the synthesis of a sulfur-containing CTF. The same group aforementioned, predict the increase in sulfur content through nucleophilic aromatic substitution reaction between perfluoroaryl units and elemental sulfur [79]. The strategy succeeded and the cathode achieved an ICE of 96.9% and remarkable capacity retention of 81.6% after 300 cycles.

1.4 MOTIVATION AND GOALS

In a very dynamic world, with significant economic and environmental challenges, the development of novel materials and catalytic processes for renewable energy production and transformation is an essential step towards a sustainable future. Covalent triazine frameworks are among the most promising class of materials regarding energy applications, mainly because of their features. Therefore, it is fundamental to keep pushing the boundaries on the design and synthesis of covalent triazine frameworks.

The major limitations in the synthesis of CTFs via ionothermal and acid approaches, e.g. the unavoidable carbonization and the restriction on the utilization of pyridinic building blocks, respectively, were the main driving forces for searching new methods of synthesis. Moreover, the recent development of polycondensation approach has enabled the design and synthesis of CTF through a modular approach, a significant advantage over the other methods. Therefore, this project has as a primary goal the understanding of the synthesis of CTFs through condensation procedure, focussing on the enhancement of molecular control and precision in the synthesis and seeking to describe the main advantages, drawbacks and challenges in comparison to the other methods.

Additionally, up to now, only non-functionalized CTFs synthesized through condensation has been reported in the literature. The lack of information regarding the utilization of functionalized amidines as precursors hinders the employment of the polycondensation method. In this regard, the present work has as a second goal: the synthesis of CTFs based on chelating functionalized building blocks.

The strategy of heterogenization of homogeneous catalysts bridges the gap between the two types of catalysis, taking advantage of both. With a well-defined molecular structure, resulting in enhanced selectivity and activity, combined with easy handling, robustness, recyclability and the benefits of working under heterogeneous conditions. For these reasons, this project will target the development of novel bipyridine-based CTFs, as a way to investigate the utilization of functionalized amidine chlorides as precursor for the synthesis of complex CTFs and also in order to use its binding properties as a functional group for supporting homogeneous catalysts.

Additionally, the imminent threat humankind is facing due to climate change will be addressed in the application of these novel bipyridine-based CTFs. As a way to mitigate climate emergency, the main target is the conversion of carbon dioxide to

valuable chemicals and fuel. Therefore, taking advantage of functional CTFs, the main goal is the utilization of a series of bipyridine-based CTFs as a scaffold for molecular Rhodium complex to investigate carbon dioxide reduction under visible light irradiation.

The next chapter will be devoted to the main challenges faced on the synthesis of the starting materials, in designing a stable photocatalytic system and later on its characterization.

CHAPTER 2: CHALLENGES

2. CHALLENGES

The fast development of porous materials, especially the organic and hybrids, can be noticed through the number of publications regarding this topic in the recent years. Figure 15 shows the number of publications per year using the terms “microporous polymer”, “nanoporous polymer” and “organic framework” [80]. Indeed, the vast possibilities in terms of structure, design, and application, made MOFs and POPs very popular, achieving impressive improvements in a short time.

The success of these classes of materials hides significant challenges in their preparation and characterization. This section will be dedicated to the main challenges faced in the synthesis and characterization of photoactive CTFs through polycondensation.

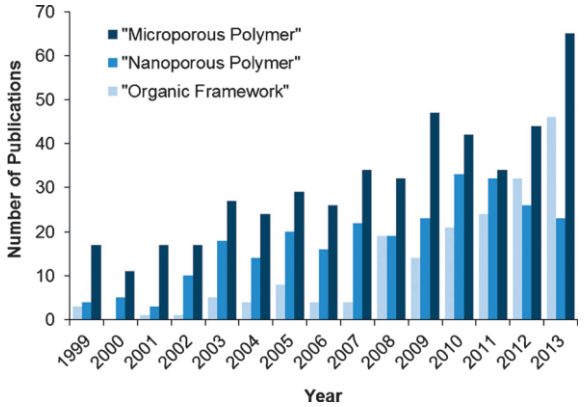

Figure 15 – Number of publications per year for terms “metal-organic-framework” and “porous organic polymer”. Adapted with permission from: Rose, M. Nanoporous Polymers: Bridging the Gap between Molecular and Solid Catalysts?. *ChemCatChem* 2014, 6, 1166-1182.

2.1 CHALLENGES IN THE SYNTHESIS OF CTFs

The successful synthesis of a porous organic polymer hides big challenges. Having control over organic matter in a chaotic polymerization reaction, resulting in a functional material, requires a good understanding not only on the mechanistic aspects but also on the experimental ones.

Because the main issues on the ionothermal and acid approaches, the synthesis of photoactive and functionalized CTFs, designed in this project, have to be done according to the polycondensation approach. The first issue in the synthesis through condensation is the preparation of precursors. As said before, the condensation is based on a reaction between aldehyde with amidine chloride to produce in situ the hydro-triazine ring, which

is further oxidized to s-triazine by the solvent, DMSO. So, the first challenge, after the design, starts with the synthesis of the aldehyde and amidine chloride.

The aldehyde can be synthesized by several different reactions like alcohol oxidation [81], reduction of esters or nitriles [82], Swern oxidation of carboxylic acids or esters [83], Sommelet oxidation of benzyl halides [84], between others. The pathway to synthesize the aldehyde will mostly depend on what kind of building block is required. On the other hand, the synthesis of amidine presents a real challenge.

Amidines or Carboxamidines (official name from IUPAC) are a group of organic compounds that can be described as carboxylic acid derivatives with ammonia, in which the −OH group is replaced by a $-NH_2$ and the =O group is replaced by =NR, resulting in the general structural formula R_1-C(= NR_2)-NH_2. The amidines are often called "free" when R_2 is a hydrogen and substituted when R_2 is a different organic radical. Furthermore, amidines are among the strongest uncharged/unionized bases. In the case of a free amidine, the base can be protonated on the sp^2 hybridized nitrogen creating a resonance, the resulting ionic specie is called amidinium. Due to high stability under air, amidines are very often found as chloride or bromide salts [85]. Figure 16 shows the amidine structure and also the resonance created to delocalize the charge.

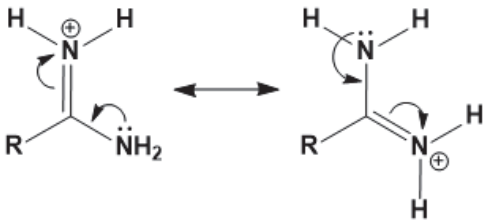

Figure 16 – General structure of a free amidine and the resonance of amidinium ion.

Carboxamidine compounds have found a very interesting application on the development of drugs. The pharmaceutical industry uses amidines as precursors for nitrogenated heterocycles derivate in drugs synthesis [86]. Additionally, some amidines also present pharmacological activity towards some diseases. Pentamidine is one example of amidine's relevance as drugs. It is an effective medicine used to treat African trypanosomiasis, leishmaniasis and pneumocystis pneumonia. The compound came into medical use in 1937 and is still in use nowadays. It is on the World Health Organization's List of Essential Medicines, the most effective and safe medicines needed in a health system.

Free amidines can be synthesized in many different ways using a wide variety of starting compounds. However, using nitriles as starting material is an advantage. Nitriles are cheap compounds and when not available, can be synthesized from halides. Additionally, nitriles are precursors for CTF synthesis in a range of different approaches, being interesting compounds to have at disposal. There are several methods to synthesize amidines from nitriles, but these three are the most relevant: Pinner reaction, Garigipati's reaction and reaction with lithium bis(trimethylsilyl)amide (LiHMDS).

The Pinner reaction [87] consists of an acid-catalyzed reaction of nitrile with alcohol, culminating in the formation of an imino ester salt (usually called Pinner salt). The intermediate salt can react with a series of compounds giving, through nucleophilic addition, various useful products like ester (when reacts with water), thionoester (when hydrogen sulphide is used), or orthoester (when the Pinner salt reacts with an excess of alcohol). Amidine is generated by reacting the intermediate pinner salt with ammonia or amine. This reaction is usually carried out at 0ºC with an excess of hydrochloric acid in a dry solvent, such as dioxane, chloroform, nitrobenzene, benzene, or ether. Figure 17 shows the Pinner reaction in detail.

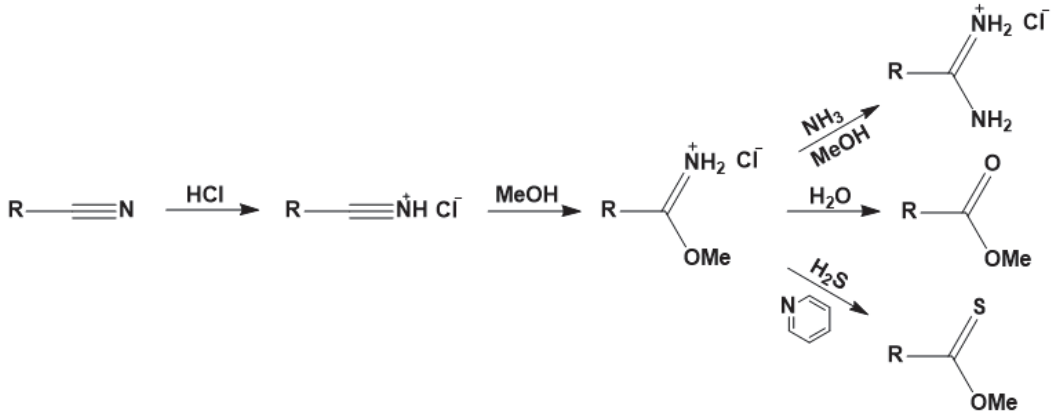

Figure 17 – Pinner reaction and the various products formation.

The reaction is very versatile, and the utilization of functionalized nitriles is possible. However, it has a few limitations. Adducts such as acyl cyanides and some ortho-substituted nitriles do not undergo a Pinner reaction. Additionally, the imidine intermediate is very sensitive to moisture, it can react with water and give an undesired product if not handled properly. Despite being a very useful reaction, Pinner reaction has some drawbacks like the utilization of HCl in the gas phase, due to the high toxicity and difficulty in handling, the need for extensive purification of the by-products, and time.

Depending on the structure of the starting material, some reaction needs more than days to complete.

There are some variations of the Pinner reaction, like using a very basic condition in order to avoid the utilization of HCl, or a different solvent composition to shorten the purification procedure of the final compound. But, despite the recent efforts on the improvement of Pinner reaction, the most common procedure still remains the acidic route.

Another pathway to obtain amidines in good yield is the addition of aluminium amide to nitriles [88]. The studies date back to 1969 when Hoberg and Barluenga Mur first studied spectroscopically a dimer aluminium-amidine, an insertion product from the interaction between benzonitrile and diethylaluminum dimethylamide. By that time, the researchers did not proceed to the complete synthesis and isolation of amidines, studying the intermediate instead. Inspired by the synthesis of carboxamides, by direct nucleophilic addition of aluminium amide to carboxylic esters, Garigipati studied the products starting from nitriles, leading to amidine formation. The reaction, also known as Garigipati's reaction, uses alkylchloroaluminum amides to conveniently synthesize amidines from nitriles. The aluminium amide can be prepared by mixing trimethyl-aluminium with ammonium chloride in toluene, and was developed by Weinreb. Figure 18 shows the general reaction.

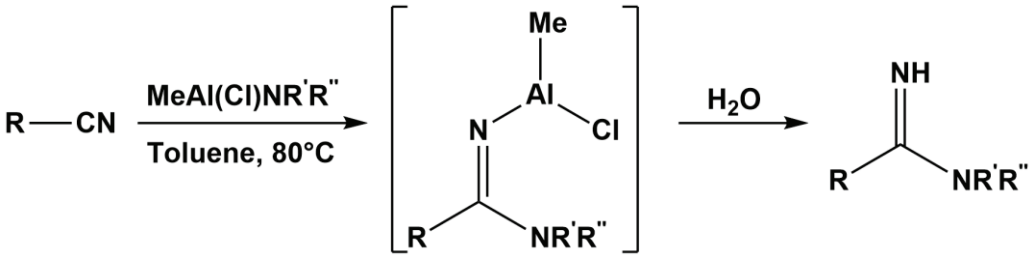

Figure 18 – General reaction of nitriles with alkylchloroaluminium for the synthesis of amides.

The preparation of alkylchloroaluminum amides by mixing ammonium chloride with trimethyl-aluminium in toluene releases lots of heat and can be dangerous if not done properly. Other issues considered on the utilization of Garigipati's reaction rely on the utilization of trimethyl-aluminium, a highly toxic and pyrophoric compound, which decomposes to aluminium oxide in a violent reaction when exposed to air.

So far, the most convenient way to synthesize amidines from nitriles is the reaction with lithium bis(trimethylsilyl)amide (LiHMDS) [89]. The reaction proceeds

under inert atmosphere and anhydrous solvent through mild conditions and leads to the formation of an intermediate, the lithium tris(trimethylsilyl)benzamidine carbanion. This lithium compound was first isolated in 1973 by Sanger. Another critical point is the solvent. Depending on the solvent, the reaction gives different products. In petroleum ether, it forms 1,3,5-s-triazine in small amounts, while in diethyl ether and THF the reaction proceeds to amidine formation. This synthetic route applies to any nitrile lacking an α-hydrogen atom. The presence of an α-hydrogen leads to the formation of a carbanion, which structure can be seen in Figure 19.

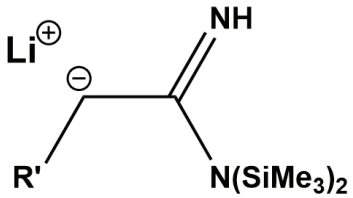

Figure 19 – General structure of a carbanion resulting from reaction of a nitrile containing a α-hydrogen with LiHMDS

The intermediate can react with hydrochloric acid in ethanol to give amidine chlorides in high yields. Reaction with Me_3SiCl in refluxing toluene gives tris(trimethylsilyl)benzamidine [90]. Figure 20 shows the reactions and the formation of the intermediate in the amidine salts synthesis.

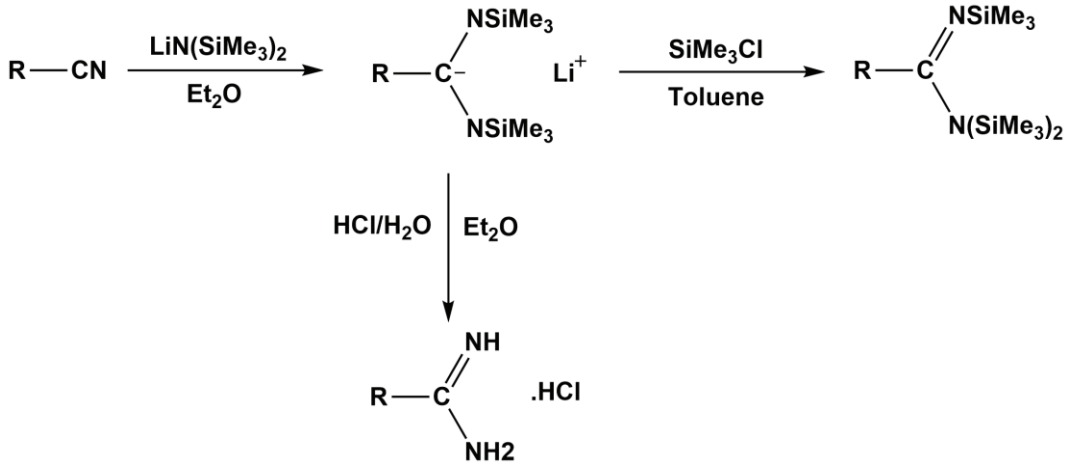

Figure 20 – Synthesis of tris(trimethylsilyl)benzamidine and amidine hydrochloride.

The former reaction presents a very simple and straightforward way to synthesize amidine chlorides from nitriles. Typically, the utilization of such reaction leads to high yields. Moreover, the reaction is selective and allows the utilization of many functionalized nitriles. For these reasons, the reaction of nitriles with lithium

bis(trimethylsilyl)amide was chosen for the synthesis of the amidine chlorides, precursors required for the synthesis of CTFs investigated in this work.

The next section will discuss the main challenges in designing stable and efficient photocatalyst for carbon dioxide reduction.

2.2 CHALLENGES IN DESIGNING A PHOTOCATALYST

Carbon dioxide conversion into valuable products like fuel and chemicals is a crucial reaction for climate change mitigation. The main approaches employed to convert CO_2 include photocatalysis, chemical fixation, hydrogenation, and electrocatalysis. However, using sunlight as a sole source of energy to trigger carbon dioxide reduction is a sustainable way to address the problem.

One electron reduction of CO_2 to $CO_2^{\cdot -}$ is thermodynamically unfavorable due to the high negative redox potential (-1.90V vs. NHE at pH 7). However, the proton-assisted multi-electron reduction is much more favorable considering the relative lower redox potential. Many products can be formed on the photocatalytic CO_2 reduction, including carbon monoxide (CO), formaldehyde (HCHO), formic acid (HCOOH), methanol (CH_3OH), and methane (CH_4). Table 1 gives the photoreduction reactions of CO_2 in aqueous solution at pH = 7 and their reduction potentials with reference to the normal hydrogen electrode (NHE) at 25°C and 1 atm [91].

Table 1 – Photoreduction reactions of CO_2 in aqueous solution at pH=7 and their reduction potentials with reference to normal hydrogen electrode (NHE) at 25°C and 1 atm.

Reaction	Thermodynamic potential (V) vs. NHE
$\mathbf{CO_2 + 2H^+ + 2e^- \rightarrow HCOOH}$	-0.61
$\mathbf{CO_2 + 4H^+ + 4e^- \rightarrow HCHO + H_2O}$	-0.52
$\mathbf{CO_2 + 2H^+ + 2e^- \rightarrow CO + H_2O}$	-0.48
$\mathbf{CO_2 + 6H^+ + 6e^- \rightarrow CH_3OH + H_2O}$	-0.38
$\mathbf{CO_2 + 8H^+ + 8e^- \rightarrow CH_4 + 2H_2O}$	-0.24
$\mathbf{H_2O \rightarrow ½O_2 + 2H^+ + 2e^-}$	+0.82
$\mathbf{2H^+ + 2e^- \rightarrow H_2}$	-0.41

A typical photocatalytic reaction can be explained in terms of four important steps. The first is the absorption of light by a semiconductor and the generation of

electron-hole pairs. The second step is the separation of charges in HOMO-LUMO orbitals (in the case of an organic photocatalyst) or valence-conduction bands (in case of an inorganic semiconductor). Then, the generated charges are transferred to the surface of the photocatalyst. In the last step, redox reactions are triggered by the charges on the surface. Although differences on reaction and mechanism can be observed depending on the system, not all photo-generated charges reach the final step. The recombination of electron-hole pairs is possible, and result in the dissipation of the harvested energy, either in the form of heat (non-radiative) or light emission (radiative), consequently dropping the quantum efficiency (QE). This last one, also known as quantum yield (QY), measures the ratio between the numbers of times a specific event occurs per photon absorbed by the system. In the case of CO_2 photoreduction, the event means the photochemical reaction.

Thermodynamically, the reduction of CO_2 is feasible if the band position of the semiconductor is suitable. Semiconductor should have conduction band (or LUMO orbitals) located at higher or more negative potential than the reduction potential of CO_2 and valence band (or HOMO orbitals) located at lower or more positive than the potential of the other half-reaction, either oxidation of water or the oxidation of a sacrificial compound.

The first photocatalytic carbon dioxide reduction reaction (CO_2RR) was reported by Fujishima *et al.* in 1979 [92]. The group employed a series of heterogeneous inorganic semiconductors (TiO_2, ZnO, CdS, and others) as photoelectrocatalyst to reduce CO_2 in water under light irradiation. Formaldehyde, formic acid, methanol and methane were found as products. After his accomplishment, many scientists pursued in this field, achieving considerable progress on the development of new catalysts. To enhance their activity, strategies were mainly focused on suppressing charge recombination, broaden visible-light absorption and consequently improving the charge utilization of the semiconductor, optimizing the solar energy conversion. Basically, photocatalysts for carbon dioxide reduction can be divided into two main groups: heterogeneous and homogeneous.

According to aspects of the photocatalytic CO_2 reduction, like light harvesting and the photogenerated charge-transfer mechanisms, heterogeneous photocatalysts can be further divided into four: one-step excitation semiconductor, one-step excitation

photosensitized semiconductor, two-step excitation semiconductor heterojunction and, two-step excitation Z-scheme systems [93].

In the first category, one-step excitation semiconductor, the role of semiconductor material is to harvest light, generate and separate the chargers, delivering it to the active site or co-catalyst to trigger the chemical reaction. Typically, co-catalyst utilization improves the photocatalytic activity of heterogeneous semiconductors. When deposited into semiconductor's surface, co-catalyst can improve their activity via two pathways: i) trapping the photogenerated charges (electron/hole pair) enhancing their separation and prolonging the lifetime of charge carriers; ii) directly activating the CO_2 molecule or providing an active intermediate state, lowering the reaction energy barrier for CO_2 reduction. The most widely used co-catalysts include noble metals such as Pt, Au, Pd, Ru, Ir, and Ag, however, due to their high cost and scarcity, alternative earth-abundant metals have been explored.

In the second group, one-step excitation photosensitized semiconductor, the semiconductor acts only as an electron acceptor. Light-harvesting, generation of charges and a further injection of photo-generated electrons into the semiconductor's conduction band is accomplished by a photosensitizing unit, such as organic dyes, metal complexes, or inorganic quantum dots. To close the cycle, the oxidized dye can be regenerated through sacrificing the electron donor or oxidizing water.

The last two groups are coupling systems of two different semiconductors, also called heterojunctions. The position of conduction and valence bands (CB and VB) will determine the direction of charge transfer. In semiconductor heterojunction systems, the electrons are mainly injected to the material with a more positive CB position, while the holes are transferred to the material with a more negative VB position. Usually, electrons and holes are transferred in opposite directions to different semiconductors. Heterojunctions may improve the catalytic activity mainly because they bring a spatial charge separation, which is beneficial for the following CO_2 reduction processes.

The Z-scheme also employs two semiconducting materials. However, the electron/hole flow directions are different than the previews case. Here, a first semiconductor absorbs light to generate the electron/hole pairs, the holes are employed in an oxidation reaction, for example, oxidation of water to oxygen, while the photo-generated electrons are injected into the valence band from the second semiconductor,

neutralizing the holes produced by the second semiconductor. Finally, the electrons generated by the second semiconductor triggers CO_2 reduction. In Z-scheme, the two semiconductors can be connected in series by a conductive medium or through reversible redox shuttles (electron donor/acceptor pairs). Figure 21 shows a schematic illustration of the four common charge separation mechanisms for heterogeneous photocatalytic CO_2 reduction aforementioned.

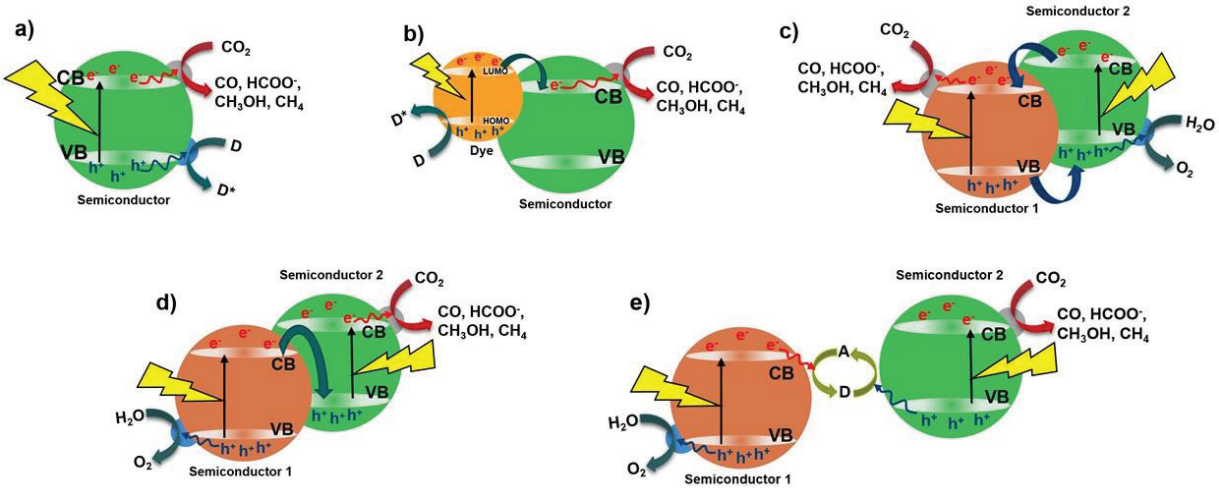

Figure 21 – Schematic illustration of four charge separation mechanisms for photocatalytic CO_2 reduction: a) one-step excitation semiconductor, b) photosensitized semiconductor, c) two-step excitation heterojunction, d) two-step excitation Z-scheme with direct injection, and e) Z-scheme with reversible redox shuttles.

After the seminal work of Fujishima, titanium dioxide has become very popular as heterogeneous photocatalytic for CO_2 reduction. Together with TiO_2, many other semiconductors materials were explored, including metal oxides containing d^0 element (Ti^{4+}, Ta^{5+}, V^{5+}, Zr^{4+}, Nb^{5+}, Mo^{6+}) [94] and d^{10} elements (Ge^{4+}, In^{3+}, Ga^{3+}), d^{10} metal nitride solid solutions, some sulfides [95] like CdS, ZnS, MnS, and others. Even though these semiconductors are thermodynamically able to perform photocatalytic CO_2 reduction, most of them show quite low activities. Such low activity is mainly due to low visible-light absorption and a high recombination rate. Many strategies have been carried out in an attempt to overcome these limitations. Some of them are bandgap structure engineering, oxidative co-catalyst utilization, bandgap doping, morphology structuration, porosity engineering, heterojunction, defect engineering, Z-scheme process, and exposed crystal facets controlling.

A considerable drawback regarding the utilization of these conventional semiconductors as photocatalysts in CO_2 reduction is their very low tunability. On the other side, molecular metal complexes have become very popular as homogeneous

photocatalysts in CO_2 reduction [96]. Their popularity comes mainly from their versatile tuning, for example, of binding sites, functional groups, metal sites, coordination number, and ligand structure. The first application of molecular metal complexes in CO_2 photoreduction dates back to 1980s [97-99]. The earliest attempts showed poor stability, low activity and quantum efficiencies, however, improving metal centers and ligands through the years have dramatically enhanced their potential. Single-site molecular complexes include the utilization of noble metals like Rhenium, Ruthenium, Iridium, Osmium and Rhodium or earth-abundant metals like Iron, Cobalt, Manganese, Nickel and Copper [100]. These organometallic complexes are often composed of one or more π-conjugated binding ligands like bipyridine and its derivatives such as porphyrin. S-containing ligands and thiol-derivatives have also been employed. Typically, the utilization of molecular catalysts in photocatalytic CO_2 reduction leads to high selectivity, producing CO, formic acid (HCOOH) and methane as main products.

In most cases of homogeneous photocatalysts, the active specie has to be used together with a photosensitizer due to the inability of metal complex to generate the charges. A photosensitizer is usually a Ru-based metal complex having a large delocalized π system, which consequently decreases the energy of the highest occupied molecular orbital (HOMO). The molecule absorbs light in the visible spectrum and generates charges that are transferred to adjacent species.

The third component in molecular photocatalyst systems is the electron donor. Also known as sacrificial reagent or sacrificial compound, the electron donor has two functions, first regenerate the photoexcited photosensitizer by donating an electron and secondly, to accept the h^+ generated during the photochemical reaction.

However, if on the one hand, the utilization of a homogeneous photosensitizer increases the activity by enhancing the charge separation, on the other hand, it is a key limitation for long-term reactions. During the photocatalytic process, the photosensitizer often changes ligand or photodegrade, consequently, the catalytic activity is slowed down or even completely lost within less than 12 hours. To overcome this issue, many researchers addressed the utilization of supramolecular structures as catalysts in CO_2 photoreduction. They are composed of two or three metal centers linked together, in which one acts as photosensitizing unit and other as active site. Nevertheless, in long-term reactions, these supramolecular structures still inefficient due to photosensitizer degradation.

Recently, many metal-organic frameworks (MOFs) have been applied in hybrid photocatalytic systems. They are composed of a molecular organometallic catalyst bonded to a functional binding ligand into the material's backbone. Even though MOFs are interesting materials, with a fully tunable chemical and physical composition, allowing the engineering of essential features for photocatalytic carbon dioxide reduction, such as bandgap position and light absorption, these photocatalytic systems still did not show remarkable activity [101].

Another class of porous materials that are attracting growing interest in photocatalytic CO_2 reduction is porous organic polymers (POPs) [102]. The key of their success also relies on the tunability of their properties. By judiciously choosing the building blocks that compose the polymer's structure, it is possible to control aspects like visible light absorption, porosity and the gap between HOMO-LUMO orbitals. Additionally, these materials exhibit higher thermal and chemical stability than MOFs, since they are based on covalent interactions between the building units.

A recent strategy to enhance the stability of these photocatalytic systems consists of heterogenizing a molecular catalysts through macroligands [103]. These last one, consists of a solid acting like ligand in the corresponding molecular complex. The utilization of macroligands bridges homogeneous and heterogeneous catalysts, profiting from both sides. On one hand, the enhanced selectivity and activity from molecular catalysts and on the other hand, the easy handling and separation from working under heterogeneous conditions. Additionally, since a well-known deactivation pathway in homogeneous photocatalysis is the formation of dimers, such strategy increases the stability of complexes due to isolation. Moreover, it also simplifies their recyclability.

Employing this strategy, Wisser *et al.* synthesized two bipyridine-based conjugated microporous polymers (CMPs) as macroligands for heterogenization of molecular rhodium Cp* complex. This complex is well-known to reduce selectively CO_2 to formate in the presence of a photosensitizer and a sacrificial compound under visible-light irradiation [104]. The macroligands were synthesized by copolymerization of two different polyethynyl units (1,3,5-triethynylbenzene and tetrakis(ethynyl-phenyl)methane for BpyMP-1 and -2, respectively) with two different building blocks: 4,4′-diiodo-biphenyl, as connector and 5,5′-dibromo-2,2′-bipyridine, as a functional unit, designed to support the Rh-based complex. Figure 22 shows the structure, reaction and post-synthetic modification for both macroligands.

After the incorporation of different amounts of Rh complex, all materials presented a decrease of nearly half its specific surface area and total pore volume. Although the group has shown from acetonitrile physisorption experiments, that in terms of accessibility, the pore blocking due to the presence of Rh complex is negligible for loadings up to 1,6 wt%. In contrast, for higher loadings, the effect is more pronounced.

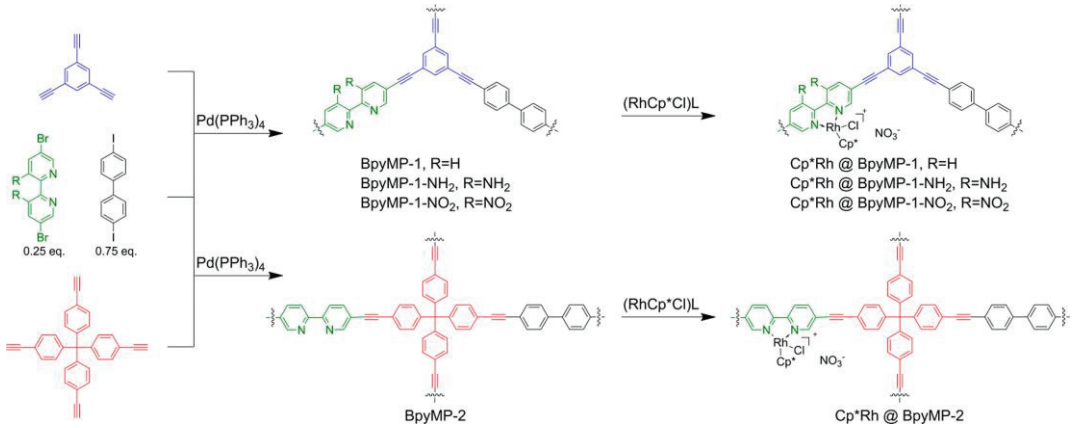

Figure 22 – Synthesis of BpyMP-1 and BpyMP-2 followed by support of RhCp* complex. Adapted with permission from: Wisser, F. M.; Berruyer, P.; Cardenas, L.; Mohr, Y.; Quadrelli, E. A.; Lesage, A.; Farrusseng, D.; Canivet, J. Hammett Parameter in Microporous Solids as Macroligands for Heterogenized Photocatalysts. *ACS Catal*. 2018, 8, 3, 1653-1661.

The reaction was carried out in acetonitrile using 1mmol of $Ru(Bpy)_3Cl_2$ as a photosensitizer, achieving maximum activity of 24.5 h^{-1}, in TOF number, for BpyMP-1 containing 1.6 wt% of Rhodium complex, which lowers upon the increase in the Rh content due to pore blocking. With the same metal loading, BpyMP-2, which is synthesized using a tetrahedral building block, and therefore has a higher specific surface area, presented similar activity. As conclusion, there is no influence from the framework regarding the activity.

Even though the group obtained relevant results, in heterogenizing a molecular metal complex for photocatalytic CO_2 reduction selectively to formate, the activity was still decreasing considerably over time due to photo-degradation of photosensitizer. In another attempt to improve the stability these photocatalytic systems for carbon dioxide reduction, the group employed the MOF MIL-101-NH_2(Al) for heterogenization of Cp*Rh(4,4'-bpydc)Cl]Cl, as active site, and $Ru(bpy)_2$(4,4'-bpydc) as photosensitizing unit (4,4'bpydc = 2,2′-bipyridine-4,4′-dicarboxylic acid) [105]. Both metal complexes were stabilized through two hydrogen bonds, one between the carboxylic acid group from the complex ligand with a terminal water molecule on the inorganic sub-unit and another

with the amino group from the MOF structure. Additionally, π-π interaction between the Cp* and terephthalate helped to stabilize the active metal complex within the metal-organic framework structure. The fully heterogeneous system Rh-Ru-MIL-101-NH_2 achieved a formate production performance of 0.33 μmol within 5 hours of reaction, corresponding to a TOF of 0.6 h^{-1}. The material showed a linear rate of formate production within 10h, slightly decreasing after that. Although the strategy of immobilization of both active site and photosensitizer unit into MOF material resulted in a more selective carbon dioxide photoreduction, the degradation of photosensitizer still an issue on the deactivation process. No leaching was observed during this time, since the main product from the completely homogeneous reaction is hydrogen, not formate, therefore, the only process that could lead to the deactivation of the catalyst is the degradation of the photosensitizer.

To overcome this key limitation for long-term photocatalytic CO_2 reduction, the group recently designed and synthesized conjugated microporous polymers that contain a photosensitizing building block integrated into the framework's backbone [106]. Here, the same active metal complex was used as an active site, rhodium Cp*, however, pyrene and perylene were employed as a photosensitizing unit. The synthesis of these new CMPs, was done through Suzuki coupling reaction, connecting bipyridine, as a chelating functional unit to bind the active molecular catalyst and perylene and pyrene moieties as a photosensitizer. Figure 23, depicts the structure of precursor, the synthesis procedure as well as the structure of the resulting materials after incorporation of RhCp* complex. The materials were named Cp*Rh@PerBpyCMP and Cp*Rh@PyBpyCMP.

Both materials were tested as fully heterogeneous systems for photocatalytic carbon dioxide reduction. The catalytic performance of these materials achieved turnover frequencies of 3 and 6 h^{-1}, for pyrene and perylene-based CMPs, respectively. Although the materials present a relatively low activity in comparison with photosystems that employ both homogeneous catalysts and photosensitizers, the group reported an unprecedented stability. The fully heterogeneous photosystem is active up to 4 days under continuous light irradiation. No degradation of the active sites and photosensitizing material was noticed after the reaction.

With these two materials, the group showed that the all-in-one strategy, when both photosensitizer and chelating unit for heterogenization of molecular catalysts are present in the same material, give rise to fully heterogeneous photosystems with remarkable

stability. Moreover, the properties of the photoactive CMP can be controlled by judiciously chosen the building blocks that compose the framework.

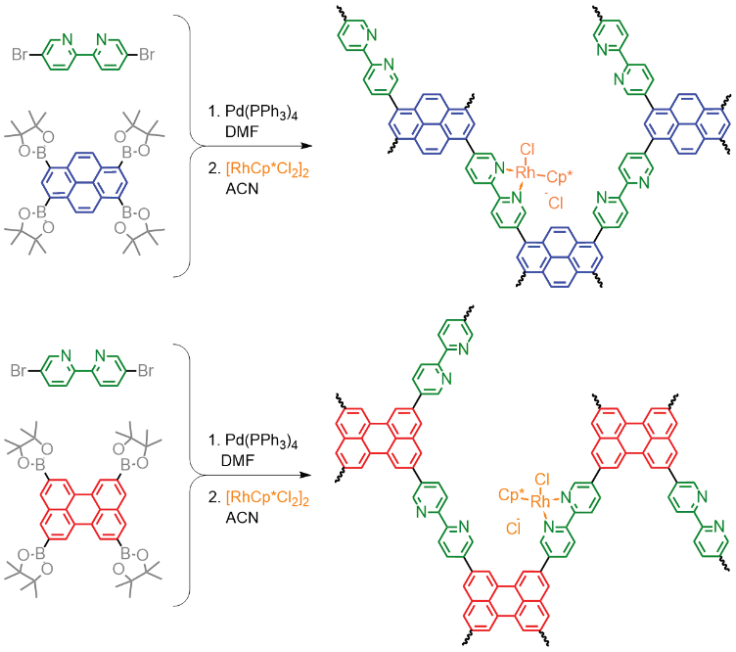

Figure 23 – Synthesis of Cp*Rh@PerBpyCMP and Cp*Rh@PyBpyCMP through Suzuki coupling reaction. Adapted with permission from: Wisser, F.M.; Duguet, M.; Perrinet, Q.; Ghosh, A. C.; Alves-Favaro, M.; Mohr, Y.; Lorentz, C.; Quadrelli E. A.; Palkovits, R.; Farrusseng, D.; Mellot-Draznieks, C.; Waele, V.; Canivet, J. Molecular Porous Photosystems Tailored for Long-Term Photocatalytic CO_2 Reduction. https://doi.org/10.1002/anie.201912883.

To conclude, the design of a photocatalytic system for CO_2 reduction is a complex task that mainly targets materials with enhanced activity, selectivity, and stability. For this purpose, the development of suitable materials is required. Between many possibilities, designing a photocatalysts might include the precise control over features like bandgap size, HOMO-LUMO positions, light-harvesting property, process of charge separation, and electron conductivity. Moreover, the main limitations for long-term stability and high activity could be addressed, like charge recombination and photodegradation of photosensitizing units. Although the development of photocatalysts and photocatalytic processes for CO_2 reduction evolved considerably over the last decades, there still big challenges to overcome.

2.3 CHALLENGES IN CHARACTERIZATION

The characterization of porous organic polymers is a real ongoing challenge [107]. All the issues in elucidating the structure and morphology of porous organic polymers are related to the lack of long-range order as well as the high chemical stability of these

materials. Solving the structure in order to establish activity-structure relationships is a difficult task, especially considering amorphous materials.

Many different techniques can be applied in the elucidation of material's structure, and although there is not a limitation on the number of techniques employed in the characterization, some techniques are used more often than others and will be discussed below.

Certainly, x-ray techniques are the most frequently used in the characterization of porous organic polymers. They provide precise insights on the long-range organization of the framework, but require crystalline materials. In the case of CTFs, most of the reported materials are amorphous, though it is possible to find some examples of crystalline polymers. In amorphous materials, the technique can be useful to speculate on the structure. Because of the intrinsic angles of triazine linkages, most CTFs have a similar hexagonal structure, making it easier to simulate primary crystal structure. Comparing the ideal model with the experimental spectra, gives insights and helps in the elucidation of the structure. It is possible, for example, to study the stacking position of a bi-dimensional materials. X-ray diffraction is one of the most common analyses done in CTFs, even to prove the lack of order and amorphous nature of these solids.

The porous properties of such polymers can be elucidated by gas physisorption. Despite nitrogen and argon, that are the most common gasses employed in this analysis, gasses such as CO_2 or ammonia can also be used. However, the utilization of these last two gasses is more focused on the application of porous polymers as adsorbent. Physisorption analysis gives essential information about surface area, pore size distribution, pore volume, and depending on the case, even the shape of the pore structure can be elucidated. Porosity is crucial in some applications. In catalysis, for example, porosity assures the accessibility of the reactants to the active sites. Substantial part of the scientific publications about porous polymers report porosity in terms of superficial area. Despite many efforts to create a standard procedure to analyze physisorption data, there is still not a definite method. The superficial area can be calculated by different methodologies. The most common is the BET (Brunauer-Emmett-Teller) theory. Although the utilization of BET theory is widely employed to calculate and express the superficial area of determined porous materials, the theory presents some limitations on the calculation of surface area, especially for microporous materials. The BET theory considers the adsorption of infinite layers of adsorbate, however, this is not true for

microporous materials, in which the confined spaces and constrict pores would allow the formation of a few layers but not infinite. Additionally, there are some insights that adsorption in microporous materials happens by pore filling and not by layers formation. Even with these limitations, BET theory still the most common method employed on the calculation of surface area for porous materials.

Furthermore, one of the most employed analysis of porous organic polymers is Fourier-transform infrared (FT-IR) spectroscopy. FT-IR allows to determine the characteristic stretching and vibrating modes of different functional groups within the material's framework. In the case of CTFs, FT-IR is often focused on the triazine main vibrations, around 1510 and 1350 cm^{-1}, corresponding to C=N and -C-N- stretching vibrations, additionally to the breathing mode of the ring around 815 cm^{-1}, in which all carbons and nitrogen vibrates into the same direction at the same time, moving forward and backward like a lung breathing. Moreover, since nitrile (C≡N) are usually precursors for the synthesis of CTFs, the band in the region of 2260-2222 cm^{-1} is also frequently investigated. Comparing the spectra of the precursors with the final material can give additional insights into the triazine formation mechanism. Furthermore, the degree of polymerization can be speculated since it is possible to check the stretching vibrations of the precursor or unreacted terminal functions that potentially leading to defects [108].

Transmission electron microscopy (TEM) and scanning electron microscopy (SEM) are also techniques commonly used in the characterization of porous materials, mainly to determine the morphology and get additional insights into the material's structure. However, organic porous polymers are typically insulators, despite the extended conjugated π-electron system, therefore, using higher voltages for high-resolution images can decompose the organic material, resulting in issues to determine morphology and the exact size of host species. In addition to the image analysis, energy dispersive X-ray (EDX) spectroscopy is often done to assure the elemental composition of the material. In the case of a supported catalyst, EDX analysis is a valuable tool to get qualitative information on the dispersion.

Another very useful technique on the evaluation of chemical composition is X-ray photoelectron spectroscopy. In practice, it is a surface technique, based on the photoelectric effect, discovered by Heinrich Hertz in 1887, and later explained by Albert Einstein in 1905. Essentially, XPS consists of irradiating a sample with x-ray and then collect the emitted photoelectrons. Measuring the kinetic energy and the number of

electrons that escape from the 10 - 20 nm depth on the surface of the sample, it is possible to construct a graph of number by kinetic energy, and identify the elements present in the sample. All the elements can be detected and quantified, with exception to hydrogen and helium. Although it is a very useful technique, it only measures the surface, which in the case of porous organic polymers can be an issue. Mainly because the surface of a polymer's particle might have a different composition than the bulk since terminal or unreacted functional groups might be at the surface. No doubts that it is a valuable technique to study supported catalysts, for example, the oxidation state of metallic complex immobilized into a functional porous organic polymer can be identified with precision, but the results have to be carefully analyzed since the technique does not provide information on the bulk material.

Despite the fact that the characterization of amorphous porous organic polymer presents some challenges, and it is possible to get insights into the complex polymeric structure, some still remain. One of them regards the utilization of porous organic frameworks as support for molecular catalysts. In this particular case, even though it is possible to make a correlation with the mechanism from the homogeneous counterpart, establishing a consistent mechanistic study to prove not only the ongoing reaction mechanism but the real active species and its interactions within the surrounding framework, is a complex task.

Additionally to the difficulty in understanding the real nature of the active site, most porous organic polymers present a very dynamic behavior. The polymer structure of these materials can twist, bend and turn their shape, depending on the external stimulus. So understanding that the characterization techniques described above, and the condition they are measured, does not reflect the real behavior of dynamic materials like CTFs and other classes of porous organic polymer. It can, in fact, elucidate and give insights into the material structure and its behavior under certain conditions, however, properly understanding the framework system is a key aspect for further optimizations, and these aspects are still to be addressed.

2.4 ADDRESSING THESE CHALLENGES

The synthesis of CTFs through condensation present challenges in many aspects. First, the synthesis of precursors that are not reported in the literature, secondly to design

a suitable material for the targeting application, photocatalytic CO_2 reduction. Lately, the challenge to properly characterize the final materials.

In the first challenge, the synthesis of precursors started by attempting to reproduce what is described in the literature so far: the synthesis of CTFs based on the condensation of terephthalamidine chloride and terephthaldehyde. In this way, the synthesis of amidine precursors was done using the same starting materials described previously, by reacting terephthalonitrile with LiHMDS in anhydrous THF under an inert atmosphere. The synthesis of these precursors was carried out in a systematic fashion, in order to identify the main advantages and limitations of this method. Furthermore, the same reaction protocol was extended to produce functionalized building blocks. Both bipyridine-based amidine and aldehyde monomers were synthesized. The aldehyde was already reported and can be synthesized by a variety of different reactions. However, the synthesis of compound 5,5′-diamidine-2,2′-bipyridine dichloride, is not reported in the literature. In the same way, this bipyridine-based amidine precursor was synthesized in a systematic fashion in order to identify possible by-products and impurities.

Secondly, the design of a photocatalyst was done according to the "all-in-one" strategy, reported recently. In his study, Wisser *et al*. showed that such strategy leads to a very stable photocatalyst with unprecedented stability, overcoming one of the key limitations for low stability in photocatalytic carbon dioxide reduction process: the utilization of a homogeneous photosensitizer [106]. So taking advantage that only the condensation approach leads to photoactive bipyridine-based CTFs, the "all-in-one" strategy was employed for the synthesis of a material that possess both the heterogeneous photosensitizing building block and the chelating unit, that will later support the homogeneous molecular catalyst.

As stated before, depending on the synthetic procedure, the final covalent triazine framework will present different attributes and features. Therefore, it is vital to investigate new methods of synthesis in order to achieve highly active, selective, and stable photocatalysts for CO_2 reduction. It is crucial to highlight that the material designed in this project, the bipyridine-based CTFs, can only be obtained through condensation. Since the ionothermal method often produces carbonized materials, unsuitable for photocatalysis, and, although the utilization of acidic approach leads to the synthesis of photoactive materials, this method does not work for pyridine derivated building blocks. Therefore, the option for using the condensation approach for the synthesis of bipyridine-

based CTFs was clear. Additionally, this project aims to investigate the polycondensation method as a way to enhance the control and precision over the synthesis of CTFs.

The challenge of characterizing the structure of the resulting CTFs will be addressed by combining the results of two or more analyses. This way it is possible to speculate on the structure and formulate the hypothesis that satisfactory explain the experimental behaviors of the samples.

One example is the combination of the results obtained in both XRD and nitrogen physisorption analysis in order to get insights into the stacking positions of these materials. Owing to the partially layered structure, when CTFs are synthesized through condensation, the stacking position of these materials is a critical feature. Typically, a material based on stacked bidimensional sheets is described in terms of different positions the layers can assume. The most common stacking positions are AA and AB. In the case of the AA position, the first layer is exactly in the same position as the subsequent one.

On the other hand, AB stacking position describes a material in which the first layer is completely shifted from the subsequent one. In the case of CTFs, if AB stacking is predominant, it would result in a material in which the triazine unit from the first layer would be located exactly in the center of the vacancy from the next layer. Moreover, Heine *et al*., demonstrated the existence of two more stacking positions for layered materials [109]. These positions will mostly depend on the strength of intramolecular forces that plays a role during the synthesis of the polymer. Depending on the bi-dimensional arrangement of these layers, the CTF will present completely different properties and features. Even though only computational analysis can give details on the exact position the layers are organized, combining the results obtained in both XRD and nitrogen physisorption analysis can elucidate the predominant stacking positions of these materials. For instance, a layered material stacked in AB position would have a much dense structure, since AB represents a better-packed form of a bi-dimensional polymer.

As a consequence of the shifting in the layers, the material would also present a low specific surface area, due to pore blocking, caused by the intercalated layers. On the other hand, from a material in which the AA stacking position is predominant, the opposite behavior would be expected. Such material would have layers located in the same position, aligning their vacancies and boosting the specific surface area.

Combining the results of two or more different characterization techniques is a way to address the main challenges regarding the evaluation of the CTF structure. Since two different techniques can give insights in the same direction, their results can be used in a way to complement one another. Like the combination of nitrogen physisorption and XRD, results obtained in FT-IR and solid-state NMR can give insights on the polymerization degree of these materials. Both techniques are able to show the formation of triazine moiety after reaction as well as identify unreacted precursors that can further lead to defects in the final framework.

In the next chapters, the results will be presented and discussed. They were divided into four chapters: chapter three will discuss the synthesis and characterization of all precursors employed in the synthesis of the materials described in this project, chapter four, is focused on discussing the synthesis, characterization and further optimization of CTFs through condensation. Chapter five describes the synthesis, characterization and further application of bipyridine-based CTFs in photocatalytic CO_2 reduction. The following chapter six, will discuss the synthesis, characterization, and application of porphyrin-based CTFs also developed during this project.

CHAPTER 3: SYNTHESIS OF PRECURSORS

3. SYNTHESIS OF PRECURSORS

The synthesis of precursors is divided according to their structure. Up to now, only CTFs based on the condensation of terephthalamidine were reported. So the phenyl-based building blocks were the first to be synthesized. Further, with the attempt to synthesize CTFs with functionalized building blocks, bipyridine and biphenyl-based precursors were addressed. Furthermore, since our main goal is the utilization of these CTFs as photocatalysts, other functionalized building blocks like porphyrin were considered during the project and will be described at the end of this section.

3.1 PHENYL-BASED PRECURSORS

In order to understand and investigate the role of the polycondensation approach in the synthesis of Covalent Triazine Frameworks, the first materials addressed in this project were based on a reaction between terephthalamidine chloride and terephthaldehyde. Their structures are depicted in Figure 24.

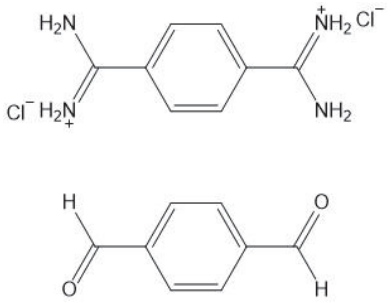

Figure 24 – Structure of phenyl-based precursors: terephthalamidine chloride (up) and terephthaldehyde (down).

The aldehyde is available commercially and was bought from abcr. The compound was used as received. On the other hand, terephthalamidine had to be synthesized. The synthesis of terephthalamidine chloride was done by reacting the commercially available 1,4-dicyanobenzene with Lithium bis(trimethylsilyl)amide in dry THF. Following the previews procedure [30], the nitrile was mixed with dry THF under a nitrogen atmosphere. After complete dissolution, the mixture was cooled to 0°C in an ice-water bath and 1M LiHMDS solution in THF was added dropwise over 15 minutes. After complete addition, the reaction was allowed to stir at room temperature for 3 hours. After this time, the reaction was once again cooled to 0°C in an ice-water bath, and HCl

in ethanol was added dropwise to quench the reaction. The mixture was set aside overnight. Further details can be found in appendix page 226.

The white precipitate was then filtrated and washed with THF and ether, to afford crude terephthalamidine chloride. The compound showed high solubility in water, DMSO, and DMF. In the beginning, yields higher than 100% were obtained, pointing out that the compound was not pure. In order to verify the structure and the possible impurities, liquid ^{1}H NMR was recorded in deuterated DMSO. The result is depicted in Figure 25.

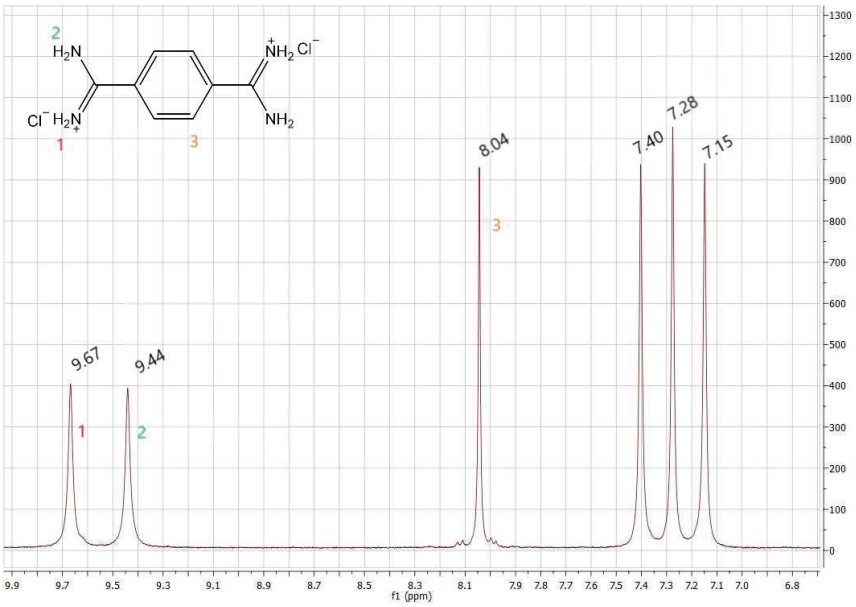

Figure 25 – ^{1}H-NMR spectrum of terephthalamidine chloride, recorded in d_6-DMSO.

According to the spectra, the first two signals can be assigned to the hydrogens at the amidine function. They have chemical shifts of 9.67 and 9.44 ppm. Moreover, a small shift from the previously reported synthesis was found, the same hydrogens were reported to have chemical shifts of 9.63 and 9.37 ppm, respectively. Additionally, the hydrogens from the phenyl group can be assigned to the signal at 8.04, in accordance with the ^{1}H-NMR previously reported. However, a prominent triplet can be found at 7.28 ppm. Such a signal was not reported in the synthesis of terephthalamidine chloride. Possibly, the triplet comes from a by-product, changing the final yield and, if interacting with the amidine functionality, changing the chemical shift from the reported NMR.

In an attempt to purify the compound, recrystallization was done using an ethanol/water mixture. 0.5 grams of the crude product was added into 20 mL of ethanol/water mixture at 1:1 volume ratio. The mixture was heated until boiling point for

10 minutes, then cooled down to room temperature. The solid was filtrated and dried in the oven at 80°C. Liquid ^{1}H-NMR from the recrystallized sample was recorded in deuterated DMSO, and once again, the triplet at 7.28 ppm was found. To verify the elemental composition of samples before and after the recrystallization, CHN analysis was performed. The samples were measured more than one time. The results are presented in Table 2.

Table 2 – Elemental analysis of terephthalamidine chloride before and after recrystallization.

SAMPLE	RUN	WEIGHT (mg)	CARBON (%)	HYDROGEN (%)	NITROGEN (%)
terephthalamidine chloride	1	1.432	23.1	6.5	23.2
terephthalamidine chloride	2	1.549	22.5	6.5	22.2
terephthalamidine chloride recrystallized	1	1.945	5.5	7.6	24.7
terephthalamidine chloride recrystallized	2	1.910	15.3	6.9	22.9
terephthalamidine chloride recrystallized	3	1.934	23.1	6.5	22.6

From the results in Table 2, both samples, especially the one measured after the recrystallization, were found to be very inhomogeneous. The elemental composition of the recrystallized therephthalamidine chloride showed carbon contents varying from 5.5 to 23%. In conclusion, the sample is not pure and the recrystallization procedure did not show satisfactory results in the purification of this compound.

The purification of amidine salts is not frequently reported in the literature. Attempts to purify the compound by traditional separation methods like flash column chromatography failed to obtain a pure compound. According to the experiments, the by-product, produced together with amidine, which can be seen in the liquid ^{1}H-NMR as a triplet, has the same solubility than the amidine, resulting in very poor separation in the case of column chromatography and persistent contamination in the case of recrystallization.

Inspired by the work of Morshedi and co-workers [110], in which the group synthesized supramolecular frameworks based in amidinium compounds with different counter-anions, the attempt to purify terephthalamidine chloride was done by changing its counter-ion in order change their solubility, seeking to separate the amidine from the

impurity. According to Morshedi *et al.* study, amidine chloride, bromide and nitride have high solubility in water, while amidine tetraphenylborate is completely insoluble.

Since amidine containing organic counter-ions might give insoluble compounds in water, the first attempt to change the counter-ion of terephthalamidine chloride was done by using sodium hexafluorophosphate. The reaction was done by simply mixing the amidine chloride in water with an excess of $NaPF_6$. However, no precipitated was observed. Following the same approach employed by Morshedi *et al.* the next attempt was made using $NaBPh_4$. Both amidine chloride and sodium tetraphenylborate salts were solubilized separately in water to form clear solutions. When mixed, a white compound readily precipitates. This compound was identified as terephthalamidine tetraphenylborate. To confirm the structure, the ^{1}H-NMR was recorded in deuterated DMSO. Figure 26 depicts the resulting spectrum.

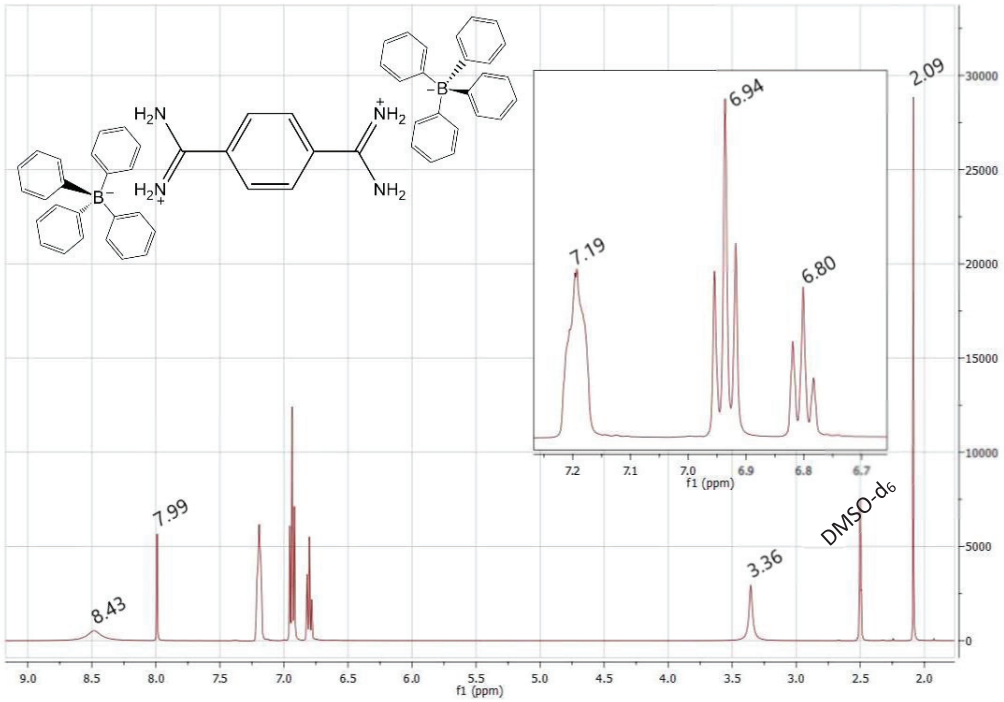

Figure 26 – ^{1}H-NMR spectrum of terephthalamidine tetraphenylborate, recorded in d_6-DMSO.

As evidenced, the signal at 8.43 and 7.99 ppm, belongs to the hydrogens from the amidine function and phenyl group, respectively. It is interesting to notice the signal broadening from the hydrogen located in the amidine function. Such behavior can be explained through proton exchange since remaining water can be found in the system, confirmed by the signal at 3.36 ppm. The signal showed in detail both triplets at 6.80 and 6.94 ppm and the broad peak at 7.19 can be assigned to the hydrogens in para, meta and

ortho position in the phenyl ring from tetraphenylborate counter-ion. The signal at 2.09 ppm belongs to the remaining acetone, used to wash the amidine chloride after the synthesis.

From liquid ^{1}H-NMR, it can be noticed that the impurity leading to the triplet at 7.28 ppm is no longer contamination in the sample. However, since the tetraphenylborate anion has a big radius, there could be influence from the counter-ion over the porous properties of CTFs. Steric effects could lead to pore blocking and consequently lower the specific surface area. Therefore, the counter-ion was again changed, this time to bromide. Since terephthalamidine tetraphenyl borate is very soluble in acetone, the counter-ion exchange was done using acetone as solvent and tetrabutylammonium bromide as a counter-ion source. After the complete addition of the salt into the homogeneous solution of amidine tetraphenylborate, a pale solid started to precipitate. The fine powder was filtered off and washed with acetone and THF. To confirm the structure, liquid ^{1}H-NMR was recorded in deuterated DMSO, the spectrum is depicted in Figure 27.

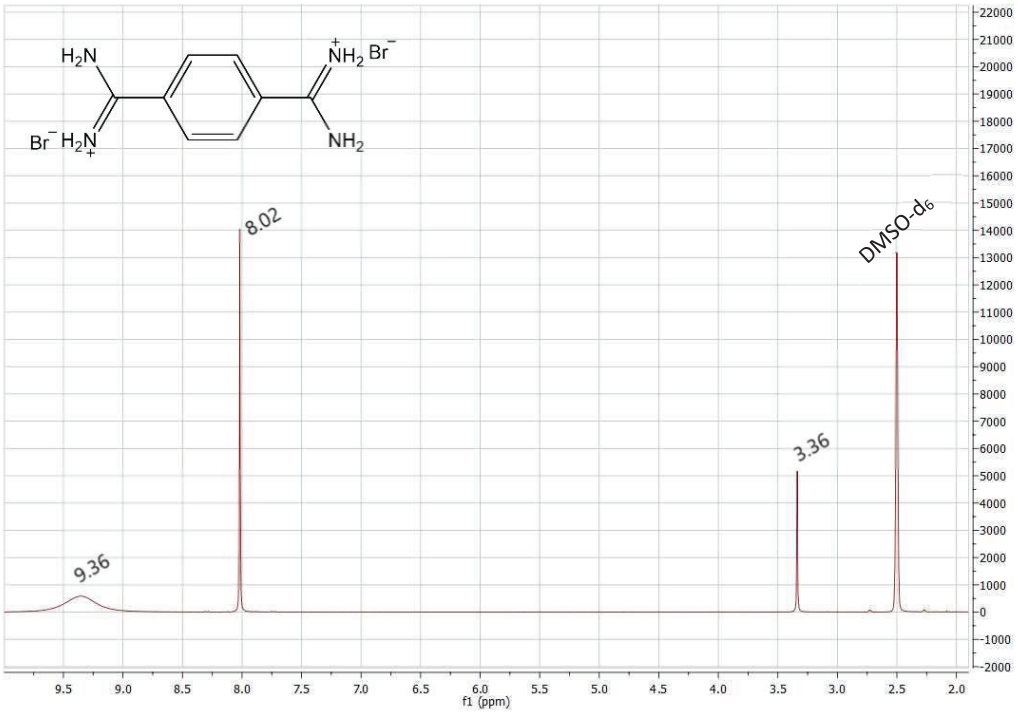

Figure 27 – ^{1}H-NMR spectrum of terephthalamidine bromide, recorded in d_6-DMSO.

As can be found in Figure 27, the signals at 9.36 and 8.02 ppm belongs to the hydrogens in the amidine function and the phenyl moiety, respectively. The signal at 3.36 ppm belongs to the remaining water.

As a conclusion, the synthesis of phenyl-based monomers, especially the amidine chloride, was successfully carried out through the addition of LiHMDS to nitrile precursor. Although recrystallization and flash column chromatography did not work well for the purification of these starting materials, the pure compound was obtained by exchanging the counter-ion of amidine. The by-product that leads to the prominent triplet signal in liquid ^{1}H-NMR will be investigated. All these terephthalamidine compounds were employed as precursors on the synthesis of covalent triazine frameworks through condensation. The results and discussions regarding the synthesis of the materials will be described in chapter 4.

3.2 BIPHENYL-BASED PRECURSORS

Another goal of this project is the synthesis of functionalized CTFs for heterogenization of homogeneous photocatalyst. For this purpose, a series of bipyridine-based covalent triazine framework was designed. Moreover, in order to show the potential of the polycondensation approach in the synthesis of CTFs, the content of bipyridine ligand within the framework was intentionally controlled. For this reason, together with the bipyridine, biphenyl-based precursors were employed as a non-functionalized building block. The option for biphenyl as precursors, together with bipyridine, rely on the length os the ligand. Since both have the same size, the CTFs synthesized containing biphenyl and bipyridine ligands would result in a material with a symmetric pore structure. The synthesis of CTFs through condensation demanded the starting compounds, 4,4'-biphenyldiamidine chloride, 4,4'-biphenyldicarboxaldehyde, 5,5′-diamidine-2,2′-bipyridine dichloride and 5,5′-diacarbaldehyde-2,2′-bipyridine. This section will describe the synthesis of biphenyl-based precursors, while section 3.3 presents the synthesis of bipyridine-based building blocks.

In the case of biphenyl-based monomers, the aldehyde 4,4'-biphenyldicarboxaldehyde is commercially available and was bought from Tokyo Chemical Industry (TCI) and used as received. The synthesis of 4,4'-biphenyldiamidine chloride, was done using the same reaction as described for terephthalamidine, a reaction between nitrile and LiHMDS. The nitrile precursor, 4,4′-biphenyldicarbonitrile, is commercially available, it was bought from Sigma Aldrich and used as received.

The complete experimental procedure for the synthesis of 4,4'-biphenyldiamidine chloride can be seen in appendix page 227. The pale white solid resulting from the reaction between 4,4′-biphenyldicarbonitrile and LiHMDS was filtered off after quenching the reaction with hydrochloric acid in ethanol. In order to analyze its structure, liquid ^{1}H-NMR was recorded in deuterated DMSO. The spectrum is depicted in Figure 28.

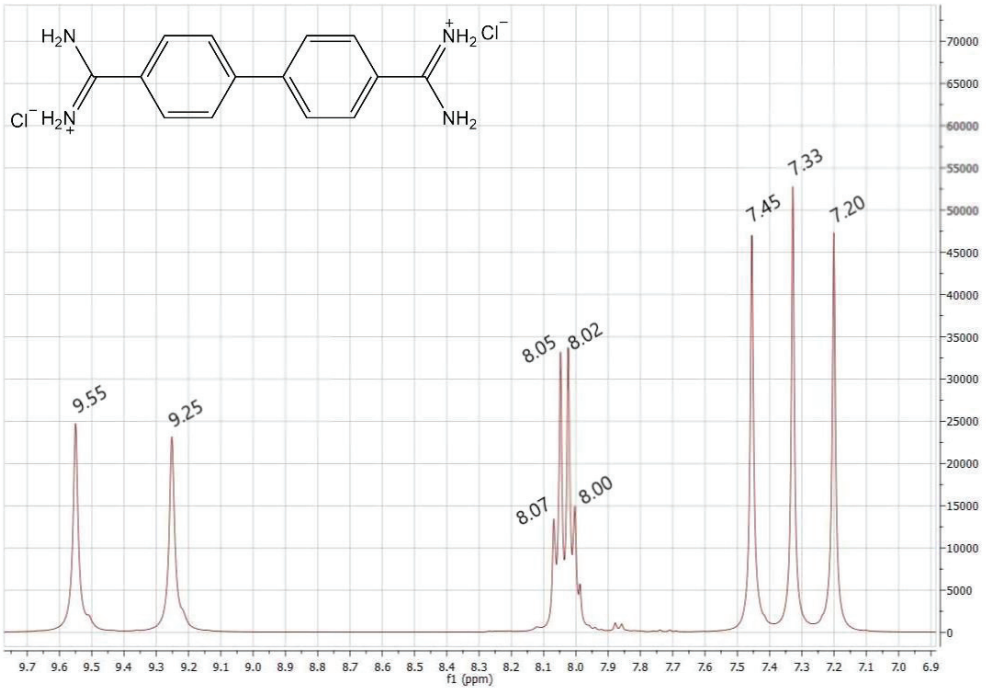

Figure 28 – ^{1}H-NMR spectrum of 4,4'-biphenyldiamidine chloride, recorded in d_6-DMSO.

From the ^{1}H-NMR spectrum, the signals at 9.55 and 9.25 ppm can be assigned to the hydrogens from the amidine function. The quartet at 8.05 ppm can be assigned to the hydrogens from the phenyl ring. Additionally, the same triplet signal coming from a by-product can be noticed at 7.33 ppm, in a slightly higher chemical shift than in the case of terephthalamidine synthesis.

Once again, aiming to purify the compound, the counter-ion was changed from chloride to tertraphenylborate and later to bromide. Figure 29 depicts the spectra of the resulting 4,4'-biphenyldiamidine tetraphenylborate.

From the ^{1}H-NMR spectrum, it is possible to see the pattern signals from the tetraphenylborate in detail. The pattern contains three signals: two triplets at 6.80 and 6.94 ppm and one broader signal at 7.19 ppm. They correspond to hydrogens in para, meta and ortho positions from the tetraphenylborate counter-ion, respectively. The double

doublets at 7.97 and 8.04 ppm can be assigned to the hydrogens in the phenyl ring, while the broad signals at 9.01 and 9.31 ppm can be assigned to both hydrogens in the amidine function. The broader feature is due to proton exchange with water. Moreover, no signal from impurity can be observed.

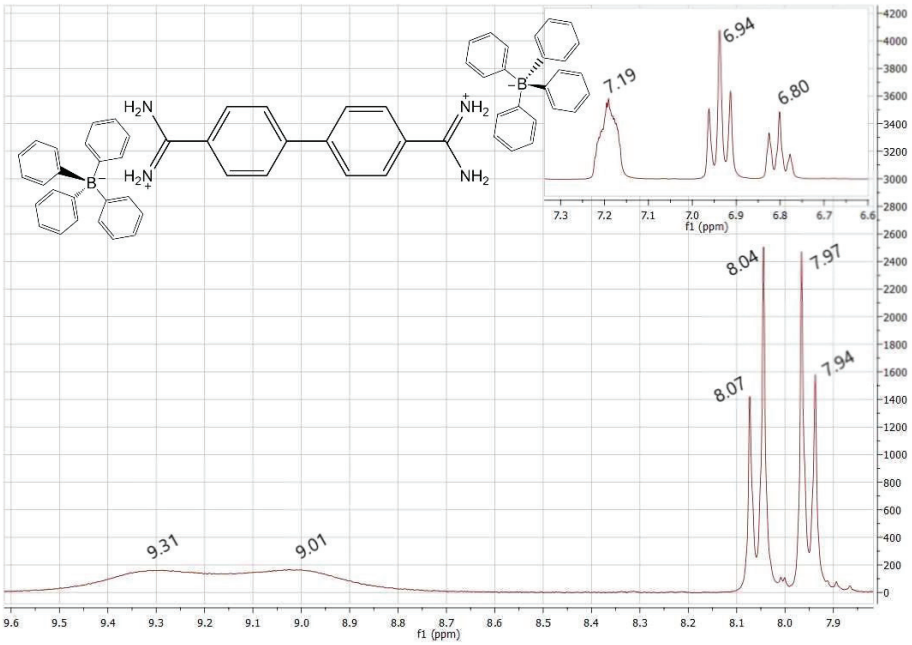

Figure 29 – ^{1}H-NMR spectrum of 4,4'-biphenyldiamidine tetraphenylborate, recorded in d_6-DMSO.

In the last reaction, the counter-ion of 4,4'-biphenyldiamidine was exchanged from tetraphenylborate to bromide. The exchange was done in acetone. The complete experimental procedure is described in appendix page 227. Figure 30 shows the ^{1}H-NMR spectrum from 4,4'-biphenyldiamidine bromide.

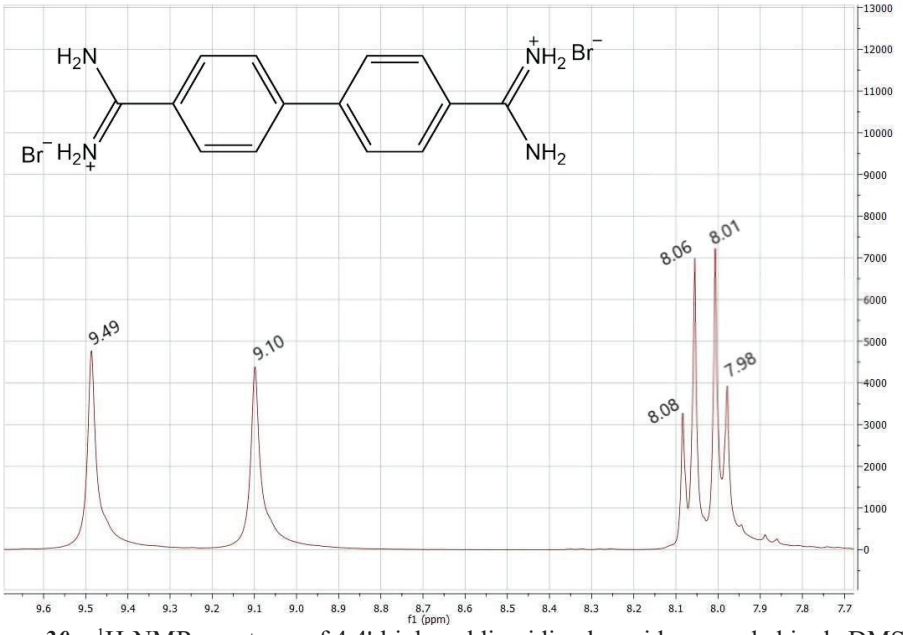

Figure 30 – ^{1}H-NMR spectrum of 4,4'-biphenyldiamidine bromide, recorded in d_6-DMSO.

In the spectrum of 4,4'-biphenyldiamidine bromide, it is possible to see only the signals relative to the amidine. No signals from by-products are observed. Signals at 9.49 and 9.10 ppm are assigned to the hydrogens from the amidine function, while the double doublets at 8.01 and 8.06 ppm are assigned to the hydrogens in the phenyl ring.

All these biphenyl-based monomers were successfully synthesized by reacting the nitrile precursor with LiHMDS and further exchanging their counter-ion. Furthermore, the by-product that leads to a triplet signal in the liquid ^{1}H-NMR could be found in the synthesis of biphenyl precursors and still unidentified. Once again, the strategy of exchanging the counter-ion to purify the amidines worked well. All the monomers synthesized in this section were employed as a non-functionalized building block and together with the bipyridine, these ligands were used in the synthesis of a series of covalent triazine frameworks containing different amounts of chelating monomer. The synthesis of these materials will be described in chapter 5. The next section will describe the synthesis of precursors based in bipyridine.

3.3 BIPYRIDINE-BASED PRECURSORS

Since the synthesis of CTFs through condensation is based on the reaction of aldehyde and amidine chloride, two main compounds are required: 2,2'-bipyridine-5,5'-dicarboxyaldehyde and 5,5′-diamidine-2,2′-bipyridine dichloride. The aldehyde can be synthesized in many ways. In the beginning, it was synthesized through Kornblum oxidation of 5,5′-bis(bromomethyl)-2,2′-bipyridine in microwave [111]. The complete pathway can be seen in Figure 31.

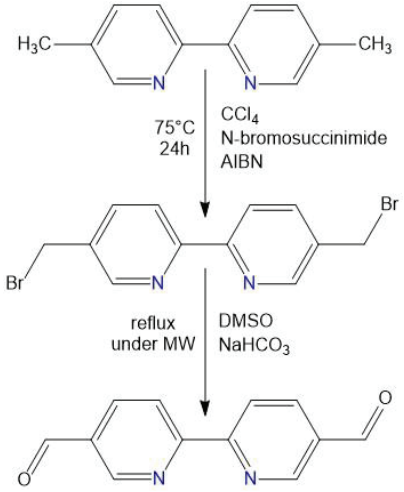

Figure 31 – Pathway for the synthesis of 2,2'-bipyridine-5,5'-dicarboxyaldehyde through microwave-assisted Kornblum oxidation.

The synthesis of the aldehyde started with the bromination of commercially available 5,5′-dimethyl-2,2′-bipyridine in tetrachloromethane (CCl_4) and using N-bromosuccinimide as bromine source. The complete procedure is described in the appendix, page 222. The ^{1}H-NMR of the resulting compound is shown in Figure 32. Signals at 8.61, 8.35 and 7.80 ppm can be assigned to hydrogens from carbons C5/5', C2/2' and C3/3' from the bipyridine, respectively. The signal at 4.47 ppm is assigned to the methyl group from the aliphatic part. Small signals below 4 ppm can be assigned to residual solvents and remaining by-products from the reaction.

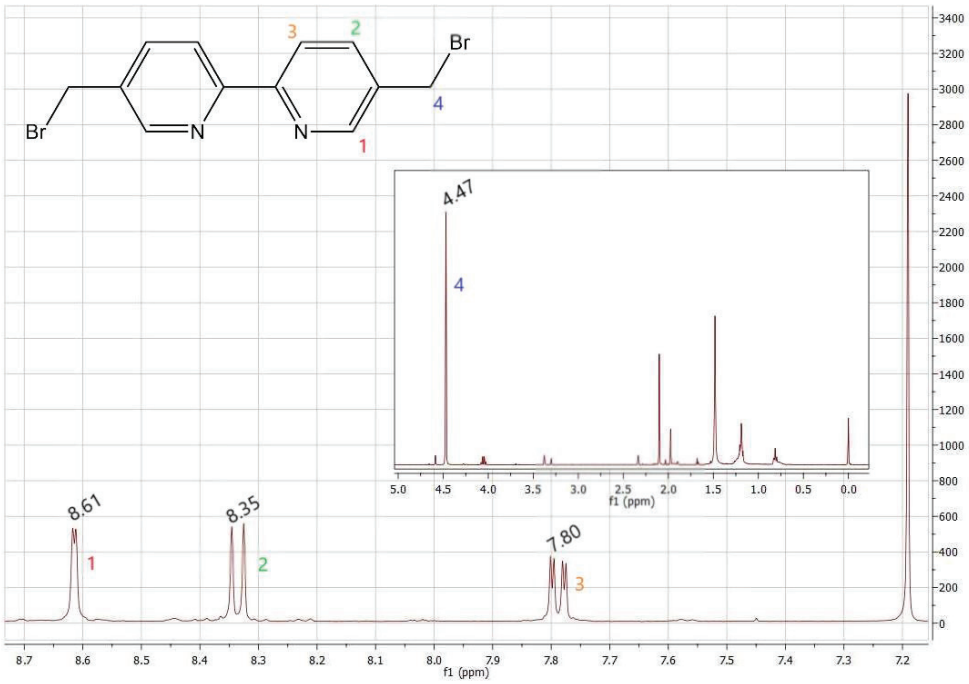

Figure 32 – ^{1}H-NMR spectrum of 5,5′-bis(bromomethyl)-2,2′-bipyridine, recorded in $CDCl_3$.

After the synthesis of 5,5′-bis(bromomethyl)-2,2′-bipyridine, the compound was oxidized to the aldehyde using a microwave-assisted Kornblum reaction. A mixture of DMSO, $NaHCO_3$, and 5,5′-bis(bromomethyl)-2,2′-bipyridine was set to reflux under microwave irradiation. After the reaction was completed, water was added to the system, and the mixture extracted with toluene. The combined organic extracts were washed with brine, and the solvent was evaporated. The crude product was purified by chromatography (n-hexane/ethyl acetate in a volume ratio of 10:1). Figure 33 depicts the liquid ^{1}H-NMR from the corresponding aldehyde, recorded in deuterated chloroform.

As can be noticed from the ^{1}H-NMR spectrum, the signals from bipyridine shifted to higher values. Signals at 9.17, 8.72, and 8.34 ppm can be assigned to hydrogens from

the bipyridine moiety, following the same pattern, from hydrogens in carbons C5/5', C2/2' and C3/3', respectively. In higher chemical shifts, the signal at 10.21 ppm is assigned to the aldehyde function. Signals below 7 ppm are not showed in the Figure, however, they belong to residual solvents. Minimal impurities can be seen close to double doublet at 8.34 ppm and can be assigned to the remaining starting material.

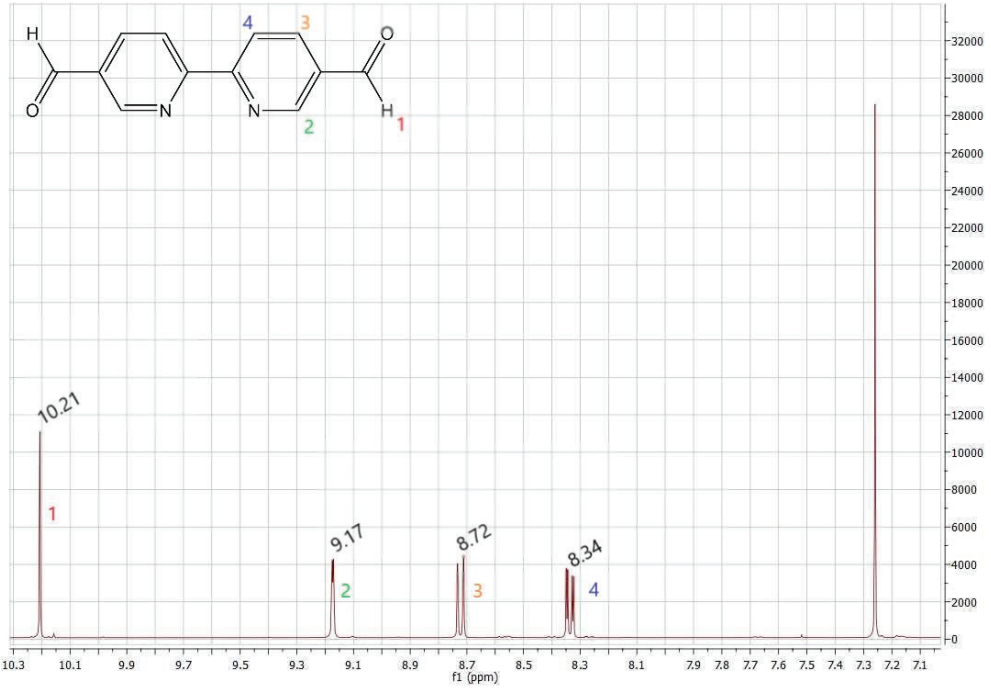

Figure 33 – ^{1}H-NMR spectrum of 2,2'-bipyridine-5,5'-dicarboxyaldehyde, recorded in $CDCl_3$.

Although the synthesis of 2,2'-bipyridine-5,5'-dicarboxyaldehyde has been carried out successfully through microwave-assisted Korblum oxidation, the synthesis of the precursor 5,5′-bis(bromomethyl)-2,2′-bipyridine require the utilization of tetrachloromethane, a compound widely employed in the past as precursor for Chlorofluorocarbons (CFCs) production. Additionally, CCl_4 is both ozone-depleting and greenhouse gas, with a lifetime of approximately 85 years in the atmosphere. Moreover, due to its toxicity, exposure to high concentrations of carbon tetrachloride (including vapor) can affect the central nervous system and degenerate liver and kidneys. Therefore, avoiding the utilization of this solvent is an important task. Other pathways for the synthesis of 2,2'-bipyridine-5,5'-dicarboxyaldehyde was also considered, like Dess-Martin or Swern oxidation reactions, however, due to other issues like high price and short time for the synthesis of this monomer, the compound was bought from abcr and used as received.

Although the synthesis of aldehydes can be performed through several pathways, the synthesis of functionalized amidine chloride salts is not reported in the literature and presented a challenge in synthesis and purification of such precursor. The synthesis of bipyridine-based amidine chloride starts with the production of 2,2'-bipyridine-5,5'-dicarbonitrile. Since the nitrile is not available to purchase for a reasonable price, it is common to find cyanation of halides as the main pathway used in the synthesis of nitrile.

The cyanation of aryl halides is usually done under reflux in high boiling point solvents, like DMF. CuCN is used as a catalyst and CN^- source. At the beginning of this project, the adduct was synthesized under microwave irradiation, using anhydrous DMF as a solvent, tetrakis(triphenylphosphine)palladium(0) as catalyst and ZnCN as CN^- source. The complete experimental procedure, as well as the synthesis of the precursor 2,2'-bipyridine-5,5'-dibromo, can be found on page 223 in the appendix.

Even though 2,2'-bipyridine-5,5'-dicarbonitrile was successfully obtained through cyanation of 2,2'-bipyridine-5,5'-dibromo in DMF, the pathway to synthesize the nitrile had to be reconsidered for many reasons. First, the issues regarding scaling-up this reaction. Since the reaction is done under microwave irradiation and the biggest reactor available holds 50 mL, only 0,7 g of the desired nitrile can be synthesized in each batch. Furthermore, extensive purification has to be carried out in order to obtain a pure product. Beyond the limitations in quantity, toxicity is often the main drawback in cyanation reactions. Highly toxic cyanides compounds like CuCN and ZnCN are commonly used in this reaction. Because of all the reasons, the synthesis of 2,2'-bipyridine-5,5'-dicarbonitrile was reconsidered, and after extensive research, it was done according to the pathway illustrated in Figure 34.

The synthesis started with the oxidation of 2,2'-bipyridine-5,5'-dimethyl over $KMnO_4$ in water. After the filtration of the MnO_2, the acidification of the final water solution results in precipitation of pure 2,2′-bipyridine-5,5′-dicarboxylic acid. This last compound was too insoluble in common organic solvents for recording a liquid ^{1}H-NMR. Therefore, the reaction followed to esterification without previews purification. The acid was esterified in refluxing ethanol/sulfuric acid solution, to afford diethyl 2,2'-bipyridine-5,5'-dicarboxylate. Figure 35 shows the liquid ^{1}H-NMR and the corresponding structure of the ester, measured in deuterated chloroform.

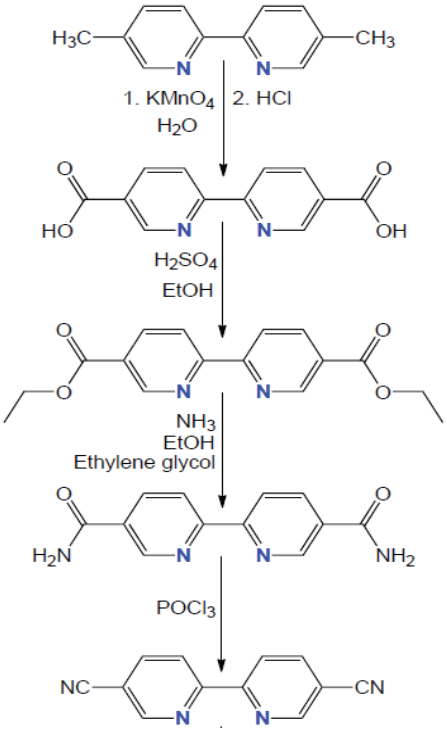

Figure 34 – Pathway for the synthesis of 2,2'-bipyridine-5,5'-dicarbonitrile.

From the resulting spectrum shown in Figure 35, signals at 9.27, 8.55, and 8.44 ppm follow the pattern from bipyridine unit, assigning to hydrogens in position H5/5', H2/2' and H3/3', respectively. Signals at 4.42 and 1.42 ppm belong to hydrogens in the diethyl group, been assigned to methylene and terminal methyl group, respectively.

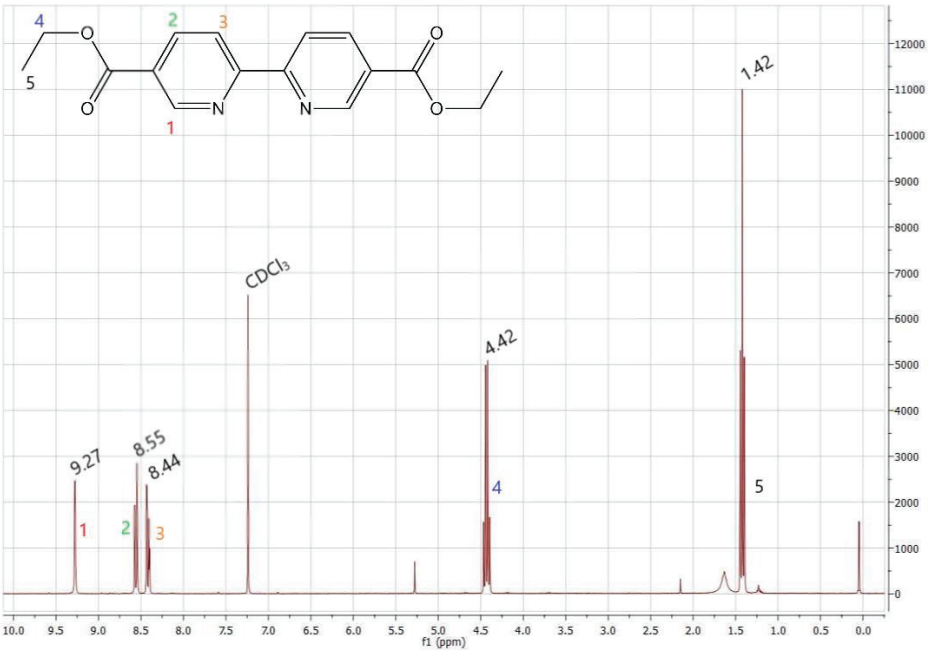

Figure 35 – ^{1}H-NMR spectrum of diethyl 2,2'-bipyridine-5,5'-dicarboxylate, recorded in $CDCl_3$.

In a subsequent reaction, the diethyl ester was converted to carboxamide by reacting with ammonia in ethanol/ethylene glycol solution in a closed reactor. This reaction is not described very often in the literature. So first, a mixture of ethanol/ethylene glycol in equal volumetric ratio was saturated with ammonia for 1 hour until pH reached 11. The saturation was done by slowly heating an ammonium hydroxide solution at 60°C and constantly bubbling N_2 through the solution. The gas containing ammonia is then dried through a trap full of potassium hydroxide in pellets and later bubbled into the ice-cooled mixture of ethanol/ethylene glycol for one hour. A schematic illustration shows the whole apparatus in Figure 36.

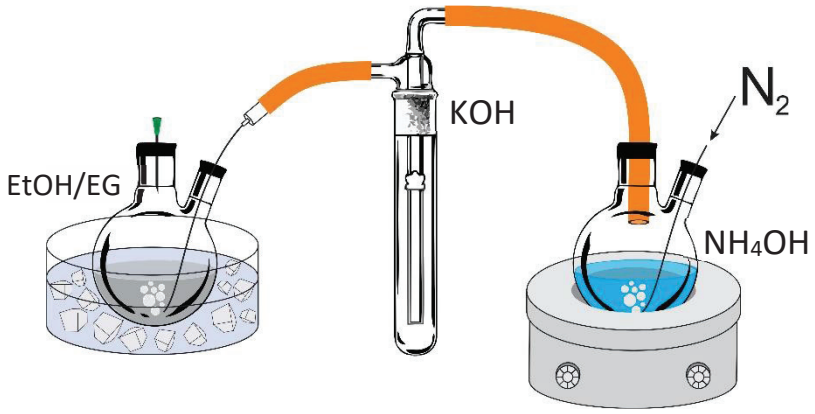

Figure 36 – Schematic illustration of the apparatus used to saturate the mixture of ethylene glycol and ethanol with ammonia.

This ammonia-saturated ethanol/ethylene glycol mixture was placed together with diethyl 2,2'-bipyridine-5,5'-dicarboxylate in a stainless steel autoclave. After properly closed, the reaction was heated up to 90°C for 40 hours. The complete experimental procedure can be seen in appendix page 224. After this time, the autoclave was cooled with ice-water bath and opened. The resulting fine white powder was removed by filtration and washed with boiling ethanol. After dried, the resulting solid could not be analyzed through liquid ^{1}H-NMR due to insolubility issues. Therefore, the structure was investigated using Fourier-transform infrared spectroscopy (FT-IR). Figure 37 depicts the infrared analysis of compound 2,2'-bipyridine-5,5'-dicarboxamide.

From the FT-IR spectrum, it is possible to assign the main stretching vibration from carboxamide. The band at 3420 cm^{-1} is assigned to N-H stretch from primary amide, while the bands in the 3000 cm^{-1} regions are assigned to C-H stretching vibration. Bands at 1723 and 1677 cm^{-1} can be assigned to C=O from amide function and C=N from the bipyridine unit. Additionally, bands at 1550 and 1450 cm^{-1} are assigned to N-H bending

from amide and C-N stretching vibration from the bipyridine. The spectrum is in accordance with the literature.

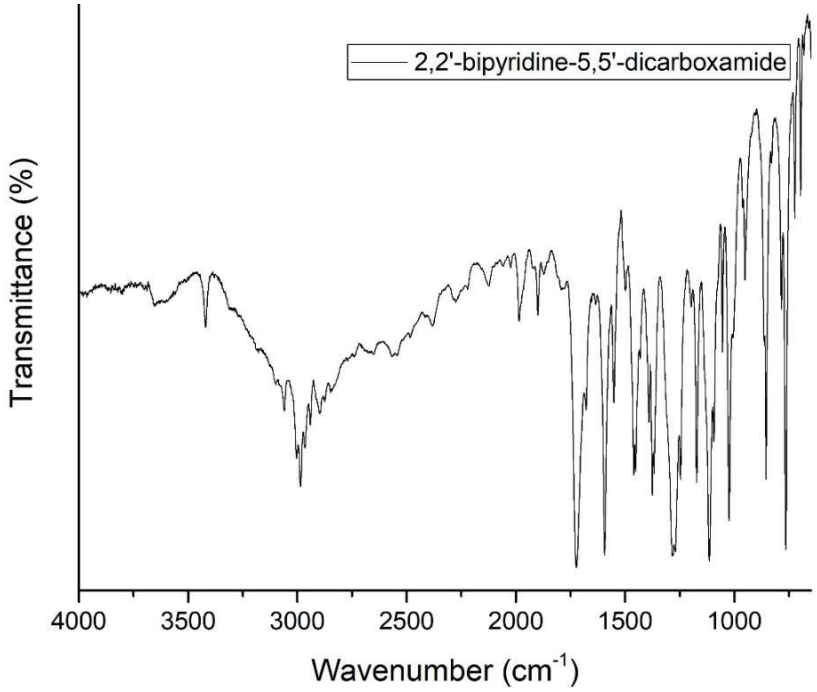

Figure 37 – FT-IR spectrum of 2,2'-bipyridine-5,5'-dicarboxamide.

Afterwards, 2,2'-bipyridine-5,5'-dicarbonitrile was obtained by dehydration of carboxamide in $POCl_3$ under ultrasonic bath. The final compound was purified by recrystallization in acetonitrile to afford colorless needle-like crystals. The advantages of this pathway for the synthesis of 2,2'-bipyridine-5,5'-dicarbonitrile rely on the simple purification step. Only simple recrystallization is needed to obtain a pure product, while the product of cyanation often requires column chromatography. Additionally, this approach employs only chemicals with low toxicity. The only drawback is the overall yield of nitrile, which is around 60-70%, while the cyanation of aryl halides typically reaches 90-100%. Figure 38 shows the liquid ^{1}H-NMR of the resulting nitrile, recorded in deuterated chloroform.

As can be noticed from the liquid ^{1}H-NMR, the compound is pure enough for the next step in the synthesis. The recrystallization procedure successfully purified the compound. From the spectrum, it is possible to notice one doublet at 8.95 ppm, corresponding to the hydrogen in position H5/5', and two double doublets at 8.63 and 8.13 ppm. These two last signals are assigned to hydrogens in positions H2/2' and H3/3' in the bipyridine moiety, respectively. Carbon NMR was also recorded in deuterated

chloroform and is in accordance with the literature. The signals from ^{13}C-NMR can found in appendix page 225.

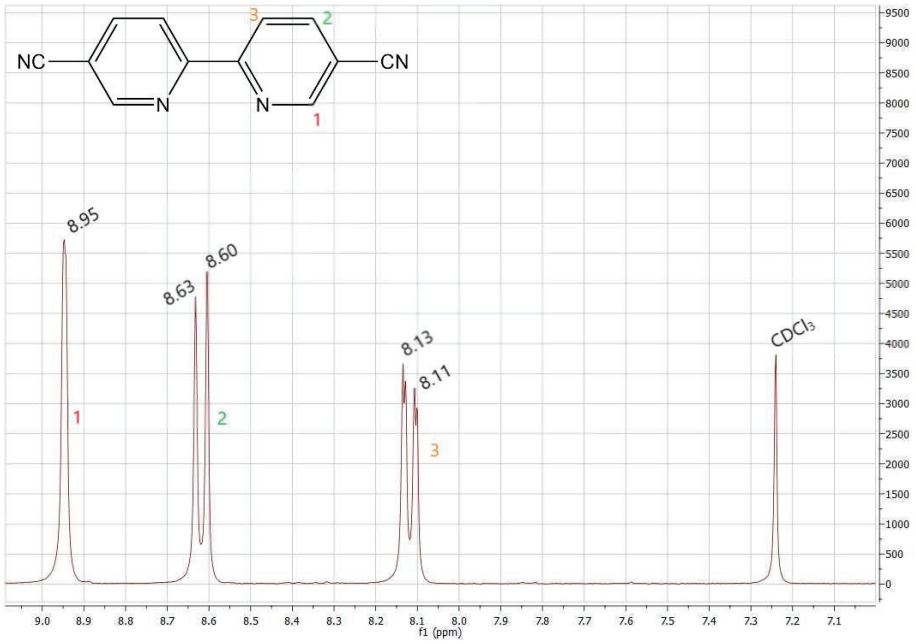

Figure 38 – ^{1}H-NMR spectrum of 2,2'-bipyridine-5,5'-dicarbonitrile, recorded in $CDCl_3$.

In the last step, the nitrile was converted to amidine. The reaction followed the same procedure described for the synthesis of terephthalamidine and 4,4'-biphenyldiamidine chloride, using LiHMDS and nitrile as starting compounds. Figure 39 shows the ^{1}H-NMR spectrum of the resulting 5,5′-diamidine-2,2′-bipyridine dichloride, recorded in deuterated DMSO.

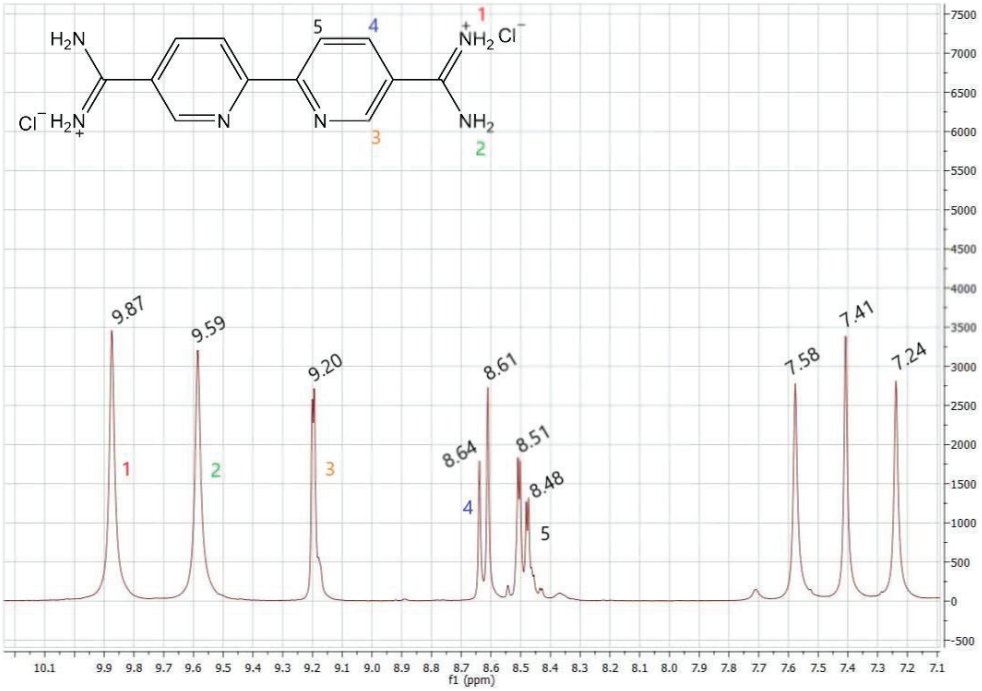

Figure 39 – ^{1}H-NMR spectrum of 5,5′-diamidine-2,2′-bipyridine dichloride, recorded in d_6-DMSO.

From the resulting spectrum, it is possible to notice a prominent triplet signal at 7.41 ppm, the same signal reported previously in the synthesis of terephthalamidine and 4,4'-biphenyldiamidine. The other signals can be assigned to the 5,5′-diamidine-2,2′-bipyridine. The signals at 9.87 and 9.59 ppm, are assigned to the hydrogens from the amidine function, while the doublet at 9.20, and both double doublets at 8.64 and 8.51 ppm can be assigned to the bipyridine unit, following the same pattern as described before, H5/5', H2/2' and H3/3', respectively.

Following the counter-ion exchange in order to purify the amidine chloride, the first compound obtained was 5,5′-diamidine-2,2′-bipyridine tetraphenylborate. The ^{1}H-NMR spectrum is depicted in Figure 40.

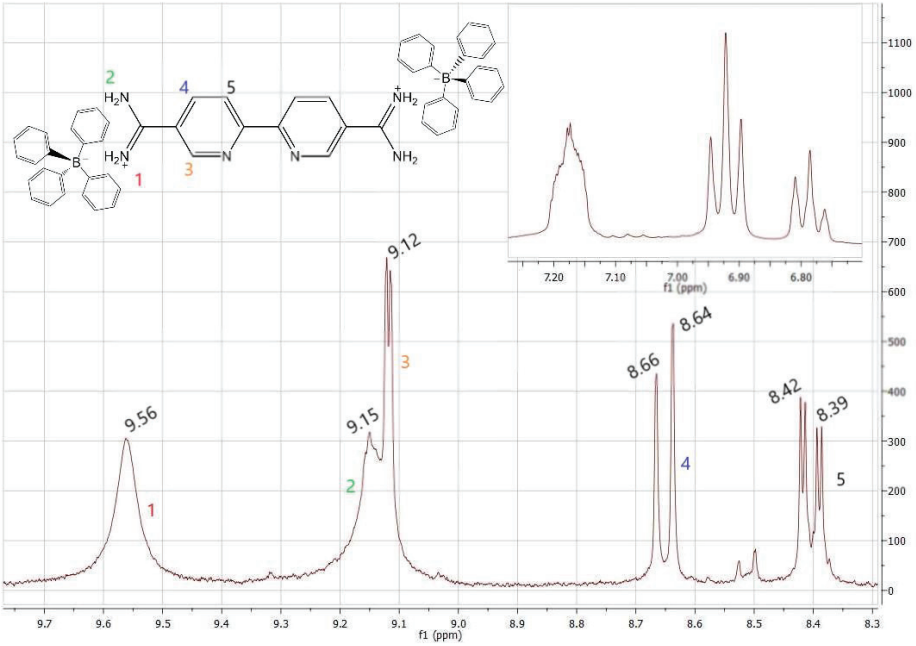

Figure 40 – ^{1}H-NMR spectrum of 5,5′-diamidine-2,2′-bipyridine tetraphenylborate, recorded in d_6-DMSO.

According to the result in Figure 40, both patterns from tetraphenylborate counter-ion and bipyridine can be observed. The pattern from the counter-ion is showed in detail, with the typical three signals, one broad signal from the hydrogen in ortho position at 7.19 ppm, and two triplets at 6.94 and 6.80 ppm, corresponding to hydrogens in meta e para positions, respectively. The typical signals from bipyridine can also be assigned. The first two double doublets at 8.42 and 8.66 ppm, corresponds to hydrogens adjacent to carbons C3/3' and C2/2'. The doublet with the higher chemical shift, at 9.12 ppm is assigned to hydrogen adjacent to carbon C5/5'. This last signal from bipyridine is overlapping the signal from the hydrogen in the amidine function at 9.15 ppm. Another

signal from amidine hydrogen can be noticed at 9.56 ppm. Once more, no signals from the by-product can be found in the region of 7.60-7.20 ppm.

In the last step, the counter-ion was changed once again. This time from tetraphenylborate to bromide. Liquid ^{1}H-NMR was recorded in deuterated DMSO. The spectrum from 5,5′-diamidine-2,2′-bipyridine bromide can be seen in Figure 41.

The spectrum shows five signals in which the two at higher chemical shifts, 9.59 and 9.17 ppm, can be assigned to the hydrogens from the amidine, while the other three follow the pattern from bipyridine. The first on at 9.13 ppm belongs to hydrogen in position H5/5', the second at 8.66 ppm is assigned to hydrogen H2/2', and lately, the signal at 8.44 ppm corresponds to hydrogen in position H3/3'.

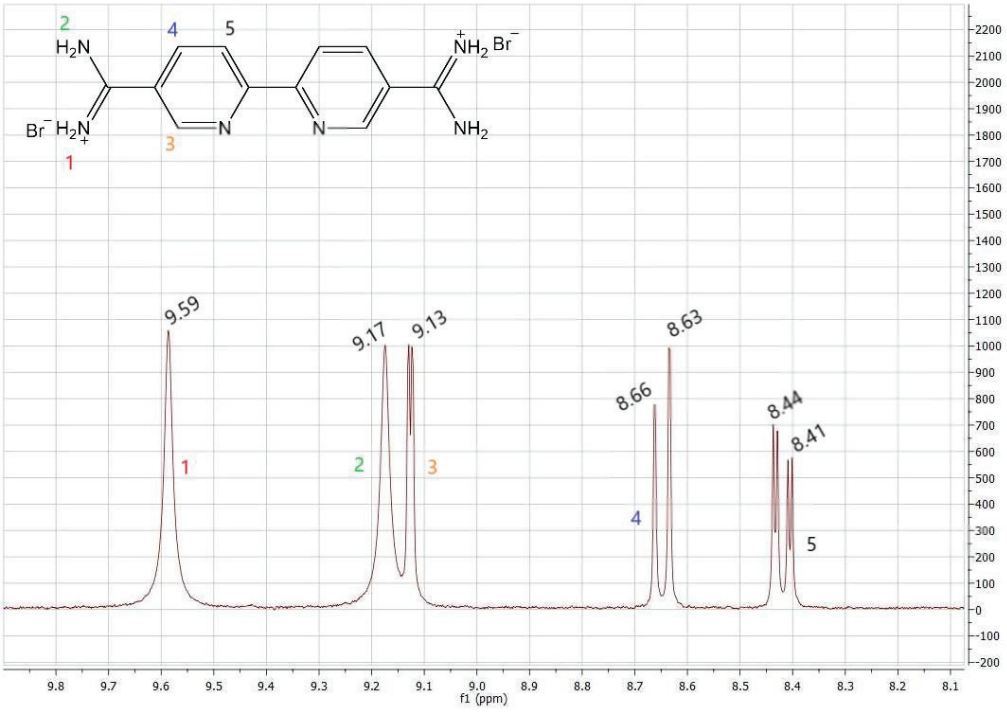

Figure 41 – ^{1}H-NMR spectra of 5,5′-diamidine-2,2′-bipyridine bromide, recorded in d_6-DMSO.

Although the utilization of LiHMDS for the synthesis of amidine chlorides is a convenient route, it also has some drawbacks. After a long research attempting to identify the structure of the by-product that leads to a significant triplet in liquid ^{1}H-NMR at 7.44 ppm, the compound was confirmed to be ammonium chloride.

When the reaction between nitrile and the lithium base (LiHMDS) is quenched with HCl, some side-products can be formed together with the amidine chloride. Salts

such as LiCl and NH_4Cl have already been reported in the literature [112]. However, the separation of both salts, the amidine and the ammonium chloride, is a challenging task.

Depending on the solubility of the resulting amidine chloride, the compound can be purified by exhaustively washing it amidine with ethanol, since ammonium chloride is soluble in this solvent. To properly separate both salts, the amidine was suspended in ethanol and stirred for one hour, filtrated, washed with clean ethanol, and dried. This procedure was done three times until no signal from the ammonium chloride could be found in liquid ^{1}H-NMR. After treating the crude amidine compound with ethanol, the solvent separated from the amidine was dried and a white solid residue collected. In an attempt to identify the residue, FT-IR and liquid ^{1}H-NMR were measured. Figure 42 depicts the FT-IR spectra of the residue.

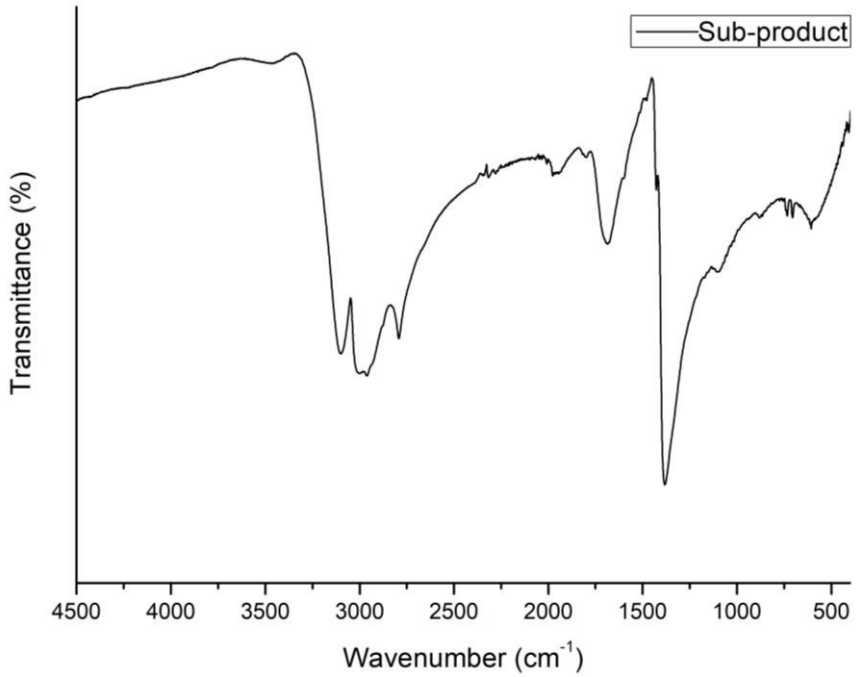

Figure 42 – FT-IR of the by-product formed during the synthesis of amidine chlorides.

It is clear from the FT-IR that the by-product formed when the reaction between nitriles and LiHMSD is quenched with HCl is ammonium chloride. In order to understand the role of ammonium chloride with amidine, liquid ^{1}H-NMR of ammonium chloride was measured with and without pure terephthalamidine. Both measurements were done in deuterated DMSO. Figure 43 shows the resulting spectra.

From the resulting liquid ^{1}H-NMR spectra, only a singlet at 7.50 ppm can be observed when ammonium chloride is recorded alone. This singlet is assigned to the

hydrogens present in the ammonium cation. However, when amidine is present, the singlet became a triplet, shifting to lower chemical shift, clearly showing that the hydrogens in ammonium chloride are coupling with the ones at amidine function. The presence of ammonium chloride in the amidine sample can disturb the synthesis of covalent triazine frameworks and will be discussed in section 3.2.

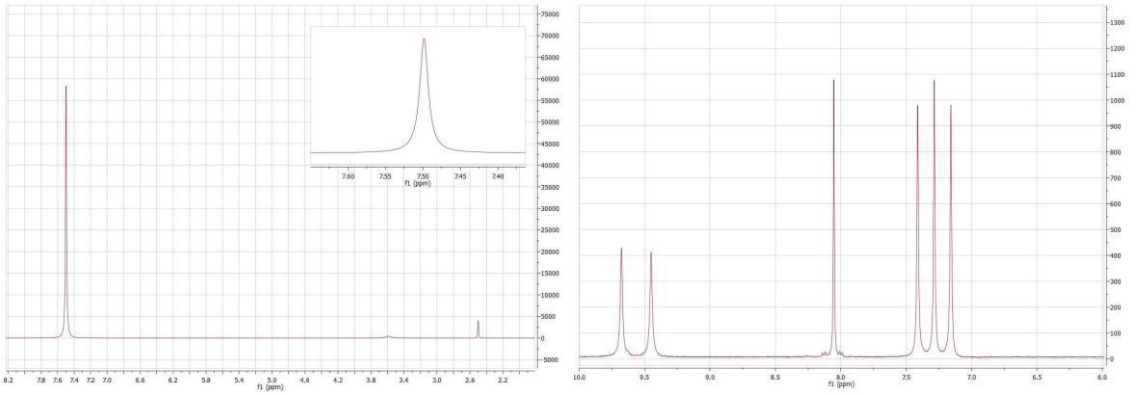

Figure 43 – ^{1}H-NMR spectra of ammonium chloride (left) and terephthalamidine chloride in the presence of ammonium chloride (right), both recorded in d_6-DMSO.

By employing the same protocol described in the synthesis of phenyl and biphenyl-based precursors, the synthesis of bipyridine-base precursors, starting from the preparation of nitrile, was carried out with success. The developed pathway for the synthesis of 2,2'-bipyridine-5,5'-dicarbonitrile showed lower final yield in comparison with the traditional cyanation of halides. However, as an advantage, the pathway described here only needs recrystallization as a purification procedure to obtain the pure nitrile. Furthermore, the synthesis of bipyridine-based amidines was successfully done by the same reaction described before, the addition of LiHMDS to the nitrile precursor. The amidine purification was done by exchanging the counter-ion from chloride to tetraphenylborate and later to bromine. The by-product leading to the prominent triplet signal in liquid ^{1}H-NMR has been identified by FT-IT as being ammonium chloride, a salt already reported elsewhere as an impurity in the synthesis of amidine chlorides. All these bipyridine-based monomers were employed as starting materials in the synthesis of functionalized CTFs. The results regarding the synthesis, characterization and further application of these CTFs as macroligands in photocatalytic CO_2 reduction are described in chapter 5.

3.4 PORPHYRIN PRECURSOR

Porphyrins are heterocyclic macrocycle organic compounds composed of four pyrrole subunits interconnected via double bonds. One of the consequences of its large conjugated structure is that porphyrins typically absorb strongly in the visible region. Moreover, the macrocycle can be metallated with different metal species to form a single atom organometallic complex. Due to its interesting properties, this thesis also reports the attempt to incorporate porphyrin building blocks into the covalent triazine framework's backbone, in order to analyze their activity in photocatalytic CO_2 reduction.

The synthesis of 5,10,15,20-tetrakis(4'-cyanophenyl)porphyrin, which structure is illustrated in Figure 44, was done according to previews reports [113]. The full experimental procedure can be found in the appendix page 229.

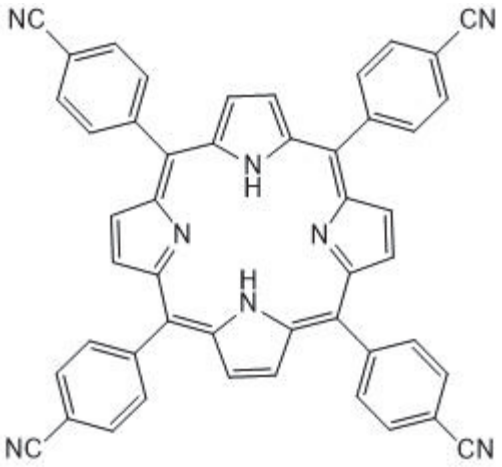

Figure 44 – Structure of 5,10,15,20-tetrakis(4'-cyanophenyl)porphyrin.

To confirm the porphyrin structure, liquid ^{1}H-NMR was recorded in deuterated chloroform. Spectra is depicted in Figure 45.

From the resulting spectra, it is possible to observe a signal at 8.80 ppm, corresponding to both hydrogens at the pyrrole moiety. Two doublets at 8.33 and 8.10 ppm are assigned to hydrogens in the ortho and meta-cyanophenyl group, respectively. Additionally, the signal at -2.87 ppm is assigned to inner hydrogens from the pyrrole group.

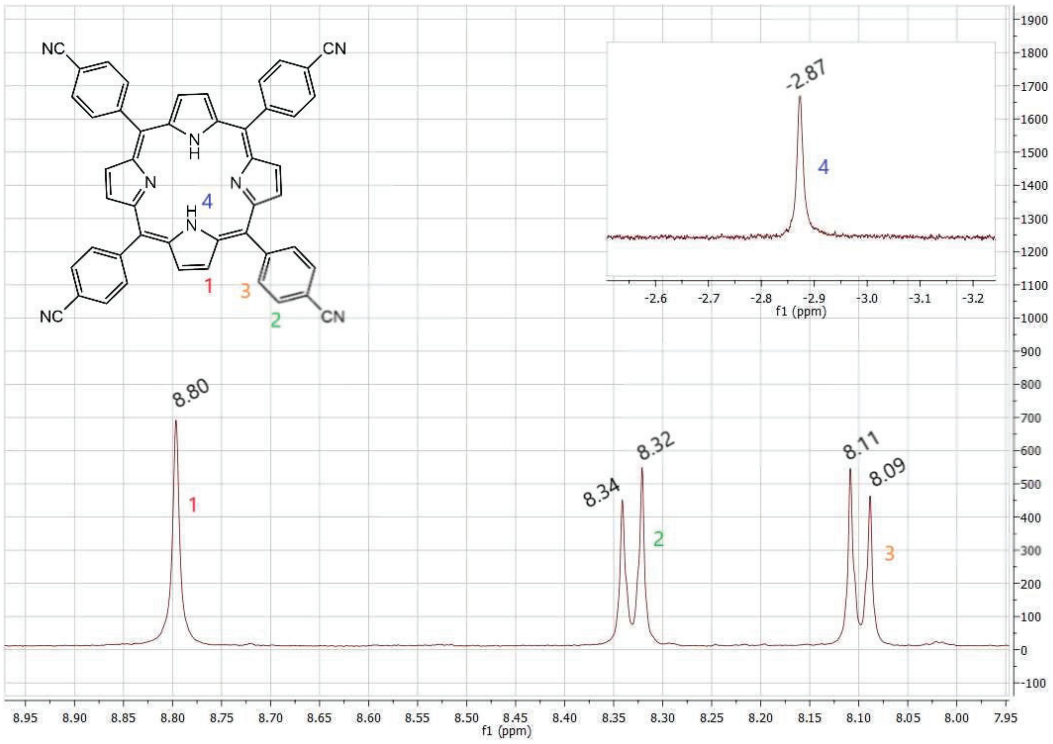

Figure 45 – ^{1}H-NMR spectrum of 5,10,15,20-tetrakis(4-cyanophenyl)porphyrin, recorded in $CDCl_3$.

With the nitrile, it is possible to synthesize CTFs through the acid or ionothermal approach, however, the synthesis through condensation requires amidine and aldehyde monomers. Different attempts to synthesize 5,10,15,20-tetrakis(4'-amidinophenyl)porphyrin by reacting the nitrile precursor with Lithium bis(trimethylsilyl)amide in dry THF had failed, leading to another products. In the last attempt, the reaction was done at room temperature under ultrasonic bath, following the procedure described by Wong *et al* [114]. In this procedure, a homogeneous solution of 5,10,15,20-tetrakis(4'-cyanophenyl)porphyrin in dry THF under an inert atmosphere is mixed with LiHMDS. The mixture was set to an ultrasonic bath for 2 hours. During this time, the temperature of the reaction increased to 50°C. After the reaction, the solvent was removed under vacuum and the residue treated with acetonitrile, water, and diethyl ether. After the recrystallization in methanol/acetonitrile, the compound 5,10,15,20-tetrakis(4'-cyanophenyl)porphyrin was obtained as fine purple solid. To confirm the structure, liquid ^{1}H-NMR was measured in deuterated DMSO. Figure 46 depicts the spectrum.

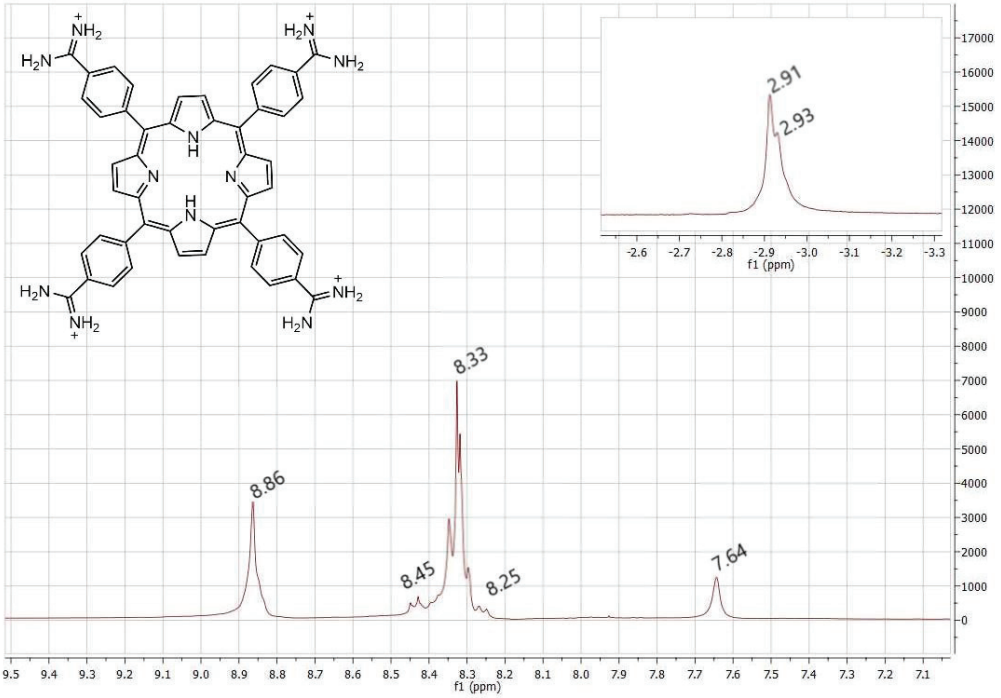

Figure 46 – ^{1}H-NMR spectrum of 5,10,15,20-tetrakis(4-amidinophenyl)porphyrin, recorded in d_6-DMSO.

As can be noticed from the spectrum, the signal at 8.86 ppm can be assigned to the hydrogens in the pyrrole moiety. Moreover, the signal at -2.93 ppm corresponds to the pyrrole hydrogens from the inner cycle. Even though the multiplet from 8.45 to 8.25 ppm include two singlets corresponding to the hydrogens in the phenyl group from the structure of 5,10,15,20-tetrakis(4'-amidinophenyl)porphyrin, the other signals might come from a different structure. After dried, a strong ammonia odor could be felt coming from the resulting purple solid. One hypothesis is that two amidines condensed to form the intermediate shown in Figure 47, producing ammonia as a by-product. Such intermediate, studied by Pinner *et al.*, could explain the ammonia smell and also the differences in the ^{1}H-NMR spectrum.

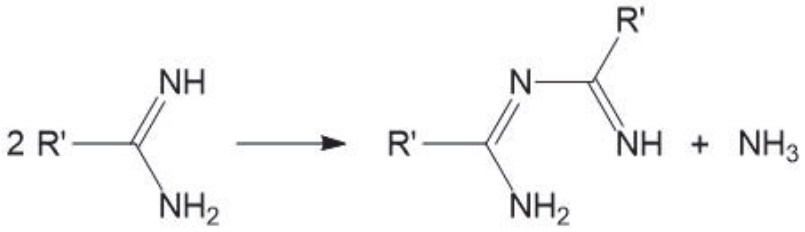

Figure 47 – Formation of non-cyclic intermediate from two amidines.

Even though 5,10,15,20-tetrakis(4'-amidinophenyl)porphyrin could not be obtained, the nitrile can be used in the synthesis of porphyrin-based CTFs using the acid

approach. The synthesis of this material, as well as its application, are described in chapter 6.

CHAPTER 4: SYNTHESIS OF CTF THROUGH CONDENSATION

4 SYNTHESIS OF CTF THROUGH CONDENSATION

The materials synthesized by polycondensation present characteristics that cannot be found when other methods are employed, such as partially layered structure, yellow to orange color (corresponding to the absorption of light in the visible spectra) and semiconducting properties. Additionally, no limitations regarding the geometry or the nature of the precursor were found, increasing the range of materials based on triazine units that can be synthesized.

To verify the main advantages and drawbacks of this method, the first experiments were done aiming to reproduce the materials previously reported in the literature [30]. The synthesis of CTF-HUST-1, the first CTF synthesized by condensation, is based on the reaction of terephthaldehyde with terephthalamidine dichloride. Following the procedure described in the literature, the precursors were mixed with caesium carbonate in DMSO. The homogeneous solution was heated for 12 hours at 60º, 80º, and 100°C, each, before being heated at 120°C for three days. The solid was recovered by filtration and was washed with diluted hydrochloric acid to remove the caesium carbonate salt, water, and organic solvents such as THF and acetone to remove the unreacted precursors.

The resulting yellow solid, hereafter called CTF-MAS-01, was analysed by FT-IR and N_2 physisorption at 77K. Figure 47 shows a comparison between precursors (terephthalamidine and terephthaldehyde) with CTF-MAS-01 material. According to FT-IR, two main stretching vibrations from the triazine centre, at 1515 and 1356 cm^{-1}, assigned to C=N and –C-N-, respectively can be found in CTF-MAS-01. In the FT-IR spectra of the aldehyde precursor, it is possible to see a strong stretching vibration at 1670 cm^{-1}, characteristic from the carbonyl group in the aldehyde. In the case of amidine, the stretching vibrations at 1660 and 1540 cm^{-1} can be assigned to $C=N^{+}H_2$ and N-H bending respectively. It is interesting to notice a small band at 2240 cm^{-1}, corresponding to nitrile stretch C≡N. Such band is evidence of a persistent contamination from the precursor therephtalnitrile. This contamination has been reported elsewhere [90].

Even though FT-IR shows the formation of triazine centers, proving the material CTF-MAS-01 is a covalent triazine framework, from nitrogen adsorption experiments, the material presented unsatisfactory porosity. Figure 48 shows the N_2 adsorption/desorption isotherms. Using the BET method, the superficial area was found to be 2 m^2/g, in comparison to 663 m^2/g, for CTF-HUST-1 reported previously [30].

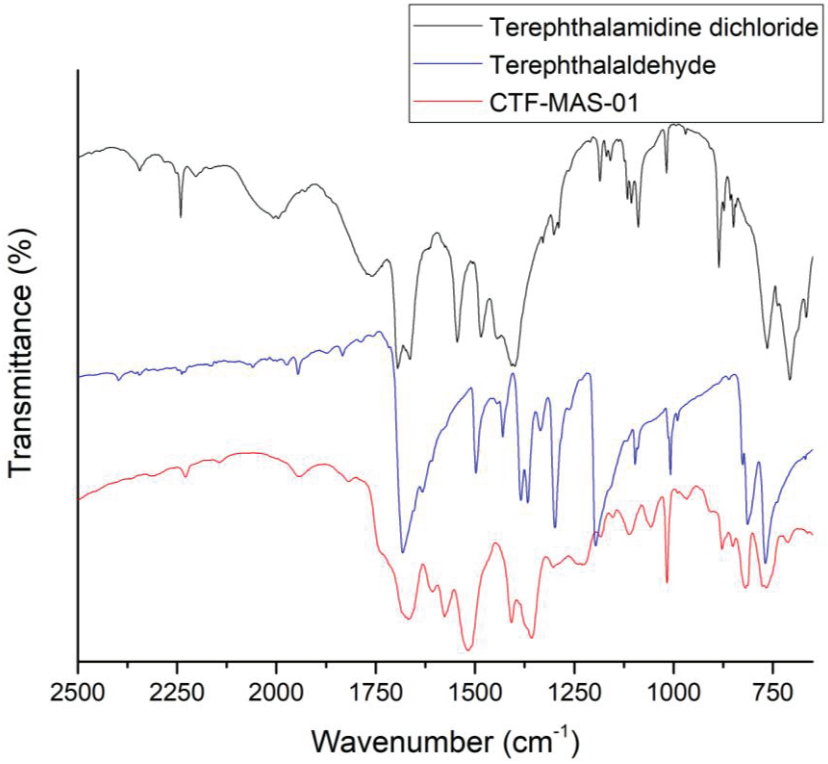

Figure 47 – FT-IR spectra of CTF-MAS-01 and its precursors terephthalaldehyde and terephthalamidine dichloride.

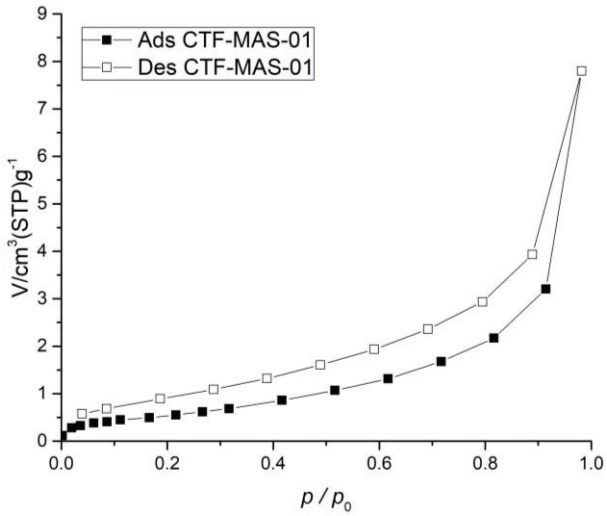

Figure 48 – N_2 physisorption isotherms for CTF-MAS-01 measured at 77K.

Porosity is critical when these materials are applied in catalysis. The presence of structured vacancies over the material assures accessibility of the active sites and better diffusion of reactants and products through the catalyst.

Furthermore, the characterization of non-porous material, synthesized by the same route, can be useful to predict the mechanisms that lead to the lack of porosity and find a way to overcome this issue and boosts its superficial area.

From the literature, it is known that CTFs synthesized by this method hold a partially layered structure. In this case, the stacking position is a crucial feature in order to obtain porous materials. Figure 49 shows the two different stacking positions for CTF-HUST-1. If the layers are organized in AA position, the vacancies are aligned, creating channels which lead to porosity, while when the AB stacking is predominant, the triazine ring from the first layer is precisely in the center of a vacancy in the next layer, causing pore blocking and leading to low porosity.

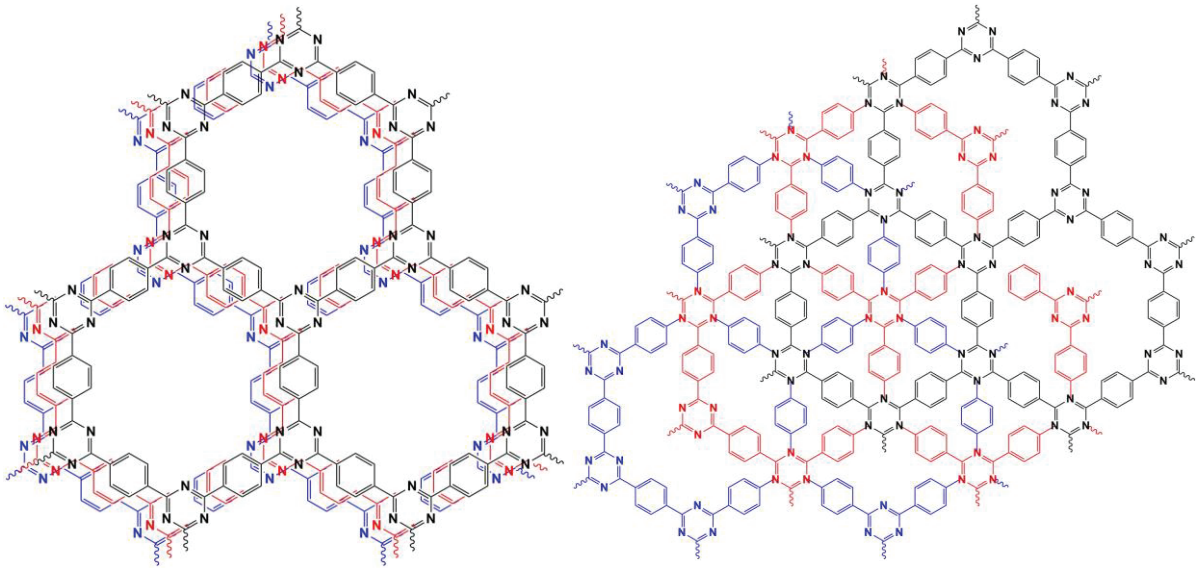

Figure 49 – Simulated model with stacking position in AA (a) and AB (b) orientations.

To investigate the stacking position, an XRD study was carried out. Figure 50 shows a comparison between the first material synthesized in this project (CTF-MAS-01), the material reported by Cooper *et al.* (CTF-HUST-1 [30]), and the ideal calculated XRD pattern for each stacking position. The main difference between the spectra is in the region from 10 to 20 2θ degrees. According to the simulated pattern, the peaks situated in this region possess higher intensity when AB stacking is predominant. Therefore, it can be suggested that AB stacking really leads to pore blocking, although it might not be the only reason for low porosity.

Most porous materials have to be activated. The activation process usually is an extraction method to clean up the pores from remaining salts or unreacted precursors. In this way, Soxhlet extraction was used to activate CTF-MAS-01 in an attempt to clean the pores and increase the superficial area. N_2 physisorption measurements were carried out before and after Soxhlet extraction with THF and toluene. The samples were named CTF-

MAS-01-02 and CTF-MAS-01-03 for treatment with THF and toluene, respectively. Figure 51 shows the N_2 adsorption/desorption isotherms measured at 77K.

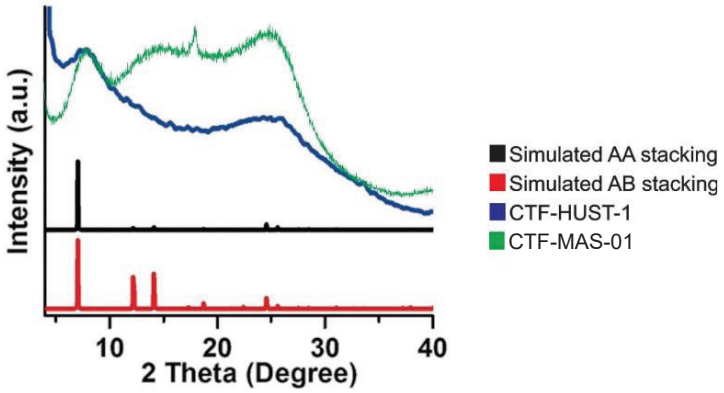

Figure 50 – Comparison between XRD pattern of CTF-MAS-01, CTF-HUST-1 and simulated spectra for AA and AB stacking position.

THF was used mainly because the precursors and triazine compounds are soluble, and toluene in order to try to insert solvent between the layers, increasing the space and opening the material, increasing the superficial area. The BET area for CTF-MAS-01, the fresh synthesized material was 2 m^2/g, in comparison to 24 m^2/g after extraction with THF and 76 m^2/g after toluene extraction. All the isotherms presented the same shape (Type III), although the isotherms of samples CTF-MAS-01-02 and 03, show some features from type IV, slightly increasing the adsorption at low pressure, but significantly increasing the adsorption at higher pressures, suggesting the presence of mesopores. Even though unsatisfactory changes in the specific surface area were obtained.

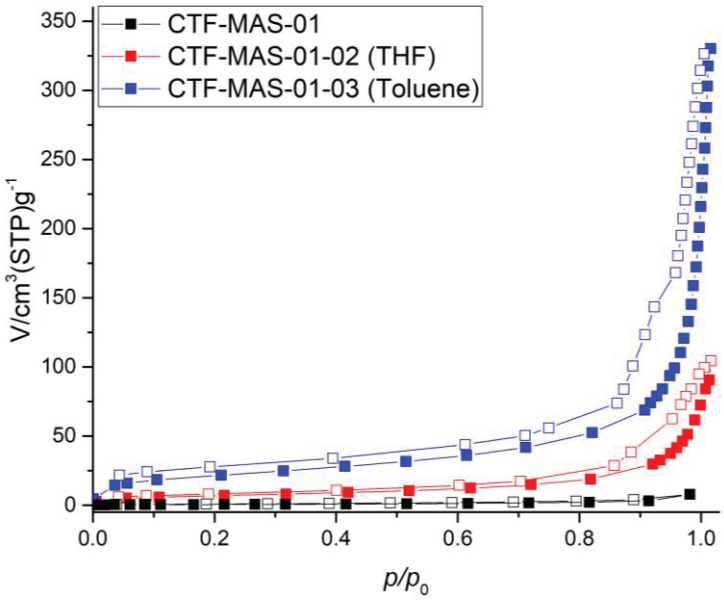

Figure 51 – N_2 physisorption isotherms measured at 77K for CTF-MAS-01 before and after soxhlet extraction with THF and toluene.

Therefore, since the objective is the synthesis of porous CTFs using the polycondensation method, an investigation of how the synthetic parameters influence the porous structure was carried out. Parameters such as solvent composition, temperature, amount and nature of base, time and purity of precursors were investigated.

The first parameter investigated was the amount and nature of base. In the polycondensation reaction, the base is needed to catalyze the trimerization reaction. To investigate this parameter, three samples were synthesized. The first one using two times more Cs_2CO_3 named CTF-MAS-04. The second, triethylamine was used instead of Cs_2CO_3 in the same molar ratio (sample CTF-MAS-05). Lately, both bases were employed on the synthesis of sample CTF-MAS-07. All synthesis was done following the same procedure described in the literature. Because amidine often has a hydrochloric acid as counter-ion, the utilization of a higher amount of base is based on the need to neutralize the counter-ion during synthesis. The N_2 physisorption isotherms for samples CTF-MAS-04, CTF-MAS-05 and CTF-MAS-07 can be seen in Figure 52.

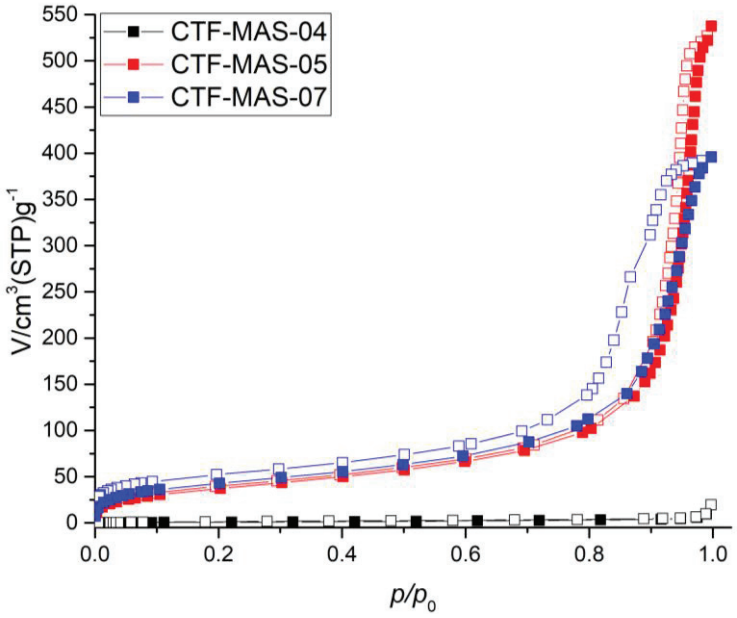

Figure 52 – N_2 physisorption isotherms measured at 77K for CTF-MAS-04, 05 and 07.

A BET area of 2 m^2/g was found for sample CTF-MAS-04 when twice more Cs_2CO_3 was used. Using more carbonate did not change anything regarding the porous properties of these materials. Another test using three times more carbonate was also carried out and resulted in a material with a BET surface area of 5 m^2/g. However, when triethylamine (TEA) was used as a base, sample CTF-MAS-05, the BET superficial area reached 137 m^2/g. Isotherms of this sample also changed from type to a mixture between

type IV and III. The microporous structure can be assigned to the small steep rise at the very begging of the isotherms. The reason might be linked to the liquid nature and the higher solubility of TEA in water, easier to wash out from the sample's pores. Although the superficial area had increased with the utilization of TEA as a base, the yield that usually is around 96-99% when Cs_2CO_3 is employed, dropped to 46%.

Additionally, the color of the resulting material changed from yellow to dark brow. For sample CTF-MAS-07, synthesized with both bases TEA and Cs_2CO_3, comprising the same molar ratio employed in the synthesis of previews samples, a superficial BET area of 155 m^2/g was obtained. The same reason above-mentioned could explain such behavior, the liquid nature of TEA combined with the strength of Cs_2CO_3. Although changing the base can lead to an increase in the specific surface area, the results achieved by employing a different base were not comparable with the one reported in the literature.

The next variable investigated was solvent composition. DMSO is very important to oxidize 1,3,5-dihydrotriazine to s-triazine, in the last step of the condensation mechanism. For this reason, dimethyl sulfoxide was used in all synthesis. The amount of DMSO employed in the synthesis, as well as mixtures of DMSO with water or toluene were investigated. The utilization of toluene is based on the attempt to insert molecules in between the CTF layers, opening the material, and increasing the superficial area. None of the samples presented a substantial change of the surface area or shape of isotherms.

None of the attempts to increase the CTF surface area after the synthesis was successful. Therefore, a study regarding the precursors was carried out. At first, the purity of the precursors was checked. Since the aldehyde used was commercially available and both NMR and FT-IR analyses did not show any contamination, the investigation was mainly focussed on purifying the amidine chloride.

The synthesis of amidine chloride followed the same procedure described in the literature [30]. The reaction of nitrile with LiHMDS was carried out in THF under inert atmosphere. In the reported article, after the synthesis, the amidine is recrystallized in a water-ethanol mixture with a final yield of 96%. That was the first hint that amidine chloride should be purified before CTF synthesis. The second hint was the overall yield of amidine obtained in the reaction. Usually, yields higher than 100% was achieved, thus, indicating the presence of impurities. From the elemental analysis, two measurements on

the same sample had shown more than 10% difference in carbon composition. Additionally, the nitrogen content also did not match. All the results were indicating the presence of impurities.

The attempt to recrystallize the amidine chloride was made using 20 mL of (1:1) ethanol-water mixture at boiling point with 0.5 g of the fresh synthesized terephthalamidine dichloride. After complete solubilization of amidine, the solution was removed from heat and placed into the fridge for three days at 5ºC. After this time, very crystalline amidine was deposited as crystals on the bottom of the flask. The yield was very low (25%), in comparison with 96% found in the literature [30].

A CTF was synthesized using this very crystalline and pure amidine. The sample named CTF-MAS-08 was synthesized using the same parameters described in the literature, the reaction afforded a very fine yellow powder. The BET area for this sample reached 350 m^2/g, therefore indicating the relevance of amidine purity for the synthesis of porous CTFs through condensation. Figure 53 shows the N_2 physisorption isotherms for the most relevant materials, measured at 77K. Its respective superficial area calculated using the BET theory is shown in table 3.

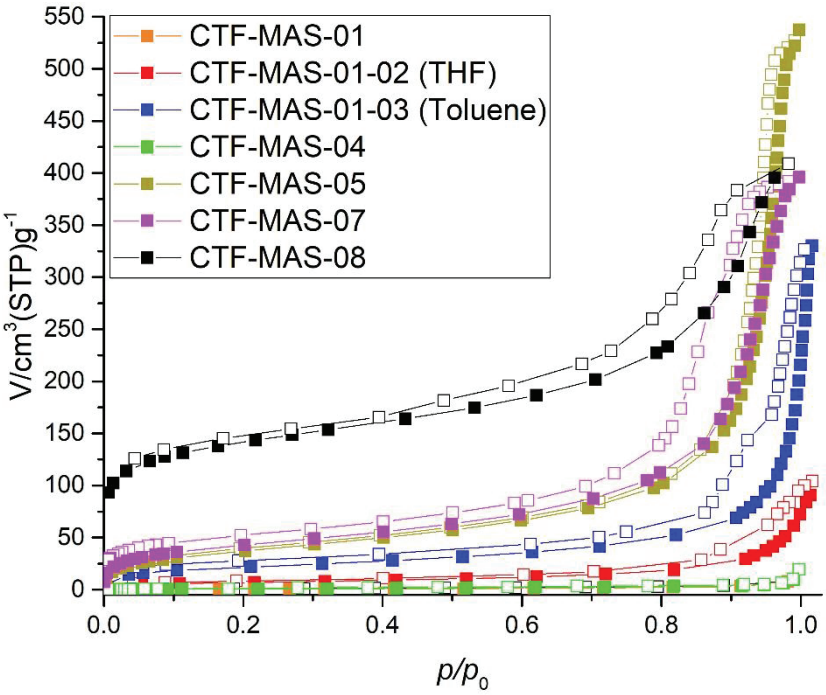

Figure 53 – N_2 adsorption isotherms for the most relevant samples of CTF-1.

Amidine purification is a crucial step for the synthesis of porous CTFs by polycondensation. Side-products such as ammonium chloride and lithium chloride have

been reported in the literature as impurities on the synthesis of amidines. The salts are formed upon addition of hydrochloric acid during quenching of lithium base. Most probably, the salt is what drives the stacking position to AB, leading to pore blocking and low porosity.

Table 3 – The most relevant CTFs synthesized and its corresponding BET area.

Material	BET area (m^2/g)	Description
CTF-MAS-01	2	First material synthesized through condensation
CTF-MAS-01-02	24	Sample after Soxhlet extraction with THF
CTF-MAS-01-03	76	Sample after Soxhlet extraction with toluene
CTF-MAS-04	5	Sample synthesized using two more Cs_2CO_3
CTF-MAS-05	137	Sample synthesized using triethylamine as base
CTF-MAS-07	155	Sample synthesized using half triethylamine and half Cs_2CO_3
CTF-MAS-08	350	Sample synthesized using very crystalline amidine chloride

As described in chapter 3, amidine had its counter-ion exchanged from chloride to tetraphenylborate and later to bromine. Figure 54 shows the scheme used to change the counter-ion of the amidines.

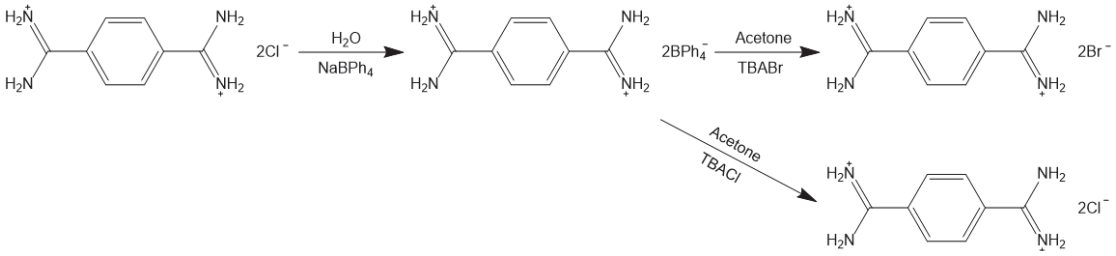

Figure 54 – Scheme for changing the counter-ion of terephthalamidine.

In order to analyze the influence of the amidine's counter-ion on the porosity of the final material, CTFs were synthesized employing terephthalamidine chloride, tetraphenylborate, and bromide. The synthesis was carried out using the same procedure described in the experimental part. Figure 55 shows the nitrogen adsorption isotherms measured at 77K for samples CTF-MAS-75, CTF-MAS-84, and CTF-MAS-99, corresponding to materials synthesized with terephthalamidine tetraphenylborate, bromide, and chloride, respectively.

Due to the very long time needed to stabilize the pressure during the measurement, only the adsorption branch from the full isotherm could be obtained. When synthesized with amidine bromide (sample CTF-MAS-84), the BET area reached 505 m^2/g, while 335

m^2/g and 157 m^2/g were obtained for samples CTF-MAS-99 and CTF-MAS-75, materials synthesized with terephthalamidine chloride and tetraphenylborate, respectively.

The material with the lowest superficial area from this series, CTF-MAS-75, could be attributed to steric effects from tetraphenylborate anion, leading to pore blocking and consequently lowering the specific surface area. In the case of bromide and chloride, the higher solubility of terephthalamidine bromide in DMSO might explain such behavior, although more analyses has to be done to prove which effect plays a role on the porosity, depending on the case.

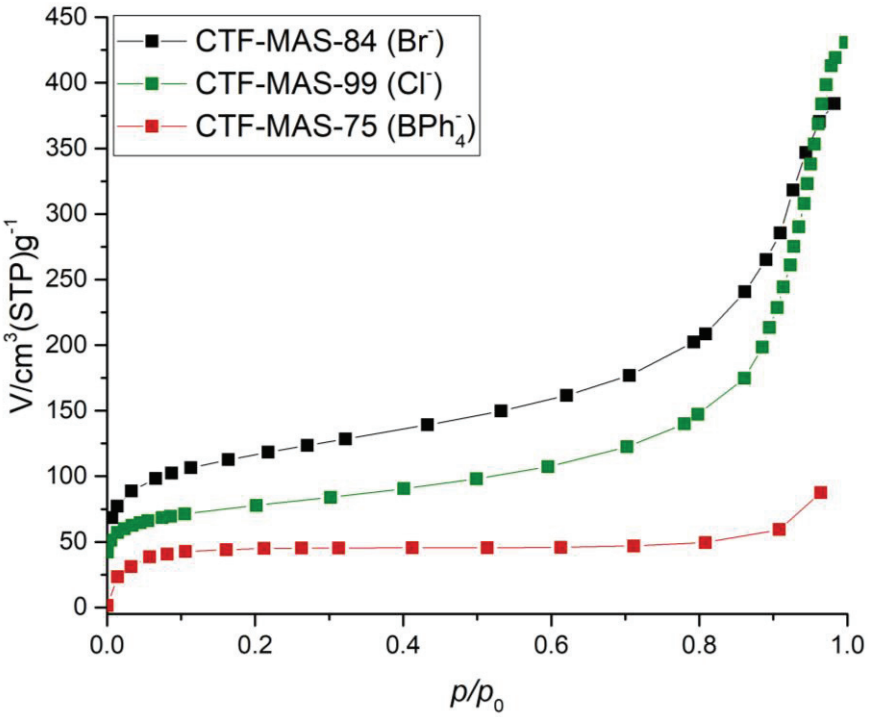

Figure 55 – N_2 adsorption isotherms for samples CTF-MAS-84, 99 and 75, synthesized using terephthalamidine bromide, chloride and tetraphenylborate, respectively.

To investigate the triazine formation, infrared measurements were carried out in transmission mode using KBr for dilution. Figure 56 shows the infrared spectra of the precursor terephthalamidine bromide and also the final material CTF-MAS-84. The main stretching vibrations at 1515 and 1354 cm^{-1} are assigned to -C=N- and -C-N- from the triazine ring, respectively. It is also important to notice the stretch at 2226 cm^{-1} from nitrile. This band can be assigned to the amidine's precursor and is a persistent contamination of nitrile when amidine is synthesized. Even though the unreacted nitrile groups represent the presence of defects and might cause a lower polymerization degree in the final material, the obtained spectrum is completely in accordance with the literature.

The persistent contamination in the case of 1,4-dicyanobenzeno was also reported elsewhere.

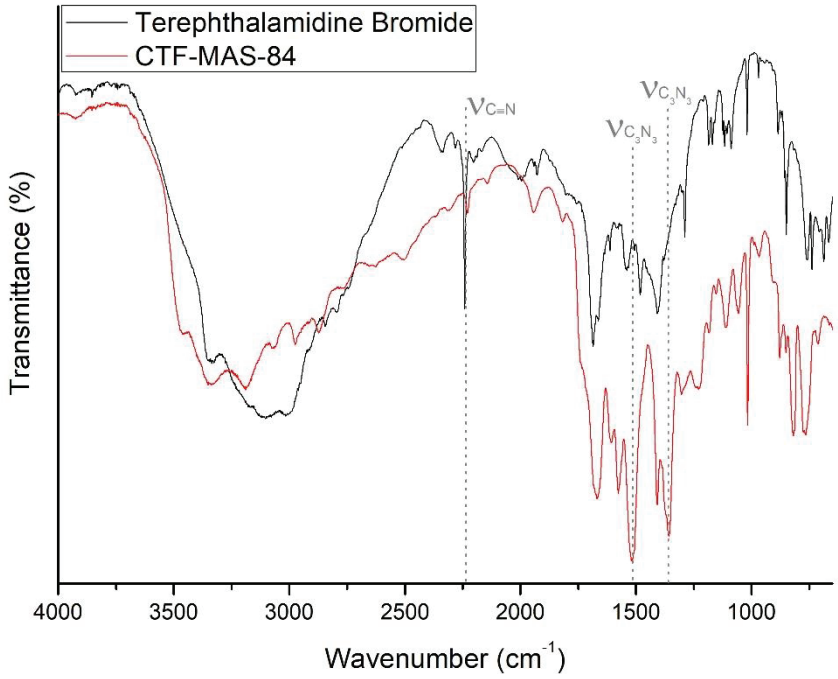

Figure 56 – Infrared spectra for amidine bromide and CTF-1.

To further investigate the difference between CTFs synthesized with terephthalamidine bromide and chloride, cross-polarization magic angle spinning carbon-13 nuclear magnetic resonance (CP-MAS ^{13}C-NMR) experiments were carried out in samples CTF-MAS-84 and 99. Figure 57 shows the spectra for both samples. According to literature, the signals at 128.7 and 138.8 ppm, can be assigned to carbons from the phenyl group, aromatic C-H and quaternary carbon, respectively. The signal at 170.4 ppm is assigned to the carbon from the triazine ring. Signals with the * denote spinning sidebands. The signals # from 0 to 50 ppm denote the remaining solvent trapped into the framework and could not be identified.

From X-ray photoelectron spectroscopy analysis (XPS), the content of elements like carbon and nitrogen can be calculated. For the sample CTF-MAS-84, synthesized with terephthalamidine bromide, the content found was 78.0% and 18.0% for carbon and nitrogen, respectively. The calculated one is 73.8% and 21.5%. Although the contents slightly deviate from the ideal, it is important to highlight that XPS analysis does not provide information over the bulk material, but only concerning the first 10-20 nm depth in the sample. Therefore, the elemental content obtained from XPS analysis is a

qualitative measurement. The difference between the experimental and calculated nitrogen and carbon contents evidence the presence of defects and also points out the amount of nitrogen lost during the synthesis.

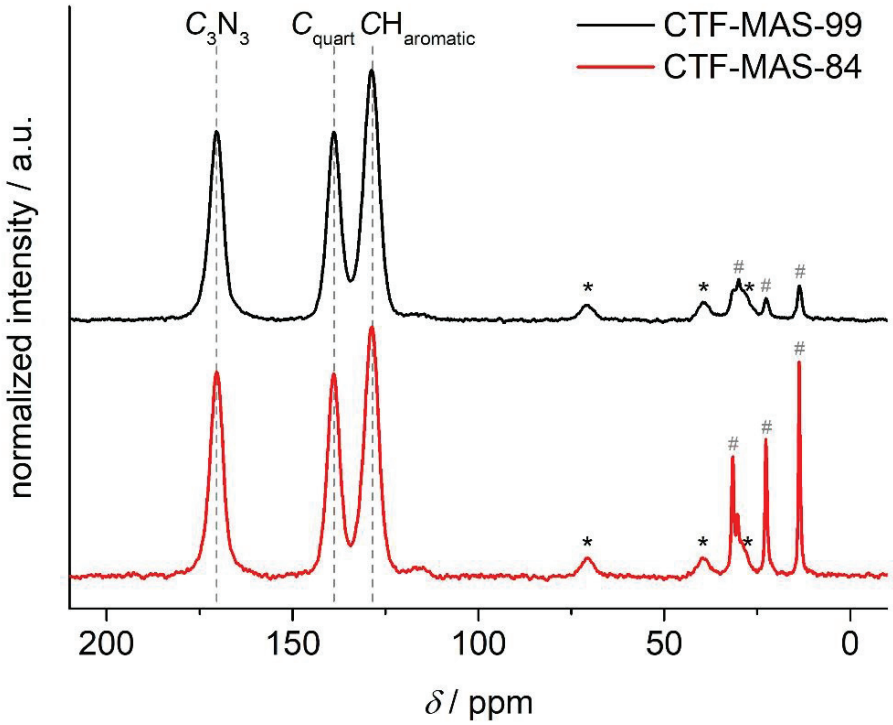

Figure 57 – CP-MAS ^{13}C-NMR for samples CTF-MAS-84 and 99, synthesized with terephthalamidine bromide and chloride, respectively.

The analysis is also in good agreement with the literature, regarding the nitrogen species [115]. Figure 58 shows the N1s XPS analysis for sample CTF-MAS-84. Three peaks are observed, at 398.38, 399.41 and 402.41 eV. They are assigned to pyridinic, pyrrolic and pyridinic N-oxide species, respectively. In comparison with literature, the same peaks can be observed with no significant divergence in the energy-related to each species. However, the contribution of each species seems to change significantly. While in the materials described in this project, the pyridinic nitrogen is the dominant species, followed by pyrrolic and N-oxide in the material reported in literature, pyrrolic nitrogen presents the dominant species followed by pyridinic and N-oxide species.

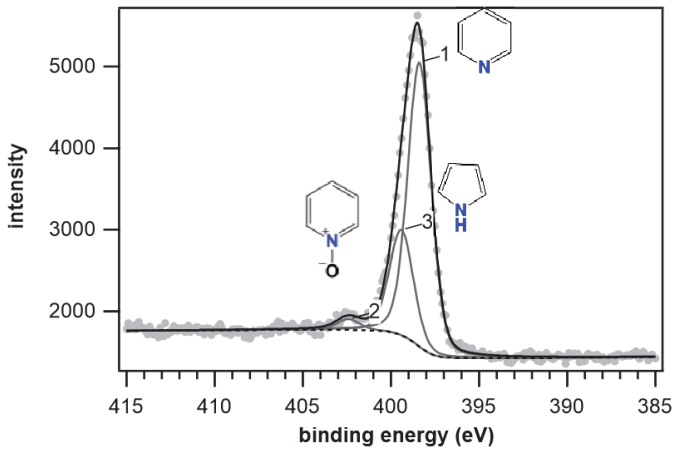

Figure 58 – N1s XPS analysis of CTF-MAS-84 including fitting.

Such a behaviour could be explained through the reaction time. In the synthesis described in the literature, the reaction starts at 60ºC and is heated up to 80ºC and 100ºC for 12h each step, followed by heating at 120ºC for three days. The temperature schedule employed in the synthesis is the same, however, the times were prolonged. Instead of using 12h each step, the reaction was allowed to stay 24h.

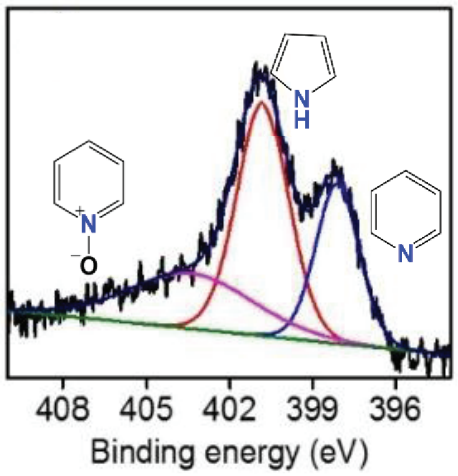

Figure 59 – N1s XPS analysis of CTF-HUST-1 reported in literature and respective fitting. Adapted with permission from: Wang, K.; Yang, L. M.; Wang, X.; Guo, L.; Cheng, G.; Zhang, C.; Jin, S.; Tan, B.; Cooper, A. Covalent Triazine Frameworks via a Low-Temperature Polycondensation Approach. Angewandte Chemie, 2017, v.56 pp14149-14153.

As stated before, the condensation reaction produces hydro-triazine, which is further oxidized by DMSO to triazine. Since hydro-triazine has pyrrolic nitrogen species, a shorter reaction time would favour the synthesis of materials containing a higher amount of pyrrolic species. On the other hand, a longer reaction time produces materials with a higher amount of pyridinic nitrogen species, since the oxidation of hydro-triazine ring is

more effective for longer reaction time. Figure 59 shows the N1s XPS analysis of CTF-HUST-1 reported in the literature [30].

In an attempt to improve the synthesis of CTF through polycondensation and also to reduce the time needed to complete the polymerization, a CTF based on the reaction of terephthalamidine bromide with terephthalaldehyde, was made using a microwave reactor. The same amount of starting material and solvent was charged in a regular round-bottom flask. The flask was equipped with a condenser and placed in the microwave. The mixture was irradiated for 45 minutes (15 min at 80ºC, 15 min at 100ºC and 15 min at 120ºC), after cooling down to room temperature, the precipitate was filtered, washed with dilute HCl, water, acetone, THF and dried in an oven at 60ºC to afford a yellow powder. The solid was obtained in 98% yield.

That was the first time a microwave reactor was used to perform the synthesis of CTF by polycondensation. The main advantage of the microwave synthesis is the short time and lower energy consumption to synthesize the material. Instead of 5 days in conventional heating, the microwave-irradiated reaction was done in 45 minutes. This is an important step towards the industrial use of these materials since microwave synthesis is easier to scale-up. To investigate their porous properties, nitrogen physisorption measurements were carried out at 77K. Figure 60 illustrates the adsorption/desorption isotherms of CTF-MAS-84, synthesized by conventional heating, and CTF-MAS-95 derived from this novel microwave synthesis.

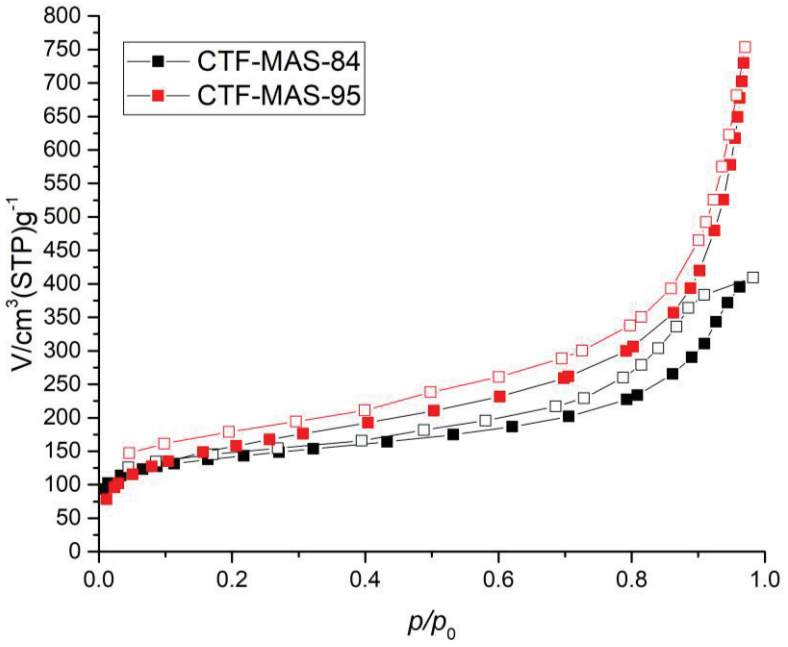

Figure 60 – N_2 physisorption isotherms of CTFs MAS-84 and MAS-95, synthesized by conventional heating and microwave-assisted reaction, respectively.

According to the physisorption data showed in Figure 60, the BET area for CTF-MAS-84 synthesized by conventional polycondensation is 500 m^2/g while for the material synthesized using the microwave, CTF-MAS-95, the specific surface area reached 560 m^2/g. For both materials, the isotherms present a mixture of type I and IV shape, characteristic of microporous and mesoporous materials. The steep rise at low pressure is due to micropore filling, while the one at high relative pressure may be related to condensation in macropores (formed between the particles). In the case of CTF-MAS-95 (MW), the isotherm shows a higher contribution of meso/macro-pores, reflected by the presence of a hysteresis type H3 over a broad range of relative pressure, especially at high pressure. Additionally, the material synthesized in the microwave presents lower micropore volume. From t-plot, the micropore volume of sample CTF-MAS-84 is 0,111 cm^3/g while for CTF-MAS-95 it is 0,037 cm^3/g. Once again, indicating a bigger contribution of mesopores in CTF synthesized by the microwave-assisted reaction.

According to the literature [30], all CTF materials synthesized through the condensation between amidine and aldehyde present an amorphous structure. In order to confirm their structure, powder x-ray diffraction was carried out in samples CTF-MAS-84 and CTF-MAS-95. Figure 61 shows the XRD pattern for samples CTF-MAS-84, CTF-MAS-95, and the non-porous CTF-MAS-01.

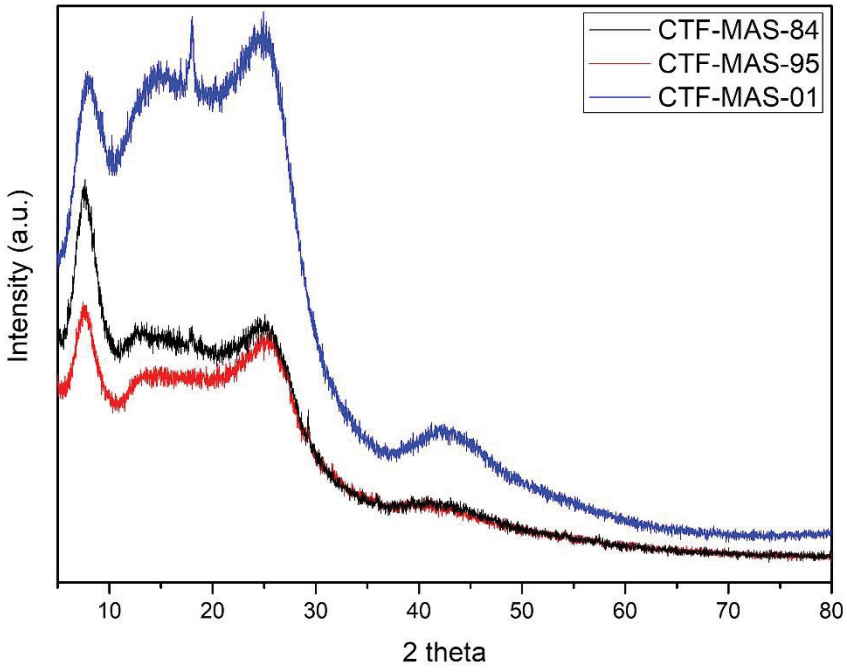

Figure 61 – X-ray powder pattern for CTF-MAS-01, CTF-MAS-84 and CTF-MAS-95.

Although amorphous, both samples CTF-MAS-84 and CTF-MAS-95 have a very similar pattern. The main difference from both samples to CTF-MAS-01 is the peak in the 10-15° 2θ region. Such a peak indicates predominantly AB stacking position, which can explain the non-porous feature, while for the porous samples (CTF-MAS-84 and 95), the peak is not so intense. As expected, both porous samples might have a predominant AA stacking position, which leads to the creation of channels within the framework structure and as a consequence enhance their porous properties.

As can be noticed from the XRD pattern, these materials do not possess long-range order, by the lack of crystalline features. However, FT-IR studies have shown sharp and defined stretching vibrations, suggesting a high degree of order on the local scale. Figure 62 depicts the FT-IR spectra for samples CTF-MAS-84 and 95.

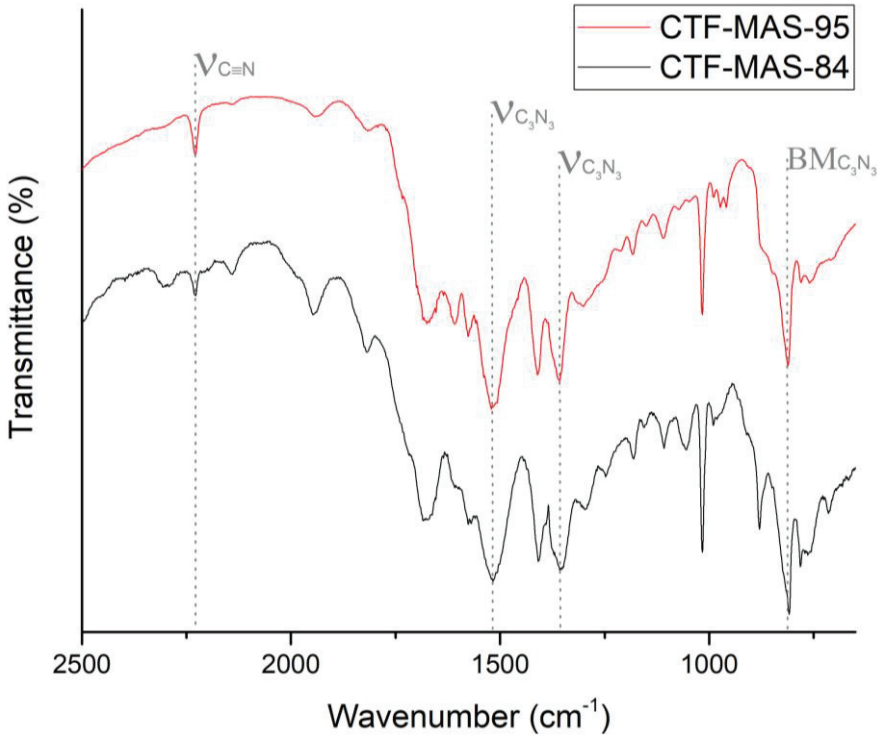

Figure 62 – FT-IR spectra of CTF-MAS-95 and CTF-MAS-84.

Notably, the mains stretching vibrations from the triazine ring can be found in both samples. Bands at 1516, 1355 and 810 cm^{-1} are assigned to C=N, -C-N- and breathing mode from the triazine ring, respectively. Additionally, the band at 2226 cm^{-1} shows the persistent contamination of the amidine's precursor in both samples.

In order to investigate the optical properties of these materials, UV-Vis spectroscopy was carried out for both materials in reflectance mode. Figure 63 depicts the analyses.

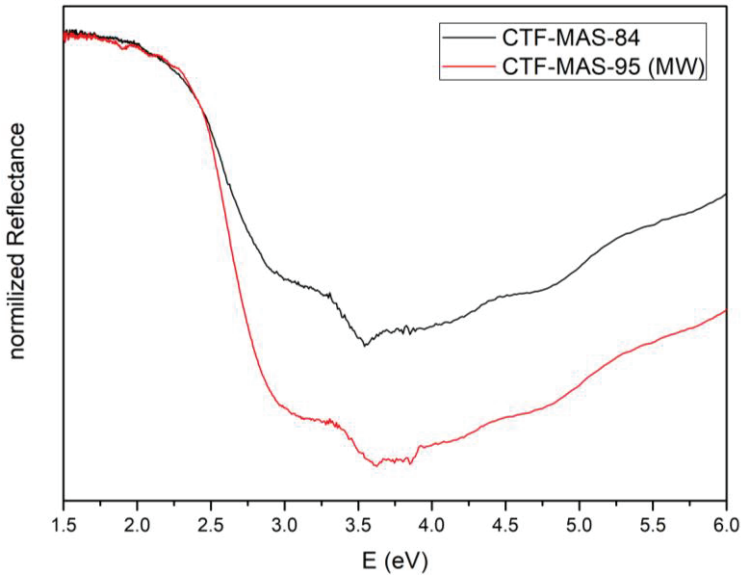

Figure 63 – Uv-Vis spectra for CTFs MAS-95 and MAS-84.

According to the UV-Vis spectra, both materials have similar absorption properties. Using Tauc-plot, the bandgap was calculated to be 2.33 and 2.43 eV for CTF-MAS-84 and CTF-MAS-95 (MW), respectively. The correlation between reflectance and absorbance was found using the Kubelka-Munk equation. The bandgap found for CTF-MAS-84 is in accordance with preview data reported in the literature [30].

The synthesis of simple CTFs by condensation worked well. Based on phenyl building blocks, these materials were investigated in order to determine the main limitations of this approach and also to optimize the parameters for the synthesis of more complex CTFs. According to the results described here, the main limitation of the condensation approach is the synthesis of amidines. Even though these precursors are easy to synthesize, the ammonium chloride, generated as a by-product when the reaction of nitrile with LiHMDS is quenched with hydrochloric acid, changes significantly the features of this materials, in particular the stacking position, leading to non-porous materials. Although the amidines can be purified by exchanging their counter-ions, this strategy is not conventional and doesn't work for all types of building blocks.

Additionally, washing the precursor with ethanol to get rid of the ammonium chloride in the crude amidine sample, can be done only in amidines insoluble in this solvent. Therefore, these purification methods depend on the solubility of the resulting

amidine chloride. For instance, exchanging the counter-ion of amidine chloride was an efficient method to purify the phenyl-based precursor. Another conclusion is that the counter-ion can significantly change the properties of the final CTF. This was evident in the N_2 physisorption experiments for samples synthesized using amidines containing different counter-ions.

Furthermore, a CTF was synthesized for the first time using a microwave-assisted condensation reaction. Although both materials look similar, according to the characterization, some considerations have to be done. The first regard its porous structure. While the material synthesized by conventional heating is mainly microporous, the CTF formed under microwave irradiation has a more significant contribution of macro and mesopores. Additionally, the difference in 0.1 eV shows that the optical properties are not the same, implying changes in the framework structure.

Further analysis has to be done in order to better understand the microwave-irradiated synthesis and the implications it consequently gives to the material's structure. XPS and SEM are interesting characterization techniques that could bring light to the carbon and nitrogen composition as well as their distribution. Moreover, imagens can explain morphologic features.

The sample CTF-MAS-84 showed very similar properties compared to the material CTF-HUST-1, reported previously. The strategy of changing the counter-ion to purify the precursor worked well for simple amidines, like terephthalamidine. The next step was to use the same purification procedure to synthesize more sophisticated materials, based on bipyridine building blocks.

CHAPTER 5: SYNTHESIS, CHARACTERIZATION, AND APPLICATION OF BIPYRIDINE-BASED CTFs

5 SYNTHESIS, CHARACTERIZATION, AND APPLICATION OF BIPYRIDINE-BASED CTFs

5.1 SYNTHESIS AND CHARACTERIZATION

Bipyridine-based CTFs were designed for the heterogenization of molecular catalysts. The reason why condensation is preferred over other methods relies not only on the issues regarding the utilization of ionothermal and acid procedures, but on the advantage of using the modular design to enhance molecular control and precision during the synthesis.

The condensation approach made possible the synthesis of materials containing different amounts of bipyridine ligand. Since the method is based on the condensation of two molecules of amidine chloride and one of aldehyde, the series of bipyridine-based CTFs were conveniently synthesized with 0%, 33%, 66% and 100% of bipyridine ligands.

Together with bipyridine, biphenyl was employed as a non-functionalized building block. The utilization of building units with the same length leads to the synthesis of materials with uniform distribution of shape and pore size. Due to the linear geometry of the building blocks composing the material, and their potentially layered nature, one can expect a symmetrical hexagonal (honeycomb-like) structure.

The synthesis and characterization of the precursors 5,5′-diamidine-2,2′-bipyridine dibromide; 5,5’-diamidine-2,2’-biphenyl dibromide; 5,5’-dicarbaldehyde-2,2’-bipyridine and 5,5′-diacarbaldehyde-2,2′-biphenyl, which structure are illustrated in Figure 64, are described in chapter 3.

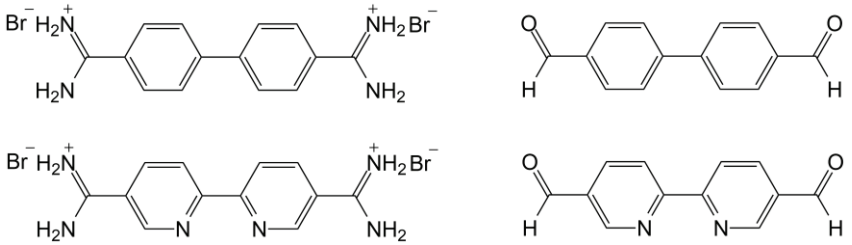

Figure 64 – Structure of amidine bromides and aldehydes employed in the synthesis of bipyridine-based CTF series.

The synthesis of CTF-BPY series was done according to the same procedure described previously for CTF-1 [30]. Although the condensation procedure, especially in the case of aldehyde as starting material, results in amorphous materials, the molecular

control involved in the presented synthesis was never achieved before. This method is the only one until today that allows the synthesis of CTFs using two different building blocks.

Therefore, only with the condensation approach, it is possible to precisely control the amount of specific building blocks in the material structure. In total, a series of four materials were synthesized. The structure of repetition units for all materials is illustrated in Figure 65. The series was named CTF-BPY-X, in which X represents the conceptual percentage of bipyridine present in the material. To complete the series, representing a material without bipyridine, the polymer-based only on biphenyl units was named CTF-BPH.

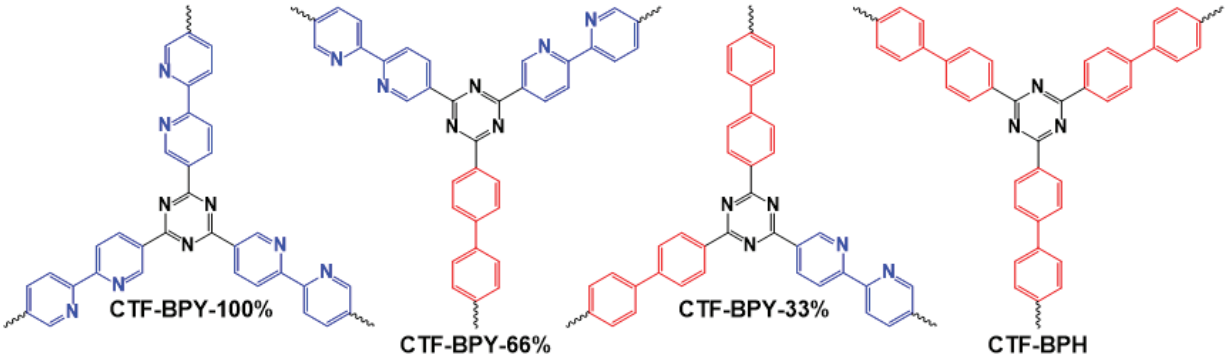

Figure 65 – Structure of the repetition units for the bipyridine-based CTFs.

As explained in the first chapter, the condensation approach leads to amorphous materials, especially when aldehyde is used as a precursor. Therefore, to confirm the amorphous nature of these polymers, powder x-ray diffraction (PXRD) analysis was carried out. Figures 66 shows the PXRD pattern for the series.

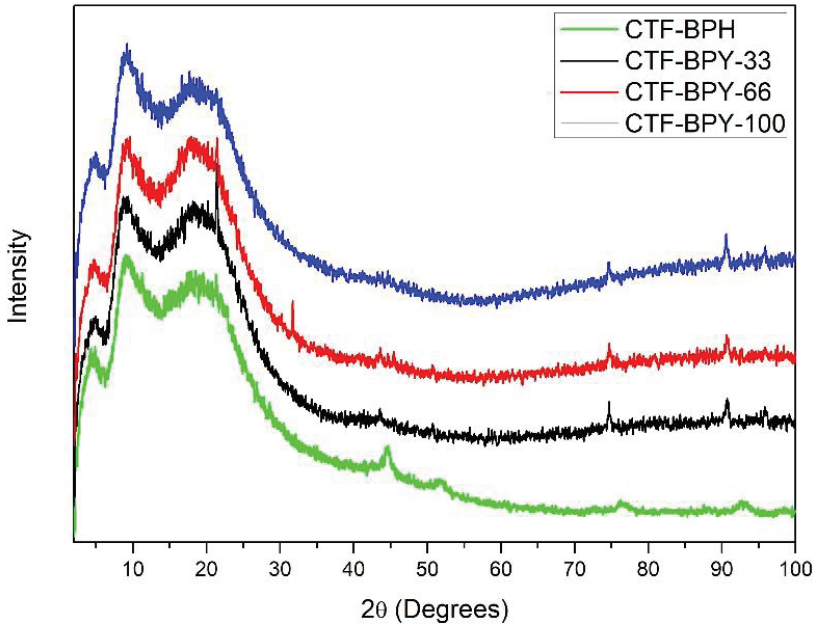

Figure 66 – PXRD pattern for samples CTF-BPH and CTF-BPY-33, 66 and 100.

As expected, the PXRD pattern confirm the amorphous nature of the CTF series. Three very broad diffraction peaks can be observed at 5, 9 and 18º 2θ degrees. Even though these peaks are too broad to give a conclusive insight about the atomic arrangement of the frameworks, typically, the low angle reflexes are assigned to the in-plane reflection of the layered structure, while the peak at ~18° could be attributed to the vertical space between stacked sheets.

To confirm the structure of triazine moieties, an FT-IR study was carried out in transmission mode for the CTF series. The samples were diluted with KBr prior to the measurement. Figure 67 depicts the IR spectra for all materials.

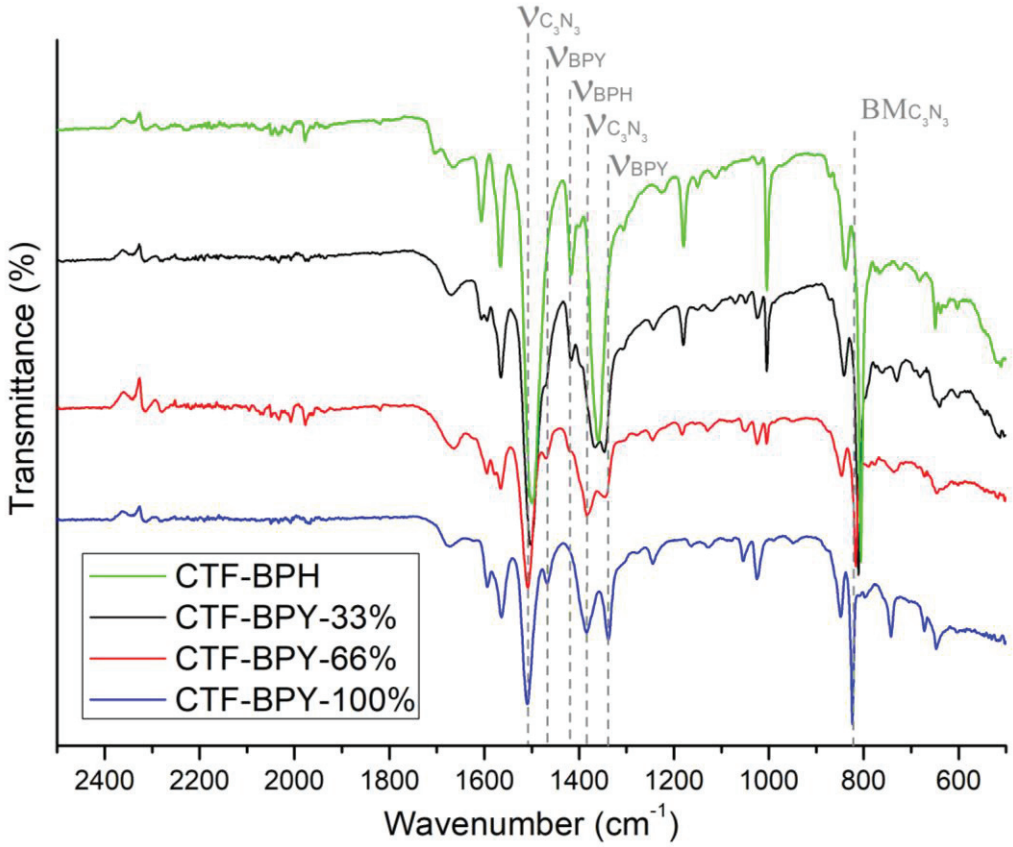

Figure 67 – FT-IR spectra for samples CTF-BPH and CTF-BPY series.

Even though the materials show an amorphous structure, due to the lack of long-range order in the framework, the well-defined sharp starching vibrations from FT-IR, suggests a high degree of order at the local scale. According to the FT-IR study, the main bands of the triazine ring can be found at 1510, 1379 and 817 cm^{-1}. They are assigned to -C=N-; -C-N- and the breathing mode of triazine, respectively. Additionally, it is possible to note three more stretches, at 1467, 1416 and 1335 cm^{-1}. The stretch at 1416 cm^{-1} is assigned to -C=C- from biphenyl units while both at 1467 and 1335 cm^{-1} belong to -C=N-

and –C-N- from the bipyridine units, respectively. It is interesting to notice, though, that the stretches at 1419 and 1335 cm^{-1} do not appear in the spectrum of CTF-BPH, due to the lack of bipyridine ligands in this material. On the other hand, the -C=C- stretch from biphenyl moieties, does not appear in the case of CTF-BPY-100. However, all stretches can be found in the IR spectra of samples CTF-BPY-33 and 66, confirming the presence of both bipyridine and biphenyl units. The absence of a stretch at 2226 cm^{-1}, confirms the absence of nitrile contamination in the series.

The porous properties of the CTF-BPY series were investigated by N_2 physisorption measurements at 77 K. All the isotherms can be classified as a mixture of type I and II according to IUPAC classification, characteristic for partially microporous materials. Figure 68 shows the adsorption/desorption isotherms for all CTF-BPY materials, including the material based on biphenyl units, CTF-BPH.

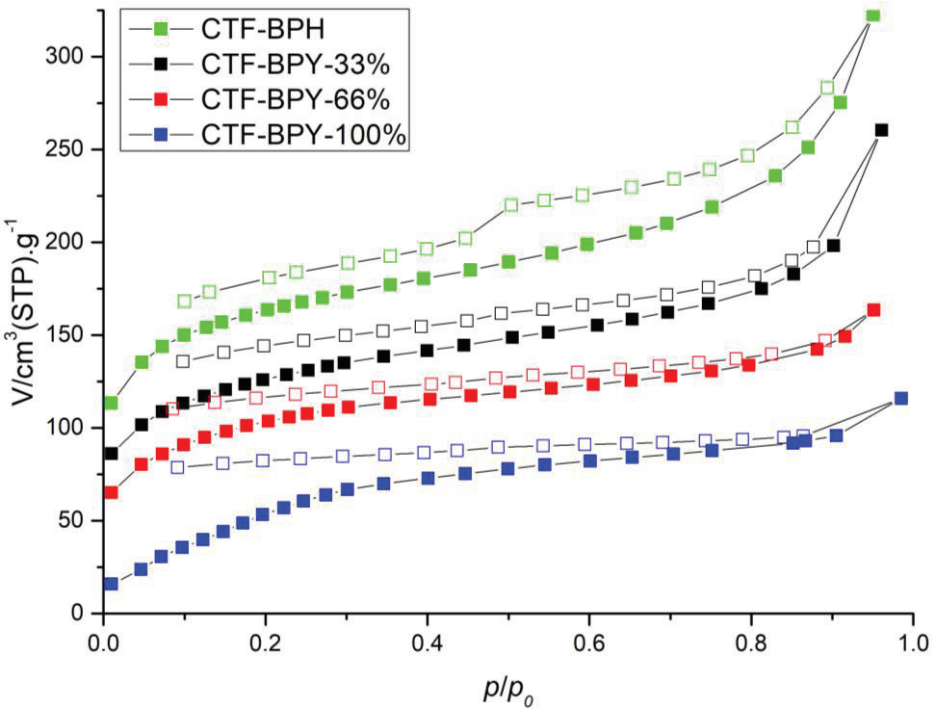

Figure 68 – N_2 adsorption/desorption isotherms for CTF-BPY series and CTF-BPH.

The BET equation was used to calculate the specific superficial area, at the range of relative pressure from $0.01 < p/p_0 < 0.2$. In this region, the constant c is always positive. In all isotherms, a steep rise at low relative pressure indicates the presence of a microporous structure. On the other hand, the steep rise at high relative pressure (when p/p_0 is close to 1) is due to macropores filling. Such macropores potentially form between particles aggregate. This behavior can be easily noted in the first two samples (CTF-BPH

and CTF-BPY-33). The calculated BET surface areas were found to be 572, 400, 368 and 235 m^2/g for CTF-BPH, CTF-BPY-33, 66 and 100, respectively. The decrease in surface area is relative to the increase in the nitrogen content. The fact can be explained by the quadrupolar moment in the nitrogen gas molecule. Its repulsive interaction with the nitrogen present at the surface of the adsorbent, disturbs considerably the monolayer and consequently the calculation of specific superficial area. Another explanation would be the shift in stacking position, since the increase in nitrogen content would disturb the packing of CTF layers, consequently changing its porous properties. However, this hypothesis is not supported by XRD, since no significant change in the spectra can be observed.

Since the BET theory might have some limitations in calculating the specific surface area for microporous materials, the area was also calculated by using Langmuir and DFT theories. Table 4 gives the values.

Table 4 – The most relevant CTFs synthesized and its corresponding BET area.

Material	Theory		
	BET (m^2/g)	Langmuir	DFT
CTF-MAS-BPH	572	761	643
CTF-MAS-BPY-33%	400	530	429
CTF-MAS-BPY-66%	368	496	355
CTF-MAS-BPY-100%	234	370	187

As can be noticed from results in Table 4, using other theories to calculate the specific surface area leads to the same trend, while the nitrogen content increases, the specific surface area decreases.

Another important observation found in the isotherms is the hysteresis. Due to capillary condensation, the gas adsorption and desorption isotherms do not coincide, resulting in a hysteresis loop. The shape of such hysteresis is dependent on the pore structure, therefore, some valuable information can be obtained from the shape of the isotherm. Figure 68 shows the type of hysteresis, related to the shape of the pore structure.

From the isotherms depicted in Figure 68, it is possible to identify a hysteresis at relative pressures around 0.5 ($p/p_0 \sim 0.5$) in all CTFs. The hysteresis notably present in CTF-BPH isotherms can be assigned as H3 type, relative to wedged-shaped pores. This

information is consistent with the layered nature of the CTFs synthesized via condensation, reported in literature for previews materials [7].

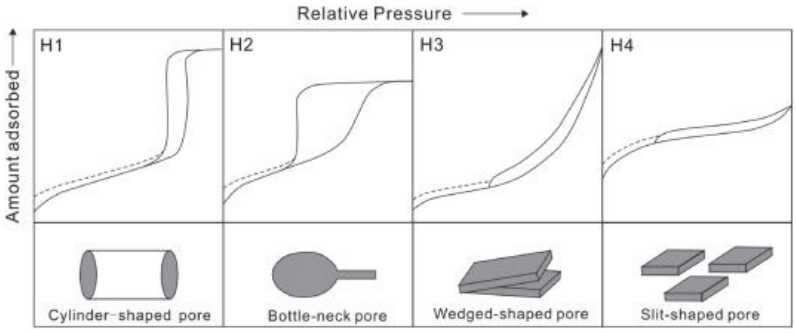

Figure 69 – Type of hysteresis loop in N_2 adsorption/desorption isotherms according to the relative shape or pores. Adapted with permission from: Sing, K. S. W.; Everett, D. H.; Haul, R. A. W.; Moscou, L.; Pierotti , R. A.; Rouquerol, J.; Siemieniewska, T. Reporting Physisorption Data for gas/solid Systems. *Pure Appl. Chem*. 54, 2201 (1982).

Because of the very long time needed to stabilize the pressure in each step of the isotherm measurement, combined with the disconnection of desorptions and adsorption branches in all isotherms, it suggests the materials might be flexible. Even though these observations are more pronounced for other materials reported in the literature, this swelling behavior is found in many porous materials like MOFs and other classes of POPs, since their structure can bend, twist and reshape according to the external stimulus.

The porous nature of these materials is essential for catalysis. The accessibility of active sites and the diffusion of reactants and products through the catalyst can be assured by a high surface area and pore volume. Therefore, because the nitrogen physisorption analysis had shown a considerable difference upon the increase in the nitrogen content, acetonitrile physisorption experiments, measured at 298K were performed to investigate the porous properties of these CTFs. Because acetonitrile is a standard solvent employed in CO_2 photoreduction, its adsorption analysis is relevant to identify the wettability of these materials, and its consequences during catalysis. Figure 70 shows the acetonitrile adsorption/desorption isotherms for the CTF-BPH and CTF-BPY series.

The isotherms presented in Figure 70 can be classified as type II according to IUPAC classification. Moreover, the continuous increase in acetonitrile uptake with the increase in the pressure, with the disconnected adsorption/desorption branches, and the significant hysteresis present in all isotherms, together with the results from N_2 physisorption experiments, strongly suggests swelling behavior. A feature commonly found in MOFs and porous polymers containing flexible structure.

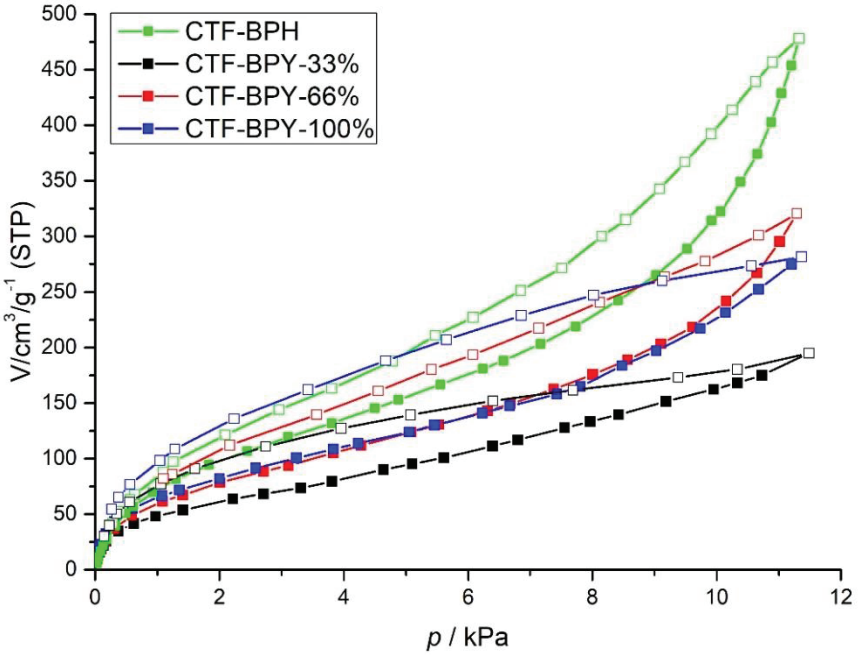

Figure 70 – Acetonitrile adsorption/desorption isotherms for CTF-BPY series and CTF-BPH.

From the initial slope of acetonitrile adsorption, shown in Figure 71, it is possible to calculate the Henry constant (K_H). This constant can give the affinity of a determined solvent for the surface chemistry of the CTF. The value is calculated from the linear regression of the adsorption isotherms for $p/p_0 < 0.1$, according to Canivet *et al* [116].

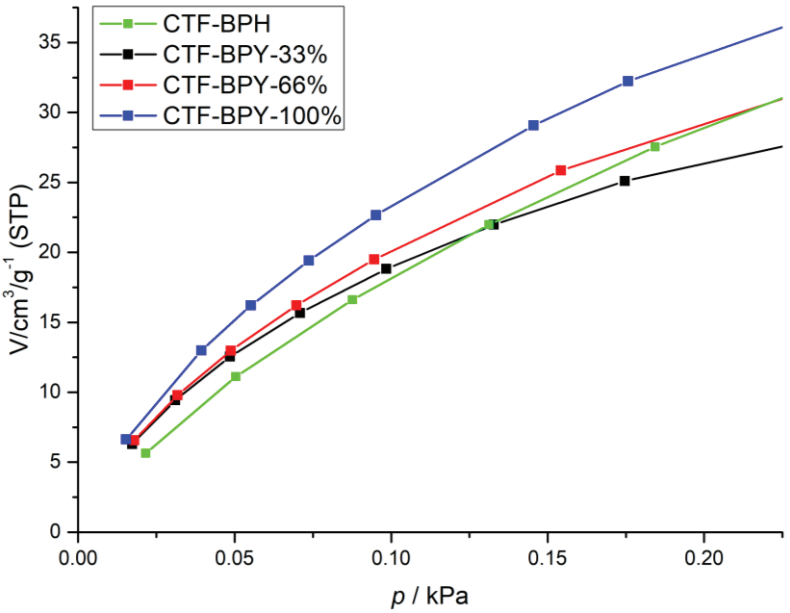

Figure 71 – Acetonitrile adsorption/desorption isotherms for CTF-BPY series and CTF-BPH from $0 < p/kPa < 0.1$.

The calculated Henry constant was found to be 7.3×10^{-6}, 9.1×10^{-6}, 8.9×10^{-6} and 10.8×10^{-6} mol/g/Pa for samples CTF-BPH, CTF-BPY-33%, CTF-BPY-66% and CTF-

BPY-100%, respectively. As can be noticed, the deviation on the Henry constant between the series is assigned to the increase in nitrogen content and their influence on the material's surface interaction with the solvent. In the series, CTF-BPH shows the weakest solid-solvent interaction, while CTF-BPY-100% shows the strongest. Even though some small deviations can be noticed, they are relatively close, showing the acetonitrile-solid interaction are in the same order of magnitude. Moreover, very low discrepancies can be found in the adsorption isotherms at low relative pressure, suggesting very similar behavior from different materials within the series.

Further investigation on the consequences of different nitrogen content in physisorption was done using water as the adsorbate. Figure 72 depicts the adsorption/desorption isotherms of CTF-BPH and CTF-BPYs, measured at 298 K.

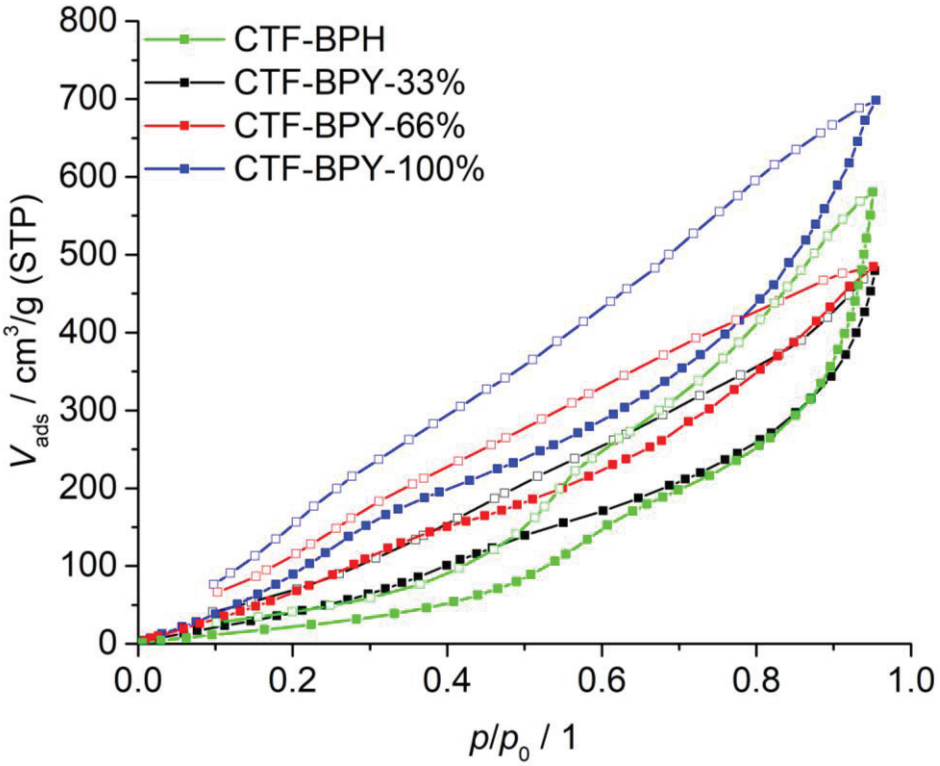

Figure 72 – Water adsorption/dessorption isotherms for CTF-BPY series and CTF-BPH.

According to IUPAC classification, the isotherms of samples CTF-BPY-100% and 66% present a shape corresponding to type II. The shape of isotherms for samples CTF-BPY-33% and CTF-BPH present a mixture of types II and III. From the series, it is possible to notice a strong deviation in the range of relative pressure from 0 to 0.5 ($0 < p/p0 < 0.5$). Since stronger interaction through hydrogen bond formation between

nitrogen and hydrogen can be expected, the higher the nitrogen content in the material, the strongest the interaction between water-solid. Such interaction gives information on the hydrophobicity and hydrophilicity of the CTFs.

The Henry constant (K_H) was calculated for all samples using the range of pressure $0 < p/p_0 < 0.1$. Figure 73 depicts the water vapor adsorption isotherms for all samples in the relative pressure range in which the Henry constant was calculated.

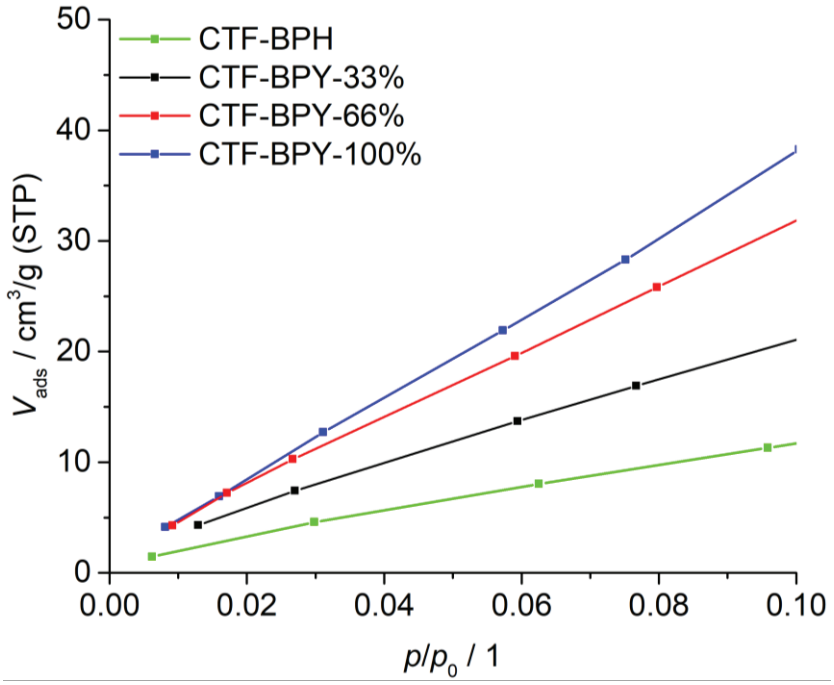

Figure 73 – Water adsorption isotherms for CTF-BPY series and CTF-BPH at $p/p_0 < 0.1$.

As is can be noticed from results in Figure 73, the constant K_H, calculates from the slope of the linear fitting of adsorption isotherms at low relative pressure, are different for all the materials. As expected, the lowest value for the constant, 1.5×10^{-6} mol/g/Pa, is given to CTF-BPH, which contains only biphenyl ligands. The lowest value represents the weaker interaction water-material from the series. Upon the increase in nitrogen content, the slope of the water adsorption curve gets higher. For CTF-BPY-33, the Henry constant reached 2.5×10^{-6} mol/g/Pa. With an additional increase in nitrogen content, K_H also increases, suggesting a stronger interaction between water and the porous polymer. K_H values of 3.8×10^{-6} and 5.2×10^{-6} mol/g/Pa were found for CTF-BPY-66% and CTF-BPY-100%, respectively. As expected, CTF-BPY-100% have the strongest interaction water-CTF, evidencing the higher nitrogen content of this material, resulting in more hydrogen bond formation at the surface.

Furthermore, using the data from water adsorption/desorption isotherms, pore filling degree was calculated as a ratio between the total pore volume for water adsorption isotherms at p/p_0 of 0.95 over the total pore volume found in nitrogen physisorption experiments at p/p_0 of 0.97. The results of pore filling degree and Henry constant for all samples were plotted in a graph depicted in Figure 74.

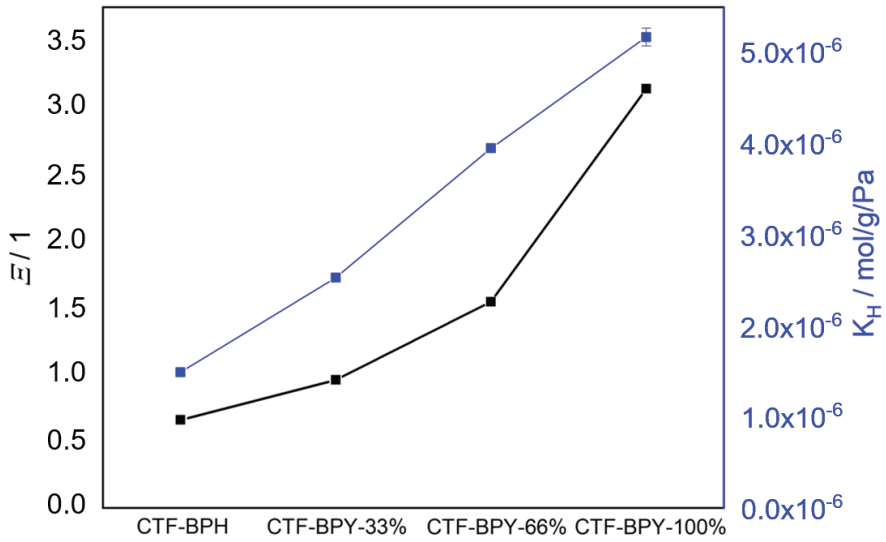

Figure 74 – Pore filling degree and Henry constant for samples CTF-BPH and CTF-BPY series.

Notably, the pore filling degree follows the same trend found in Henry's constant. Upon an increase in the bipyridine content within the framework, both pore filling degree and K_H also increases. Therefore, as expected, CTF-BPH represents the most hydrophobic material from the series, followed by CTF-BPY-33%. Both CTF-BPY-66% and CTF-BPY-100% are hydrophilic materials, with strong water-CTF interactions. Sample CTF-BPY-100% is the most hydrophilic material from the series.

Further characterization was done by elemental analysis. The theoretical content of carbon, nitrogen, and hydrogen was calculated using the repetition unit described in Figure 65. Both theoretical and experimental values can be found in table 5.

From the elemental analysis, it is possible to follow the increase in nitrogen content. In the first material, CTF-BPH, the amount of nitrogen is only derived from the triazine ring. The subsequent samples, include the bipyridine moiety, increasing gradually the nitrogen content. However, there is a significant deviation of the experimental values from the theoretical one. The high experimental hydrogen content indicates the adsorption

of water before the experiment since no thermic treatment was done before analyses. Therefore, the values of nitrogen and carbon consequently changed.

Table 5 – Elemental analysis of CTF-BPY series.

		Theoretical			**Experimental**		
Material	Formula	C%	H%	N%	C%	H%	N%
CTF-BPH	$C_{21}H_{12}N_3$	82.3	3.9	13.7	73.4	4.6	12.8
CTF-BPY-33	$C_{20}H_{11}N_4$	78.2	3.6	18.2	68.2	5.2	15.9
CTF-BPY-66	$C_{19}H_{10}N_5$	74.0	3.3	22.7	58.4	4.5	18.1
CTF-BPY-100	$C_{18}H_9N_6$	69.9	2.9	27.2	55.2	4.3	22.1

In order to better elucidate the structure of these materials, cross-polarization magic angle spinning carbon-13 nuclear magnetic resonance (CP-MAS ^{13}C-NMR) experiments were carried out in the CTF-BPY series. The resulting spectra are shown in Figure 75 as well as the fitting.

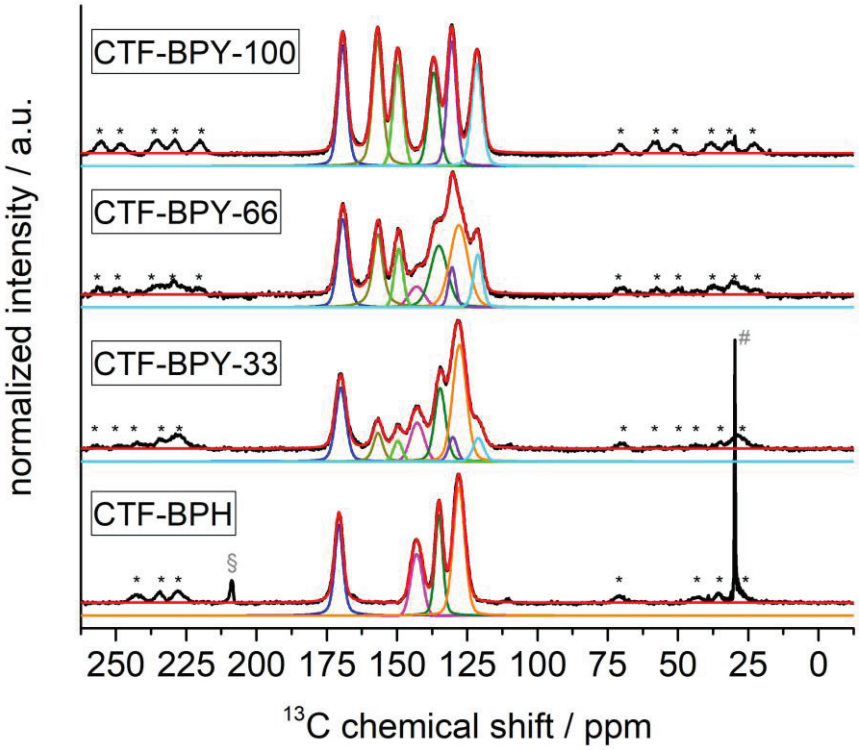

Figure 75 – CP-MAS ^{13}C-ssNMR spectra for CTF-BPY series and CTF-BPH.

From the ^{13}C-ssNMR spectra, it is possible to assign the signal at 170 ppm to the carbon from the triazine unit. Such a signal can be found in all samples. However, the other signals in the 160-115 ppm region change significantly according to the composition of the material. As expected, the resulting spectra of CTF-BPH contain only

signals from biphenyl and triazine building blocks, the signals at 142.8 and 135.1 ppm can be assigned to carbons at 1/1' and 4/4' positions while the signal at 128.1 ppm belongs to carbons in positions 2/2', 3/3', 5/5' and 6/6'. Figure 76 shows the color code with the structure of a biphenyl building block.

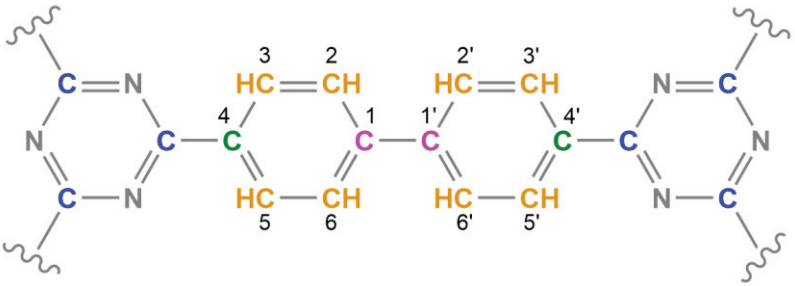

Figure 76 – Structure of biphenyl building block with color code from ss-NMR.

For material CTF-BPY-100, the ^{13}C-ssNMR spectra show 6 signals. All of them are assigned to the bipyridine and triazine building units. The signal at 170 ppm is assigned to the carbon in the triazine unit. The signal at 157 ppm is assigned to carbon in position 4/4', while the signal at 149.6 ppm can be assigned to carbon in position 5/5'. These two last signals are from carbons closed to the nitrogen atom in the bipyridine ligand and therefore have higher chemical shifts than the others. Subsequent signals at 137.1, 130.5 and 121.5 ppm are assigned to carbons in positions 2/2', 1/1' and 3/3', respectively. Figure 77 shows the structure of the bipyridine building block with the color code and the exact position of the carbons.

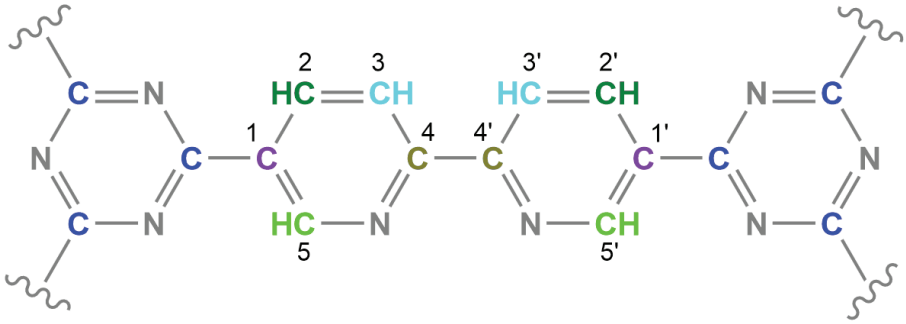

Figure 77 – Structure of bipyridine building block with color code from ss-NMR.

Furthermore, the spectra of both materials CTF-BPY-66 and CTF-BPY-33, present the signals from carbon assigned in the biphenyl and bipyridine ligands in different intensities, according to their composition. From the ss-NMR spectra of CTF-BPY-33, the signal at 170 ppm is assigned to the carbons in the triazine ring, while signals

at 156.8 and 149.9 ppm are assigned to carbons in position 4/4’ and 5/5’ from bipyridine building unit, respectively. The signal at 142.5 ppm belongs to carbon in position 1/1’ from the biphenyl unit. The region from 149 to 115 ppm contains three signals. Such signals are contributions from four different carbons in both bipyridine and biphenyl. Notably, the signals corresponding to carbons from the biphenyl are more intense than the ones from bipyridine.

The ^{13}C ss-NMR spectra of sample CTF-BPY-66 follow the same trend from previews sample, however, for this sample, the signals derived from carbons in bipyridine are more intense. Like all the other samples, the signal at 170 ppm is assigned to carbon in the triazine ring. Two well-defined signals at 156.9 and 149.6 ppm are assigned to carbons in positions 4/4’ and 5/5’ from the bipyridine ligand, respectively. In the region from 145 to 115 ppm, the signals from 5 different carbons from both ligands, biphenyl and bipyridine, can be assigned. As can be noticed from the spectra, the signals coming from carbons in the biphenyl are less intense than the last sample in which this ligand was in higher ratio, on the other hand, the contribution from carbons in bipyridine ligand to the resulting signals are more pronounced and intense, compared with sample CTF-BPY-33.

The CP-MAS ^{13}C-NMR clearly shows that by using the condensation approach it is possible to precisely control the ratio between two different ligands within the covalent triazine framework structure. Such achievement is a step forward the molecular control over CTFs structures, demonstrating the potential of the synthesis through condensation.

To investigate the optical properties of these covalent triazine frameworks, solid-state UV-Vis spectroscopy experiments were carried out. Notably, the differences in color can be seen with the naked eye. Figure 78 depicts an image from the three samples containing different amounts of bipyridine ligands.

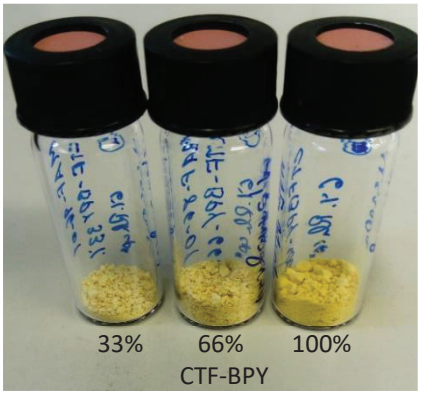

Figure 78 – Picture of samples CTF-BPY-33%, CTF-BPY-66%, and CTF-BPY-100%.

The resulting UV-Vis reflectance spectra for samples CTF-BPH, CTF-BPY-33, 66, 100% is depicted in Figure 79.

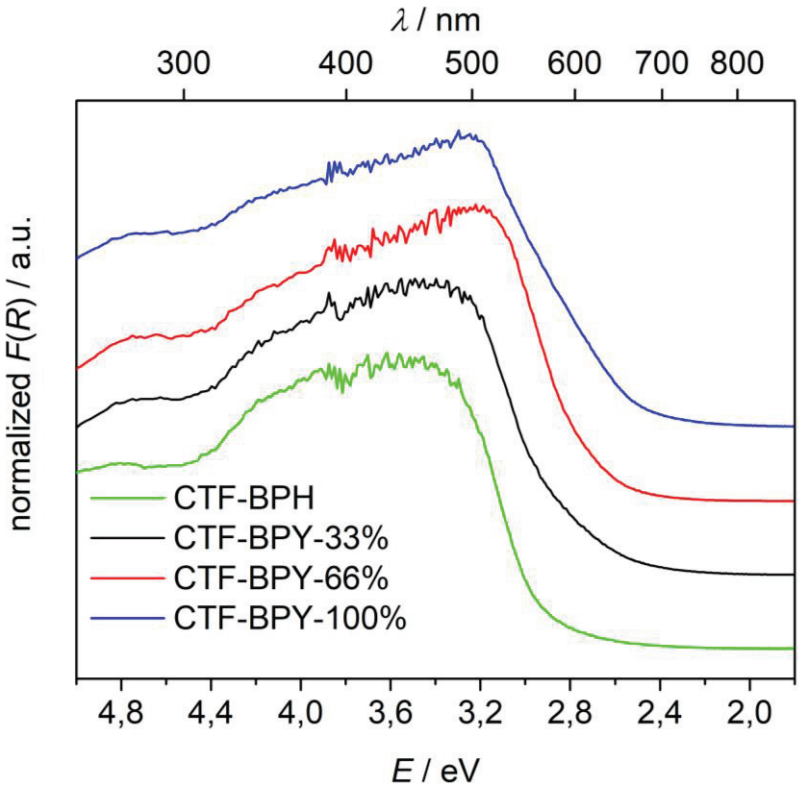

Figure 79 – Solid state UV-Vis analysis for CTF-BPY series and CTF-BPH, measured in reflectance mode.

As expected, with the increase in the bipyridine content, the light absorption shifts to higher wavelengths. CTF-BPH holds the narrowest absorption in the visible light spectrum, the material absorbs light up to 420 nm. On the other extreme, CTF-BPY-100% has the broadest absorption spectrum (up to 500 nm). CTF-BPY-33% and 66% possess similar properties, they absorb light up to 440 and 450 nm, respectively. Using UV-Vis data, the size of the bandgap was calculated using Tauc-plot. Figure 80 shows the calculation for all samples.

According to Tauc-plot, the bandgap of CTF-BPH is 2.93 eV, while the bipyridine-based CTFs possess values of 2.83; 2.75 and 2.53 eV for CTF-BPY-33%, CTF-BPY-66% and CTF-BPY-100%, respectively. These results are in accordance with the literature. With a higher amount of bipyridine, the heteroatom effect is more pronounced, allowing the material to absorb more light in the visible region, narrowing its bandgap. On the other hand, since CTF-BPH is based on biphenyl units, possessing

the lowest nitrogen content, the material has the smaller absorbance in the visible region and, consequently the bigger bandgap in the series.

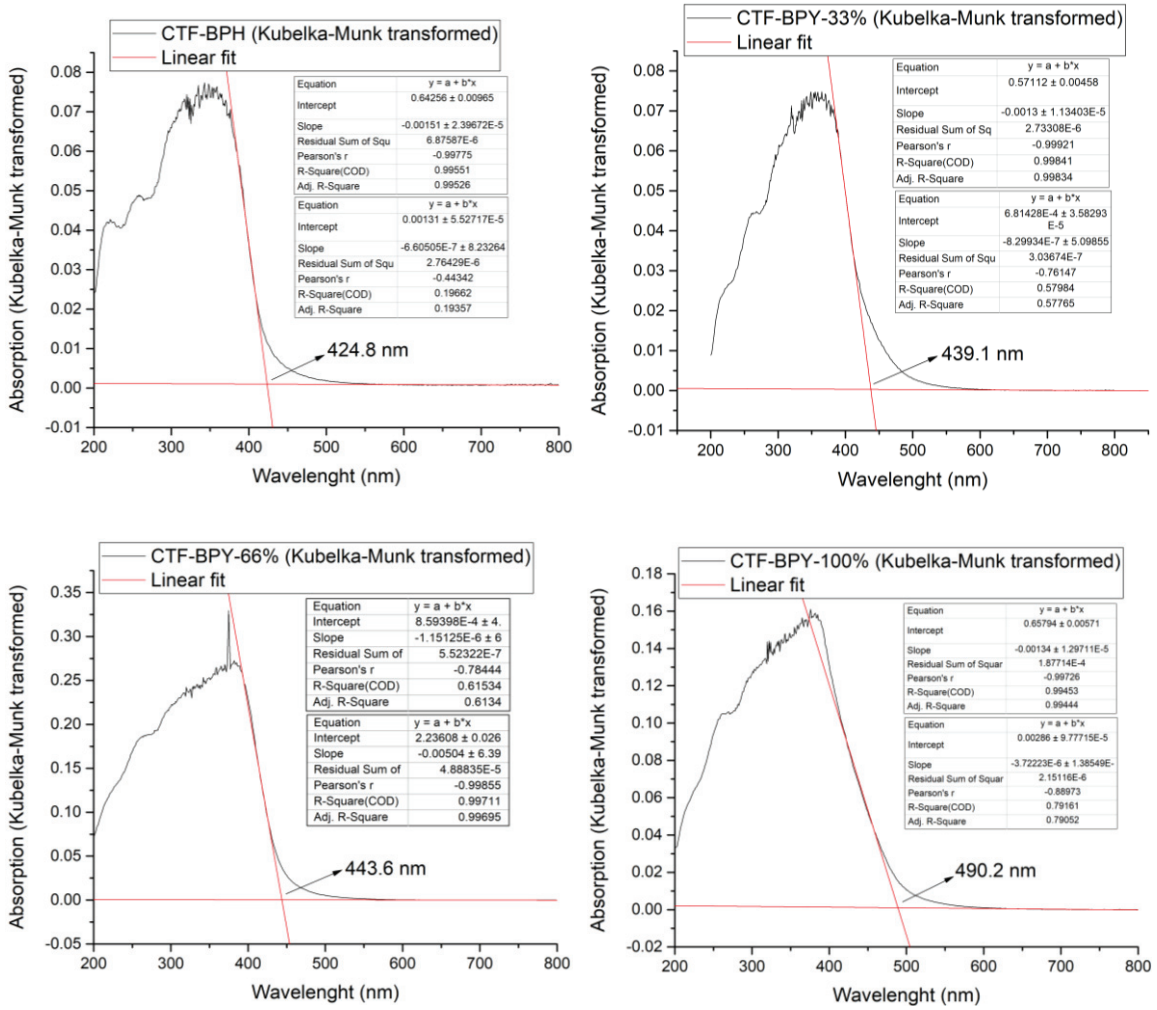

Figure 80 – Tauc-plot for samples CTF-BPH, CTF-BPY-33, 66 and 100.

When the bandgap is plotted against the nitrogen content, a clear correlation can be found. Figure 81 depicts the bandgap in terms of nm and eV for all CTFs in the series.

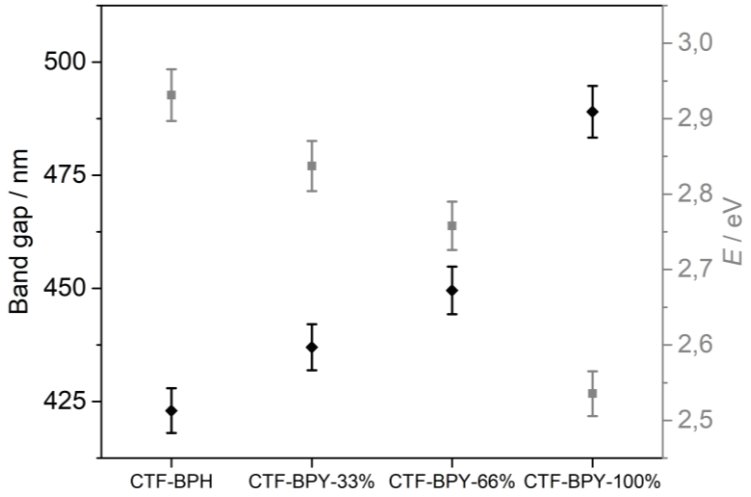

Figure 81 – Plot of bandgap in terms of nm and eV for all CTF-BPY series, including CTF-BPH.

According to Figure 81, the bandgaps calculated by Tauc-plot clearly follow a trend with regard to the bipyridine content. Starting with biphenyl-based CTF, holding the biggest bandgap, and following the decrease in bandgap according to the increase of bipyridine ligand within the framework. This trend shows another advantage of the condensation method in the synthesis of CTF in detriment to more conventional approaches like ionothermal and acid. Besides being a method in which it is possible to precisely control the content of a ligand within the CTF structure, it is also possible to control their properties by judiciously choosing the right building block. In the case of bipyridine-based CTFs, it is possible to control properties like porosity or visible light absorption, fundamental features in photocatalysis. The control over the molecular structure and its properties regarding the synthesis of these materials through condensation is unprecedented and it is a considerable step towards the development of high performing CTFs in many fields.

To get more insights into the structure of CTF-BPY-66%, XPS analysis carried out. Although the next experiment was done only in CTF-BPY-66%, there is a strong indication that both CTF-BPY-33% and CTF-BPY-100% possess the same properties. Figure 82 and 83 show the resulting spectra for carbon and nitrogen, respectively.

Three signals were found in carbon XPS. Their binding energies are 284.55, 286.65 and 288.65 eV. The signals are assigned to C-C, C=N and C-N moieties. Which is in accordance with the structure of CTF-BPY-66%.

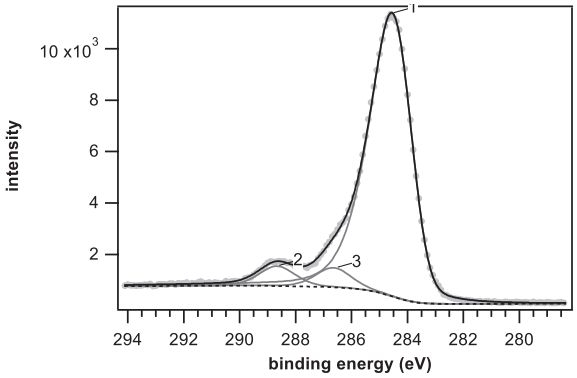

Figure 82 – C1s XPS analysis of CTF-BPY-66%.

Furthermore, the N1s spectra show only two nitrogen species. They are reflected by signals at 398,45 and 399,39 eV binding energies. The signals can be assigned to pyridinic and pyrrolic nitrogen species, respectively. No oxidized pyridinic units were

found. In comparison with CTF-MAS-84, based on the condensation of terephthalamidine chloride and terephthaldehyde, the materials CTF-BPY-66% shows a better polymerization.

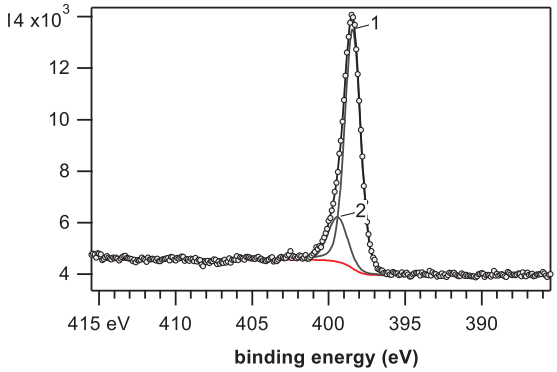

Figure 83 – N1s XPS analysis of CTF-BPY-66%.

In the next section, an attempt to synthesize a crystalline CTF is described. Further, the metalation process, in which the rhodium Cp* complex is infiltrated within the bipyridine-based CTF, will be discussed and later the application of this fully heterogeneous photocatalytic system in CO_2 reduction under visible light irradiation will be described in section 5.4.

5.2 ATTEMPT TO SYNTHESIZE A CRYSTALLINE BYPIRIDINE-BASED CTF

Additionally, to the samples described above, an attempt to synthesize crystalline CTF based on bipyridine units by changing the precursor from aldehyde to alcohol was investigated. The structure of the starting materials is illustrated in Figure 84.

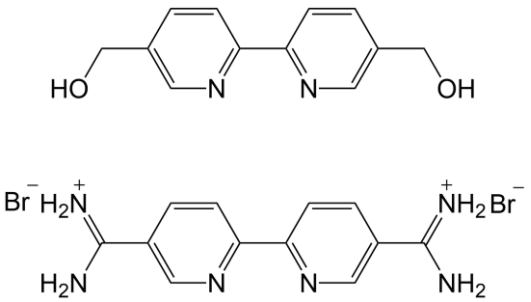

Figure 84 – Structure of 5,5'-di(hydroxymethyl)-2,2'-bipyridine and 5,5′-diamidine-2,2′-bipyridine dibromide.

The enhancement in crystallinity is due to the low nucleation rate. The triazine formation only happens upon condensation of aldehyde and amidine. Therefore, the alcohol has to be oxidized to the aldehyde prior reaction. Such oxidation occurs in situ, employing DMSO and air as oxidant. With the aldehyde feeding rate controlled by the in-situ oxidation of alcohol, the nucleation rate slows down. As a consequence, crystals with better quality and superior crystallinity can be obtained.

The synthesis of CTF using alcohol as a precursor, is done at higher temperatures. The maximum temperature when aldehyde is employed is 120ºC, while for alcohol, this value reaches the boiling point of DMSO, about 189ºC. At the boiling point, DMSO starts to decompose. The main decomposition products are paraformaldehyde, dimethyl sulfide, dimethyl disulfide, bis-(methylthio)methane and water. Judging by the brownish color and strong persistent smell of dimethyl sulfide, one could expect sulfur insertion in the framework structure. Therefore, the attempt to synthesize crystalline CTFs was done at a lower temperature. The sample was named CTF-MAF-101. The complete experimental procedure for the synthesis of precursors as well as the resulting material can be found in the appendix, pages 229 and 232. Figure 85 shows a comparison between CTF-BPY-100 and CTF-MAF-101.

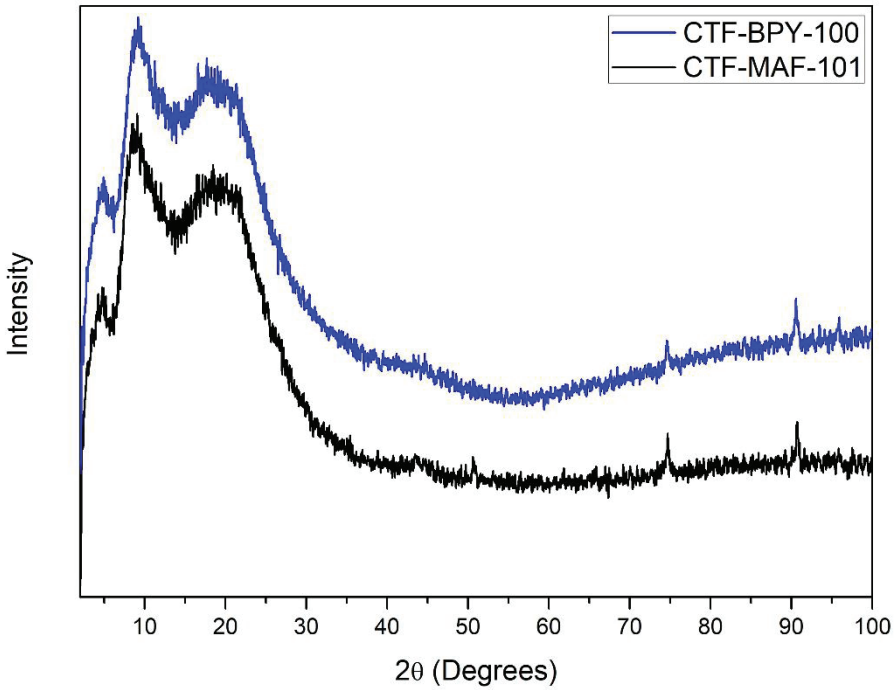

Figure 85 – PXRD pattern for samples CTF-MAF-101 and CTF-BPY-100.

As can be noticed from PXRD, changing the precursor from aldehyde to alcohol and conducting the reaction at a lower temperature, in the case of bipyridine CTFs, did not enhance the crystallinity.

FT-IR analysis was carried out to investigate the formation of the triazine bonds. The spectra of the resulting CTF-MAS-101, synthesized with the alcohol precursor is depicted together with the FT-IR spectra of CTF-PY100%, synthesized with aldehyde as starting material. Figure 86 depicts the spectra.

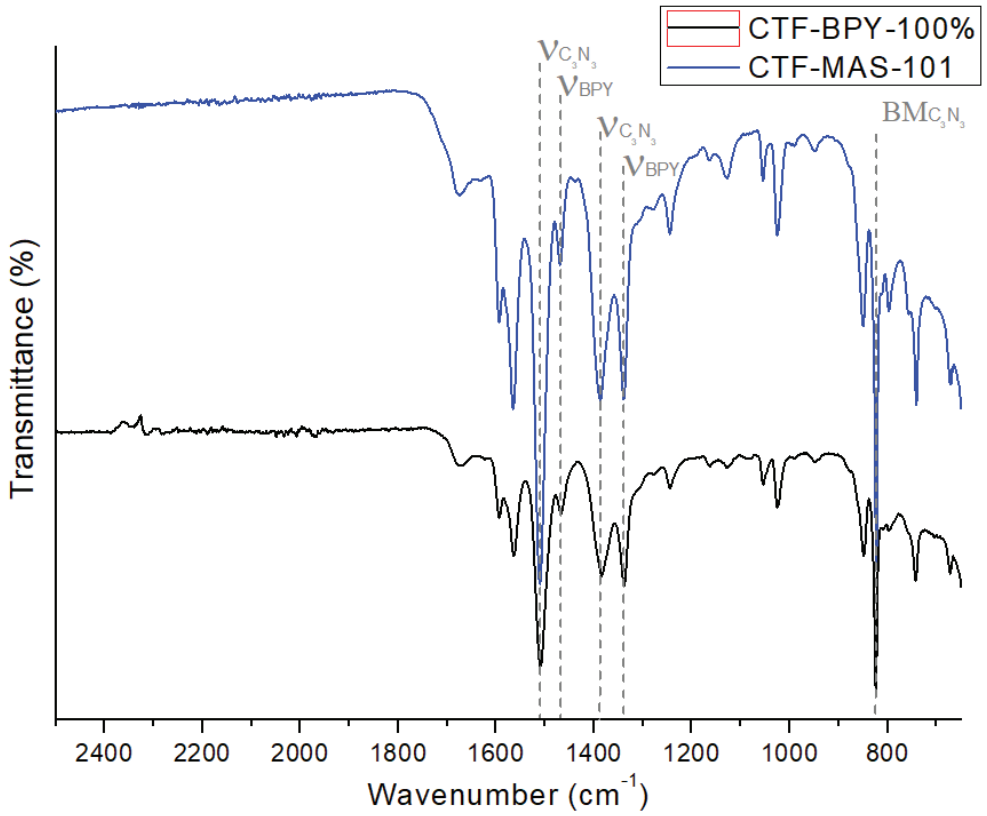

Figure 86 – FT-IR spectra of CTF-BPY-100% and CTF-MAS-101.

From the FT-IR analysis, it is possible to assign the main bands of the triazine linkage. Stretching vibrations at 1510, 1385 and 816 cm^{-1} can be assigned to C=N, C-N and breathing mode of triazine. Additionally, two stretches from the bipyridine building block can be found at 1465 and 1336 cm^{-1}. These bands can be assigned to -C=N- and –C-N- from the bipyridine units.

An investigation on the porous structure of the resulting material was done through N_2 physisorption analysis, measured at 77K. Figure 87 depicts the N_2 adsorption/desorption isotherms for sample CTF-BPY-100%, synthesized from the

amidine and aldehyde condensation, and CTF-MAS-101, in which the alcohol was employed as aldehyde substitute.

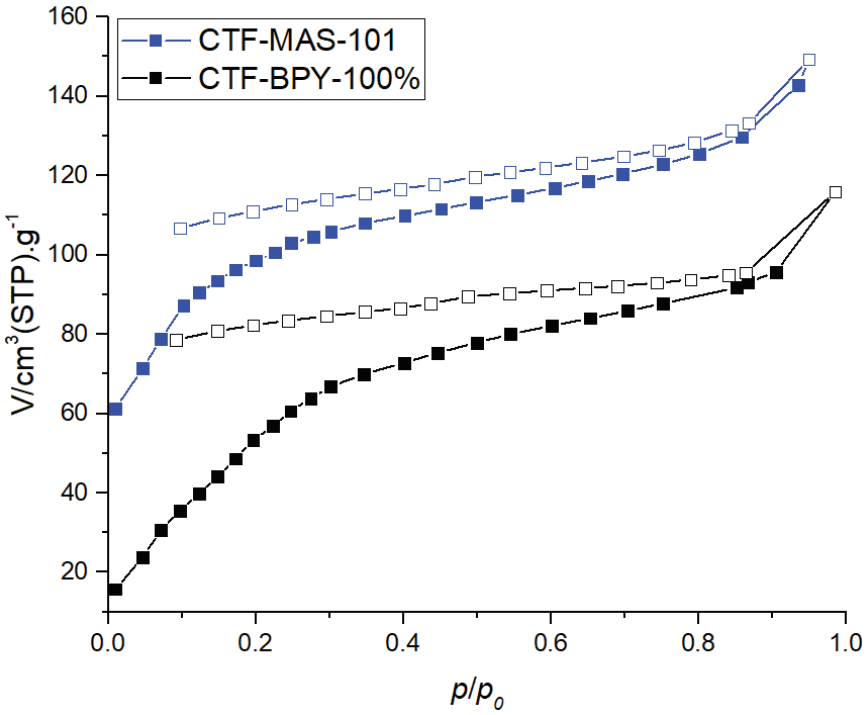

Figure 87 – N_2 adsorption/desorption isotherms of CTF-BPY-100% and CTF-MAS-101.

According to the N_2 physisorption, both isotherms present very similar behavior. They can be assigned to shape type II from the IUPAC classification. Moreover, the calculated specific surface area calculated from the BET theory, the material synthesized with the alcohol precursor, CTF-MAS-101, achieved 364 m^2/g in comparison to 234 m^2/g from the material synthesized with the aldehyde. This improvement in the surface area could be explained due to better alignment in the bi-dimensional CTF sheets since the material is organized at a slower rate.

The attempt to synthesize a crystalline bipyridine-based CTF had failed, as evidenced by the powder XRD analysis. Even though the material synthesized with the alcohol precursor have shown an enhancement in specific surface area, CTF-MAS-101 was not employed in the catalytic reduction of CO_2 under visible light irradiation. Further characterization analysis and optimization on the protocol of CTF synthesis through condensation using the alcohol precursor, has to be carried out to achieve better results.

The next section describes the infiltration of rhodium Cp* catalyst within the CTF-BPY series.

5.3 METALATION OF BYPIRIDINE-BASED CTFs

The main reason for the utilization of bipyridine ligands in the synthesis of covalent triazine frameworks was to use the materials as scaffolds for catalytically active species. Therefore, using its chelating properties, the infiltration of the molecular complex rhodium Cp* prior to the catalytic application in CO_2 photoreduction was carried out.

First, to infiltrate the rhodium Cp* complex, the dimer pentamethylcyclopentadienyl rhodium dichloride ($[Cp^*RhCl_2]_2$) had to be converted to the mono rhodium complex. The cleavage in the bridge-bonded complex was carried out using $AgNO_3$ in acetonitrile (the complete experimental procedure can be found in the appendix page 233). The infiltration of the rhodium complex into the material was carried out by mixing the rhodium complex solution and the CTF in anhydrous methanol. The mixture was stirred for 24 hours, and during this time, the dark yellow solution became clear, as a result of the infiltration. After this time, the mixture was centrifuged and the solvent exchanged to clean the unbounded complexes. After exchanging the solvent five times, the material was dried in an oven at 60ºC to afford the rhodium-functionalized material. Figure 88 illustrates the structure of one layer of the rhodium-functionalized CTF-BPY-66.

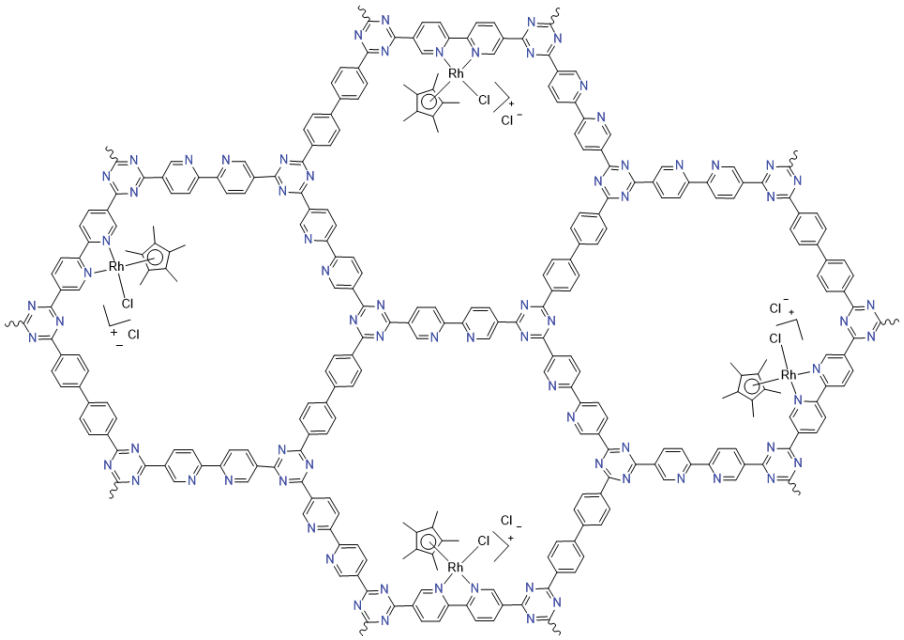

Figure 88 – Ideal structure of CTF-BPY-66% functionalized with rhodium Cp* complex.

In order to investigate the local structure of this bipyridine-based covalent triazine framework, a magic angle spinning solid-state NMR measurement was performed on sample CTF-BPY-66%. The analysis was done with the material before and after loading with a rhodium complex. Figure 89 depicts the ^{13}C MAS ssNMR for sample CTF-BPY-66 with 6 and 12% rhodium complex in mol, as well as the material without the complex.

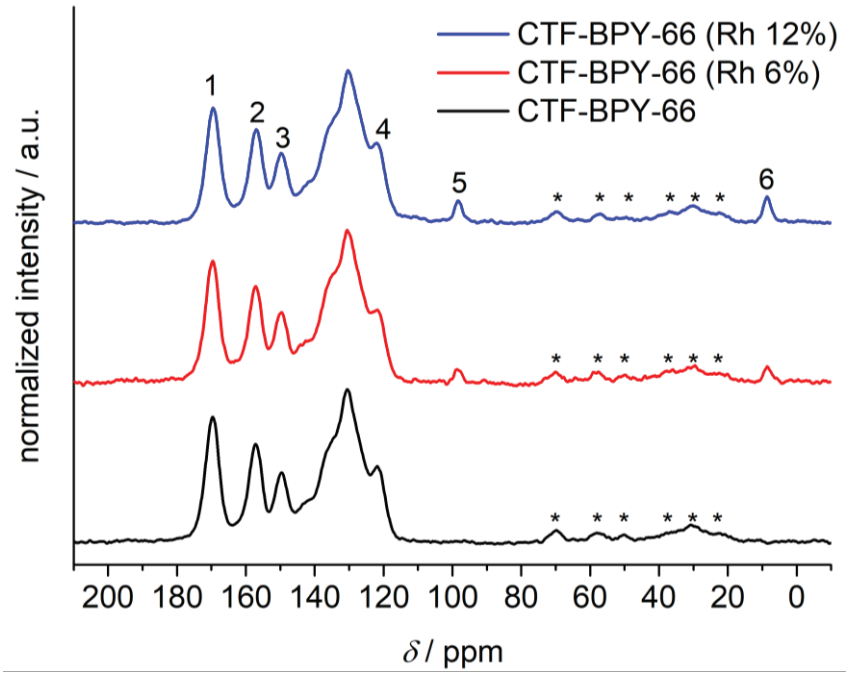

Figure 89 – ^{13}C ssNMR analysis of CTF-BPY-66 and RhCp*@CTF-BPY-66%.

According to the resulting spectra, the signal at 169.3 (1) ppm corresponds to the carbon atoms located in the triazine ring. The signals at 156.8 (2) and 148.9 (3) ppm can be assigned to carbons in position C5/5' and C6/6' from the bipyridine ligand. The signals in the range of 145-123 ppm are assigned to carbons in the biphenyl building block overlapped with signals from carbons in positions C4/4' from the bipyridine unit. Moreover, the signal at 121.7 (4) ppm corresponds to carbon in position C3/3' from bipyridine. Both signals (5) and (6) at 98.2 and 8.5 ppm, can be assigned to the rhodium metal complex. The absence of these signals in the spectrum of CTF-BPY-66% without the molecular catalyst supports this assignment, as well as the increase in the peak intensity with the increase in the metal loading. Signals with * denote spinning sidebands. Figure 90 illustrates the structure of RhCp*@CTF-BPY-66% and the assignment of signals in the ssNMR spectra.

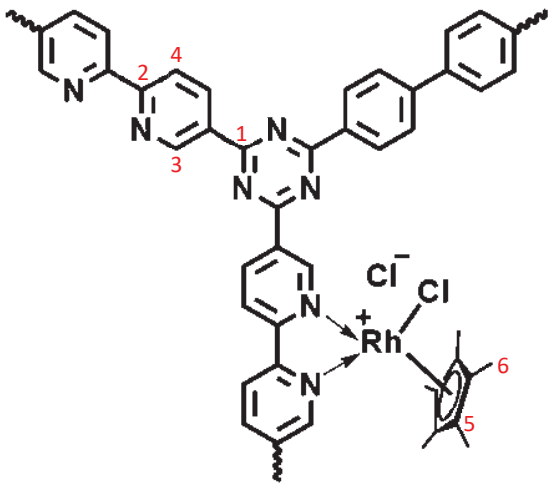

Figure 90 – ^{13}C ssNMR signals assignment for sample RhCp*@CTF-BPY-66%.

Attempting to verify the site of coordination of the rhodium Cp* complex, FT-IR study was carried out comparing samples with and without the metal complex. Figures 91, 92 and 93 depict both spectra for samples with and without rhodium for samples CTF-BPY33%, CTF-BPY-66%, and CTF-BPY-100%, respectively.

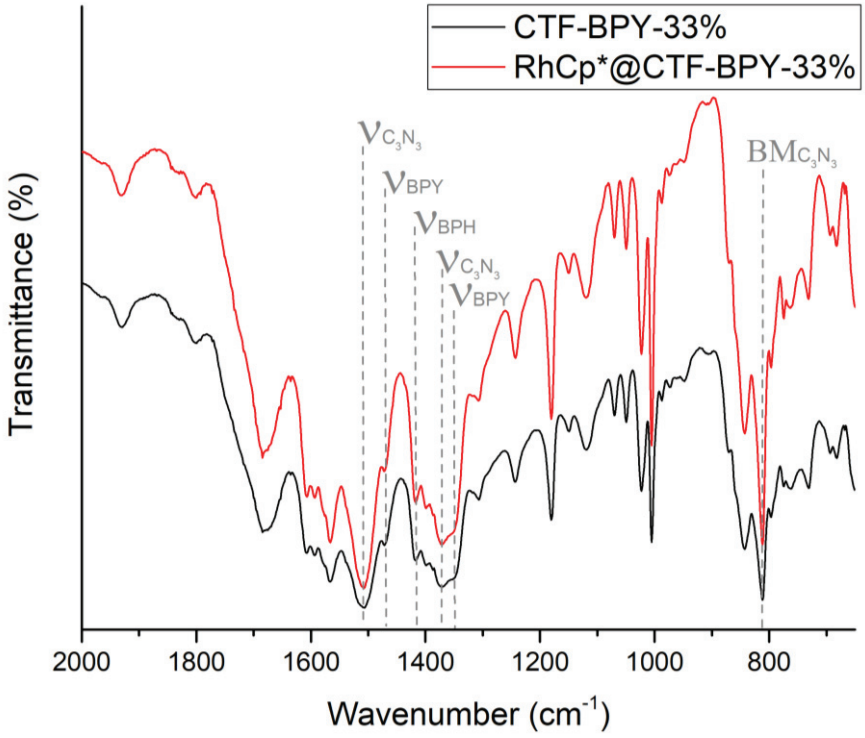

Figure 91 – FT-IR spectra of sample CTF-BPY-33% and RhCp*@CTF-BPY-33%.

As can be noticed from FT-IR spectra, no deviation or shifting in the main stretching vibration is identified. Both spectra, with and without rhodium, present the

same features. In some cases, even the same intensity. All samples have shown the same behavior, therefore, from FT-IR it is not possible to assure the exact coordination site from the metal complex.

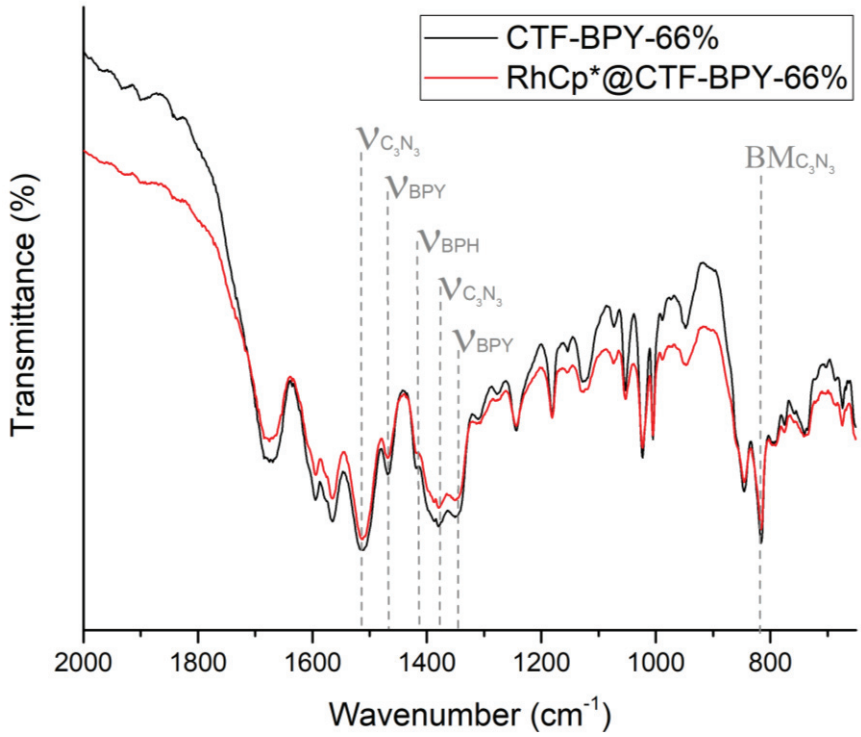

Figure 92 – FT-IR spectra of sample CTF-BPY-66% and RhCp*@CTF-BPY-66%.

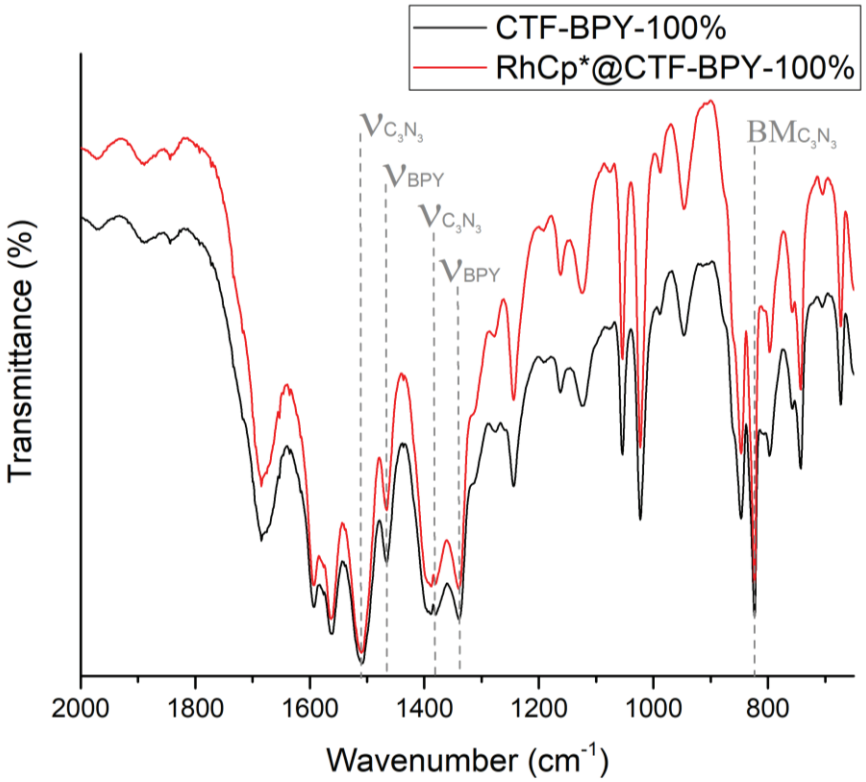

Figure 93 – FT-IR spectra of sample CTF-BPY-100% and RhCp*@CTF-BPY-100%.

All the stretching vibrations for triazine ring, bipyridine and biphenyl building blocks can be assigned from the spectra depicted in Figures 87, 88 and 89. The main bands of the triazine ring can be found at 1510, 1375 and 817 cm^{-1}. They are assigned to -C=N-; -C-N- and the breathing mode of triazine, respectively. Moreover, the stretches at 1467 and 1335 cm^{-1} are assigned to -C=N- and –C-N- from the bipyridine units, respectively. The stretch at 1416 cm^{-1} is assigned to -C=C- from biphenyl building blocks and can be found only in samples CTF-BPY-33% and CTF-BPY-66%, since this ligand is not present in sample CTF-BPY-100%, as evidenced by the FT-IR spectra. Although not shown in the spectra, no stretch at 2226 cm^{-1} was found, confirming the absence of nitrile contamination in the series.

In order to evaluate the consequences of the rhodium infiltration on the porous structure of these materials, as well as their wettability, water vapor and acetonitrile adsorption studies were carried out at 279 K. Acetonitrile adsorption/desorption isotherms for samples with and without rhodium Cp* complex are depicted in Figure 94.

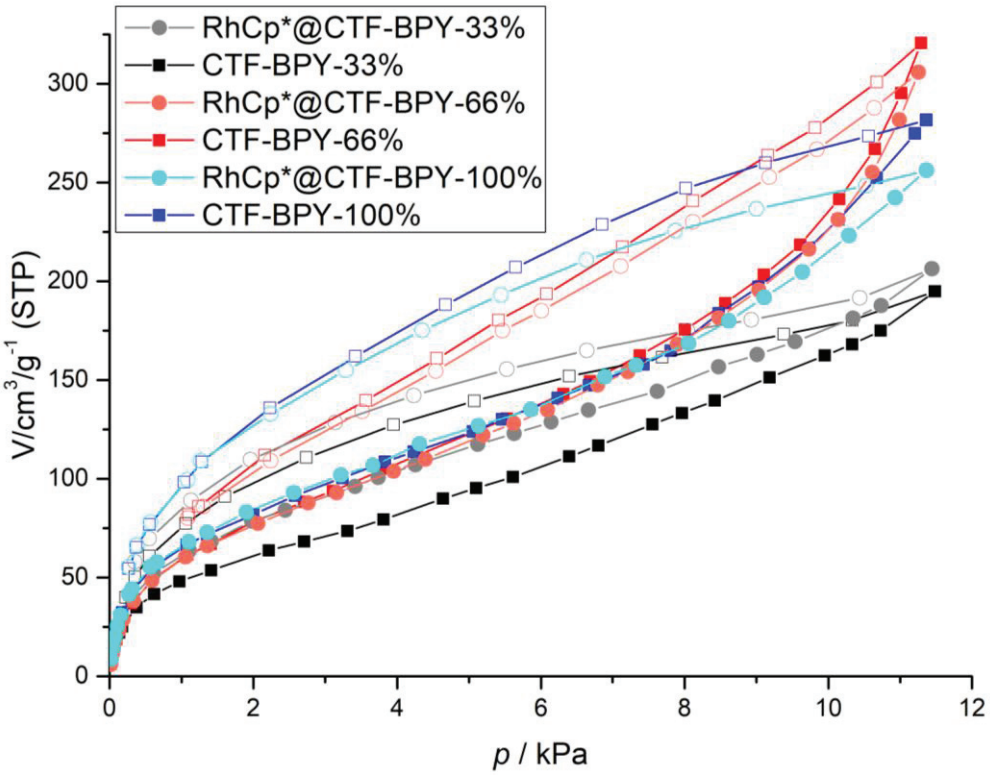

Figure 94 – Acetonitrile adsorption/desorption isotherms for CTF-BPY series with and without RhCp*.

The isotherms depicted in Figure 94 are classified as type II according to IUPAC classification. The continuous increase in acetonitrile uptake and the significant hysteresis present in all isotherms, suggests swelling behavior. Only a small deviation in sample

CTF-BPY-33% with and without rhodium complex can be noticed. The sample with rhodium-infiltrated complex possesses a slightly higher uptake of acetonitrile, compared with samples without the molecular catalyst. In the other samples, CTF-BPY-66% and CTF-BPY-100% the materials containing the metal complex within the structure did not show any difference in acetonitrile adsorption/desorption isotherms.

From the slope of the adsorption curve at lower pressure, it is possible to calculate the Henry constant. This constant is fundamental in order to investigate if the presence of the rhodium Cp* complex has changed the interaction between acetonitrile solvent and the surface of these CTFs. Figure 95 shows the acetonitrile adsorption curves for samples CTF-BPY-33%, 66% and 100% with and without rhodium complex at low pressure ($p<0.1$).

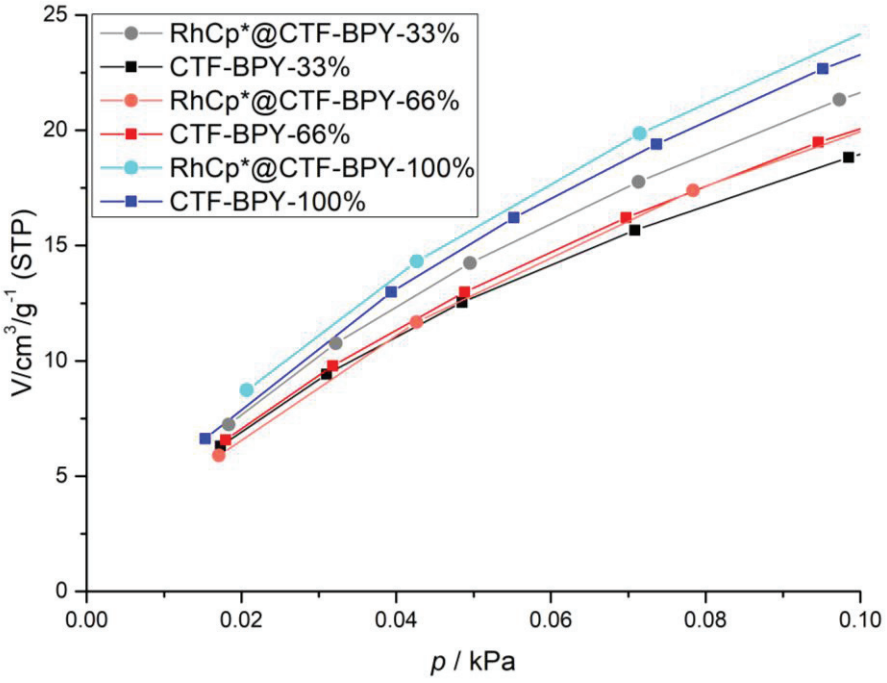

Figure 95 – Acetonitrile adsorption isotherms for CTF-BPY series with and without RhCp* at low pressure.

From the slope at lower pressure, the infiltration of 6% in mol of rhodium Cp* complex did not change the adsorptions isotherms for samples CTF-BPY-66% and CTF-BPY-100%. However, for sample RhCp*@CTF-BPY-33% the slope is higher than the material without the metal complex, showing a higher uptake. One hypothesis to explain this deviation is due to the alignment of bi-dimensional CTF sheets to accommodate the rhodium, increasing the uptake. Another hypothesis is due to the activation process and errors during the measurement.

The calculated Henry constants for the CTF-BPY series before and after the infiltration are shown in Table 6.

Table 6 – Henry constant calculated from acetonitrile adsorption isotherm at low temperature for CTF-BPY series with and without RhCp*.

BPY content	Henry constant (K_H) in mol/g/Pa	
	CTF-BPY-X	RhCp*@CTF-BPY-X
33%	$9.1x10^{-6}$	$8.4x10^{-6}$
66%	$8.9x10^{-6}$	$8.6x10^{-6}$
100%	$10.8x10^{-6}$	$10.3x10^{-6}$

From the results showed in Table 6 it is possible to assure that the materials with and without rhodium have the same order of acetonitrile wettability. All the calculated constants present the same order of magnitude, indicating very similar behavior in terms of acetonitrile-CTF interaction. Assuring the same solvent-catalyst interaction is essential to compare the results obtained in photocatalysis.

Further investigation on the pore structure of these materials has been carried out using water adsorption experiments, measured at 289K. The resulting isotherms are depicted in Figure 96.

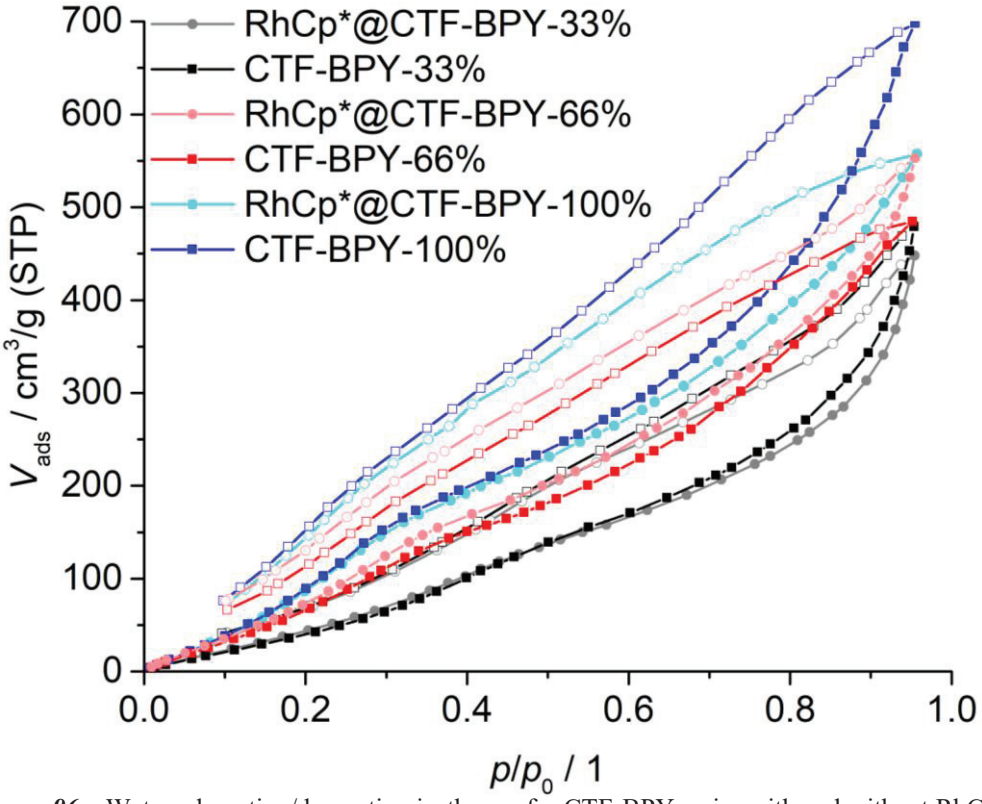

Figure 96 – Water adsorption/desorption isotherms for CTF-BPY series with and without RhCp*.

From the isotherms presented in Figure 96, the isotherms for samples CTF-BPY-100% and 66% are assigned to type II, according to IUPAC classification. The isotherms for samples RhCp*@CTF-BPY-100% and RhCp*@CTF-BPY-66% follow precisely the same behavior, and therefore, can be assigned to the same type. The shape of isotherms for samples CTF-BPY-33% and RhCp*@CTF-BPY-33% present a mixture of types II and III. When comparing the samples containing the rhodium complex and the pristine ones, no deviation is found.

The Henry constant (K_H) was calculated for all samples using the range of pressure $0 < p/p_0 < 0.1$. Figure 97 depicts the water vapor adsorption isotherms for all samples in the range of relative pressure of $0 < p/p_0 < 0.3$.

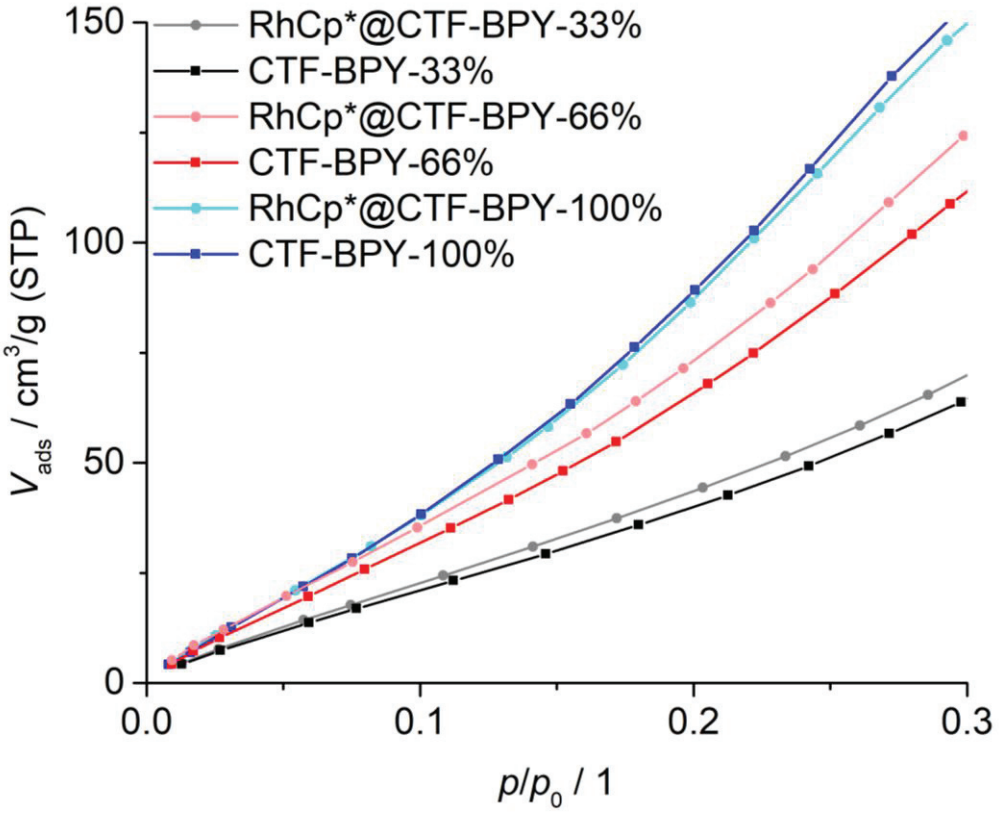

Figure 97 – Water adsorption/desorption isotherms for CTF-BPY series with and without RhCp*.

The comparison of Henry's constant between the samples containing the rhodium complex and the pristine ones are shown in Table 7.

Table 7 – Henry constant calculated from water adsorption isotherm at low temperature for CTF-BPY series with and without RhCp*.

BPY content	Henry constant (K_H) in mol/g/Pa	
	CTF-BPY-X	RhCp*@CTF-BPY-X
33%	$2.5x10^{-6}$	$2.7x10^{-6}$
66%	$3.9x10^{-6}$	$4.0x10^{-6}$
100%	$5.4x10^{-6}$	$5.1x10^{-6}$

According to the Henry constant showed in Table 7, the samples containing the metal complex present the same trend as the pristine materials. Therefore, the presence of rhodium Cp* molecular catalysts did not change the wettability properties for the bipyridine-based materials. In this regard, the materials have shown the same trend in hydrophilicity, while the nitrogen content increases, the water-CTF interaction gets stronger, indicating more hydrophilic behavior.

After loaded with the rhodium complex, all the materials were tested as photoactive support for carbon dioxide conversion. The next section will explain and discuss in detail the photocatalytic tests.

5.4 PHOTOCATALYTIC TEST

The main reason for the utilization of bipyridine ligands for the synthesis of covalent triazine frameworks was to use the materials as scaffolds for catalytically active species. Taking advantage of the condensation approach, which leads to photoactive materials, the series of bipyridine-based covalent triazine framework was applied in CO_2 photoreduction.

The utilization of a photosensitizer in the photocatalytic system normally leads to very high activity due to the enhanced charge separation. However, its utilization is also a drawback for long-term reactions. Photosensitizers typically are ruthenium or iridium metal complex containing ligands with a large delocalized π-system ($[Ru(bpy)_3]^{2+}$ for example). During catalysis, irreversible reactions like ligand exchange or oxidation of the metal center take place, causing the complete degradation of the photosensitizer over time. As a consequence, the electrons stop flowing to the active site, resulting in loss of activity.

In an attempt to enhance the stability of these photocatalytic systems, different research groups attempt to heterogenize the photosensitizer. Different materials like MOFs and POPs were employed as binding material for heterogenization of the $[Ru(bpy)_3]^{2+}$ complex. Up to now, no heterogenized system enabled higher activity towards photocatalytic CO_2 than the homogeneous ones. However, concerning the stability of these systems in the long-term reaction, the heterogenized systems typically surpass the homogeneous one by far. Additionally, the heterogenized system profit from easy handling and separation from the products. Moreover, the recyclability is also an advantage over the homogeneous systems.

As explained in section 2.2 in chapter 2, a typical photocatalytic reaction can be described in terms of four steps:

1- Absorption of light by a semiconductor and the generation of electron-hole pairs;

2- Charge separation HOMO-LUMO orbitals;

3- Transfer of generated charges to the surface of the photocatalyst

4- The charges at surface triggers redox reactions.

Comparing the homogeneous and heterogenized systems, all the four steps described above occur in different locations of material and photosensitizer. Figure 98 illustrates all four steps in a homogeneous photocatalytic cycle.

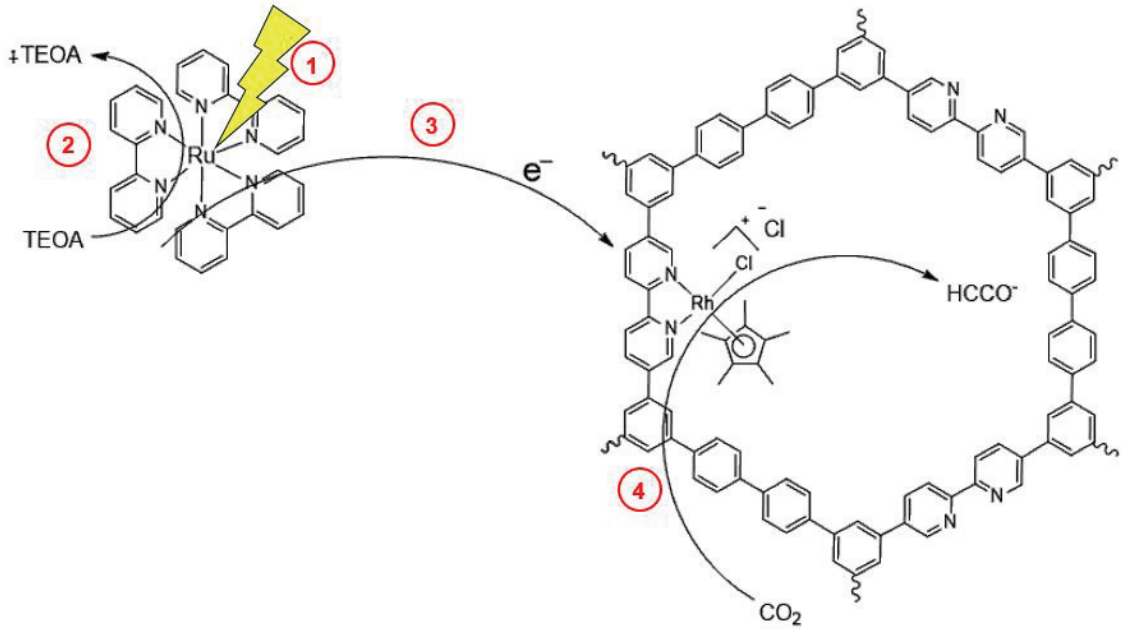

Figure 98 – Four steps of homogeneous photocatalytic CO_2 reduction using a $[Ru(bpy)3]^{2+}$ photosensitizer.

Seeking for long-term stability, the "all-in-one" strategy was employed to synthesize materials in which the photosensitizing unit heterogenized. The ability of the triazine ring to generate the electron-hole pairs, oxidize triethanolamine (sacrificial reagent), deliver electrons to the active rhodium Cp* complex to trigger the CO_2 reduction, dispenses the utilization of a homogeneous photosensitizer. Figure 99 depicts the steps of a photocatalytic reaction in the case of a heterogenized system.

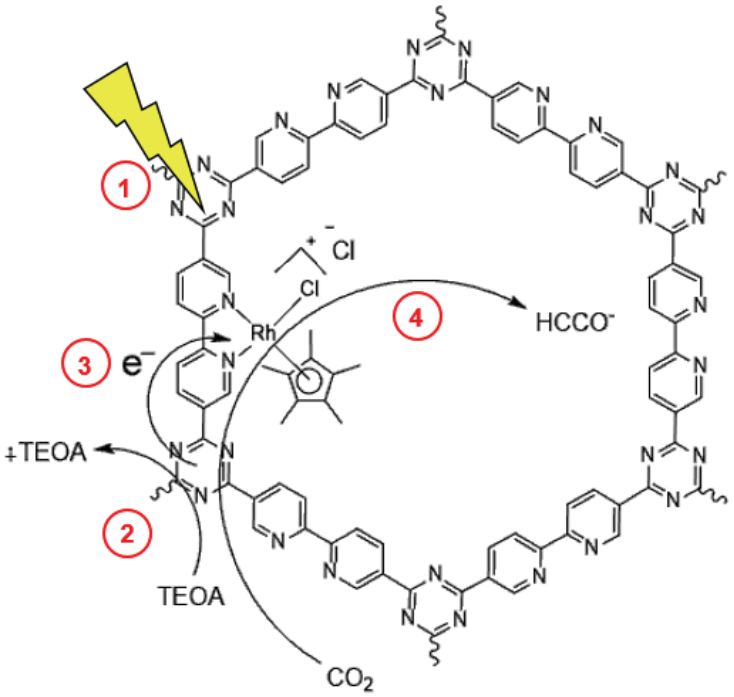

Figure 99 – Four steps of photocatalytic CO_2 reduction in a fully heterogeneous system. The triazine is the photosensitizer while the bipyridine supports the active metal centre.

The first material to be synthesized in the bipyridine-based CTF series was CTF-BPY-66%. The technique of exchanging the counter-ion to purify the amidine chloride worked well in the case of 5,5′-diamidine-2,2′-bipyridine dibromide. The amidine was used in the synthesis of porous bipyridine-based CTFs through condensation. Moreover, CTF-BPY-66% was the first material to be infiltrated with rhodium Cp* complex and tested in photocatalytic CO_2 reduction.

The material CTF-BPY-66% was loaded with 6% Rh complex in mol. The utilization of rhodium Cp* complex leads only to formate production, no other product was detected during the reaction, not even hydrogen.

For a typical photocatalysis experiment, about 1 mg of the porous framework was weighed into a UV-Vis cuvette (path length: 10 mm). Then 2 ml of acetonitrile and

triethanolamine (5:1 in volume) were added. The solution was saturated with CO_2 for 15 min. The cuvette was sealed, and the solution irradiated for 4 h using a 200 W Hg(Xe) lamp (Newport Research Arc Lamp), equipped with a 420 nm UV cutoff filter and a water-based IR filter unit, cutoff 950 nm, using a working distance of 10 cm, and an irradiance of 1030 W/h.m^2 (for a typical catalysis of 4 h, this corresponds to a total irradiation of 4120 W/m^2). After 4 h the material was removed by centrifugation and the liquid phase was analyzed by quantitative ^{1}H-NMR.

The results from catalytic tests, regarding the application of RhCp*@CTF-BPY-66% as photocatalyst in CO_2 conversion, are shown in Table 8.

Table 8 – Results of the application of RhCp*@CTF-BPY-66% in photocatalytic reduction of CO_2.

Reaction	Material	TON_{HCOO-}	TOF (h^{-1})	R / μmol/g_{cat}/h
Anhydrous	RhCp*(6%)@CTF-BPY-66	15.9	3.97 ± 0.39	376.05
4 hours	RhCp*(6%)@CTF-BPY-66	14.5	3.64 ± 0.36	344.31
Leaching test	RhCp*(6%)@CTF-BPY-66	-	-	340.58
8 hours	RhCp*(6%)@CTF-BPY-66	25.3	3.16 ± 0.31	298.97

The reactions were done three times to assure reproducibility. At first, the reaction was done in an anhydrous solvent. The reason to use dry solvent relies on the ability of CTF to split water for hydrogen production. Therefore, if water is present in the solvent, the electrons produced might also trigger the water reduction reaction, leading to low activity towards CO_2 reduction. To avoid side reactions, the first test was done in the complete absence of water. Turnover number (TON) of 15.9 was achieved for formate production.

In the second entry in Table 8, the reaction was done using standard grade solvents. TON of 14.5 was achieved in such a system, moreover, the production rate of formate was 344.31 μmol/g_{cat}/h, representing 31.74 μmol/g_{cat}/h lower than the first entry, when the anhydrous solvent was employed. Such result is consistent with the strong ability of CTFs to reduce water under visible light irradiation. Therefore, a small decrease in activity might be related to hydrogen production.

After four hours of reaction (entry 2), the mixture was centrifuged and the solid removed. The solution was again irradiated for another 4 hours without the solid. At the end, the sample was analyzed by quantitative ^{1}H-NMR. No increase in the formate

production was observed. Entry 3 was an attempt to check for rhodium leaching. However, because the CTF is the heterogeneous photosensitizer, even though there was leaching of rhodium, the metal complex is not capable to reduce CO_2 by itself. The right approach to detect rhodium leaching is to measure ICP-OES from the solution.

Looking for long-term stability, the reaction was performed at a longer time. Entry 4 shows the result for 8 hours reaction. TONs of 25.3 were achieved during this time. The rate of formate production was 298.97 $\mu mol/g_{cat}/h$. The result shows a lower production rate over a longer reaction time, it might indicate leaching of the active rhodium metal complex, or other deactivation processes taking place.

In comparison with the state-of-art, RhCp*@CTF-BPY-66% showed the highest activity in a heterogenized system. Up to now, all the materials tested in CO_2 photoreduction, using a heterogeneous photosensitizer, are based on ligand exchange in Metal-Organic-Frameworks. Table 9 shows the materials and the respective turnover number for formate production of the relevant state-of-art.

Table 9 – Activity of the fully heterogeneous systems from the state-of-art in CO_2 photoreduction.

Support	Catalyst	TON_{HCOO-}	Reference
UiO-66-catechole	Cr^{3+}	11.2	[117]
UiO-66-catechole	Ga^{3+}	6.14	[117]
UiO-66-NH_2 (Zr/Ti)	Zr, Ti sites	6.3 ± 0.2	[118]
UiO-66-$(NH_2)_2$ (Zr/Ti)	Zr, Ti sites	4.7 ± 0.2	[118]
NH_2-MIL-125 (Ti)	Ti sites	1.52	[119]
MIL-101-NH_2 (Al)	[Cp*Rh(bpy)Cl]NO_3	3.3	[105]

Later, CTFs BPY-33% and BPY-100% were infiltrated with 6% of rhodium Cp* complex in mol, using the same protocol described for CTF-BPY-66%. The materials containing the rhodium Cp* were tested in CO_2 photoreduction. Table 10 shows the results obtained for samples RhCp*@CTF-BPY-33% and RhCp*@CTF-BPY-100%.

Table 10 – Results of the application of RhCp*@CTF-BPY-33% and RhCp*@CTF-BPY-100% in photocatalytic reduction of CO_2.

Reaction	Material	TON_{HCOO-}	TOF (h^{-1})	R / μmol/g_{cat}/h
4 hours	RhCp*(6%)@CTF-BPY-33%	1.23	0.31 ± 0.001	53.88
4 hours	RhCp*(6%)@CTF-BPY-33%	0.92	0.23 ± 0.02	40.10
8 hours	RhCp*(6%)@CTF-BPY-33%	1.30	0.16 ± 0.001	28.51
4 hours	RhCp*(6%)@CTF-BPY-100%	1.21	0.30 ± 0.002	52.74
4 hours	RhCp*(6%)@CTF-BPY-100%	1.54	0.38 ± 0.05	67.43
8 hours	RhCp*(6%)@CTF-BPY-100%	1.53	0.19 ± 0.01	33.43

It can be noticed in Table 10, that both RhCp*@CTF-BPY-33% and 100% present a very inconsistent results in comparison to RhCp*@CTF-BPY-66%. The first two materials were synthesized in Aachen, while the last one was synthesized and tested in Lyon. In terms of structure, all the series present very consistent and reproducible results, however, in catalysis the activity of both RhCp*@CTF-BPY-33% and 100% does not match with the trend found before.

One hypothesis to explain the experimental results regards the active site. In the same way the rhodium Cp* complex can bind to bipyridine sites in different ways, it probably binds to triazine nitrogen as well. Therefore, two different active sites might be possible. The problem is while the bipyridine moiety is a weak acceptor, the triazine ring however, is a very strong electron acceptor. This way, the electronic properties of the local structure that surrounds the rhodium complex, change the catalytic activity. Since 1mg of material is used per catalytic test, the influence of different active sites is relevant. Figure 100 shows both possible active sites for CTF-BPY.

These two different active sites might explain the big deviation for CTF-BPY-33 and 100. The strong acceptor character of the triazine ring, reduces the availability of electrons for the rhodium complex, leading to very low activity. Even though the low activity can be explained in terms of different active sites, proving its existence is quite challenging due to the lack of long-range order in the framework. Therefore, it is necessary to carry out new analyses or improve the material's crystallinity in order to prove the existence of two rhodium sites.

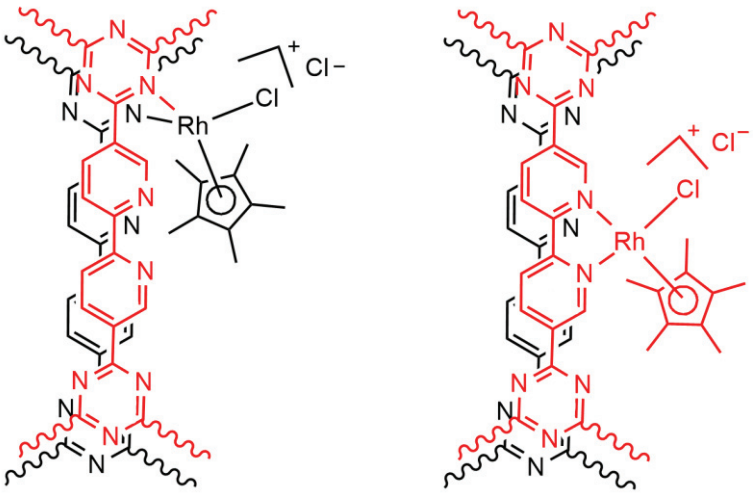

Figure 100 – Two possible active sites for RhCp* in CTF-BPY.

In conclusion, the strategy of exchanging the counter-ion of the amidine precursor worked well for the purification of 5,5′-diamidine-2,2′-bipyridine dibromide. The compound was used together with 4,4'-biphenyldiamidine bromide and both aldehydes 2,2'-bipyridine-5,5'-dicarbaldehyde and 4,4'-biphenyldicarboxaldehyde in the synthesis of a series of porous covalent triazine frameworks through condensation. Taking advantage that the synthesis of CTF through condensation enables the design of materials using the modular approach, the content of bipyridine ligand was controlled within the CTF structure. For the first time, the synthesis of functionalized CTFs was accomplished through condensation of amidine chloride and aldehyde. Moreover, the precision and molecular control over the content of a building block within the CTF structure is unprecedented. Four materials were synthesized. Their content varied from 100, 66, and 33% of bipyridine ligand, and 0% which correspond to the CTF based entirely on biphenyl units. Their structural features were characterized through FT-IR, N_2 physisorption, XRD, acetonitrile adsorption, XPS, water adsorption, elemental analysis, solid-state NMR and UV-Vis. Later, the material was employed as a fully heterogenized photocatalytic system in CO_2 photoreduction, in which the triazine linkage was used as a heterogeneous photosensitizer and the bipyridine units as a chelating agent for heterogenization of rhodium Cp* complex. When applied in CO_2 photoreduction, the material RhCp*@CTF-BPY-66% showed an activity of 15.9 h^{-1} in terms of turnover number (TON) exhibiting a rate of formate production of 376.05 $\mu mol/g_{cat}/h$, surpassing most of the fully heterogeneous systems applied in this reaction.

CHAPTER 6: SYNTHESIS, CHARACTERIZATION, AND APPLICATION OF PORPHYRIN-BASED CTF

6 SYNTHESIS, CHARACTERIZATION, AND APPLICATION OF PORPHYRIN-BASED CTF

6.1 SYNTHESIS AND CHARACTERIZATION

As shown in chapter 3, porphyrin was another building block investigated during this thesis. This heterocyclic organic compound is composed of four pyrrole subunits interconnected via double bonds. Due to its large conjugated structure, porphyrins are typically colorful compounds strongly absorbing in the visible spectra. Additionally, the macrocycle can be metallated with different metal species to form a single atom organometallic complex. In literature, many examples of porphyrin-based porous polymers have attracted attention from researchers worldwide, not only in photocatalysis but in many applications like photovoltaics [120], electrocatalysis [64], sensors [121], and others.

Due to its interesting properties, attempts to synthesize porphyrins-based covalent triazine frameworks were conducted. Targeting their application in photocatalytic CO_2 reduction.

Since the main focus of this work is the synthesis of CTFs through condensation, the first attempt was carried out by condensing therephthaldehyde and 5,10,15,20-tetrakis(4'-amidinophenyl)porphyrin.

The condensation of therephthaldehyde and 5,10,15,20-tetrakis(4'-amidinophenyl)porphyrin was done under the same protocol developed in the synthesis of phenyl and bipyridine-based materials described previously. Both compounds were mixed with Cs_2CO_3 in DMSO and the resulting solution was heated to 60, 80, 100 and 120°C for 24 hours each. After this time, the mixture was cooled down to room temperature and a solid was recovered by filtration. The resulting purple material was washed with THF and acetone, before drying in an oven at 60°C.

To analyze the resulting polymer, N_2 physisorption experiments were carried out at 77K. Figure 101 shows the resulting adsorption/desorption isotherms of sample CTF-MAS-99.

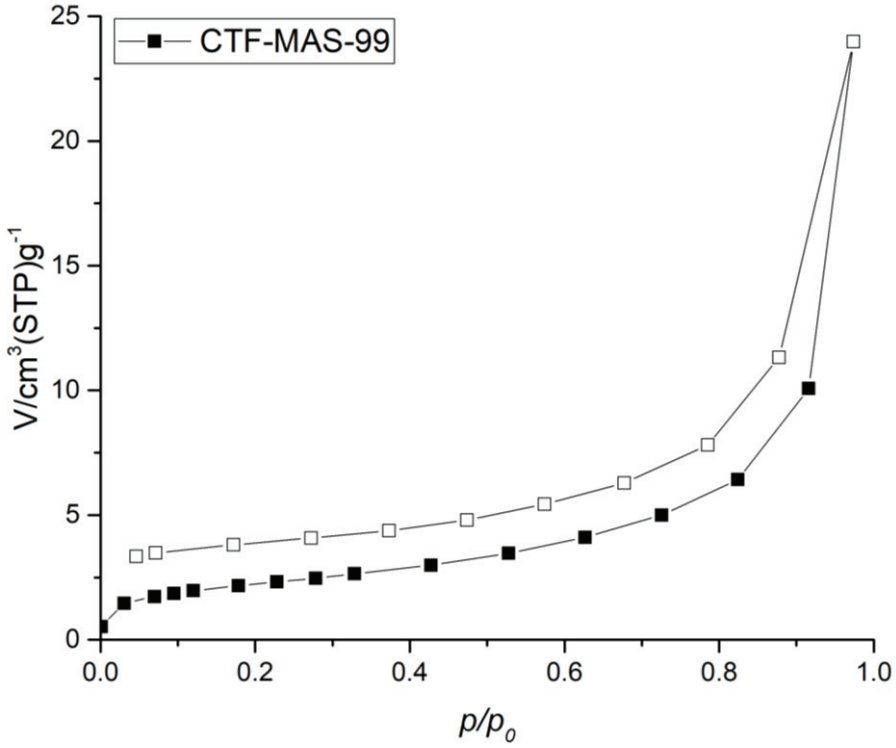

Figure 101 – N_2 adsorption/desorption isotherms from sample CTF-MAS-99, measured at 77K.

The N_2 isotherms depicted in Figure 101 are classified as type II, according to IUPAC classification. This type of isotherm is characteristic for microporous materials, as a small steep rise can be seen at low pressures. However, the specific surface area of CTF-MAS-99, calculated using the BET theory achieved 12 m^2/g. Compared to other polymers based in porphyrin, this specific surface area is low.

Even though the synthesis of porphyrin-based CTF did not work through condensation, most probably due to the flawed synthesis of 5,10,15,20-tetrakis(4'-amidinophenyl)porphyrin precursor, the nitrile can still be used for the synthesis of CTFs through the acid approach.

The first attempt was done using microwave-assisted synthesis. In this synthesis, the nitrile precursor, 5,10,15,20-tetrakis(4'-cyanophenyl)porphyrin, was mixed with trifluoromethanesulfonic acid in a microwave glass reactor, resulting in a deep green solution. This solution was irradiated with microwave until 100°C for 30 min. The resulting solution was carefully poured in diluted ammonium hydroxide in water, until complete neutralization. From this reaction, no precipitate was formed. Employing another variation of the acid approach, the nitrile precursor was first solubilized in chloroform, resulting in a purple solution. To this solution, small amounts of the triflic

acid were added, turning the solution green. After 24 hours stirring at room temperature, a green solid precipitates. The solution was neutralized using ammonium hydroxide and the solid recovered by filtration. After been washed with water, acetone and chloroform, the resulting purple material was dried in the oven at 80°C. The sample was hereafter named CTF-PORF. Figure 102 illustrates the synthesis of porphyrin-based CTF through the acid approach.

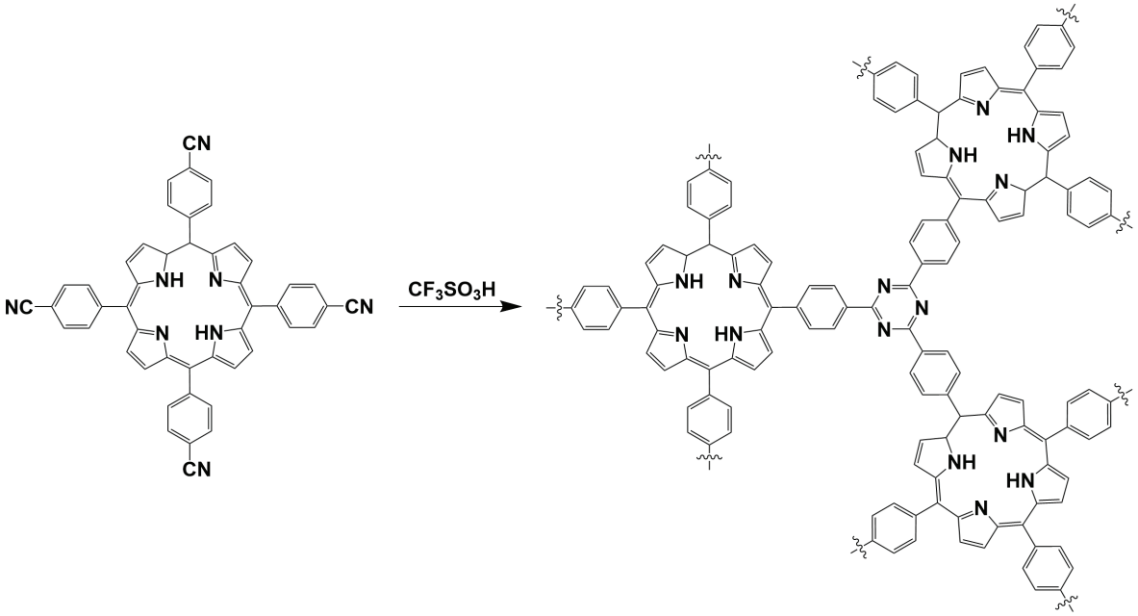

Figure 102 – Illustration of CTF-PORF synthesis through trimerization of 5,10,15,20-tetrakis(4'-cyanophenyl)porphyrin in triflic acid.

In order to characterize the resulting framework, FT-IR, XPS, XRD, and N_2 physisorption experiments were carried out. Figure 103 shows the resulting FT-IR spectra comparing 5,10,15,20-tetrakis(4'-cyanophenyl)porphyrin, named PORF-CN, and the resulting framework CTF-PORF.

According to the spectra, it is possible to notice the main stretching vibration of the triazine ring at 1507 and 1365 cm^{-1}. These bands can not be found in the starting material and are assigned to C=N and C-N from the triazine ring, suggesting the material is a framework based on this linkage. Additionally, the stretching vibration from the nitrile group C≡N can be found at 2227 cm^{-1} in the precursor spectrum, but not in the resulting framework, indicating complete polymerization of the nitrile groups into triazine.

N_2 adsorption/desorption isotherms of sample CTF-PORF is depicted in Figure 104. The experiments were carried out at 77K.

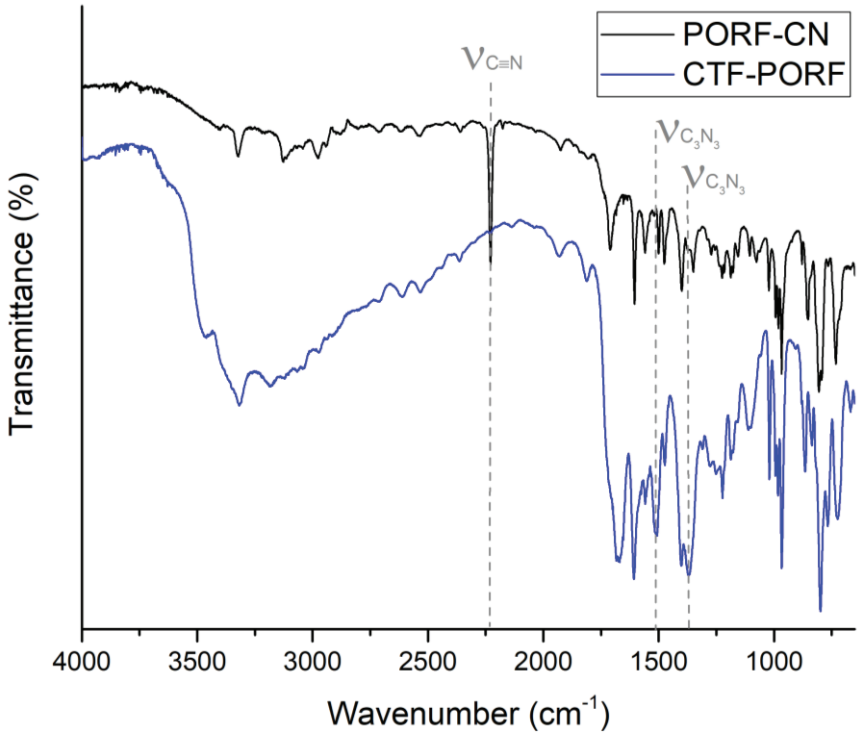

Figure 103 – FT-IR spectra of 5,10,15,20-tetrakis(4'-cyanophenyl)porphyrin (PORF-CN) and sample CTF-PORF.

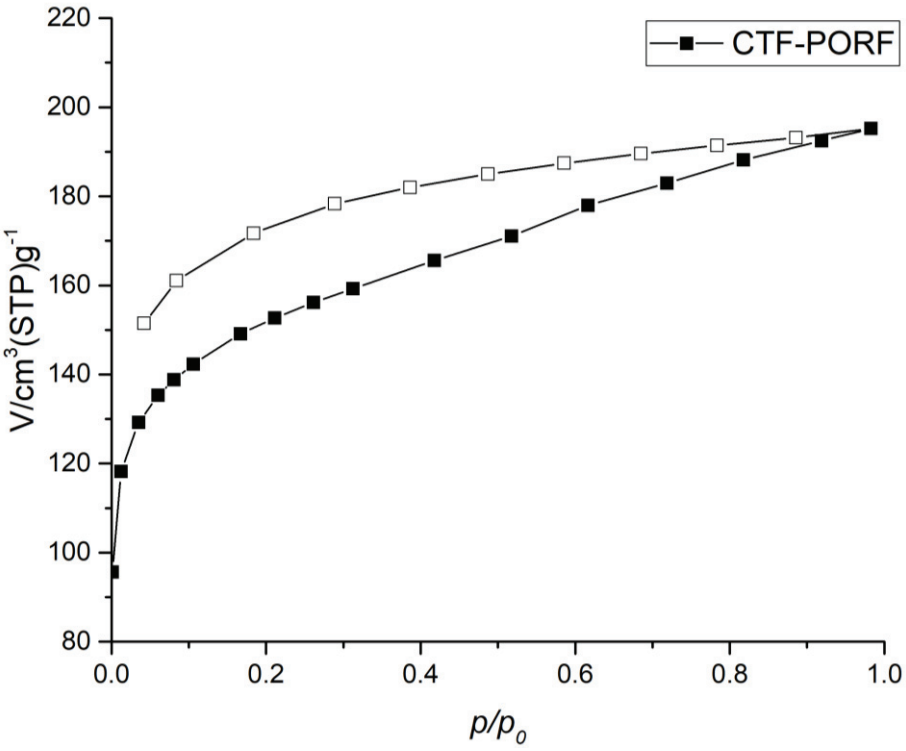

Figure 104 – N_2 adsorption/desorption isotherms from sample CTF-PORF, measured at 77K.

The N_2 adsorption/desorption isotherms depicted in Figure 104 are assigned to type I, according to IUPAC classification. This type is characteristic of microporous materials, as a steep rise can be seen at low relative pressures. Using the BET theory, a specific surface area of 670 m^2/g was achieved.

Powder x-ray diffraction was carried out to investigate the range of organization within the CTF-PORF structure. Figure 105 depicts the XRD pattern of CTF-PORF.

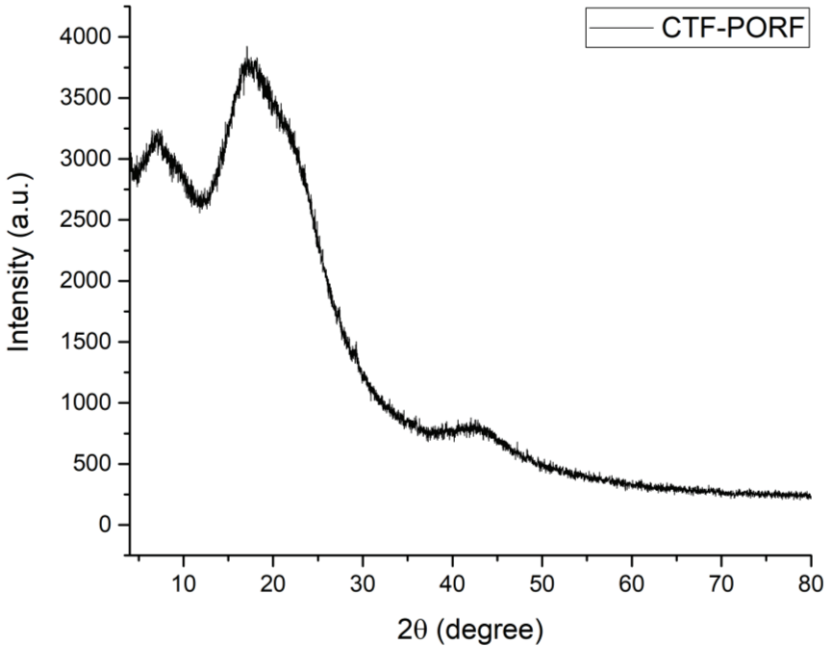

Figure 105 – XRD pattern from sample CTF-PORF.

As noticed from the XRD pattern, the material CTF-PORF is amorphous. No long-range organization was found in sample CTF-PORF's structure. However, the FT-IR spectrum, suggests local organization, due to the well-defined shape of the stretches.

Further characterization was carried out using XPS. The resulting spectra for carbon and nitrogen as well as the fitting can be seen in Figures 106 and 107.

According to C1s XPS analyses, 4 signals can be found. Their binding energy was found at 284.6, 286.9, 291.3 and 288.8 eV. These signals can be assigned to C=C, C=N, C-OOH, and C-N, respectively.

The only signal that the assignment with the porphyrin structure is not obvious is the carboxylic acid C-OOH at 291.3 eV. Such a signal can arise due to the nitrile hydrolysis. This reaction happens in a strong acid or basic environment. Since the synthesis of the material is realized in strongly acidic media, some nitrile groups can be

oxidized to the corresponding carboxylic acid. Additionally, the XPS analysis provides information only from the surface, not on the bulk. Therefore, the hypothesis that the nitrile gets oxidized due to the strong acid environment is plausible, especially considering that the terminal nitrile groups at the surface stay in contact with the acid solution for a longer time.

The other signals, C=C, C=N, and C-N at 284.6, 286.9, and 288.8 eV binding energies, can be assigned to aromatic carbons, and both C-N and C=N moieties from the pyrrole within the porphyrin structure.

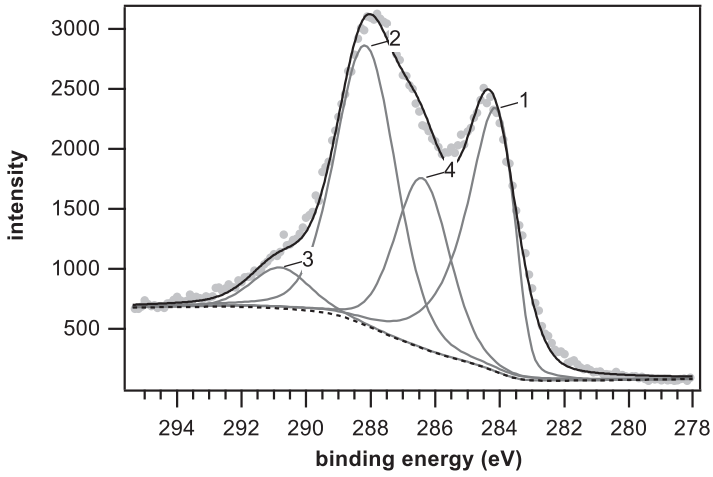

Figure 106 – C1s XPS analysis of CTF-PORF.

In nitrogen XPS analysis, three signals are noticed at binding energies of 397.7, 401.7, and 399.4 eV. These signals are assigned to N=C, N-H, and N-C, respectively.

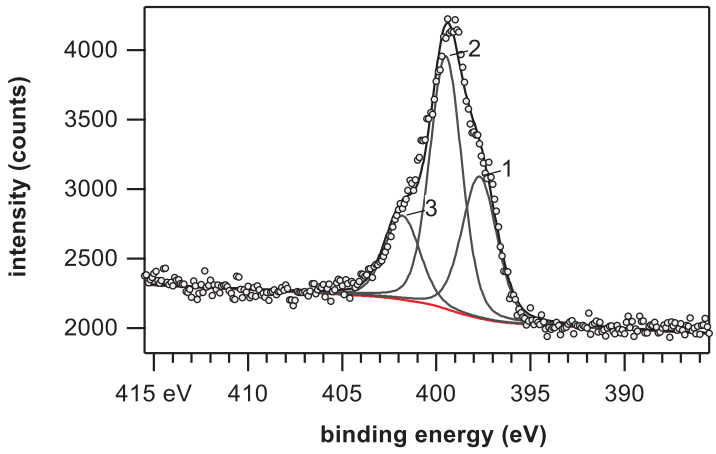

Figure 107 – N1s XPS analisys of sample CTF-PORF.

Signals N=C and N-C are assigned to the pyrrole and triazine structures, while the N-H signal at 401.7 eV is assigned to the nitrogen species at the center of the macrocycle.

The synthesis of a porphyrin-based CTF through the acid procedure, by trimerization of 5,10,15,20-tetrakis(4'-cyanophenyl)porphyrin resulted in a porous framework based in porphyrin and triazine building blocks. Since the porphyrin can be metallated to give rise to an organometallic complex, CTF-PORF was metallated and applied as a catalyst. The next section will describe the metalation procedure.

6.2 METALLATION

The metalation of the porphyrin macrocycle gives rise to very active complexes. Typically, the metalation is done by refluxing chloride or nitride salts from the metal precursor and the porphyrin in high boiling points solvents like DMF. This solvent also promotes the deprotonation of the nitrogens from the inner porphyrin core, assisting the metalation.

Metal-porphyrin complexes drive selectively the CO_2 photoreduction to different products, depending on the metal center. For instance, rhodium porphyrins selectively convert CO_2 into formate while copper-based porphyrins mainly produce methanol. In an attempt to insert rhodium metal into the porphyrin core, the salt precursors $RhCl_3$ was refluxed in DMF together with the pristine CTF-PORF framework. After 24 hours, the mixture was cooled to room temperature and the solid separated by filtration. An evident change in the color suggests a successful metalation.

Moreover, CTF-PORF was also metallated with copper. Like the metalation with rhodium, pristine CTF-PORF was refluxed with $CuNO_3$ in DMF for 24 hours. The resulting material was collected by filtration and washed with water and acetone before drying in the oven at 80°C. Once again, the significant change in color is evidence of metallation success.

Both materials were employed in photocatalytic CO_2 reduction, however, no product was formed during 4 hours of reaction. Since the application of rhodium and copper-based porphyrin CTFs in CO_2 photoreduction did not work, CTF-PORF was metallated iron and applied in the methane oxidation reaction.

As a greenhouse gas, the release of methane into the atmosphere is harmful, together with carbon dioxide, methane emissions affect the global energy balance, resulting in changes on Earth's climate. Since oil has become depleted, natural gas, which corresponds to 70 to 90% methane, has been used as an option in energy production. However, transportation of methane over long distances gas is quite challenging. Liquefaction of natural gas is also not a viable option, as the boiling point of methane is 109 K at 1 atm. On the other hand, the conversion of methane into chemicals and fuel is difficult due to its chemical inertness [122].

Inspired by nature, in which iron-based methane monooxygenase enzymes convert methane to methanol at mild reaction conditions, research groups around the world are employing iron-functionalized porous materials for conversion of methane to methanol [123]. In this context, the attempt to metallate the CTF-PORF with iron and its further application in methane oxidation in water is reported.

First, the metalation proceeded in the same way as rhodium and copper metalation. The pristine CTF-PORF framework was refluxed together with $FeCl_3$ in DMF for 24 hours. The resulting solid was filtered off and washed with water and acetone, before drying in an oven at 80°C. The color changed significantly from purple to dark brownish. In order to characterize the resulting material, FT-IR and nitrogen adsorption was carried out in sample CTF-PORF(Fe). Figure 108 depicts the FT-IR spectra from the nitrile precursor, 5,10,15,20-tetrakis(4'-cyanophenyl)porphyrin, named PORF-CN, the pristine CTF-PORF and the resulting CTF-PORF(Fe) after metalation.

From the spectra depicted in Figure 108, the sample CTF-PORF(Fe) presents the same stretching vibrations from the triazine ring at 1507 and 1365 cm^{-1}, corresponding to C=N and C-N groups from the triazine linkage, respectively. Moreover, the nitrile stretch can be noticed at 2227 cm^{-1}. Interestingly this stretch can not be found in the FT-IT spectrum of pristine CTF-PORF, however, after the metallation, the stretch notably reappears. Since the metalation reaction is done under the reflux of high boiling point solvent, in the case DMF, the structure of the framework seems to be damaged. Moreover, the weel-defined bands of the FT-IR spectrum of pristine CTF-PORF, significantly change to more broad featured bands after metalation with iron. This evidence suggests changes in the local structure of the framework after metallation.

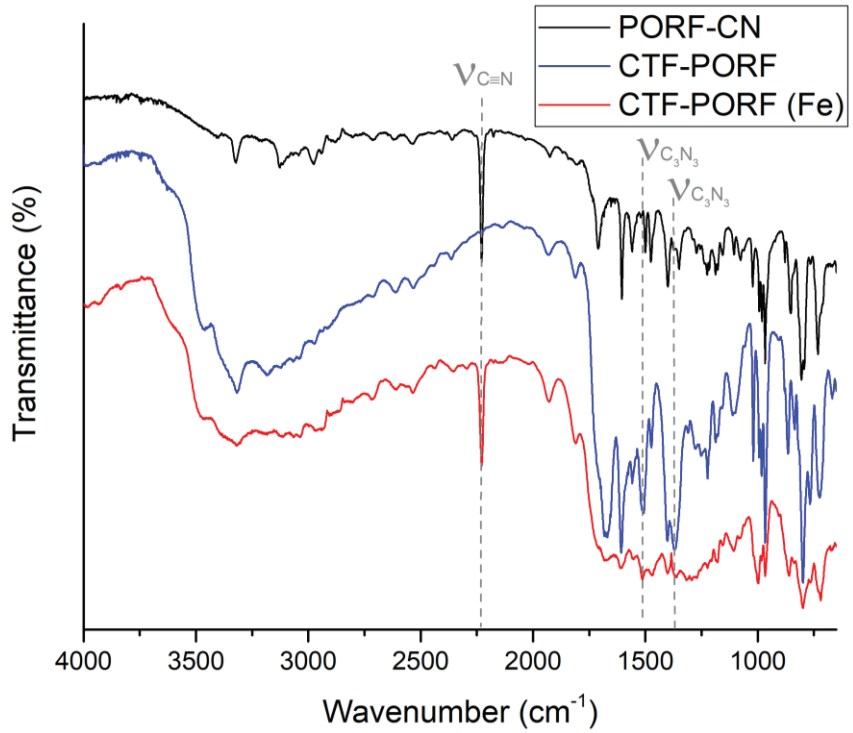

Figure 108 – FT-IR of spectra of PORF-CN, CTF-PORF and CTF-PORF (Fe).

The porous properties of CTF-PORF after metalation with iron were verified through N_2 adsorption/desorption isotherms, measured at 77K. Figure 109 shows the adsorption/desorption isotherms comparing pristine CTF-PORF and CTF-PORF(Fe).

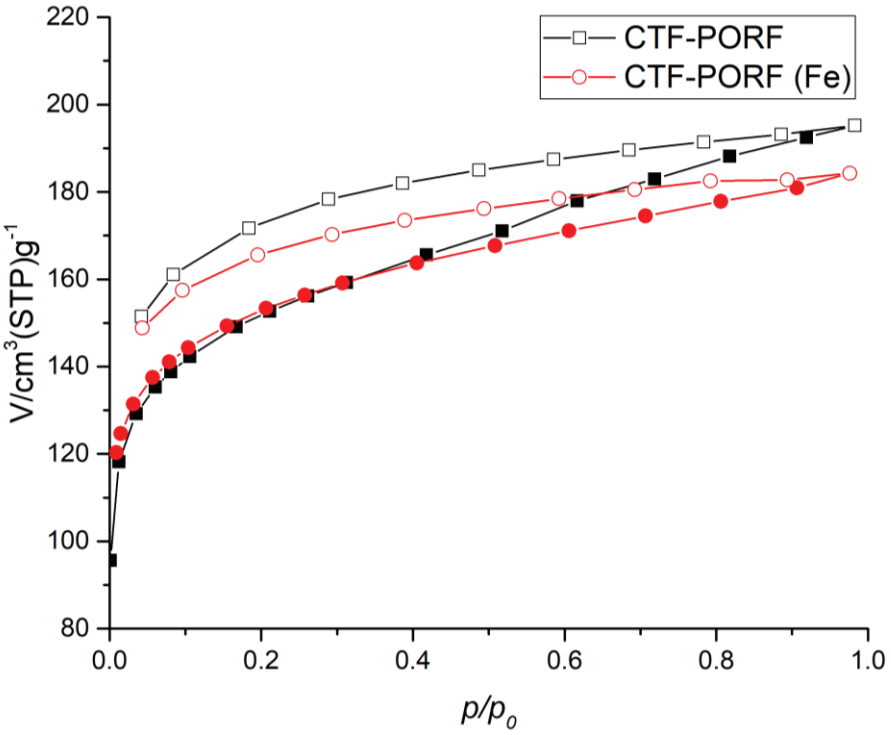

Figure 109 – N_2 adsorption/desorption isotherms from sample CTF-PORF and CTF-PORF(Fe), measured at 77K.

From the resulting isotherms, it is evident that the insertion of iron atoms into the porphyrin heterocycle did not change significantly the porous properties of the framework, especially at low pressure. Both isotherms present type III, according to IUPAC classification. A specific surface area of 680 m^2/g was found using the BET equation.

Although the significant change in the color indicates a successful metalation, further analysis has to be done to prove the iron insertion. Typically, the UV-Vis analysis is carried out to get insights over the metalation procedure. Commonly UV-Vis analysis of porphyrin is divided into two parts. The first, absorption between 380-500 nm is assigned to transitions from the ground state to the second excited (S0→S2), depending on whether the porphyrin is β or meso-substituted. This band is called Soret or B band, and is a classical transition in porphyrin UV-Vis analysis. The second region, between 500-750 nm consists of a weak transition from the ground to the first excited state (S0→S1) and is called Q bands. These spectroscopic features of porphyrins are due to the conjugation of 18 π-electrons and they provide an easy and precise way to monitor the binding of gest metals into the porphyrin structure. Additionally, ICP-OES should be carried out in order to investigate the content of iron into the CTF-PORF.

After metalation with iron, the resulting CTF-PORF(Fe) was applied in methane oxidation. The results are shown in the next section.

6.3 APPLICATION

The oxidation of methane was carried out in water, using H_2O_2 as oxidant and 30 mg of CTF-PORF (Fe) was employed as a catalyst. The reaction was done in an autoclave under 20 bars of methane at 60°C for 2 hours. After the reaction, the solid was separated by centrifugation and the solution analyzed by quantitative NMR.

Figure 110 depicts the ^{1}H-NMR analysis from the resulting solution after the reaction.

According to the ^{1}H-NMR analysis, when applied in methane oxidation, the material CTF-PORF (Fe) selectively produced formate. The rate of production was found to be 603.2 $\mu mol/g_{cat}/h$, which corresponds to a turnover number of 1.35 h^{-1}.

Up to now, MOFs are the main class of porous materials applied in the methane oxidation. However, metal-organic frameworks did not show enhanced stability when applied as a catalyst for methane oxidation. The main issue is the collapse of the MOF structure during the reaction. Moreover, no material has ever reported resulting in only one product, in all the examples of the application of MOFs as catalysts, both methanol and formate can be found as products, at different rates. When CTF-PORF (Fe) is compared with the states-of-the-art, it presents much lower activity, for example, MOF MIL-53(Fe) have shown activity of 12 h^{-1} in terms of turnover number [124]. However, CTF-PORF (Fe) is the very first example of material applied in methane oxidation that is 100% selective towards formate production.

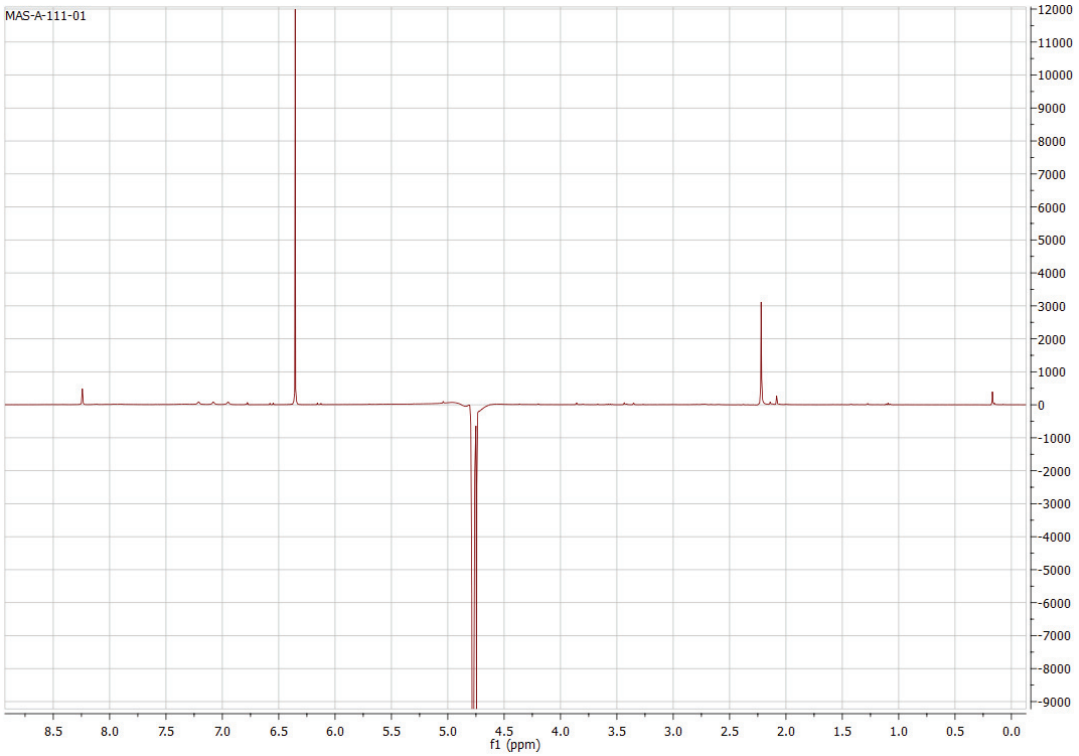

Figure 110 – NMR analysis for the resulting water solution after application of CTF-PORF(Fe) in methane oxidation.

In chapter 6, the synthesis, characterization, and application of a porphyrin-based CTF were reported. Since the synthesis of precursor 5,10,15,20-tetrakis(4'-amidinophenyl)porphyrin had failed to obtain a pure product, the nitrile monomer, 5,10,15,20-tetrakis(4'-cyanophenyl)porphyrin was employed in the synthesis of CTF using the acid approach. In this method, the trimerization of nitrile is carried out by the addition of triflic acid. After the reaction, a porous framework based on porphyrin building blocks, linked by triazine rings was recovered. Notably, the material possess a

specific surface area of 670 m^2/g. After an unsuccessful application of rhodium and copper-based porphyrin CTF in photocatalytic CO_2 reduction, the material CTF-PORF was loaded with iron and applied in the oxidation of methane. Although the material did not show a remarkable activity, CTF-PORF (Fe) produced selectively formate from methane at a rate of 603.2 $\mu mol/g_{cat}/h$.

CHAPTER 7: CONCLUSION AND OUTLOOK

7 CONCLUSION

Covalent Triazine Frameworks have been identified as a very promising class of materials for future challenges in the energy field. The electronic properties of the triazine ring, combined with the heteroatom effect, boosted the application of CTFs as catalyst for hydrogen production from water and many other interesting reactions related to clean energy production.

Seeking to produce suitable materials for a sustainable catalytic process, pushing the boundaries on the development of new materials and new synthesis pathways is crucial to overcome the main challenges humankind is facing. However, controlling the molecular structure within a framework is a big challenge.

In the case of CTFs, the investigation over the condensation approach, brought precision to the synthesis of these materials. Even though these materials lack long-range order, especially when employing amidine chloride and aldehyde as precursors, the condensation approach made possible the synthesis of materials with more than one functionalized building block. Moreover, the proper control over the content of a specific moiety within the framework, cannot be achieved by employing different synthetic methods than condensation.

In this context, the polycondensation approach for the synthesis of CTFs was investigated in order to highlight the main advantages and drawbacks of the employment of this method. At first, phenyl-based CTFs were synthesized, following previously reported procedures. In the course of this investigation, the amidine chloride purity has shown to be the major factor in the synthesis of porous covalent triazine frameworks through condensation. The presence of ammonium chloride as a by-product, was identified as one of the causes for the shifting in the stacking position, which can lead to non-porous and denser materials. As a strategy to purify the amidine precursor, the counter-ion of this monomer was exchanged from chloride to tetraphenylborate, and later to bromide. Such a strategy worked well, succeeding in obtain a pure amidine. The utilization of a pure amidine for the synthesis of CTF, leads to porous materials due to the alignment of the bi-dimensional sheets that compose the materials, resulting in channels within the material's structure.

After establishing a protocol for the purification of the starting materials and the successful synthesis of phenyl-based CTFs, the material was synthesized, for the first

time, through a microwave-assisted pathway. In comparison to the conventional heating procedure, the CTF synthesized under microwave irradiation showed enhanced specific surface area, achieving 580 m^2/g with a more significant contribution of macro and mesopores, in addition to the micropore structure. Moreover, the synthesis done under microwave irradiation, give rise to a material with a bandgap of 2.43 eV while the bandgap of the material synthesized under conventional heating was 2.33 eV.

After the successful synthesis of simple CTFs based on phenyl precursors, the purification strategy was employed in functionalized building blocks, in an attempt to synthesize more complex materials based on bipyridine moieties. Taking advantage of the precision and enhanced molecular control when polycondensation is employed for the synthesis of CTFs, the concept of modular design was employed in order to control the content of a particular ligand within the framework.

In this regard, a series of bipyridine-based CTFs were synthesized through condensation of functionalized building blocks. The content of bipyridine within the CTF structure was precisely controlled, giving rise to materials containing 0, 33, 66 and 100% bipyridine units. In order to produce materials with symmetric pore structure, biphenyl was employed as a non-functionalized building block. Therefore, the material containing 0% of bipyridine units is, in fact, a biphenyl-based CTF.

The unprecedented control and precision over the CTF structure were investigated through solid-state NMR, clearly showing the composition of these materials. The formation of triazine bonds was followed by FT-IR studies. As expected, the powder x-ray diffraction evidenced the amorphous nature of these bipyridine-based CTFs series. From N_2 physisorption experiments, the specific surface areas were found to be 572, 400, 368 and 235 m^2/g, for samples CTF-BPH, CTF-BPY-33%, CTF-BPY-66%, and CTF-BPY-100%, respectively. The higher the nitrogen content within the CTF structure, the lower is the specific surface area. Although this trend was found when nitrogen is employed as a probe molecule, acetonitrile and water adsorption experiments have shown very similar behavior within the series.

From solid-state UV-Vis analysis, the bandgap of all materials in the series was found to be 2.93, 2.83, 2.75 and 2.53 eV for CTF-BPH, CTF-BPY-33%, CTF-BPY-66%, and CTF-BPY-100%, respectively. These results highlight the precise control over the molecular structure which consequently allows the unprecedented and remarkable control

over properties like visible light absorption and porosity. The control over such properties is a major step towards the rational synthesis of CTF.

Materials based on bipyridine units are relevant for catalysis and can be used to host many different active metal species. The general approach can bridge homogeneous and heterogeneous catalysis fields, taking advantage of the enhanced selectivity and activity from molecular catalysts and at the same time from the easy handling and recyclability of heterogeneous catalysts. Due to the photoactive bandgap, the first application of bipyridine-based CTFs was in CO_2 photoreduction. The triazine moiety acts as a heterogeneous photosensitizer, absorbing light, producing the electron-hole pairs and sending them to the active rhodium Cp* complex to trigger selectively the CO_2 reduction to formate.

RhCp*(6%)@CTF-BPY-66 showed the highest activity toward CO_2 photoreduction in comparison to the state-of-art. A turnover number of 15,9 and a formate production rate of 376,05 $\mu mol/g_{cat}/h$ have been achieved. The result shows the high photocatalytic potential of these CTFs.

Overall, the investigation of the condensation approach enables the design and synthesis of a series of bipyridine-based CTFs containing different amounts of ligand, for the first time. The resulting photoactive materials, were employed as support for rhodium metal complex and applied as heterogeneous catalyst for selective CO_2 reduction to formate. Presenting higher activity than the state-of-the-art.

In addition to the functionalized bipyridine-based CTFs, this project also reported the synthesis, characterization, and application of porphyrin-based CTF. After a flawed attempt to produce 5,10,15,20-tetrakis(4'-amidinophenyl)porphyrin, the nitrile precursor was employed in the synthesis of a porphyrin-based CTF through the acid approach.

The resulting porphyrin-based CTF has shown microporous structure, achieving a specific surface area of 670 m^2/g. The material was metallated with rhodium and copper, in an attempt to reduce CO_2 to formate and methanol under visible light irradiation. However, both attempts have failed. Another important application in the energy field is the oxidation of methane to methanol at mild reaction conditions and employing earth-abundant metal as catalyst. In this context, the porphyrin-based CTF (CTF-PORF) was metallated with iron and used as a catalyst in methane oxidation.

Using H_2O_2 as an oxidant, the reaction was carried out in water and employing the CTF-PORF (Fe) as a catalyst. Although the material did not show a remarkable activity, achieving a formate rate production of 603.2 μmol/g_{cat}/h, this was the first example of porphyrin-based porous organic polymer to produce only formate in the oxidation of methane.

8 OUTLOOK

Besides the main achievements in design and synthesis of CTFs using the condensation approach, there are still some limitations. The first is the amidine purification. Since ammonium chloride is produced as a by-product and this impurity causes major changes in the structure of these materials, other methods of synthesis of purification of amidine chloride have to be addressed.

Moreover, most challenges and limitations are linked to the lack of long-range order in these frameworks. Therefore, a significant improvement would be the enhancement of crystallinity. As described before, the synthesis using alcohol precursor, for in-situ oxidation to aldehyde, has been described by Liu *et al*. However, this approach did not work well when applied in the synthesis of functionalized CTFs. Therefore, the protocol has to be optimized for the synthesis of functionalized crystalline CTFs.

Furthermore, the condensation approach opened an avenue to precisely control the structure of covalent organic frameworks. With crystalline CTFs, the understanding of structure-activity relationship is facilitated. Therefore, the design of materials with specific functionalities can boost the activity towards an application. Further, the achievement of crystalline materials through condensation brings CTFs close to COFs and MOFs, and enable the design of these materials through the application of reticular chemistry fundaments.

Taking advantage of reticular chemistry, all the possible topologies for CTF can be studied in theory. Giving insights on the geometry of precursors and their relative functionalities. Having control over the structure of CTFs opens new possibilities in the application of these materials in many different fields, especially in energy production and mitigation of climate change, by targeting water splitting and CO_2 conversion.

Regarding the application of CTFs in photocatalysis, the materials have shown encouraging activities. Although a strong variation between the materials could be noticed when applied in photocatalytic CO_2 reduction, the photoactive bipyridine-based CTFs series could find application in other reactions, like photocatalytic water splitting. Currently, the application of bipyridine-based CTFs in other photocatalytic reactions has been addressed since these materials will be tested in hydrogen evolution reaction under visible light irradiation in a recent collaboration with Professor Arne Thomas at Technische Universität Berlin.

Additionally, other characterization techniques, like photoluminescence spectroscopy, steady-state emission spectroscopy, time-correlated single-photon counting, and DFT calculation, would be interesting analysis in order to fully elucidate these bipyridine-based photosystems and better understand the role of triazine moieties within the CTF structure.

In the case of porphyrin-based CTF, the synthesis protocol has to be optimized. Further characterizations analysis has to be carried out to prove the insertion of the metal center and to better understand the structure of this material. Since porphyrin can be metallated with different metals, this material needs to be optimized and has the potential to become a platform, allowing the application in many different reactions. For instance, considering only carbon dioxide photoreduction, an active porphyrin-based CTF would allow to shift between different products, according to the metal center. In a future perspective, the synthesis of porphyrin-based CTFs through condensation will be addressed, as well as its application in photocatalytic CO_2 reduction and methane oxidation reactions.

Another important improvement achievement to be addressed as future perspectives is the synthesis of CTFs in different shapes. The ability to shape functional materials in different morphologies also enhance their applicability. Thin films are interesting for the production of membranes or electrodes. Different particle sizes have a big influence when these materials interact with light. Therefore, looking back to the past few years and the revolution in material chemistry, driven by the discovery of novel classes of materials such as metal-organic-frameworks and porous organic polymers, the coming years hold major advances on the application of these materials, addressing the main challenges in our society and helping to shift to a more sustainable world.

REFERENCES

9 REFERENCES

[1] D. Spencer, “BP Statistical Review of World Energy Statistical Review of World,” *Ed. BP Stat. Rev. World Energy*, pp. 1–69, 2019.

[2] R. J. Zedalis, “International Energy Law,” *Int. Energy Law*, 2017.

[3] D. Roberts, R. Pidcock, Y. Chen, S. Connors, and M. Tignor, Global warming of 1.5°C IPCC Report, https://www.ipcc.ch/.

[4] Y. Luo, L. Dong, J. Liu, S. Li, and Y. Lan, “From molecular metal complex to metal-organic framework : The CO_2 reduction photocatalysts with clear and tunable structure,” *Coordination Chemistry Reviews*, vol. 390, pp. 86-126, 2019.

[5] J. M. Barlow and J. Y. Yang, “Thermodynamic Considerations for Optimizing Selective CO_2 Reduction by Molecular Catalysts,” *ACS Cent. Sci.*, vol. 5, no. 4, pp. 580-588, 2019.

[6] Y. Gu, J. Zhao, and J. A. Johnson, “A unifying review of polymer networks: from rubbers and gels to porous frameworks,” *Angew. Chemie Int. Ed.*, 2019. https://doi.org/10.1002/anie.201902900

[7] K. S. W. Sing, D. H. Everett, R. Haul, L. Moscou, R. A. Pierotti, J. Rouquerol, T. Siemieniewska. “Reporting Physisorption Data for Gas/Solid Systems with Special Reference to the Determination of Surface Area and Porosity” *Pure & Appl.Chem*., vol.54, no.11, pp. 2201-22l8, 1982

[8] Q. Huo, "Synthetic Chemistry of the Inorganic Ordered Porous Materials". *Modern Inorganic Synthetic Chemistry* 2011, pp 339-373.

[9] B. M. Weckhuysen and J. Yu, “Recent advances in zeolite chemistry and catalysis,” *Chem. Soc. Rev.*, vol. 44, no. 20, pp. 7022-7024, 2015.

[10] G. Maurin, C. Serre, A. Cooper, and G. Férey, “The new age of MOFs and of their porous-related solids,” *Chem. Soc. Rev.*, vol. 46, no. 11, pp. 3104-3107, 2017.

[11] Y. Kinoshita, I. Matsubara, T. Higuchi, and Y. Saito, “The Crystal Structure of Bis(adiponitrilo)copper(I) Nitrate,” *Bull. Chem. Soc. Jpn.*, vol. 32, no. 11, pp. 1221-1226, 1959.

[12] N. L. Rosi *et al.*, “Hydrogen Storage in Microporous Metal-Organic Frameworks,”

Science, v.300, pp. 1127-1129, 2003.

[13] T. Hasell and A. I. Cooper, “Porous organic cages: Soluble, modular and molecular pores,” *Nat. Rev. Mater.*, vol. 1, no. 9, 2016.

[14] R-B. Lin, Y. He, P. Li, H. Wang, W. Zhou and B. Chen, “Multifunctional porous hydrogen-bonded organic framework materials”. *Chem. Soc. Rev.*, v.48, pp. 1362-1389, 2019.

[15] J. Tian, L. Chen, D-W. Zhang, Y. Liu and Z-T. Li. " Supramolecular organic frameworks: engineering periodicity in water through host-guest chemistry". *ChemComm*, v.52, pp. 6351-6362, 2016.

[16] N. B. McKeown, “Polymers of Intrinsic Microporosity,” *Mater. Sci.*, vol. 2012, pp. 1-16, 2012.

[17] J. Huang and S. R. Turner, “Hypercrosslinked Polymers: A Review,” *Polym. Rev.*, vol. 58, no. 1, pp. 1-41, 2018.

[18] S. J. Lyle, P. J. Waller, and O. M. Yaghi, “Covalent Organic Frameworks: Organic Chemistry Extended into Two and Three Dimensions,” *Trends Chem.*, vol. 1, no. 2, pp. 172-184, 2019.

[19] Y. Xu, S. Jin, H. Xu, A. Nagai, and D. Jiang, “Conjugated microporous polymers: Design, synthesis and application,” *Chem. Soc. Rev.*, vol. 42, no. 20, pp. 8012-8031, 2013.

[20] P. Chen, J. S. Sun, L. Zhang, W. Y. Ma, F. Sun, and G. Zhu, “Porous aromatic framework (PAF-1) as hyperstable platform for enantioselective organocatalysis,” *Sci. China Mater.*, vol. 62, no. 2, pp. 194-202, 2019.

[21] S. Das, P. Heasman, T. Ben, and S. Qiu, “Porous Organic Materials: Strategic Design and Structure-Function Correlation,” *Chem. Rev.*, vol. 117, no. 3, pp. 1515-1563, 2017.

[22] X. Wang *et al.*, “A metal-free polymeric photocatalyst for hydrogen production from water under visible light,” *Nat. Mater.*, vol. 8, no. 1, pp. 76-80, 2008.

[23] P. Kuhn, M. Antonietti, and A. Thomas, “Porous, covalent triazine-based frameworks prepared by ionothermal synthesis,” *Angew. Chemie - Int. Ed.*, vol.

47, no. 18, pp. 3450-3453, 2008.

[24] M. Liu, L. Guo, S. Jin, and B. Tan, “Covalent triazine frameworks: Synthesis and applications,” *J. Mater. Chem. A*, vol. 7, no. 10, pp. 5153-5172, 2019.

[25] Y. Zhang and S. Jin, “Recent advancements in the synthesis of covalent triazine frameworks for energy and environmental applications,” *Polymers (Basel).*, vol. 11, no. 1, pp. 30-43, 2018.

[26] S. Ren *et al.*, “Porous, fluorescent, covalent triazine-based frameworks via room-temperature and microwave-assisted synthesis,” *Adv. Mater.*, vol. 24, no. 17, pp. 2357-2361, 2012.

[27] X. Zhu *et al.*, “A superacid-catalyzed synthesis of porous membranes based on triazine frameworks for CO_2 separation,” *J. Am. Chem. Soc.*, vol. 134, no. 25, pp. 10478-10484, 2012.

[28] T. Chen *et al.*, “Direct synthesis of covalent triazine-based frameworks (CTFs) through aromatic nucleophilic substitution reactions,” *RSC Adv.*, vol. 9, no. 31, pp. 18008-18012, 2019.

[29] S. Y. Yu *et al.*, “Direct Synthesis of a Covalent Triazine-Based Framework from Aromatic Amides,” *Angew. Chemie - Int. Ed.*, vol. 57, no. 28, pp. 8438-8442, 2018.

[30] K. Wang *et al.*, “Covalent Triazine Frameworks via a Low-Temperature Polycondensation Approach,” *Angew. Chemie - Int. Ed.*, vol. 56, no. 45, pp. 14149-14153, 2017.

[31] S. Biswas and S. Batra, “One-step synthesis of 2-amino-5h-pyrimido[5,4-b]indoles, substituted 2-(1,3,5-triazin-2-yl)-1h-indoles, and 1,3,5-triazines from aldehydes,” *European J. Org. Chem.*, no. 18, pp. 3492-3499, 2012.

[32] M. Liu *et al.*, “Crystalline Covalent Triazine Frameworks by In Situ Oxidation of Alcohols to Aldehyde Monomers,” *Angew. Chemie - Int. Ed.*, vol. 57, no. 37, pp. 11968-11972, 2018.

[33] D. Wu, F. Xu, B. Sun, R. Fu, H. He, and K. Matyjaszewski, “Design and preparation of porous polymers,” *Chem. Rev.*, vol. 112, no. 7, pp. 3959-4015, 2012.

[34] O. M. Yaghi, M. J. Kalmutzki, and C. S. Diercks, "Introduction to Reticular

Chemistry: Metal-Organic Frameworks and Covalent Organic Frameworks". ISBN: 9783527821099, 2019.

[35] O. M. Yaghi, “Reticular Chemistry: Molecular Precision in Infinite 2D and 3D,” *Mol. Front. J.*, vol. 03, no. 01, pp. 66-83, 2019.

[36] B. Lukose, A. Kuc, J. Frenzel, and T. Heine, “On the reticular construction concept of covalent organic frameworks,” *Beilstein J. Nanotechnol.*, vol. 1, no. 1, pp. 60-70, 2010.

[37] C. S. Diercks and O. M. Yaghi, “The atom, the molecule, and the covalent organic framework,” *Science*, vol. 355, no. 6328, p. 1585, 2017.

[38] J. Wu *et al.*, “Porous Polymers as Multifunctional Material Platforms toward Task-Specific Applications,” *Adv. Mater.*, vol. 31, no. 4, pp. 1-45, 2019.

[39] A. G. Slater and A. I. Cooper, “Function-led design of new porous materials,” *Science*, vol. 348, no. 6238, p. 8075, 2015.

[40] D. Ramimoghadam, E. M. A. Gray, and C. J. Webb, “Review of polymers of intrinsic microporosity for hydrogen storage applications,” *Int. J. Hydrogen Energy*, vol. 41, no. 38, pp. 16944-16965, 2016.

[41] X. Hu, Q. Chen, Y. Zhao, B. W. Laursen, and B. Han, “Microporous and Mesoporous Materials Facile synthesis of hierarchical triazine-based porous carbons for hydrogen storage,” *Microporous Mesoporous Mater.*, vol. 224, pp. 129-134, 2016.

[42] Y. J. Lee, S. N. Talapaneni and A. Coskun, “Chemically Activated Covalent Triazine Frameworks with Enhanced Textural Properties for High Capacity Gas Storage Chemically Activated Covalent Triazine Frameworks with Enhanced Textural Properties for High Capacity Gas Storage”. *ACS Appl. Mater. Interfaces*, v.9, pp. 30679-30685, 2017.

[43] W. Wang, M. Zhou, and D. Yuan, “Carbon dioxide capture in amorphous porous organic polymers,” *J. Mater. Chem. A*, vol. 5, no. 4, pp. 1334-1347, 2017.

[44] S. Dey, A. Bhunia, I. Boldog and C. Janiak. “A mixed-linker approach towards improving covalent triazine-based frameworks for CO_2 capture and separation”. *Microporous and Mesoporous Materials,* v. 241, pp. 303-315, 2017.

[45] C. Gu, D. Liu, W. Huang, J. Liu, and R. Yang, “Synthesis of covalent triazine-based frameworks with high CO_2 adsorption and selectivity,” *Polym. Chem.*, vol. 6, no. 42, pp. 7410-7417, 2015.

[46] O. Buyukcakir, S. H. Je, S. N. Talapaneni, D. Kim, and A. Coskun, “Charged Covalent Triazine Frameworks for CO_2 Capture and Conversion”. *ACS Appl. Mater. Interfaces*, v.9 (8), pp.7209-7216, 2017.

[47] S. Mukherjee, M. Das, A. Manna, R. Krishna, and S. Das, “Dual Strategic Approach to Prepare Defluorinated Triazole-Embedded Covalent Triazine Frameworks with High Gas Uptake Performance”. *Chem. Mater.*, v. 31 (11), pp. 3929-3940, 2019.

[48] B. D. Freeman, “Basis of permeability/selectivity tradeoff relations in polymeric gas separation membranes,” *Macromolecules*, vol. 32, no. 2, pp. 375-380, 1999.

[49] H. B. Park, J. Kamcev, L. M. Robeson, M. Elimelech, and B. D. Freeman, “Maximizing the right stuff: The trade-off between membrane permeability and selectivity,” *Science*, vol. 356, no. 6343, pp. 1138-1148, 2017.

[50] Y. Ying, D. Liu, *et al.* “A GO-assisted method for the preparation of ultrathin covalent organic framework membranes for gas separation”. *J. Mater. Chem. A*, v. 4, pp. 13444-13449, 2016.

[51] L-C. Lin, J. Choi and J. C. Grossman. “Two-dimensional covalent triazine framework as an ultrathin-film nanoporous membrane for desalination”. *Chem. Commun*., v. 51, pp. 14921-14924, 2015.

[52] Y. Wang, J. Li, Q. Yang and C. Zhong. “Two-Dimensional Covalent Triazine Framework Membrane For Helium Separation And Hydrogen Purification”. *ACS Appl. Mater. Interfaces*, v. 8 (13), pp. 8694-8701, 2016.

[53] J. Artz, “Covalent Triazine-based Frameworks: Tailor-made Catalysts and Catalyst Supports for Molecular and Nanoparticulate Species,” *ChemCatChem*, vol. 10, no. 8, pp. 1753-1771, 2018.

[54] J. Roeser, K. Kailasam, and A. Thomas, “Covalent Triazine Frameworks as Heterogeneous Catalysts for the Synthesis of Cyclic and Linear Carbonates from Carbon Dioxide and Epoxides”. *ChemSUSChem,* v. 5 (9), pp. 1793-1799, 2012.

[55] J. Artz and R. Palkovits, “Base-Free Aqueous-Phase Oxidation of 5-Hydroxymethylfurfural over Ruthenium Catalysts Supported on Covalent Triazine Frameworks”. *ChemSUSChem,* v.8 (22), pp. 3832-3838, 2015.

[56] J. Artz, S. Mallmann, and R. Palkovits, “Selective Aerobic Oxidation of HMF to 2 , 5-Diformylfuran on Covalent Triazine Frameworks-Supported Ru Catalysts”. *ChemSUSChem,* v. 8 (4), pp. 672-679, 2015.

[57] M. Soorholtz *et al.*, “Local Platinum Environments in a Solid Analogue of the Molecular Periana Catalyst”. *ACS Catal*., v. 6 (4), pp. 2332-2340, 2016.

[58] P. Sudakar, G. H. Gunasekar, I. H. Baek, and S. Yoon, “Recyclable and efficient heterogenized Rh and Ir catalysts for the transfer hydrogenation of carbonyl compounds in aqueous medium”. *Green Chem.*, vol. 18, no. 24, pp. 6456-6461, 2016.

[59] G. H. Gunasekar, K. D. Jung, and S. Yoon, “Hydrogenation of CO_2 to Formate using a Simple, Recyclable, and Efficient Heterogeneous Catalyst”. *Inorg. Chem*., v. 58 (6), pp. 3717-3723, 2019.

[60] K. Kamiya, R. Kamai, K. Hashimoto, and S. Nakanishi, “Platinum-modified covalent triazine frameworks hybridized with carbon nanoparticles as methanol-tolerant oxygen reduction electrocatalysts”. *Nat. Commun.*, no. May, pp. 1-5, 2014.

[61] J. Stacy, Y. N. Regmi, B. Leonard, and M. Fan, “The recent progress and future of oxygen reduction reaction catalysis: A review”. *Renew. Sustain. Energy Rev.*, vol. 69, pp. 401-414, 2017.

[62] K. Iwase, T. Yoshioka, S. Nakanishi, K. Hashimoto, and K. Kamiya. “Copper-Modified Covalent Triazine Frameworks as Non-Noble-Metal Electrocatalysts for Oxygen Reduction”. *Angewandte Chemie Int. Ed*., v. 54, pp. 11068-11072, 2015.

[63] H. Wang and L. Gao, “Recent developments in electrochemical hydrogen evolution reaction,” *Curr. Opin. Electrochem.*, vol. 7, pp. 7-14, 2018.

[64] J. Yi, R. Xu, G. Chai, T. Zhang, K. Zang, *et al.* “Cobalt single-atoms anchored on porphyrinic triazine-based frameworks as bifunctional electrocatalysts for oxygen reduction and hydrogen evolution reactions”. *J. Mater. Chem. A*, v. 7, pp. 1252-1259, 2019.

[65] C. Lu, J. Yang, *et al.*, “Atomic Ni Anchored Covalent Triazine Framework as High Efficient Electrocatalyst for Carbon Dioxide Conversion”. *Advanced Functional Materials*., v. 29, pp. 1806884, 2019.

[66] K. Schwinghammer, S. Hug, M. B. Mesch, J. Senker, and B. V Lotsch, “Phenyl-triazine oligomers for light-driven hydrogen evolution". *Energy Environ. Sci.*, vol. 8, pp. 3345-3353, 2015.

[67] C. B. Meier, A. Cooper, *et al.*, “Structure-property relationships for covalent triazine-based frameworks: The effect of spacer length on photocatalytic hydrogen evolution from water,” *Polymer.*, v. 126, pp. 283-290, 2017.

[68] L. Guo, Y. Niu, *et al.* “Engineering heteroatoms with atomic precision in donor–acceptor covalent triazine frameworks to boost photocatalytic hydrogen production”. *J. Mater. Chem. A*, v. 6, pp. 19775-19781, 2018.

[69] R. Xu, X-S. Wang, *et al.* “Rhenium-modified porous covalent triazine framework for highly efficient photocatalytic carbon dioxide reduction in a solid–gas system”. *Catal. Sci. Technol.*, v.8, pp. 2224-2230, 2018.

[70] J. Bi, B. Xu, *et al*. “A Cobalt-Modified Covalent Triazine-Based Framework as an Efficient Cocatalyst for Visible-Light-Driven Photocatalytic CO_2 Reduction”. *ChemPLUSChem*., v. 84, pp. 1149-1154, 2019.

[71] R. K. Yadav, A. Kumar, D. Yadav, N. J. Park, J. Y. Kim, and J. O. Baeg, “In Situ Prepared Flexible 3D Polymer Film Photocatalyst for Highly Selective Solar Fuel Production from CO_2”. *ChemCatChem*, vol. 10, no. 9, pp. 2024-2029, 2018.

[72] S. Yang *et al.*, “2D Covalent Organic Frameworks as Intrinsic Photocatalysts for Visible Light-Driven CO_2 Reduction,” *J. Am. Chem. Soc.*, vol. 140, no. 44, pp. 14614-14618, 2018.

[73] A. Bhunia, S. Dey, M. Bous, C. Zhang, W. Von Rybinski, and C. Janiak. “High adsorptive properties of covalent triazine-based frameworks (CTFs) for surfactants from aqueous solution”. *Chem. Commun.*, vol. 51, pp. 484-486, 2014.

[74] J. Ren, X. Wang, X. Li, M. Wang, R. Zhao, and J. Lin, “Magnetic covalent triazine-based frameworks as magnetic solid-phase extraction adsorbents for sensitive determination of perfluorinated compounds in environmental water samples”.

Analytical and Bioanalytical Chemistry., v. 410, pp. 1657-1665, 2018.

[75] Y. Shen, C. Zhu, S. Song, T. Zeng, L. Li, and Z. Cai, "Defect-Abundant Covalent Triazine Frameworks as Sunlight-Driven Self-Cleaning Adsorbents for Volatile Aromatic Pollutants in Water". *Environ. Sci. Technol.,* v. 53, pp. 9091-9101, 2019.

[76] X. Deng, B. Zhao, *et al.* "Molten salt synthesis of nitrogen-doped carbon with hierarchical pore structures for use as high-performance electrodes in supercapacitors". *Carbon.*, vol. 93, pp. 48-58, 2015.

[77] Y. Li, S. Zheng, *et al.*"Conductive Microporous Covalent Triazine-Based Framework for High-Performance Electrochemical Capacitive Energy Storage". *Angewandte Chemie Int. Ed*., v. 57, pp. 7992-7996, 2018.

[78] S. N. Talapaneni, T. H. Hwang, S. H. Je, O. Buyukcakir, J. W. Choi, and A. Coskun, "Elemental-Sulfur-Mediated Facile Synthesis of a Covalent Triazine Framework for High-Performance Lithium–Sulfur Batteries". *Angewandte Chemie Int. Ed*., v.128, pp. 3158-3163, 2016.

[79] S. H. Je, H. J. Kim, J. Kim, J. W. Choi, and A. Coskun, "Perfluoroaryl-Elemental Sulfur S N Ar Chemistry in Covalent Triazine Frameworks with High Sulfur Contents for Lithium – Sulfur Batteries". *Advanced Functional Materials*., vol. 27, p.1703947, 2017.

[80] M. Rose, "Nanoporous polymers: Bridging the gap between molecular and solid catalysts?," *ChemCatChem*, vol. 6, no. 5, pp. 1166-1182, 2014.

[81] M. Besson and P. Gallezot, "Selective oxidation of alcohols and aldehydes on metal catalysts". *Catalysis Today,*v. 57, pp. 127-141, 2000.

[82] R. Mouselmani, A. Hachem, A. Alaaeddine, E. Métay, and M. Lemaire, "Reduction of aromatic nitriles into aldehydes using calcium hypophosphite and a nickel precursor". *Org. Biomol. Chem.*, v.16, pp. 6600–6605, 2018.

[83] A. J. Mancuso, S-L. Huang and D. Swern, "Oxidation of Long-chain and Related Alcohols to Carbonyls by Dimethyl Sulfoxide "Activated" by Oxalyl Chloride". *J. Org. Chem.*, v. 43, No12, 1978.

[84] J. H. Wood, C. C. Tung, M. A. Perry, and R. E. Gibson, "The Sommelet Reaction in the Synthesis of Aromatic Dialdehyde". vol. 654, no. 6, pp. 2992-2993, 1950.

[85] R. L. Shriner and F. W. Neumann, “The chemistry of the amidines,” *Chem. Rev.*, vol. 35, no. 3, pp. 351-425, 1944.

[86] W. Guo, M. Zhao, *et al*. “Developments towards synthesis of N-heterocycles from amidines via C–N/C–C bond formation”. *Org. Chem. Front*., v. 6, pp. 2120-2141, 2019.

[87] Z. Wang, “Pinner Reaction,” *Compr. Org. Name React. Reagents*, pp. 2237-2240, 2010.

[88] R. S. Garigipati, “An efficient conversion of nitriles to amidines,” *Tetrahedron Lett.*, vol. 31, no. 14, pp. 1969-1972, 1990.

[89] M. S. Eisen and M. Kapon, “Synthesis, molecular structure and solution dynamics of dimeric benzamidinates containing a double diazaallyl lithium bridge. A rapid interconversion of σ and π bonds,” *J. Chem. Soc. Dalt. Trans.*, no. 23, pp. 3507–3510, 1994.

[90] R. T. Boeré, R. T. Oakley, and R. W. Reed, “Preparation of N,N,N′-tris(trimethylsilyl)amidines; a convenient route to unsubstituted amidines”. *J. Organomet. Chem.*, vol. 331, no. 2, pp. 161-167, 1987.

[91] K. Li, X. An, K. H. Park, M. Khraisheh, and J. Tang, “A critical review of CO2 photoconversion: Catalysts and reactors”. *Catal. Today*, vol. 224, pp. 3-12, 2014.

[92] T. Inoue, A. Fujishima, S. Konishi and K. Honda “Photoelectrocatalytic reduction of carbon dioxide in aqueous suspensions of semiconductor powders”. *Nature,* v. 277, pp. 637-638, 1979.

[93] K. Li, B. Peng, and T. Peng, “Recent Advances in Heterogeneous Photocatalytic CO 2 Conversion to Solar Fuels,” 2016.

[94] S. Navalón and A. Dhakshinamoorthy, “Photocatalytic CO_2 Reduction using Non-Titanium Metal Oxides and Sulfides”. *ChemSUSChem*., v. 6, pp. 562-577, 2013.

[95] K. Chan, C. Tsai, H. A. Hansen, and J. K. Nørskov, “Molybdenum Sulfides and Selenides as Possible Electrocatalysts for CO_2 Reduction”. *ChemCATChem*., v. 6, pp. 1899-1905, 2014.

[96] Y. Yamazaki, H. Takeda, and O. Ishitani, “Photocatalytic reduction of CO_2 using

metal complexes," *Journal of Photochemistry and Photobiology C : Photochemistry Reviews.,* vol. 25, pp. 106–137, 2015.

[97] J. Lehn and R. Ziessel, "Photochemical generation of carbon monoxide and hydrogen by reduction of carbon dioxide and water under visible light irradiation," vol. 79, pp. 701–704, 1982.

[98] "Electrocatalytic reduction of carbon dioxide by using macrocycles of nickel and cobalt". *J. Am. Chem. Soc.*, v. 102, pp. 7361-7363, 1980.

[99] R. Ziessel, J. Hawecker, and J. Lehn, "Photogeneration of Carbon Monoxide and of Hydrogen via Simultaneous Photochemical Reduction of Carbon Dioxide and Water by Visible-Light Irradiation of Organic Solutions Containing Tris(2,2′-bipyridine)ruthenium(II) and Cobalt(II) Species as Homogeneous Catalysts". *Helvetica*., v. 69, pp. 1065-1084, 1986.

[100] M. Complexes, D. Photocatalysts, Y. Zhao, and Z. Liu, "Recent Advances in Photocatalytic CO_2 Reduction Using Earth - Abundant". *Chinese Journal of Chemistry*., v. 36, pp. 455-460, 2018.

[101] "Metal-organic frameworks for photocatalytic CO_2 reduction under visible radiation: A review of strategies and applications". *Catalysis Today.,* v. 340, pp. 209-224, 2020.

[102] V. S. Vyas, V. W. H. Lau, and B. V. Lotsch, "Soft Photocatalysis: Organic Polymers for Solar Fuel Production". *Chem. Mater.*, vol. 28, no. 15, pp. 5191-5204, 2016.

[103] F. M. Wisser, Y. Mohr, A. Quadrelli, and J. Canivet, "Porous Macroligands : Materials for Heterogeneous Molecular Catalysis". *ChemCATChem*., https://doi.org/10.1002/cctc.201902064, 2020.

[104] F. M. Wisser *et al.*, "Hammett Parameter in Microporous Solids as Macroligands for Heterogenized Photocatalysts". *ACS Catal.*, vol. 8, no. 3, pp. 1653-1661, 2018.

[105] X. Wang, F. M. Wisser, *et al*, "Immobilization of a Full Photosystem in the Large-Pore MIL-101 Metal–Organic Framework for CO_2 reduction". *ChemSUSChem*., v.11, pp. 3315-3322, 2018.

[106] F. M. Wisser, M. Duguet, *et al*. "Molecular Porous Photosystems Tailored for

Long-Term Photocatalytic CO_2 Reduction". https://doi.org/10.1002/anie.201912883, 2020

[107] A. Trewin and A. I. Cooper, "Porous organic polymers: Distinction from disorder?". *Angew. Chemie - Int. Ed.*, vol. 49, no. 9, pp. 1533-1535, 2010.

[108] G. Paul *et al.*, "Combined solid-state NMR, FT-IR and computational studies on layered and porous materials," *Chem. Soc. Rev.*, vol. 47, no. 15, pp. 5684-5739, 2018.

[109] B. Lukose, A. Kuc, and T. Heine, "The structure of layered covalent-organic frameworks". *Chem. - A Eur. J.*, vol. 17, no. 8, pp. 2388–2392, 2011.

[110] M. Morshedi, M. Thomas, A. Tarzia, J. Doonan, and N. G. White, "Chemical Science Supramolecular anion recognition in water : synthesis of hydrogen-bonded supramolecular frameworks". *Chem. Sci.*, v. 8, pp. 3019-3025, 2017.

[111] G. Xu, J. P. Wu, X. M. Ai, and L. R. Yang, "Microwave-assisted Kornblum oxidation of organic halides," *Chinese Chem. Lett.*, vol. 18, no. 6, pp. 643-646, 2007.

[112] A. R. Sanger, "Reactions Of Benzonitrile With Lithium Amides". *Inorg. Nucl. Chem. Lett.*, vol. 9, pp. 351-354, 1973.

[113] B. Steiger and F. C. Anson, "New Electrocatalysts for the Four-Electron Reduction of Dioxygen Based on (5,10,15-Tris(pentaammineruthenium(II)-4-cyanophenyl)-20- (1-methylpyridinium-4-yl)porphyrinato)cobalt(II) Immobilized on Graphite Electrodes". *Inorg. Chem*., v. 33, pp. 5767–5779, 1994.

[114] X. Zhu, W. Wong, F. Jiang, C. Poon, and W. Wong, "An ultrasonic wave-assisted synthesis of meso-amidinophenyl substituted porphyrins". *Tetrahedron Letters*., v. 49, pp. 2114–2118, 2008.

[115] A. I. Olivos-suarez, A. V Bavykina, and J. Gascon, "Revisiting Nitrogen Species in Covalent Triazine Frameworks". *Langmuir,* v. 33, pp. 14278-14285, 2017.

[116] J. Bonnefoy, A. Legrand, B. Coasne, and D. Farrusseng, "Structure-property relationships of water adsorption in Metal-Organic Frameworks". *New J. Chem.*, v. 38, pp. 3102-3111, 2014.

[117] Y. Lee, S. Kim, *et al*."Photocatalytic CO_2 reduction using visible light by metal-monocatecholato species in a metalorganic framework". *Chem. Commun*., v. 51, pp. 16549-16552, 2015.

[118] D. Sun, W. Liu, M. Qiu, Y. Zhang, and Z. Li, "Introduction of a mediator for enhancing photocatalytic performance via post-synthetic metal exchange in metal-organic frameworks (MOFs)". *Chem. Commun.*, vol. 66, pp. 3-6, 2014.

[119] Y. Fu, D. Sun, Y. Chen, R. Huang, Z. Ding, and X. Fu, "An Amine-Functionalized Titanium Metal – Organic Framework Photocatalyst with Visible-Light-Induced Activity for CO_2 Reduction". *Angewandte Chemie Int. Ed.*, vol. 125, pp. 3364–3367, 2012.

[120] A. Mahmood, J-Y. Hu, *et al.* "Recent progress in porphyrin-based materials for organic solar cells". *J. Mater. Chem. A*, v. 6, pp. 16769-16797, 2018.

[121] R. Paolesse, S. Nardis, D. Monti, M. Stefanelli, and C. Di Natale, "Porphyrinoids for Chemical Sensor Applications". *Chem. Rev.,* v. 117, pp. 2517-2583, 2017.

[122] M. Ravi, M. Ranocchiari, and J. A. Van Bokhoven, "The Direct Catalytic Oxidation of Methane to Methanol - A Critical Assessment". *Angewandte Chemie Int. Ed.*, v. 56, pp. 16464-16483, 2017.

[123] G. Li, J. Gascon, E. A. Pidko, and A. Sze, "Mechanistic Complexity of Methane Oxidation with H_2O_2 by Single- Site Fe/ZSM-5 Catalyst". *ACS Catal.,* v. 8, pp. 7961-7972, 2018.

[124] M. A. Nasalevich *et al.*, "Isolated Fe Sites in Metal Organic Frameworks Catalyze the Direct Conversion of Methane to Methanol". *ACS Catal*., v.8, pp. 5542-5548, 2018.

APPENDIX

10 APPENDIX

10.1 EXPERIMENTAL PART

10.1.1 MATERIALS AND METHODS

Acetonitrile (anhydrous, 99.8%), biphenyl-4,4′-dicarboxylic acid (97 %), 2,2′-bipyridine-5,5′-dicarbonitrile (97 %), bis(triphenylphosphine)palladium(II) diacetate (98 %), maleic acid (standard for quantitative NMR, TraceCERT), methanol (anhydrous, 99.8 %), pentamethylcyclopentadienylrhodium(III) chloride dimer, sodium hydrogen carbonate (99 %), tetrahydrofurane (99.9 %), toluene (anhydrous, 99.8 %), triethanolamine (99 %), were purchased from Sigma Aldrich. Silver nitrate was purchased from Alfa Aesar. Deuterated solvents were purchased from euriso-top. All chemicals were used as received.

Nitrogen physisorption experiments were carried out using a BELSORP-mini II. Prior to measurements the samples were degassed at 80 °C for at least 12 h. Acetonitrile and water vapor physisorption isotherms were recorded on a BELSORP-max at 25 °C. Prior to measurement the porous materials were degassed at 80 °C for at least 12 h. The equilibrium condition was set to a relative pressure change (p/p0) below 0.3 % for 300 s for acetonitrile vapour and water physisorption experiments.

Liquid NMR spectra were recorded on a Bruker Ascend 400 spectrometer (9.4 T, 1H at 400.13 MHz, 13C at 100.61 MHz). The spectra were referenced against the deuterated solvent. Quantitative NMR (q-NMR) spectra were recorded using a stem coaxial insert (Wilmad-LabGlass) filled with 0.25 M maleic acid in D_2O. Prior to measurement the filling ratio between the NMR tube and the inserts used was determined according to Henderson using maleic acid in D_2O, maleic acid in D_2O/NaOD and benzoic acid in DMSO-d6. The quantitative inaccuracy of the q-NMR spectroscopy was $\leq 2\%$, which is considered to be sufficiently precise for q-NMR determination.

Elemental analyses were carried out using a LECO TruSpec Micro (Mikrolabor, ETH Zurich).

IR spectra were recorded using a Nicolet Magna IR 550 FT-IR spectrometer (Thermo Fisher Scientific) in diffuse reflection (resolution 2 cm^{-1}, 64 scans, Praying Mantis Diffuse Reflection Accessory, Harrick Scientific). Diffuse reflectance UV-Vis

spectra were recorded using an AvaLight-DHS source and an AvaSpec-2048 Fiber Optic Spectrometer (Avantes). Powders were diluted in $BaSO_4$ prior to measurement. The same setup was used to measure the spectra of the 200W Hg(Xe) lamp (Newport Research Arc Lamp), used for photocatalysis.

X-ray photoelectron spectroscopy (XPS) was performed using a monochromatic Alkα source in a commercial instrument (KRATOS AXIS ULTRA DLD), and revealed well-resolved peaks corresponding to C1s, N1s, and Rh3d core levels. Each high-resolution spectrum was decomposed into a combination of Voigt functions, each with an overall full-width at half maximum (FWHM) of approximately 2 eV.

Solid-state NMR spectra at room temperature were recorded on a Bruker AVANCE III 500 WB spectrometer (11.7 T, ^{1}H at 500.04 MHz, ^{13}C at 125.73 MHz) equipped with a 2.5 mm MAS (magic angle spinning) probe. ^{13}C cross polarization (CP) MAS spectra were referenced against glycine.

10.1.2 SYNTHESIS OF PRECURSOR

5,5’- Bis(bromomethyl)-2,2’-bipyridine:

The synthesis was done according to a literature procedure. To a solution of 5,5'-dimethyl-2,2'-bipyridine (10 mmol) in 50 mL of CCl_4, N-bromosuccinimide (20.5 mmol) and AIBN (0,02 mmol) were added. The reaction mixture was refluxed for 24 h, cooled to room temperature, filtered and the solvent was removed under reduced pressure. The crude product was solubilized in 50 mL of $CHCl_3$, washed with 100 mL 0,5 mol/L of aqueous $Na_2S_2O_3$. The aqueous phase was washed with 50 mL of $CHCl_3$ and all the organic phases were dried over sodium sulfate. The evaporation of the solvent gave the product, pure enough for the next step. Yield 80-90%.

^{1}H NMR (500 M Hz, $CDCl_3$, TMS) δ 4.47 (s, 4H, CH2Br), 7.80 (m, 2H, aromatic), 8.35 (m, 2H, aromatic), 8.61 (m, 2H, aromatic);

^{13}C NMR ($CDCl_3$, 125 MHz) δ 29.43, 121.25, 133.28, 137.70, 149.27, 155.19;

5,5′-dibromo-2,2′-bipyridine:

The synthesis was done according to a literature procedure. To 100g of 2,2′-bipyridine in 500 ml of methanol, 215 ml of 48% (wt/wt) aqueous HBr was added at 0 °C. The mixture was allowed to warm up to room temperature and stirred for 30 minutes. The solvent was removed using a rotary evaporator in a fume hood resulting in 2,2′-bipyridine dihydrobromide. A mortar was charged with 12.0 g of 2,2′-bipyridine dihydrobromide and gridded with 4 ml of bromine. The resulting orange powder was transferred to a 15-ml sample vial using a plastic funnel and compressed with a spatula. The vial was placed into a stainless steel bomb and heat to 185 °C for 72 h. After cooling to room temperature, the monolith was grounded and added to 200 ml of 2M NaOH solution. 10 g of EDTA tetrasodium salt and 10 g of Na_2SO_3 was added and stirred for 1 hour. The solution was extracted with DCM. The organic phases were separated and dried over Na_2SO_4. Evaporation of the solvent gave 5,5′-dibromo-2,2′-bipyridine as white powder. Yield: 8.88 g (28.30 mmol, 75%).

^{1}H NMR: (500 MHz, $CDCl_3$): δ in ppm: 7.93 (dd, 2H), 8.29 (d, 2H), 8.70 (d, 2H);

^{13}C NMR: (125 MHz, $CDCl_3$): δ in ppm: 121.4, 122.2, 139.6, 150.3, 153.7;

5,5′-dicyano-2,2′-bipyridine (cyanation - microwave):

A microwave vial was charged with degassed DMF (20.0 mL), 5,5'-dibromo-2,2'-bipyridine (1.25 g, 4.00 mmol), $Zn(CN)_2$ (0.94 g, 8.00 mmol), $Pd(PPh_3)_4$ (0.28 g, 0.24 mmol), and bis(diphenylphosphino)pentane (0.11 g, 0.24 mmol). A stream of argon was then bubbled through the mixture for 2 min and the vial was sealed. The yellow mixture was heated in the microwave for 5 min at 150 °C. The resulting greenish suspension was poured into H_2O (300 mL) and $CHCl_3$ (300 mL) and was stirred for 1 h. The solvent layers were separated and the water layer was extracted with $CHCl_3$ (3 × 300 mL). The combined organic layers were dried over $MgSO_4$ and concentrated in vacuo. The crude product was purified by flash column chromatography (CH_2Cl_2/ethyl acetate 9:1) to give 5,5’dicyano-2,2’-bipyridine as colourless crystals (0.76 g, 3.69 mmol, 92%).

^{1}H NMR (400 MHz; $CDCl_3$): δ in ppm: 8.95 (2 H, d, 4JHH = 2 Hz, C5/5’H), 8.63 (2 H, dd, 3JHH = 8 Hz, 5JHH = 1 Hz, C2/2’H), 8.13 (2 H, dd, 3JHH = 8 Hz, 4JHH = 2 Hz, C3/3’H);

^{13}C NMR (100 MHz; $CDCl_3$): δ in ppm: 157.0 (C1/1'), 152.2 (C5/5'), 140.6 (C3/3'), 121.8 (C2/2'), 116.6 (C4/4'), 110.8 (C6/6');

2,2'-bipyridine-5,5'-dicarboxylic acid:

5,5'-dimethyl-2,2'-bipyridine (9.45 g, 51 mmol) were added to a solution of 50.0 g of $KMnO_4$ in 600 mL of water. The mixture was refluxed for two days until decolourization. The solution was filtered from precipitated MnO_2 and the filtrate was acidified with 0,5M HCl. A fine colourless powder of 2,2'-bipyridine-5,5'-dicarboxylic precipitated. The solid was recovered by filtration, washed with water (3 x 100 mL) and dried in oven at 60ºC to afford the pure diacid. The solid was too insoluble for NMR experiments. Yield: (11.83 g, 95%).

Diethyl-2,2'-bipyridine-5,5'-dicarboxylate:

To a suspension of the diacid (1.0 g, 4.1 mmol) in ethanol (15 mL) was added sulphuric acid (2mL) and the mixture was refluxed overnight. Then, the reaction mixture was cooled to 0 °C by an ice-bath and was slowly poured to a saturated $NaHCO_3$ until complete neutralization. After evaporation of ethanol, the mixture was extracted with DCM (3 × 20 mL). The combined organic layers were dried over Na_2SO_4, filtered, and concentrated under reduced pressure to afford the desired product as a white solid. Yield: (1.0 g, 85%).

^{1}H NMR (300 MHz, $CDCl_3$): δ in ppm: 1.42 (t, 6H,), 4.42 (dd, 4H,), 8.44 (dd, 2H), 8.55 (dd, 2H), 9.27 (s, 2H);

2,2'-bipyridine-5,5'-bis(carboxamide):

A mixture of diethyl-2,2'-bipyridine-5,5'-dicarboxylate (0.5 g), ethanol (25 mL) and ethylene glycol (25 mL) was saturated with ammonia and heated in a closed vessel at 90ºC for 40h. After cooling to room temperature, the resulting insoluble solid was filtered off and washed with boiling ethanol. The carboxamide was obtained as white powder in quantitative yield. The solid was too insoluble for NMR experiments. The compound was identified by FT-IR. Yield: (0.4 g, 100%).

5,5′-dicyano-2,2′-bipyridine (dehydration):

2,2’-bipyridine-5,5’-bis(carboxamide) (0.168 g, 0.694 mmol) was added to trichlorooxophosphorus(V) (6.58 g, 43 mmol) in a normal round-bottom flask. The flask, fitted with a condenser containing and drying tube ($CaCl_2$) on top, was placed in ultrasonic bath containing water at room temperature. The mixture was sonicated (50 kHz) until the suspension had disappeared (72 h). The temperature of the water in the bath rose to 45ºC during this time. 5,5′-dicyano-2,2′-bipyridine was isolated from the reaction mixture following hydrolysis (of $POCl_5$), neutralisation (with aqueous NaOH) and extraction ($CHCl_3$). The solid was recrystallized with acetonitrile and filtered off as colorless needles. Yield: (0.13 g, 86%).

^{1}H NMR (400 MHz; $CDCl_3$): δ in ppm: 8.95 (2 H, d, 4JHH = 2 Hz, C5/5’H), 8.63 (2 H, dd, 3JHH = 8 Hz, 5JHH = 1 Hz, C2/2’H), 8.13 (2 H, dd, 3JHH = 8 Hz, 4JHH = 2 Hz, C3/3’H);

^{13}C NMR (100 MHz; $CDCl_3$) δ 157.0 (C1/1’), 152.2 (C5/5’), 140.6 (C3/3’), 121.8 (C2/2’), 116.6 (C4/4’), 110.8 (C6/6’);

5,5′-dicarbaldehyde-2,2′-bipyridine:

The synthesis was done according to a modified literature procedure. To a 25 mL MW reactor, 5,5’- Bis(bromomethyl)-2,2’-bipyridine (20 mmol; 6.85g), $NaHCO_3$ (60 mmol; 5.04g) and DMSO (20 mL) were added. The microwave heating was carried out with a single cavity mode, set to 250W. After set the condenser, the reaction was heated to reflux and kept at this temperature for 15 min. After the reaction, the dark solution was cooled to room temperature, then 40 mL of water was added to the system and toluene (50mL) was used to extract the desired product. The combined organic phase was washed with brine and the solvent evaporated. The crude product was purified by chromatography (silica gel, THF/n-Hexane = 1/3) to get the pure aldehyde. Yield: (2.97 g, 70%).

^{1}H NMR (400 MHz, $CDCl_3$): 10.21 (s, 2H, 2x –CH=O); 9.17 (dd, 2H, 2x H-6 (Pyr)); 8.72 (dd, 2H, 2x H-3 (Pyr)); 8.34 (dd, 2 H, 2x H-4 (Pyr));

^{13}C NMR (75 MHz, $CDCl_3$): 190.37 (2x –CH=O); 159.11 (2x C-2(Pyr)); 151.59 (2x C-6 (Pyr)); 137.16 (2x C-4 (Pyr)); 131.65 (2x C-5 (Pyr)); 122.37 (2x C-3(Pyr));

terephthalamidine dihydrochloride:

In a schlenk flask, benzene-1,4-dicarbonitrile (1.28 g, 10.0 mmol) was added. The flask was degassed and flushed with nitrogen three times. Then 20 mL of anhydrous THF was added to complete solubilization of nitrile. The mixture was cooled to 0ºC under water-ice bath. Under inert atmosphere, 40 mL of 1M $LiN(SiMe_3)_2$ solution was added dropwise over 30 min. The mixture was allowed to warm up to room temperature and stirred for 3h. After this time, the light brown solution was again cooled to 0 °C, and carefully quenched by addition of 40 mL of 2M HCl in ethanol. The mixture was set aside overnight. The precipitate was then filtered, washed with Et_2O, THF and ethanol. Yield: (2.26 g, 96%);

^{1}H NMR (400MHz, DMSOd6): δ = 9.67 (s, 4H, NH), 9.44 (s, 4H, NH), 8.04 (s, 4H, aromatic H);

^{13}C NMR (75 MHz, D2O) δ =165.87, 132.89, 138.72;

terephthalamidine ditetraphenylborate:

A 0.5 M aqueous solution of sodium tetraphenylborate was added to a solution of terephthalamidine dihydrochloride (0.5 g) in water (50 mL) causing the immediate precipitation of terephthalamidine ditetraphenylborate. When no precipitate is formed upon further addition of sodium tetraphenylborate, the product was filtered off, washed with water and dried in oven at 60°C. Yield: 98%.

^{1}H NMR (400MHz, DMSO d6): δ = 8.43 (s), 7.99 (s), 7.19 (s), 6.94 (t), 6.80 (t);

^{11}B NMR (100 MHz, DMSO d6) δ = -6.65;

terephthalamidine dibromide:

A 0.5M solution of tetrabutyl ammonium bromide in acetone was added to a solution of terephthalamidine ditetraphenylborate (0.5 g) in acetone (50 mL) causing the precipitation of terephthalamidine dibromide. When no precipitate is formed upon further addition of tetrabutyl ammonium bromide, the product was recovered by centrifugation,

washed with acetone (3 x 50 mL) and ethanol (3 x 50 mL) and dried in oven at 60°C. Yield: 85%.

^{1}H NMR (400MHz, DMSO d6): δ = 9.36 (s), 8.02 (s);

4,4'-biphenyldiamidine dichloride:

To a solution of 4,4′-biphenyldicarbonitrile (2.042 g, 10.0 mmol) in 30 mL of THF, 40 mL of 1 M $LiN(SiMe_3)_2$ solution was added dropwise in 15 min at 0 °C in ice-water bath. After addition, the ice-water bath was removed and the mixture was stirred at room temperature for 3h. After this time, the brownish solution was cooled to 0 °C and the reaction was quenched by careful addition of 2 M HCl–EtOH (40 mL). The mixture was set aside overnight. The precipitate was then filtered off, washed with THF, acetone, and dried in oven at 60ºC. Yield: (2.9876 g, 96%).

^{1}H NMR (400MHz, DMSO d6): δ = 9.55 (s), 9.25 (s), 8.07 (d), 8.02 (d);

^{13}C NMR (100 MHz, DMSO d6) δ =165.87, 132.89, 138.72;

4,4'-biphenyldiamidine ditetraphenylborate:

A 0.5 M aqueous solution of sodium tetraphenylborate was added to a solution of 4,4'-biphenyldiamidine dichloride (0.75 mmol; 0.2334 g) in water (50 mL) causing the immediate precipitation of 5,5′-diamidine-2,2′-bipyridine ditetraphenylborate. When no precipitate is formed upon further addition of sodium tetraphenylborate, the product was filtered off, washed with water and dried in oven at 60°C. Yield: (0.4112 g, 98%).

^{1}H NMR (400MHz, DMSO d6): δ = 9.31 (s), 9.01 (s), 8.07 (d), 7.97 (d), 7.19 (s), 6.94 (t), 6.80 (t);

^{11}B NMR (100 MHz, DMSO d6) δ = -6.65;

4,4'-biphenyldiamidine dibromide:

A 0.5M solution of tetrabutyl ammonium bromide in acetone was added to a solution of 4,4'-biphenyldiamidine ditetraphenylborate (0.75 mmol; 0.42 g) in acetone (50 mL) causing the precipitation of 4,4'-biphenyldiamidine dibromide. When no precipitate is formed upon further addition of tetrabutyl ammonium bromide, the product was

recovered by centrifugation, washed with acetone (3 x 50 mL) and ethanol (3 x 50 mL) and dried in oven at 60°C. Yield: (0.3580 g, 85%).
^{1}H NMR (400MHz, DMSO d6): δ = 9.49 (s), 9.10 (s), 8.08 (d), 8.01 (d);

5,5′-diamidine-2,2′-bipyridine dichloride:
To a solution of 5,5′-dicyano-2,2′-bipyridine (2.06 g, 10.0 mmol) in 30 mL of THF, 40 mL of 1 M $LiN(SiMe_3)_2$ solution was added dropwise in 15 min at 0 °C in ice-water bath. After addition, the ice-water bath was removed and the mixture was stirred at room temperature for 3h. After this time, the brownish solution was cooled to 0 °C and the reaction was quenched by careful addition of 2 M HCl–EtOH (40 mL). The mixture was set aside overnight. The precipitate was then filtered off, washed with THF, Acetone, and dried in oven at 60ºC. Yield: (3.00 g, 96%).
^{1}H NMR (400MHz, DMSO d6): δ = 9.87 (s, 4H, NH), 9.59 (s, 4H, NH), 9.20 (d, 2H, aromatic H), 8.64 (dd, 2H, aromatic H) 8.51 (dd, 2H, aromatic H);

5,5′-diamidine-2,2′-bipyridine ditetraphenylborate:
A 0.5 M aqueous solution of sodium tetraphenylborate was added to a solution of 5,5′-diamidine-2,2′-bipyridine dichloride (0.75 mmol; 0.235 g) in water (50 mL) causing the immediate precipitation of 5,5′-diamidine-2,2′-bipyridine ditetraphenylborate. When no precipitate is formed upon further addition of sodium tetraphenylborate, the product was filtered off, washed with water and dried in oven at 60°C. Yield: (0.413 g, 98%).
^{1}H NMR (400MHz, DMSO d6): δ = 9.56 (s, 4H, NH), 9.15 (s, 4H, NH), 9.12 (d, 2H, aromatic H), 8.66 (dd, 2H, aromatic H) 8.42 (dd, 2H, aromatic H), 7.20-7.14 (m, 8H, meso-tetraphenylborate), 6.92 (t, 8H, ortho-tetraphenylborate), 6.79 (t, 4H, para-tetraphenylborate);
^{11}B NMR (100 MHz, DMSO d6) δ = -6.65;

5,5′-diamidine-2,2′-bipyridine dibromide:
A 0.5M solution of tetrabutyl ammonium bromide in acetone was added to a solution of 5,5′-diamidine-2,2′-bipyridine ditetraphenylborate (0.75 mmol; 0.42 g) in acetone (50 mL) causing the precipitation of 5,5′-diamidine-2,2′-bipyridine dihydrobromide. When no precipitate is formed upon further addition of tetrabutyl ammonium bromide, the

product was recovered by centrifugation, washed with acetone (3 x 50 mL) and ethanol (3 x 50 mL) and dried in oven at 60°C. Yield: (0.256 g, 85%).
^{1}H NMR (400MHz, DMSO d6): δ = 9.59 (s, 4H, NH), 9.17 (s, 4H, NH), 9.16 (d, 2H, aromatic H), 8.66 (dd, 2H, aromatic H) 8.44 (dd, 2H, aromatic H);

5,10,15,20-Tetrakis(4-cyanophenyl)-21H,23H-porphyrine:
The porphyrin was synthesized and purified according to methods previously described. 4-cyanobenzaldehyde (20 mmol; 2.62g) and pyrrole (20 mmol; 1.34g) were added to 50 mL of 99% propionic acid, the mixture was stirred open to the air at 145 °C for 3 h. The reaction mixture was cooled in an ice-water bath for 15 min and added to 200 mL of acetone. Then 50 mL of 32% aqueous ammonia were slowly added to the cooled (ice-water bath) mixture. After cooling overnight to -20 °C, the precipitate was collected by filtration, washed with acetone and air-dried to give 0,95 g of violet powder. Yield: 54%.
1H NMR (400MHz, CDCl3): δ = 8.80 (s, 8H, pyrrole), 8.34 (d, 8H, o-(cyanophenyl)), 8.11 (d, 8H, m-(cyanophenyl)), -2.87 (s, 2H, pyrrole);

5,5'-bis(hydroxymethyl)-2,2'-bipyridine:
To a 1 g of diethyl 2,2'-bipyridine-5,5'-dicarboxylate was added into 500 mL round-bottom flask and a silicon septum was placed. The flask was evacuated and filled with N_2 three times. 50 mL of anhydrous THF was added under N_2 and the mixture was stirred until complete solubilization. After cooled down to 0°C in ice-water bath, 3mL of bis(2-methoxyethoxy)-aluminium hydride in toluene (Red-Al®) was added dropwise over 10 minutes. The solution turned deep red and was stirred for 3 hours at 0°C under N_2. After that, the excess of Red-Al was carefully decomposed by addition of 2 ml of a saturated solution of ammonium chloride in water. The solid was filtered off and extracted with hot acetone 3 times (3x100 mL). The filtrate was evaporated and the solid washed with petroleum ether (2 x 50 mL). Recrystallization in acetone/petroleum ether afforded a pale orange solid. Yield: (0.648 g, 90%).
1H NMR (400MHz, DMSO d6): δ = 8.62 (d, 2H, aromatic H), 8.37 (d, 2H, aromatic H), 7.98 (dd, 2H, aromatic H), 4.62 (d, 4H, aliphatic H);

5,10,15,20-Tetrakis(4-alidinophenyl)-21H,23H-porphyrine:

To a 0.21 mmol of 5,10,15,20-Tetrakis(4-alidinophenyl)-21H,23H-porphyrine, 20 mL of anhydrous THF is added to a 100 mL schlenk flask under inert athmosphere. The mixture is stirred until the complete dissolution. To this mixture, 1.28 mmol of LiHMDS is added. This mixture is placed in the ultrasonic bath for 2h. During this time, the temperature rose to 50°C. After this time, 50 mL of acetonitrile is added to the mixture and the material was filtered off. The solid was washed with acetone and acetonitrile prior drying at 80°C in oven to afford a green powder.

10.1.3 SYNTHESIS OF MATERIALS

Synthesis of CTF-1 (CTF-MAS-84):

1,4-phthalaldehyde (67.2 mg, 0.5 mmol), terephthalamidine dibromide (324.0 mg, 1.0 mmol), and caesium carbonate (716.8 mg, 2.2 mmol) were added to a solution of DMSO (5.0 mL) in 25 mL round-bottom flask. The mixture was heated at 60°C, 80°C, and 100°C for 24h each, before being heated at 120°C for 3 days to yield a yellow solid. The resulting precipitate was washed with dilute HCl (3 × 10 mL) to remove the salt and residual caesium carbonate, and with water (3 × 10 mL), acetone (3 × 10 mL), and THF (3 × 10 mL), before drying at 80 °C under vacuum for 12h to yield CTF-1 as a yellow powder. Yield: 98%.

Synthesis of CTF-1 (MW) (CTF-MAS-95):

To a 25 mL round-bottom flask, 1,4-phthalaldehyde (67.2 mg, 0.5 mmol), terephthalamidine dibromide (324.0 mg, 1.0 mmol), caesium carbonate (716.8 mg, 2.2 mmol) and DMSO (5.0 mL) were added. A condenser was settled in the flask and placed into a microwave reactor. The mixture was heated under microwave irradiation at 80ºC and 100ºC for 10 min each temperature, before being heated at 120ºC for 20 minutes under dynamic mode. After cooling down, the resulting yellow solid was recovered by filtration and washed with dilute HCl (3 × 10 mL) to remove the residual caesium carbonate, water (3 × 10 mL), acetone (3 × 10 mL), and THF (3 × 10 mL), before drying at 80 °C under vacuum for 12h to yield CTF-1 (MW) as a yellow powder. Yield: 98%.

Synthesis of CTF-BPY-33:

2,2'-bipyridine-5,5'-dicarboxaldehyde (0.107 g, 0.5 mmol), 4,4'-biphenyldiamidine dibromide (0.400 g, 1.0 mmol), and caesium carbonate (0.720 g, 2.2 mmol) were added to DMSO (8.0 mL) in 50 mL round-bottom flask. The mixture was heated at 60°C, 80°C, and 100°C for 24h each, before being heated at 120°C for 3 days. After cooling to room temperature, 30 mL of 1M HCl was added and the resulting yellow mixture was stirred for 30 min to remove the residual caesium carbonate. The solid was recovered by filtration and washed with dilute HCl (3 × 15 mL), water (3 × 15 mL), acetone (3 × 15 mL), and THF (3 × 15 mL), before drying at 80 °C under vacuum for 12h to yield CTF-BPY-33 as a yellow powder. Yield: 97%.

Synthesis of CTF-BPY-66:

biphenyl-4,4'-dicarboxaldehyde (0.0559 g, 0.263 mmol), 5,5′-diamidine-2,2′-bipyridine dibromide (0.2119 g, 0.527 mmol), and caesium carbonate (0.3776 mg, 1.16 mmol) were added to DMSO (5.0 mL) in 50 mL round-bottom flask. The mixture was heated at 60°C, 80°C, and 100°C for 24h each, before being heated at 120°C for 3 days. After cooling to room temperature, 30 mL of 1M HCl was added and the resulting yellow mixture was stirred for 30 min to remove the residual caesium carbonate. The solid was recovered by filtration and washed with dilute HCl (3 × 15 mL), water (3 × 15 mL), acetone (3 × 15 mL), and THF (3 × 15 mL), before drying at 80 °C under vacuum for 12h to yield a CTF-BPY-66 as a yellow powder. Yield: 97%.

Synthesis of CTF-BPY-100:

2,2'-bipyridine-5,5'-dicarboxaldehyde (0.1061 g, 0.5 mmol), 5,5′-diamidine-2,2′-bipyridine dibromide (0.402 g, 1.0 mmol), and caesium carbonate (0.3776 mg, 2.2 mmol) were added to DMSO (5.0 mL) in 50 mL round-bottom flask. The mixture was heated at 60°C, 80°C, and 100°C for 24h each, before being heated at 120°C for 3 days. After cooling to room temperature, 30 mL of 1M HCl was added and the resulting yellow mixture was stirred for 30 min to remove the residual caesium carbonate. The solid was recovered by filtration and washed with dilute HCl (3 × 15 mL), water (3 × 15 mL),

acetone (3 × 15 mL), and THF (3 × 15 mL), before drying at 80 °C under vacuum for 12h to yield a CTF-BPY-100 as a yellow powder. Yield: 97%.

Synthesis of CTF-BPY-100 (using alcohol as precursor):

5,5'-bis(hydroxymethyl)-2,2'-bipyridine (0.0818 g, 0,37 mmol), 5,5′-diamidine-2,2′-bipyridine dibromide (0.3012 g, 0.75 mmol), and caesium carbonate (0.5368 g, 1.65 mmol) were added to DMSO (10.0 mL) in 50 mL round-bottom flask. The mixture was heated at 80°C and 100°C for 24h each, before being heated at 160°C for 3 days. After cooling to room temperature, 30 mL of 1M HCl was added and the resulting yellow mixture was stirred for 30 min to remove the residual caesium carbonate. The solid was recovered by filtration and washed with dilute HCl (3 × 15 mL), water (3 × 15 mL), acetone (3 × 15 mL), and THF (3 × 15 mL), before drying at 80°C under vacuum for 12h to yield a CTF-BPY-100 as yellow powder. Yield: 96%.

Synthesis of CTF-BPH:

4,4'-biphenyldicarbaldehyde (0.0683 g, 0.325 mmol), 4,4'-biphenyldiamidine dibromide (0.2025 g, 0.65 mmol), and caesium carbonate (0.4648 g, 1.4 mmol) were added to DMSO (6.5 mL) in 50 mL round-bottom flask. The mixture was heated at 60°C, 80°C, and 100°C for 24h each, before being heated at 120°C for 3 days. After cooling to room temperature, 30 mL of 1M HCl was added and the resulting yellow mixture was stirred for 30 min to remove the residual caesium carbonate. The solid was recovered by filtration and washed with dilute HCl (3 × 15 mL), water (3 × 15 mL), acetone (3 × 15 mL), and THF (3 × 15 mL), before drying at 80 °C under vacuum for 12h to yield CTF-BPH as light yellow powder. Yield: 99%.

Synthesis of CTF-PORF:

To a 150 mg (0.2 mmol) of 5,10,15,20-Tetrakis(4-cyanophenyl)-21H,23H-porphyrine in a 100 mL round-bottom flask, 50 mL of $CHCl_3$ is added. The mixture is stirred until the formation of a homogeneous solution. 2 mL of trifluoromethanesulfonic acid is added to the previous solution and stirred for 24h at room temperature. After 24 hours, a solution

of 3 mL of 32% Ammonia solution in 50 mL of water is carefully added into the flask. After stir for 2 hours for complete neutralization of the acid, the solid is filtered off and washed with 100 mL of water and 100 mL of acetone and dried in oven at 60ºC. Yield: 99%.

Cleavage of Rhodium dimmer:

In a glass vial, 28.0 mg (44.9 µmol, 89.7 µmol $[Cp^*RhCl]^+$) $[Cp^*RhCl_2]_2$ and 15.2 mg (89.4 µmol) $AgNO_3$ were dispersed in a mixture of 5 ml anhydrous acetonitrile and 1 ml anhydrous MeOH and stirred for 2 h under light exclusion. The white solid was removed by centrifugation and the yellow solution was stored at 5°C.

Rhodium complex infiltration:

In a typical infiltration, (6 mol % Rh) 0,1 g of CTF-BPY-33 were dispersed in 3.75 ml dry MeOH, then 1.25 ml of the above-mentioned solution were added and the suspension was stirred for 24 h at room temperature. The supernatant was removed by centrifugation and the solid washed with MeOH during 2 days (exchange of MeOH every 12 h). The solid was dried under reduced pressure first at room temperature, then at 80°C.

Metallation of CTF-PORF:

To a 200 mg CTF-PORF in a 100 mL round-bottom flask, 200 mg of $FeCl_3$ and 50 mL of DMF is added. The mixture was heated until reflux. After 24 hours, the mixture was cooled to room temperature and the solid was filtered off. The material is washed with DMF and acetone prior to dry in oven at 80°C to afford a dark brown material. Yield: 99%.